THE ASTROPHYSICAL JOURNAL

AN INTERNATIONAL REVIEW OF SPECTROSCOPY AND ASTRONOMICAL PHYSICS

VOLUME 106 SEPTEMBER 1947 NUMBER 2

THE EQUATION TO THE ARM OF A SPIRAL NEBULA

E. A. MILNE

Wadham College, Oxford, England

Received July 7, 1947

ABSTRACT

The equation which should represent the arm of a spiral nebula on the basis of kinematical relativity, on a certain hypothesis, is deduced by a simple method and is shown to depend on the epoch t, reckoned from the natural zero of time. Its relation to various forms of the equation to the orbits of the individual members of the nebula is obtained. It is shown to represent to a close approximation the most general form of spiral arm to be expected.

1. In a recent paper,[1] I gave an equation which should theoretically represent the arms of spiral nebulae on the basis of kinematic relativity and the associated theory of gravitation. The purpose of the present paper is to give a somewhat simplified deduction of the equation of a spiral arm and to point out more of its properties.

2. Since rotation is the primary feature of motions in a nebula or in our own galaxy, it is natural to begin by considering a spiral nebula as a family of circular orbits described under the gravitational influence of the nucleus.[2] This phraseology refers to the ordinary dynamical or Newtonian mode of description, using τ-measure of time and the associated measure of distance. In the more fundamental t-measure of time, the circular Keplerian orbits become equiangular spirals, and an arm of a nebula is to be regarded as the locus of the present positions of a set of particles describing these orbits. We restrict attention in the first instance to the one-parameter family of orbits described by particles which have passed through a fixed point (in t-measure) near the nucleus of the nebula. A clear distinction is to be drawn between the equation of an orbit and the equation of an arm.

3. The Keplerian circular orbits in one plane are given in τ-measure by the equations[3]

$$\theta - \theta_0 = \left(\frac{\gamma M}{r_0^3}\right)^{1/2} (\tau - \tau_0) , \qquad (1)$$

[1] *M.N.*, **106**, 180, 1946.

[2] Cf. the work of S. Chandrasekhar, *Principles of Stellar Dynamics* (Chicago: University of Chicago Press, 1942), chap. iv, §§ 4.1 and 4.2 and more particularly *Ap. J.*, **92**, 441, 1940 (esp. pp. 588, 617–28). Chandrasekhar is, of course, using the classical theory of gravitation, in which γ is a constant. It may be mentioned that Chandrasekhar has also emphasized the importance of the apparently *permanent* character of the spiral form.

[3] The method of beginning with this equation is due to the referee of my paper in *M.N.*, *loc. cit.*

and

$$r = r_0 . \tag{2}$$

Here (r_0, θ_0) is the position at time τ_0 of the particle describing the orbit; τ is the current time-variable, τ_0 its present value, γ is the "constant" of gravitation, and M is the mass of the nucleus; (r, θ) are current polar co-ordinates.

On kinematic relativity we are compelled to regard the "constant" of gravitation γ as varying secularly with the epoch, and we must accordingly replace γ by the sumbol γ_0, where

$$\gamma_0 = \frac{c^3 t_0}{M_0}, \tag{3}$$

t_0 being the present age of the universe in t-measure, reckoned from the natural origin of time, c the speed of light, and M_0 the mass of the equivalent homogeneous universe.

4. We now pass to the more fundamental t-measures, in terms of which the nebulae are mutually receding. We can take τ_0 to equal t_0, and then the change of time-scale is given by

$$\tau - \tau_0 = t_0 \log \frac{t}{t_0}, \tag{4}$$

and the associated change of distance-measure results in the equation

$$r = r_0 \frac{t}{t_0}. \tag{5}$$

The Keplerian circular orbit defined by equations (1) and (2) becomes

$$\theta - \theta_0 = \left(\frac{\gamma_0 M t_0^2}{r_0^3}\right)^{1/2} \log \frac{t}{t_0}, \tag{6}$$

and

$$r = r_0 \frac{t}{t_0}. \tag{7}$$

These orbits will all have passed through the fixed point (r_1, β) at various epochs t_1, provided that

$$\beta - \theta_0 = \left(\frac{\gamma_0 M t_0^2}{r_0^3}\right)^{1/2} \log \frac{t_1}{t_0} \tag{8}$$

and

$$r_1 = r_0 \frac{t_1}{t_0}. \tag{9}$$

Eliminating t_1, the present positions (r_0, θ_0) of the particles will satisfy the relation

$$\theta_0 = \beta + \left(\frac{\gamma_0 M t_0^2}{r_0^3}\right)^{1/2} \log \frac{r_0}{r_1}. \tag{10}$$

Accordingly, the (r, θ) equation of the locus of the present positions of the particles is

$$\theta = \beta + \left(\frac{\gamma_0 M t_0^2}{r^3}\right)^{1/2} \log \frac{r}{r_1}, \tag{11}$$

which should therefore give the equation of an arm at epoch t_0. It will be noticed that equation (11) contains t_0 both explicitly and as occurring in γ_0.

5. Let us now find the equation of the arm at any epoch t by means of the equations to the orbits. We do this by eliminating θ_0 and r_0 between equations (6), (7), and (10); we find

$$\theta - \beta - \left(\frac{\gamma_0 M t_0^2 t^3}{r^3 t_0^3}\right)^{1/2} \log \frac{r t_0}{r_1 t} = \left(\frac{\gamma_0 M t_0^2 t^3}{r^3 t_0^3}\right)^{1/2} \log \frac{t}{t_0}.$$

But

$$\frac{\gamma_0 M t_0^2 t^3}{r^3 t_0^3} = \frac{\gamma_t M t^2}{r^3}, \tag{12}$$

where γ_t, the value of the "constant" of gravitation at epoch t, is given by

$$\gamma_t = \frac{c^3 t}{M_0}. \tag{13}$$

Hence the result of the elimination is

$$\theta = \beta + \left(\frac{\gamma_t M t^2}{r^3}\right)^{1/2} \log \frac{r}{r_1}. \tag{14}$$

This is, therefore, the (r, θ) equation of the arm at epoch t.

We now note the remarkable fact that, in the process of eliminating r_0 and θ_0, we have also eliminated t_0. Equation (14) is, in fact, precisely the equation we should have obtained if we had replaced the constant t_0 in equation (11), wherever it occurs (explicitly or implicitly), by the variable t. Equation (14) is thus the polar equation of an arm at *any* time t, seen *sub specie aeternitatis*, to use Spinoza's phrase.

6. The relation of equation (11) to the (r, θ) equation of the orbits can be seen more clearly as follows: Use equation (10) to eliminate θ_0 from equation (6). We get

$$\theta = \beta + \left(\frac{\gamma_0 M t_0^2}{r_0^3}\right)^{1/2} \log \frac{r_0 t}{r_1 t_0}$$

or, using equation (7),

$$\theta = \beta + \left(\frac{\gamma_0 M t_0^2}{r_0^3}\right)^{1/2} \log \frac{r}{r_1}. \tag{15}$$

This locus is the *orbit* which passes through a point at $r = r_0$ at the epoch t_0. It may be contrasted with equation (11), the equation of the *arm* at epoch t_0. In equation (15), r_0 is the parameter which characterizes the orbit under consideration. Both the loci (15) and (11) pass through the fixed point (r_1, β).

7. Equation (15) to the r_0-orbit may be transformed into another instructive form by replacing the parameter r_0 by the parameter t_1, by means of equation (9). Since

$$\frac{\gamma_0 M t_0^2}{r_0^3} = \frac{\gamma_0 M t_0^2 t_1^3}{r_1^3 t_0^3} = \frac{\gamma_1 M t_1^2}{r_1^3}, \tag{16}$$

equation (15) becomes

$$\theta = \beta + \left(\frac{\gamma_1 M t_1^2}{r_1^3}\right)^{1/2} \log \frac{r}{r_1}. \tag{17}$$

This is an alternative form of the equation to the orbit, t_1 being now the parameter; t_1 is, in fact, the epoch at which the particle passed through the fixed point (r_1, β). The orbit (17) may be written parametrically in terms of t in the form

$$\theta = \beta + \left(\frac{\gamma_1 M t_1^2}{r_1^3}\right)^{1/2} \log \frac{t}{t_1}, \tag{18}$$

and

$$r = r_1 \frac{t}{t_1}. \tag{19}$$

8. It should be noted that we have passed freely from γ_0 to γ_t and to γ_1. The variation of the "constant" of gravitation with the epoch is essential to the whole argument; γ_0 and γ_1 are, of course, constants, but γ_t is a variable. The physical meaning of the coefficient $(\gamma_0 M t_0^2/r_0^3)^{1/2}$ is seen by writing it as

$$\left(\frac{c^3 t_0^3}{M_0} \cdot \frac{M}{r_0^3}\right)^{1/2},$$

which shows that it is the square root of the pure number which is the ratio of the mean density of the matter inside r_0 to the mean density of the universe (i.e., the local mean density) at time t_0. It has been shown in the paper published in *M.N.* that the locus (11) describes ν_0 convolutions in the sense of the orbital motion followed by ν_0 convolutions in the reverse sense, where

$$\nu_0 = \frac{1}{3\pi e}\left(\frac{\gamma_0 M t_0^2}{r_1^3}\right)^{1/2} = \left(\frac{c^3 t_0^3}{M_0}\frac{M}{r_1^3}\right)^{1/2} \frac{1}{3\pi e}. \tag{20}$$

The value of $3\pi e$ being about 25.6, we see in a general way why ν_0 is of the order of 2 or 3 observationally; for $(c^3 t_0^3 M/r_1^3 M_0)^{1/2}$, being the square root of the ratio of the mean density of the matter inside r_1 to the mean local density of the smoothed-out universe, cannot be a very large number.

9. It is easily verified from comparison of equations (11) and (15) that the number of *orbital* revolutions completed by a particle up to the present moment is equal to the net number of *convolutions* of the arm between $\theta = \beta$ and the present position of the particle. Thus, as we pass from the inner parts of a spiral to the outer parts, the number of completed *orbital* revolutions increases up to ν_0 and then decreases again, ultimately approaching zero.

10. Let us try to generalize the foregoing analysis so as to cover more general initial conditions than passage at various times through a *fixed* point (r_1, β). Suppose that, quite generally, the spiral arm at epoch t has an equation in polar co-ordinates (r, θ) of the form

$$\theta = F(r, t). \tag{21}$$

Then at epoch t_0 its form is

$$\theta_0 = F(r_0, t_0). \tag{22}$$

Then $F(r_0, t_0)$ must pass into $F(r, t)$ when we pursue the family of orbits (6) and (7). Hence, eliminating θ_0, r_0 by means of equation (6) and (7) and substituting from equation (21) for θ, we must have

$$F(r, t) - F\left(\frac{r t_0}{t}, t_0\right) = \left(\frac{\gamma_t M t^2}{r^3}\right)^{1/2} \log \frac{t}{t_0}. \tag{23}$$

This is the functional equation which $F(r, t)$ must satisfy. Put

$$F(r, t) = \left(\frac{\gamma_t M t^2}{r^3}\right)^{1/2} \log \frac{r}{r_1} + \psi(r, t), \tag{24}$$

where r_1 is some constant. We find, on using equation (12), that equation (23) reduces to

$$\psi(r, t) = \psi\left(\frac{r t_0}{t}, t_0\right). \tag{25}$$

Put $r/t = x$. Then

$$\psi(xt, t) = \psi(xt_0, t_0).$$

Hence $\psi(xt, t)$ is independent of t and thus depends only on x. Hence we may put

$$\psi(xt, t) = \psi(x)$$

or

$$\psi(r, t) = \psi\left(\frac{r}{t}\right).$$

Thus the most general form of the equation of an arm of an extragalactic nebula at epoch t is

$$\theta = \psi\left(\frac{r}{t}\right) + \left(\frac{\gamma_t M t^2}{r^3}\right)^{1/2} \log \frac{r}{r_1}. \tag{26}$$

11. We now inquire what this implies as to the initial conditions satisfied by the orbits of the particles. From equation (22) the present position of the arm is given by

$$\theta_0 = \psi\left(\frac{r_0}{t_0}\right) + \left(\frac{\gamma_0 M t_0^2}{r_0^3}\right)^{1/2} \log \frac{r_0}{r_1}. \tag{27}$$

Inserting this value of θ_0 in equation (6), we find that the azimuth θ at time t of the orbit which passed through (r_0, θ_0) at time t_0 is given by

$$\theta = \psi\left(\frac{r_0}{t_0}\right) + \left(\frac{\gamma_0 M t_0^2}{r_0^3}\right)^{1/2} \log\left(\frac{r_0}{r_1}\frac{t}{t_0}\right)$$

or, using equation (7),

$$\theta = \psi\left(\frac{r_0}{t_0}\right) + \left(\frac{\gamma_0 M t_0^2}{r_0^3}\right)^{1/2} \log \frac{r}{r_1}. \tag{28}$$

Thus the orbit which passed through (r_0, θ_0) at time t_0 intersected the circle $r = r_1$ at the azimuth θ_1, given by

$$\theta_1 = \psi\left(\frac{r_0}{t_0}\right). \tag{29}$$

12. The question arises as to whether anything more can be asserted on general grounds about this distribution in azimuth. We note, first, that $\psi(r, t)$, being an angle, must be of dimensions zero and, further, that it must be a function of arguments whose dimensions are zero. Since the constants at our disposal in fixing ψ are c and r_1, we can choose for arguments of ψ any two dimensionless combinations of r and t with c and r_1, in place of r and t themselves. Thus let us write

$$\psi(r, t) = \phi\left(\frac{r}{ct}, \frac{r}{r_1}\right).$$

Put, temporarily, $r/ct = x$ and $r/r_1 = y$. Then[4] $\psi(rt_0/t, t_0)$ is obtained by giving ϕ the arguments

$$\frac{rt_0}{t}\frac{1}{ct_0} \quad \text{and} \quad \frac{rt_0}{t}\frac{1}{r_1},$$

i.e., x and xct_0/r_1. Thus the functional equation for ψ, namely, equation (25), reduces to

$$\phi(x, y) = \phi\left(x, \frac{x\,ct_0}{r_1}\right),$$

whence $\phi(x, y)$ is independent of its argument y. Hence ψ reduces to $\phi(r/ct)$. Thus (29) reduces to

$$\theta_1 = \psi\left(\frac{r_0}{ct_0}\right).$$

Now $r_0 \ll ct_0$, the ratio r_0/ct_0 being the ratio of the radius of the nebula to the radius of the universe. Hence

$$\theta_1 = \psi\left(\frac{r_0}{ct_0}\right) \sim \psi(0) = \text{constant} = \beta,$$

say. Hence equation (27), defining the present position of the spiral arm, reduces approximately to

$$\theta_0 = \beta + \left(\frac{\gamma_0 M t_0^2}{r_0^3}\right)^{1/2} \log \frac{r_0}{r_1},$$

which is precisely equation (10). Thus, in spite of the fact that the distribution of initial azimuths over the circle $r = r_1$ is represented by an arbitrary function ψ, in practice we must expect the region of emission of the particles to be concentrated in a very small range of azimuth in the vicinity of some fixed azimuth β. This conclusion, arrived at by the methods of kinematical relativity, is in agreement with conclusions of Jeans and Lindblad which were reached by very different arguments.

[4] The details here were suggested to the author by Dr. G. J. Whitrow at a colloquium.

ON THE RADIATIVE EQUILIBRIUM OF A STELLAR ATMOSPHERE. XIX

S. CHANDRASEKHAR AND FRANCES H. BREEN

Yerkes Observatory

Received June 20, 1947

ABSTRACT

In this paper H-functions which govern the law of diffuse reflection by a semi-infinite plane-parallel atmosphere scattering radiation isotropically with an albedo $\varpi_0 \leqslant 1$ are tabulated. The functions were determined numerically by solving the exact functional equations which they satisfy.

The values of the albedo for which solutions are tabulated are: $\varpi_0 = 1$, 0.975, 0.950, 0.925, 0.9, 0.8, 0.7, 0.6, 0.5, 0.4, 0.3, 0.2, and 0.1.

In continuation of Paper XVI,[1] in which we began the tabulation of exact solutions of transfer problems, we provide in this paper H-functions which govern the law of diffuse reflection by a semi-infinite isotropically scattering atmosphere for various values of the albedo, $\varpi_0 \leqslant 1$.

DIFFUSE REFLECTION UNDER CONDITIONS OF ISOTROPIC SCATTERING WITH AN ALBEDO, $\varpi_0 \leqslant 1$

The law of diffuse reflection from a semi-infinite plane-parallel atmosphere.—

$$I(\mu;\ \mu_0) = \tfrac{1}{4}\varpi_0 F \frac{\mu_0}{\mu_0 + \mu} H(\mu)\, H(\mu_0)\,.$$

The characteristic function in terms of which $H(\mu)$ is defined is

$$\Psi(\mu) = \tfrac{1}{2}\varpi_0 = \text{constant}\,.$$

TABLE 1

THE H-FUNCTIONS OBTAINED AS SOLUTIONS OF THE EXACT FUNCTIONAL EQUATIONS WHICH THEY SATISFY

μ	$\varpi_0 = 0.1$	$\varpi_0 = 0.2$	$\varpi_0 = 0.3$	$\varpi_0 = 0.4$	$\varpi_0 = 0.5$	$\varpi_0 = 0.6$	$\varpi_0 = 0.7$
0.....	1.00000	1.00000	1.00000	1.00000	1.00000	1.00000	1.00000
0.05.....	1.00783	1.01608	1.02484	1.03422	1.04439	1.05544	1.06780
0.10.....	1.01238	1.02562	1.03989	1.05535	1.07241	1.09137	1.11306
0.15.....	1.01584	1.03295	1.05155	1.07196	1.09474	1.12045	1.15036
0.20.....	1.01864	1.03892	1.06115	1.08577	1.11349	1.14517	1.18253
0.25.....	1.02099	1.04396	1.06930	1.09758	1.12968	1.16674	1.21095
0.30.....	1.02300	1.04829	1.07637	1.10789	1.14391	1.18587	1.23643
0.35.....	1.02475	1.05209	1.08259	1.11700	1.15659	1.20304	1.25951
0.40.....	1.02630	1.05546	1.08811	1.12516	1.16800	1.21861	1.28063
0.45.....	1.02768	1.05847	1.09308	1.13251	1.17833	1.23280	1.30003
0.50.....	1.02892	1.06117	1.09756	1.13918	1.18776	1.24581	1.31796
0.55.....	1.03004	1.06363	1.10164	1.14528	1.19640	1.25781	1.33459
0.60.....	1.03106	1.06587	1.10538	1.15087	1.20436	1.26893	1.35009
0.65.....	1.03199	1.06793	1.10881	1.15602	1.21173	1.27925	1.36457
0.70.....	1.03284	1.06982	1.11198	1.16080	1.21858	1.28888	1.37815
0.75.....	1.03363	1.07157	1.11491	1.16523	1.22495	1.29788	1.39090
0.80.....	1.03436	1.07319	1.11763	1.16935	1.23091	1.30631	1.40291
0.85.....	1.03504	1.07469	1.12017	1.17320	1.23648	1.31424	1.41425
0.90.....	1.03567	1.07610	1.12254	1.17681	1.24171	1.32171	1.42497
0.95.....	1.03626	1.07741	1.12476	1.18019	1.24664	1.32875	1.43512
1.00.....	1.03682	1.07864	1.12685	1.18337	1.25128	1.33541	1.44476

[1] *Ap. J.*, **105**, 435, 1947.

TABLE 1—*Continued*

μ	$\varpi_0=0.8$	$\varpi_0=0.9$	$\varpi_0=0.925$	$\varpi_0=0.95$	$\varpi_0=0.975$	$\varpi_0=1.0$
0	1.0000	1.0000	1.0000	1.0000	1.0000	1.0000
0.05	1.0820	1.0999	1.1053	1.1117	1.1196	1.1368
0.10	1.1388	1.1722	1.1828	1.1952	1.2111	1.2474
0.15	1.1866	1.2349	1.2506	1.2693	1.2936	1.3508
0.20	1.2286	1.2914	1.3123	1.3373	1.3703	1.4503
0.25	1.2663	1.3433	1.3692	1.4008	1.4427	1.5473
0.30	1.3006	1.3914	1.4224	1.4604	1.5117	1.6425
0.35	1.3320	1.4363	1.4724	1.5170	1.5778	1.7364
0.40	1.3611	1.4785	1.5197	1.5709	1.6414	1.8293
0.45	1.3881	1.5183	1.5646	1.6224	1.7027	1.9213
0.50	1.4132	1.5560	1.6073	1.6718	1.7621	2.0128
0.55	1.4368	1.5918	1.6480	1.7191	1.8195	2.1037
0.60	1.4590	1.6259	1.6869	1.7647	1.8753	2.1941
0.65	1.4798	1.6583	1.7242	1.8086	1.9295	2.2842
0.70	1.4995	1.6893	1.7600	1.8509	1.9822	2.3740
0.75	1.5182	1.7190	1.7943	1.8918	2.0334	2.4635
0.80	1.5358	1.7474	1.8274	1.9313	2.0833	2.5527
0.85	1.5526	1.7746	1.8592	1.9695	2.1320	2.6417
0.90	1.5685	1.8008	1.8898	2.0065	2.1795	2.7306
0.95	1.5837	1.8259	1.9194	2.0423	2.2258	2.8193
1.00	1.5982	1.8501	1.9479	2.0771	2.2710	2.9078

In Paper XVI (§ 2) we outlined a procedure by which the functional equations satisfied by the H-functions can be solved numerically. The same methods were adopted in the computations of the present paper, though with increased experience we were able

TABLE 2

COMPARISON OF THE INTEGRALS $\int_0^1 H(\mu)d\mu$ EVALUATED WITH THE AID OF THE TABULATED FUNCTIONS WITH THEIR EXACT VALUES $2[1-(1-\varpi_0)^{1/2}]/\varpi_0$

ϖ_0	Iterated	Exact	ϖ_0	Iterated	Exact
0.1	1.02632	1.0263340	0.8	1.3819	1.381966
.2	1.05572	1.0557281	0.9	1.5194	1.519494
.3	1.08892	1.0889331	0.925	1.5699	1.570030
.4	1.12698	1.1270167	0.950	1.6344	1.634512
.5	1.17157	1.1715729	0.975	1.7269	1.726946
.6	1.22512	1.2251482	1.000	1.9999	2.000000
0.7	1.29219	1.2922213			

to reduce appreciably the number of iterations and integrations which were required before a further iteration did not alter the function.

An idea of the accuracy reached in our present calculations can be obtained from Table 2, where we have made a comparison between the values of the integral

$$\int_0^1 H(\mu)\, d\mu\,,$$

evaluated numerically with the aid of the tabulated functions, and the exact values given by the formula

$$\frac{2}{\varpi_0}\left[1-(1-\varpi_0)^{\frac{1}{2}}\right].$$

ON THE RADIATIVE EQUILIBRIUM OF A STELLAR ATMOSPHERE. XX

S. CHANDRASEKHAR
Yerkes Observatory
Received June 20, 1947

ABSTRACT

In this paper the exact solution for a standard problem in the theory of line formation in stellar atmospheres is obtained. The problem allows for the combined effects of monochromatic line scattering and general continuous absorption but assumes that the ratio of the line (σ_ν) to the continuous (κ_ν) absorption coefficient is constant through the atmosphere and that the Planck intensity, B_ν, is a linear function of the optical thickness in ($\sigma_\nu + \kappa_\nu$).

The exact solution involves the H-functions already tabulated in Paper XIX and their first and second moments. A table of the latter is provided in this paper.

1. *Introduction.*—As is well known, an important case in the theory of line formation in stellar atmospheres arises when the combined effects of monochromatic line scattering and general continuous absorption are considered. The equation of transfer appropriate to these conditions is

$$\mu \frac{dI_\nu}{dt_\nu} = I_\nu - \tfrac{1}{2}(1-\lambda_\nu)\int_{-1}^{+1} I_\nu(t_\nu, \mu')\, d\mu' - \lambda_\nu B_\nu\,, \tag{1}$$

where B_ν is the Planck intensity at the prevailing temperature, t_ν is the optical thickness in the combined line (σ_ν) and continuous (κ_ν) absorption coefficients, and

$$\lambda_\nu = \frac{\kappa_\nu}{\sigma_\nu + \kappa_\nu}\,. \tag{2}$$

An assumption which appears not unreasonable in the context of line formation is that B_ν is a linear function of the optical thickness, τ_ν, in the *continuum*. In other words, we may write

$$B_\nu = B_\nu^{(10)} + B_\nu^{(10)}\tau_\nu\,, \tag{3}$$

where $B_\nu^{(0)}$ and $B_\nu^{(1)}$ are certain appropriately chosen constants. (It may be remarked here that in $B_\nu^{(0)}$ and $B_\nu^{(1)}$ we may replace ν by the frequency at the center of the line, ν_0, without introducing any sensible error; this cannot, of course, be done for I_ν and λ_ν.) If we now further suppose (and this is not always an equally justifiable assumption) that σ_ν/κ_ν is constant through the atmosphere,[1] then

$$B_\nu = B_\nu^{(0)} + B_\nu^{(1)}\lambda_\nu t_\nu\,. \tag{4}$$

With B_ν given by equation (4), the equation of transfer becomes

$$\mu \frac{dI}{dt} = I - \tfrac{1}{2}(1-\lambda)\int_{-1}^{+1} I(t, \mu')\, d\mu' - \lambda\,[B^{(0)} + \lambda B^{(1)} t]\,, \tag{5}$$

where, for the sake of convenience, we have suppressed the subscript ν to the various quantities.

[1] For a theory along the lines of this series of papers, in which this assumption is not made, see M. Tuberg, *Ap. J.*, **103**, 145, 1946. The basic ideas in this context are, however, due to B. Strömgren, *Ap. J.*, **86**, 1, 1937.

Equation (5) has generally been regarded as one of the fundamental equations in the theory of stellar atmospheres.

The solution of equation (5) in the method of approximation of the earlier papers of this series was given in Paper II (§ 7),[2] and numerical results relating to the solution in the second and third approximations will be found in Papers IV and VI.[3] However, in this paper we shall show how the ideas developed in Paper XIV[4] enable us to pass to the limit of infinite approximation and obtain the exact solution for this problem in the theory of line formation.

2. *The solution for the emergent intensity in closed form in the nth approximation.*—The solution of equation (5) in the nth approximation can be written in the following form (Paper II, eq. [90]):

$$I_i = \lambda B^{(1)}\left[\sum_{a=1}^{n}\frac{L_a e^{-k_a\tau}}{1+k_a\mu_i}+\mu_i+t+\frac{B^{(0)}}{\lambda B^{(1)}}\right] \qquad (i=\pm 1\ ,\ \ldots\ ,\ \pm n)\ , \quad (6)$$

where the k_a's ($a = 1, \ldots, n$) are the positive roots of the characteristic equation

$$1 = (1-\lambda)\sum_{j=1}^{n}\frac{a_j}{1-\mu_j^2k^2}\ ; \qquad (7)$$

the L_a's ($a = 1, \ldots, n$) are the n constants of integration; and the rest of the symbols have their usual meanings.

Now in transfer problems in semi-infinite plane-parallel atmospheres the boundary conditions which determine the constants of integration and the equation which gives the intensity distribution of the emergent radiation can both be expressed in terms of the same function. Thus, in the present case, the boundary conditions and the emergent intensity $I(0, \mu)$ can be expressed in the following forms:

$$S(\mu_i) = 0\ , \qquad (i=1\ ,\ \ldots\ ,\ n) \qquad (8)$$

and

$$I(0,\ \mu) = \lambda B^{(1)} S(-\mu)\ , \qquad (9)$$

where

$$S(\mu) = \sum_{a=1}^{n}\frac{L_a}{1-k_a\mu}-\mu+\frac{B^{(0)}}{\lambda B^{(1)}}\ . \qquad (10)$$

In view of the boundary conditions (eq. [8]) we can write

$$S(\mu) = (-1)^{n+1}k_1\ldots k_n\frac{P(\mu)}{R(\mu)}(\mu-c)\ , \qquad (11)$$

where c is a constant and $P(\mu)$ and $R(\mu)$ have their standard meanings.

Moreover, according to equations (10) and (11)

$$L_a = (-1)^{n+1}k_1\ldots k_n\frac{P(1/k_a)}{R_a(1/k_a)}\left(\frac{1}{k_a}-c\right) \qquad (a=1,\ \ldots\ ,\ n)\ . \quad (12)$$

For the roots of the characteristic equation (7), it can be readily shown that

$$k_1\ldots k_n\,\mu_1\ldots\mu_n = \lambda^{\frac{1}{2}}. \qquad (13)$$

[2] *Ap. J.*, **100**, 76, 1944. [3] *Ibid.*, p. 355, and **101**, 320, 1945. [4] *Ibid.*, **105**, 164, 1947.

Equation (11) therefore becomes

$$S(\mu) = -\lambda^{\frac{1}{2}} H(-\mu)(\mu - c). \tag{14}$$

To determine the constant c, we proceed as follows:
First, putting $\mu = 0$ in equations (10) and (11), we have

$$\sum_{a=1}^{n} L_a + \frac{B^{(0)}}{\lambda B^{(1)}} = c\lambda^{\frac{1}{2}}. \tag{15}$$

We next evaluate ΣL_a in accordance with equation (12). Thus

$$\left.\begin{aligned} \sum_{a=1}^{n} L_a &= (-1)^{n+1} k_1 \ldots . k_n \sum_{a=1}^{n} \frac{P(1/k_a)}{R_a(1/k_a)} \left(\frac{1}{k_a} - c\right) \\ &= (-1)^{n+1} k_1 \ldots . k_n f(0), \end{aligned}\right\} \tag{16}$$

where

$$f(x) = \sum_{a=1}^{n} \frac{P(1/k_a)}{R_a(1/k_a)} \left(\frac{1}{k_a} - c\right) R_a(x). \tag{17}$$

Defined in this manner, $f(x)$ is a polynomial of degree $(n-1)$ in x, which takes the values

$$\left(\frac{1}{k_a} - c\right) P(1/k_a) \tag{18}$$

for $x = 1/k_a$ $(a = 1, \ldots, n)$. There must, accordingly, exist a relation of the form

$$f(x) = (x - c)P(x) + R(x)(Ax + C), \tag{19}$$

where A and C are certain constants; and the constants can be determined from the condition that the coefficients of x^{n+1} and x^n must vanish on the right-hand side. We thus find that

$$A = \frac{(-1)^{n+1}}{k_1 \ldots . k_n} \quad \text{and} \quad C = \frac{(-1)^n}{k_1 \ldots . k_n} \left(\sum_{j=1}^{n} \mu_j - \sum_{a=1}^{n} \frac{1}{k_a} + c\right). \tag{20}$$

Hence

$$f(0) = (-1)^{n+1} \mu_1 \ldots . \mu_n c + \frac{(-1)^n}{k_1 \ldots . k_n} \left(\sum_{j=1}^{n} \mu_j - \sum_{a=1}^{n} \frac{1}{k_a} + c\right), \tag{21}$$

and (cf. eqs. [13] and [16])

$$\sum_{a=1}^{n} L_a = c\lambda^{\frac{1}{2}} + \left(\sum_{a=1}^{n} \frac{1}{k_a} - \sum_{j=1}^{n} \mu_j - c\right). \tag{22}$$

Inserting this value of ΣL_a in equation (15), we obtain

$$c = \frac{B^{(0)}}{\lambda B^{(1)}} + \sum_{a=1}^{n} \frac{1}{k_a} - \sum_{j=1}^{n} \mu_j. \tag{23}$$

Finally, substituting for c from equation (23) in equation (14), we have

$$S(\mu) = -\lambda^{\frac{1}{2}} H(-\mu)\left[\mu - \left(\frac{B^{(0)}}{\lambda B^{(1)}} + \sum_{a=1}^{n} \frac{1}{k_a} - \sum_{j=1}^{n} \mu_j\right)\right]. \tag{24}$$

Equation (9) governing the intensity distribution of the emergent radiation now becomes

$$I(0, \mu) = \lambda^{3/2} B^{(1)} H(\mu)\left(\mu + \frac{B^{(0)}}{\lambda B^{(1)}} + \sum_{a=1}^{n} \frac{1}{k_a} - \sum_{j=1}^{n} \mu_j\right). \tag{25}$$

This is the required solution in closed form.

3. *Passage to the limit of infinite approximation.*—According to theorem 2 of Paper XIV (§ 11), any H-function defined in the usual manner in terms of the points of the Gaussian division and the roots of a characteristic equation becomes in the limit of infinite approximation the solution of a functional equation of the standard form,

$$H(\mu) = 1 + \mu H(\mu) \int_0^1 \frac{H(\mu')}{\mu + \mu'} \Psi(\mu')\, d\mu', \tag{26}$$

considered in Paper XIV (Sec. III). Consequently, from equation (25) we conclude that the exact solution for the emergent intensity for the problem under consideration must be of the form

$$I(0, \mu) = \lambda^{3/2} B^{(1)} H(\mu)\left(\mu + \frac{B^{(0)}}{\lambda B^{(1)}} + q\right), \tag{27}$$

where $H(\mu)$ is now defined as a solution of a functional equation of the form (26) with the characteristic function

$$\Psi(\mu) = \tfrac{1}{2}(1 - \lambda) = \text{constant}, \tag{28}$$

and

$$q = \lim_{n \to \infty}\left(\sum_{a=1}^{n} \frac{1}{k_a} - \sum_{j=1}^{n} \mu_j\right). \tag{29}$$

The exact H-functions characterizing the problem of line formation are therefore the same as the ones which occur in the problem of diffuse reflection by a semi-infinite plane-parallel atmosphere with an albedo

$$\varpi_0 = 1 - \lambda. \tag{30}$$

The H-functions tabulated in the preceding paper[5] are therefore equally applicable to this problem. However, to complete the solution we must determine q as defined in equation (29).

4. *Evaluation of the limit* $\left(\sum_1^n k_a^{-1} - \sum_1^n \mu_j\right)$ *as* $n \to \infty$. *The exact solution.*—Consider the function (cf. Paper XIV, § 11)

$$s(\mu) = \sum_{a=1}^{n} \frac{l_a}{1 - k_a \mu} + 1, \tag{31}$$

where the k_a's ($a = 1, \ldots, n$) are the roots of the characteristic equation (7) and the l_a's ($a = 1, \ldots, n$) are n constants determined by the conditions

$$s(\mu_i) = 0 \qquad (i = 1, \ldots n). \tag{32}$$

[5] Paper XIX, *Ap. J.*, **106**, 143, 1947.

It is known that, defined in this manner (Paper XIV, eqs. [132]–[138]),

$$s(\mu) = k_1 \ldots . k_n \mu_1 \ldots . \mu_n H(-\mu) . \tag{33}$$

Using relation (13), we have

$$s(\mu) = \lambda^{\frac{1}{2}} H(-\mu) . \tag{34}$$

Moreover, according to equations (31) and (32),

$$l_a = (-1)^n k_1 \ldots . k_n \frac{P(1/k_a)}{R_a(1/k_a)} \qquad (a = 1, \ldots . , n) . \tag{35}$$

Now consider

$$\sum_{a=1}^{n} \frac{l_a}{k_a} = (-1)^n k_1 \ldots . k_n \sum_{a=1}^{n} \frac{P(1/k_a)}{R_a(1/k_a)} \frac{1}{k_a} . \tag{36}$$

It is seen that the summation which occurs on the right-hand side of equation (36) is a special case ($c = 0$) of the one considered in § 2 (eq. [16]). We therefore have (cf. eq. [21])

$$\sum_{a=1}^{n} \frac{l_a}{k_a} = \sum_{j=1}^{n} \mu_j - \sum_{a=1}^{n} \frac{1}{k_a} . \tag{37}$$

But $\Sigma l_a/k_a$ can also be expressed in terms of $H(\mu)$. Thus, consider

$$\sum_{i=1}^{n} a_i \mu_i s(-\mu_i) . \tag{38}$$

Since $s(+\mu_i) = 0$ ($i = 1, \ldots . , n$), we can extend the summation in (38) for negative values of i also. Hence

$$\sum_{i=1}^{n} a_i \mu_i s(-\mu_i) = \sum_{i=-n}^{+n} a_i \mu_i s(-\mu_i) . \tag{39}$$[6]

Now substitute for $s(-\mu_i)$ according to equation (31) on the right-hand side of equation (39). We obtain

$$\left.\begin{aligned} \sum_{i=1}^{n} a_i \mu_i s(-\mu_i) &= \sum_{i=-n}^{+n} a_i \mu_i \left(\sum_{a=1}^{n} \frac{l_a}{1 + k_a \mu_i} + 1 \right) \\ &= \sum_{i=-n}^{+n} a_i \mu_i \left(\sum_{a=1}^{n} \frac{l_a}{1 + k_a \mu_i} \right); \end{aligned} \right\} \tag{40}$$

or, inverting the order of the summation, we have

$$\left.\begin{aligned} \sum_{i=1}^{n} a_i \mu_i s(-\mu_i) &= \sum_{a=1}^{n} l_a \left(\sum_{i=-n}^{+n} \frac{a_i \mu_i}{1 + k_a \mu_i} \right) \\ &= \sum_{a=1}^{n} \frac{l_a}{k_a} \sum_{i=-n}^{+n} a_i \left(1 - \frac{1}{1 + k_a \mu_i} \right). \end{aligned} \right\} \tag{41}$$

[6] In the summation on the right-hand side there is no term with $i = 0$.

Using a well-known property of the Gaussian weights and also the equation defining the characteristic roots (eq. [7]), we have

$$\sum_{i=1}^{n} a_i \mu_i s(-\mu_i) = \left(2 - \frac{2}{1-\lambda}\right) \sum_{a=1}^{n} \frac{l_a}{k_a} = -\frac{2\lambda}{1-\lambda} \sum_{a=1}^{n} \frac{l_a}{k_a}. \tag{42}$$

Hence (cf. eqs. [34] and [37])

$$\sum_{i=1}^{n} a_i \mu_i H(\mu_i) = \frac{2\lambda^{\frac{1}{2}}}{1-\lambda} \left(\sum_{a=1}^{n} \frac{1}{k_a} - \sum_{j=1}^{n} \mu_j \right), \tag{43}$$

or

$$\sum_{a=1}^{n} \frac{1}{k_a} - \sum_{j=1}^{n} \mu_j = \frac{1-\lambda}{2\lambda^{\frac{1}{2}}} \sum_{i=1}^{n} a_i \mu_i H(\mu_i). \tag{44}$$

We now pass to the limit $n \to \infty$. Then $H(\mu)$ becomes the solution of the functional equation

$$H(\mu) = 1 + \tfrac{1}{2}(1-\lambda)\mu H(\mu) \int_0^1 \frac{H(\mu')}{\mu + \mu'} d\mu' \tag{45}$$

and

$$\lim_{n \to \infty} \left(\sum_{a=1}^{n} \frac{1}{k_a} - \sum_{j=1}^{n} \mu_j \right) = \frac{1-\lambda}{2\lambda^{\frac{1}{2}}} a_1 \tag{46}$$

where a_1 is the first moment of $H(\mu)$.

The exact solution for $I(0, \mu)$ is therefore given by

$$I(0, \mu) = \lambda^{3/2} B^{(1)} H(\mu) \left(\mu + \frac{B^{(0)}}{\lambda B^{(1)}} + \frac{1-\lambda}{2\lambda^{\frac{1}{2}}} a_1 \right). \tag{47}$$

5. *Exact formulae for the residual intensity. A table of the moments of* H(μ).—The intensity, $I^{(\text{cont})}(0, \mu)$, in the continuum is obtained by letting $\lambda \to 1$. In this limit

$$H(\mu) \equiv 1 \qquad (\lambda = 1), \tag{48}$$

and

$$I^{(\text{cont})}(0, \mu) = B^{(1)} \left(\mu + \frac{B^{(0)}}{B^{(1)}} \right). \tag{49}$$

(This solution can, of course, be obtained directly from eq. [5].) The residual intensity, r, in the line is therefore given by

$$r(\mu) = \frac{\lambda^{3/2}}{\mu + \dfrac{B^{(0)}}{B^{(1)}}} H(\mu) \left(\mu + \frac{B^{(0)}}{\lambda B^{(1)}} + \frac{1-\lambda}{2\lambda^{\frac{1}{2}}} a_1 \right). \tag{50}$$

Again, according to equation (47), the emergent flux is given by

$$F = 2\lambda^{3/2} B^{(1)} \left(a_2 + \frac{B^{(0)}}{\lambda B^{(1)}} a_1 + \frac{1-\lambda}{2\lambda^{\frac{1}{2}}} a_1^2 \right), \tag{51}$$

where a_2 is the second moment of $H(\mu)$. The residual intensity, R_ν, in the emergent flux is therefore given by

$$R(\nu) = \frac{\lambda^{3/2}}{\dfrac{1}{3} + \dfrac{1}{2} \dfrac{B^{(0)}}{B^{(1)}}} \left(a_2 + \frac{B^{(0)}}{\lambda B^{(1)}} a_1 + \frac{1-\lambda}{2\lambda^{\frac{1}{2}}} a_1^2 \right). \tag{52}$$

As we have already remarked, the H-functions which occur in this problem are the same as those tabulated in Paper XIX. To facilitate the use of solutions (47), (50), and (52) we now provide a table of values of the first and the second moments of $H(\mu)$ for various values of λ (Table 1).

TABLE 1

THE FIRST AND THE SECOND MOMENTS OF $H(\mu)$

ϖ_0	λ	First Moment	Second Moment	ϖ_0	λ	First Moment	Second Moment
0	1.0	0.500000	0.333333	0.7	0.3	0.678674	0.461423
0.1	0.9	.515609	.344357	0.8	.2	0.735808	.503218
.2	0.8	.533154	.356787	0.9	.1	0.825318	.569449
.3	0.7	.553123	.370985	0.925	.075	0.858734	.594404
.4	0.6	.576210	.387466	0.950	.050	0.901864	.626785
.5	0.5	.603495	.407030	0.975	0.025	0.964471	.674134
0.6	0.4	0.636636	0.430922	1.000	0	1.154701*	0.820352*

* The exact values of these entries are 1.154701 and 0.820354, respectively.

It is a pleasure to record here my indebtedness to Mrs. Frances H. Breen, who has been of very valuable assistance to me in the numerical work of this entire series of papers.

ON THE RADIATIVE EQUILIBRIUM OF A STELLAR ATMOSPHERE. XXI

S. CHANDRASEKHAR
Yerkes Observatory
Received June 20, 1947

ABSTRACT

In this paper the theory of diffuse reflection and transmission by a plane-parallel atmosphere of finite optical thickness is considered under conditions of (I) isotropic scattering with an albedo $\varpi_0 \leqslant 1$, (II) scattering in accordance with Rayleigh's phase function, (III) scattering in accordance with the phase function $\lambda(1 + x \cos \Theta)$, and (IV) Rayleigh scattering with proper allowance for the polarization of the radiation field. In all cases considered, it has been possible to eliminate the constants of integration (which are twice as many as in the case of semi-infinite atmospheres) and express the solutions for the reflected and the transmitted radiations in closed forms in a general nth approximation. It is further shown how a pair of functions, $X(\mu)$ and $Y(\mu)$, depending only on the roots of a characteristic equation and the optical thickness of the atmosphere, play the same basic role in this theory as $H(\mu)$ does in the theory of semi-infinite atmospheres. The passage to the limit of infinite approximation and the determination of the exact laws of diffuse reflection and transmission are thus made possible.

1. *Introduction.*—In the earlier papers[1] of this series, the theory of the transfer of radiation in semi-infinite plane-parallel atmospheres has been developed to a point that it is possible to obtain by a definite algorism exact solutions for the various problems. But the corresponding theory for atmospheres of finite optical thicknesses is in a far less advanced stage. The difficulties confronting the development of this latter theory do not lie in the system of linear equations which replaces the equation of transfer in our scheme of approximation: they present, in fact, no problem which does not already require solution in the semi-infinite case.[2] The difficulties actually lie in the problem of eliminating the explicit appearance of the constants of integration in the solutions and expressing the angular distributions of the emergent radiations in terms of functions which involve only the roots of certain characteristic equations. This problem of the elimination of the constants and the reduction of the solution to the evaluation of a certain basic function (or a set of functions)[3] is of particular importance for passing to the limit of infinite approximation and obtaining the exact solutions. Thus, in analogy with the theory of semi-infinite atmospheres, we may expect that the angular distributions of the emergent radiations can be expressed in terms of certain functions which will be explicitly known in any finite approximation and which in the limit of infinite approximation will become solutions of functional equations of a standard form. We shall see that this reduction can be achieved in spite of the greater complexity of the problem arising from our present requirement of explicitly satisfying boundary conditions on both sides of the atmosphere and of obtaining solutions in closed forms for the expressions governing the radiation emergent from each of the two sides.

In this paper we shall take the first of the two principal steps required for the completion of the theory of radiative transfer in plane-parallel atmospheres of finite optical thicknesses. More particularly, in this paper, we shall carry out the elimination of the constants for the basic problem of diffuse reflection and transmission under a variety

[1] See particularly Papers XIV, XVI, XIX, and XX (*Ap. J.*, **105**, 164, 435, 1947; *ibid.*, **106**, 143, 145, 1947.

[2] Cf. Paper XII (eqs. [45] and [74]) (*ibid.*, **104**, 191, 1946).

[3] We shall see that, actually, a pair of functions defined in the interval (0, 1) is involved in the solutions for finite atmospheres.

of scattering conditions and show how, in each case considered, the solution can be expressed in terms of a single function defined in the interval $(-1, +1)$. The passage to the limit of infinite approximation and the exhibition of the relationship of these solutions[4] to the functional equations derived in Paper XVII[5] are postponed to a later paper.

I. ISOTROPIC SCATTERING WITH AN ALBEDO $\varpi_0 < 1$

2. *The expression of the boundary conditions and the emergent intensities in terms of two functions.*—As we shall see, the consideration of the problem of diffuse reflection and transmission by an atmosphere scattering radiation isotropically with an albedo $\varpi_0 < 1$ introduces us, in its simplest context, to a basic mathematical problem which is characteristic of this theory and which requires solution. Considering, then, the case of a plane-parallel atmosphere of a finite optical thickness, τ_1, on which is incident a parallel beam of radiation of net flux πF per unit area normal to itself, at an angle $\cos^{-1}\mu_0$ to the normal, we have[2]

$$I_i = \tfrac{1}{4}\varpi_0 F\Big[\sum_{\alpha=-n}^{+n}\frac{L_\alpha e^{-k_\alpha\tau}}{1+\mu_i k_\alpha}+\frac{\gamma e^{-\tau/\mu_0}}{1+\mu_i/\mu_0}\Big] \qquad (i=\pm 1,\ldots,\pm n), \quad (1)^6$$

for the solution of the intensities I_i in the nth approximation. In equation (1) the L_α's ($\alpha = \pm 1, \ldots, \pm n$) are the $2n$ constants of integration, and the k_α's ($\alpha = \pm 1, \ldots, \pm n$ and $k_{+\alpha} = -k_{-\alpha}$) are the $2n$ roots of the characteristic equation

$$1 = \varpi_0\sum_{j=1}^{n}\frac{a_j}{1-k^2\mu_j^2}, \qquad (2)$$

which occurs in pairs ($k_{+\alpha} = -k_{-\alpha}$), and

$$\gamma = H(\mu_0)\,H(-\mu_0) = \frac{(-1)^n}{\mu_1^2\cdots\mu_n^2}\,\frac{\prod_{i=1}^{n}(\mu_0^2-\mu_i^2)}{\prod_{\alpha=1}^{n}(1-k_\alpha^2\mu_0^2)}. \qquad (3)$$

The boundary conditions appropriate to our present problem are

$$I_{-i} = 0 \quad \text{at} \quad \tau = 0 \quad \text{and for} \quad i = 1, \ldots, n, \qquad (4)$$

and

$$I_{+i} = 0 \quad \text{at} \quad \tau = \tau_1 \quad \text{and for} \quad i = 1, \ldots, n. \qquad (5)$$

The equations which determine the $2n$ constants of integration are, therefore,

$$\sum_{\alpha=-n}^{+n}\frac{L_\alpha}{1-k_\alpha\mu_i}+\frac{\gamma}{1-\mu_i/\mu_0} = 0 \qquad (i=1,\ldots,n) \quad (6)$$

and

$$\sum_{\alpha=-n}^{+n}\frac{L_\alpha e^{-k_\alpha\tau_1}}{1+k_\alpha\mu_i}+\frac{\gamma e^{-\tau_1/\mu_0}}{1+\mu_i/\mu_0} = 0 \qquad (i=1,\ldots,n). \quad (7)$$

[4] In the manner of Paper XIV.

[5] *Ap. J.*, **106**, 441, 1947.

[6] In the summation over α in this equation, the term $\alpha = 0$ is omitted. We shall adopt this convention throughout. It is, therefore, always to be understood that in all summations (or products) extended over α from $-n$ to $+n$ the term with $\alpha = 0$ does not occur.

In terms of the functions

$$S(\mu) = \sum_{a=-n}^{+n} \frac{L_a}{1 - k_a\mu} + \frac{\gamma}{1 - \mu/\mu_0} \tag{8}$$

and

$$T(\mu) = \sum_{a=-n}^{+n} \frac{L_a e^{-k_a\tau_1}}{1 + k_a\mu} + \frac{\gamma e^{-\tau_1/\mu_0}}{1 + \mu/\mu_0}, \tag{9}$$

the boundary conditions can be expressed in the form

$$S(\mu_i) = T(\mu_i) = 0 \qquad (i = 1, \ldots, n). \tag{10}$$

In other words, the μ_i's ($i = 1, \ldots, n$) are zeros of both S and T.

In analogy with the procedure adopted in the case of semi-infinite atmospheres, we must now try to express the reflected and the transmitted intensities, $I(0, \mu)$ and $I(\tau_1, -\mu)$, $(0 \leqslant \mu \leqslant 1)$, in terms of the same functions $S(\mu)$ and $T(\mu)$. It is, however, immediately apparent that $I(0, \mu)$ and $I(\tau_1, -\mu)$ cannot, simply, be proportional to $S(-\mu)$ and $T(-\mu)$, respectively, since these functions diverge for all those values of $\mu = k_a^{-1}$ for which $k_a^{-1} < 1$ $(a > 0)$; in nonconservative cases (such as the present) divergence from this source will occur for $(n - 1)$ values of μ in the interval $0 \leqslant \mu \leqslant 1$.[7] Consequently, a different procedure must be adopted for expressing the angular distributions of the reflected and the transmitted radiations. On consideration, it appears that the procedure which should be adopted is the following:

For the problem of diffuse reflection and transmission under consideration, the source function $\mathfrak{J}(\tau, \mu)$ is

$$\mathfrak{J}(\tau, \mu) = \tfrac{1}{2}\varpi_0 \int_{-1}^{+1} I(\tau, \mu')\, d\mu' + \tfrac{1}{4}\varpi_0 F e^{-\tau/\mu_0}, \tag{11}$$

or, in our scheme of approximation,

$$\mathfrak{J}(\tau, \mu) = \tfrac{1}{2}\varpi_0 \Sigma a_j I_j + \tfrac{1}{4}\varpi_0 F e^{-\tau/\mu_0}. \tag{12}$$

With the solution for I_i given by equation (1), the foregoing expression for $\mathfrak{J}(\tau, \mu)$ reduces to

$$\mathfrak{J}(\tau, \mu) = \tfrac{1}{4}\varpi_0 F \Big[\sum_{a=-n}^{+n} L_a e^{-k_a\tau} + \gamma e^{-\tau/\mu_0} \Big]. \tag{13}$$

Since, in general, the outward and the inward intensities, $I(\tau, +\mu)$ and $I(\tau, -\mu)$, $(0 < \mu < 1)$, at any level τ, are derivable from the source function in accordance with the equations

$$I(\tau, +\mu) = \int_{\tau}^{\tau_1} \mathfrak{J}(t, \mu)\, e^{-(t-\tau)/\mu} \frac{dt}{\mu} \tag{14}$$

and

$$I(\tau, -\mu) = \int_{0}^{\tau} \mathfrak{J}(t, -\mu)\, e^{-(\tau-t)/\mu} \frac{dt}{\mu}, \tag{15}$$

we find that in our particular case

$$\left.\begin{aligned} I(\tau, +\mu) = \tfrac{1}{4}\varpi_0 F e^{+\tau/\mu} \Bigg\{ \sum_{a=-n}^{+n} \frac{L_a}{1 + k_a\mu} \left[e^{-\tau(1+k_a\mu)/\mu} - e^{-\tau_1(1+k_a\mu)/\mu} \right] \\ + \frac{\gamma}{1 + \mu/\mu_0} \left[e^{-\tau(\mu_0+\mu)/\mu\mu_0} - e^{-\tau_1(\mu_0+\mu)/\mu\mu_0} \right] \Bigg\} \end{aligned}\right\} \tag{16}$$

[7] In addition, $T(-\mu)$ will also diverge for $\mu = \mu_0$.

and

$$I(\tau, -\mu) = \tfrac{1}{4}\varpi_0 F e^{-\tau/\mu}\left\{\sum_{a=-n}^{+n}\frac{L_a}{1-k_a\mu}\left[e^{\tau(1-k_a\mu)/\mu}-1\right] + \frac{\gamma}{1-\mu/\mu_0}\left[e^{\tau(\mu_0-\mu)/\mu\mu_0}-1\right]\right\}. \tag{17}$$

For the reflected and the transmitted intensities we therefore have

$$I(0, \mu) = \tfrac{1}{4}\varpi_0 F\left\{\sum_{a=-n}^{+n}\frac{L_a}{1+k_a\mu}\left[1-e^{-\tau_1(1+k_a\mu)/\mu}\right] + \frac{\gamma}{1+\mu/\mu_0}\left[1-e^{-\tau_1(\mu_0+\mu)/\mu\mu_0}\right]\right\} \tag{18}$$

and

$$I(\tau_1, -\mu) = \tfrac{1}{4}\varpi_0 F e^{-\tau_1/\mu}\left\{\sum_{a=-n}^{+n}\frac{L_a}{1-k_a\mu}\left[e^{\tau_1(1-k_a\mu)/\mu}-1\right] + \frac{\gamma}{1-\mu/\mu_0}\left[e^{\tau_1(\mu_0-\mu)/\mu\mu_0}-1\right]\right\}, \tag{19}$$

or, somewhat differently,

$$I(0, \mu) = \tfrac{1}{4}\varpi_0 F\left\{\sum_{a=-n}^{+n}\frac{L_a}{1+k_a\mu}+\frac{\gamma}{1+\mu/\mu_0} - e^{-\tau_1/\mu}\left[\sum_{a=-n}^{+n}\frac{L_a e^{-k_a\tau_1}}{1+k_a\mu}+\frac{\gamma e^{-\tau_1/\mu_0}}{1+\mu/\mu_0}\right]\right\}, \tag{20}$$

and

$$I(\tau_1, -\mu) = \tfrac{1}{4}\varpi_0 F\left\{\sum_{a=-n}^{+n}\frac{L_a e^{-k_a\tau_1}}{1-k_a\mu}+\frac{\gamma e^{-\tau_1/\mu_0}}{1-\mu/\mu_0} - e^{-\tau_1/\mu}\left[\sum_{a=-n}^{+n}\frac{L_a}{1-k_a\mu}+\frac{\gamma}{1-\mu/\mu_0}\right]\right\}. \tag{21}$$ [8]

According to our definitions of the functions $S(\mu)$ and $T(\mu)$, we can re-write the foregoing expressions for $I(0, +\mu)$ and $I(\tau_1, -\mu)$ in the forms

$$I(0, \mu) = \tfrac{1}{4}\varpi_0 F\left[S(-\mu) - e^{-\tau_1/\mu}T(\mu)\right] \tag{22}$$

and

$$I(\tau_1, -\mu) = \tfrac{1}{4}\varpi_0 F\left[T(-\mu) - e^{-\tau_1/\mu}S(\mu)\right]. \tag{23}$$ [9]

Thus, in the case of finite atmospheres, as in the case of semi-infinite atmospheres, there is a relationship of reciprocity between the equations which express the boundary conditions and the functions which describe the emergent radiations. The present relationship is naturally not so direct as the one encountered in the case of semi-infinite atmospheres. But it will appear that the relationship exemplified by equations (10), (22), and (23) is quite general and is precisely what is required to preserve the basic in-

[8] These expressions, do not, of course, diverge for any value of μ in the interval, $0 \leqslant \mu \leqslant 1$.

[9] Since $S(\mu_i) = T(\mu_i) = 0$,

$$I(0, \mu_i) = \tfrac{1}{4}\bar{\omega}_0 F S(-\mu_i) \quad \text{and} \quad I(\tau_1, -\mu_i) = \tfrac{1}{4}\bar{\omega}_0 F T(-\mu_i);$$

and this is in agreement with the solution (1) for the intensities at the points of the Gaussian division.

variances of the problem in all orders of approximation. And this last is, of course, an essential requirement for passing to the limit of infinite approximation on our method.

3. *The reduction to a problem in the theory of interpolation.*—In addition to the functions

$$P(\mu) = \prod_{i=1}^{n} (\mu - \mu_i) \qquad \text{and} \qquad R(\mu) = \prod_{a=1}^{n} (1 - k_a \mu)\,, \tag{24}$$

which we have extensively used in the earlier papers, we shall now introduce the functions

$$W(\mu) = R(\mu) R(-\mu) = \prod_{a=-n}^{+n} (1 - k_a \mu) = \prod_{a=1}^{n} (1 - k_a^2 \mu^2) \tag{25}$$

and

$$W_a(\mu) = \prod_{\substack{\beta=-n \\ \beta \neq a}}^{+n} (1 - k_\beta \mu) \qquad (a = \pm 1\,, \ldots\,, \pm n)\,. \tag{26}$$

Identities which follow from definitions (25) and (26) and which we shall find useful, are

$$W(\mu) = W(-\mu) \tag{27}$$

and

$$W_a(\mu) = W_{-a}(-\mu) \qquad (a = 1\,, \ldots\,, n)\,. \tag{28}$$

Now, from equations (8) and (9) it follows that

$$S(\mu) W(\mu) \left(1 - \frac{\mu}{\mu_0}\right) \qquad \text{and} \qquad T(\mu) W(\mu) \left(1 + \frac{\mu}{\mu_0}\right), \tag{29}$$

are polynomials of degree $2n$ in μ; and, according to equation (10), the μ_i's ($i = 1, \ldots, n$) are zeros of both these polynomials. We may therefore write

$$S(\mu) = \frac{1}{\mu_1^2 \ldots \mu_n^2} \frac{P(\mu)}{W(\mu)(1 - \mu/\mu_0)}\, s(\mu) \tag{30}$$

and

$$T(\mu) = \frac{1}{\mu_1^2 \ldots \mu_n^2} \frac{P(\mu)}{W(\mu)(1 + \mu/\mu_0)}\, t(\mu)\,, \tag{31}$$[10]

where $s(\mu)$ and $t(\mu)$ are polynomials of degree n in μ.

Two relations which follow immediately from equations (3), (8), (9), (30), and(31) are

$$\left.\begin{aligned} \gamma = \frac{1}{\mu_1^2 \ldots \mu_n^2} \frac{P(\mu_0) P(-\mu_0)}{W(\mu_0)} &= \lim_{\mu \to \mu_0} \left(1 - \frac{\mu}{\mu_0}\right) S(\mu) \\ &= \frac{1}{\mu_1^2 \ldots \mu_n^2} \frac{P(\mu_0)}{W(\mu_0)}\, s(\mu_0)\,, \end{aligned}\right\} \tag{32}$$

and

$$\left.\begin{aligned} \gamma e^{-\tau_1/\mu_0} = \frac{e^{-\tau_1/\mu_0}}{\mu_1^2 \ldots \mu_n^2} \frac{P(\mu_0) P(-\mu_0)}{W(\mu_0)} &= \lim_{\mu \to -\mu_0} \left(1 + \frac{\mu}{\mu_0}\right) T(\mu) \\ &= \frac{1}{\mu_1^2 \ldots \mu_n^2} \frac{P(-\mu_0)}{W(\mu_0)}\, t(-\mu_0)\,. \end{aligned}\right\} \tag{33}$$

[10] In eqs. (30) and (31) the factor $1/\mu_1^2 \ldots \mu_n^2$ is introduced for reasons of convenience (see eqs. [32] and [33] below).

Hence

$$s(\mu_0) = P(-\mu_0), \tag{34}$$

and

$$t(-\mu_0) = e^{-\tau_1/\mu_0} P(\mu_0). \tag{35}$$

We next observe that, since (cf. eqs. [8] and [9])

$$L_a = \lim_{\mu \to 1/k_a} (1 - k_a\mu)\, S(\mu) \qquad (a = \pm 1, \ldots, \pm n), \tag{36}$$

and

$$L_a e^{-k_a\tau_1} = \lim_{\mu \to -1/k_a} (1 + k_a\mu)\, T(\mu) \qquad (a = \pm 1, \ldots, \pm n), \tag{37}$$

we must have

$$L_a = \frac{1}{\mu_1^2 \ldots \mu_n^2} \frac{P(1/k_a)}{W_a(1/k_a)(1 - 1/k_a\mu_0)}\, s(1/k_a) \qquad (a = \pm 1, \ldots, \pm n) \tag{38}$$

and (cf. eq. [28])

$$L_a e^{-k_a\tau_1} = \frac{1}{\mu_1^2 \ldots \mu_n^2} \frac{P(-1/k_a)}{W_a(1/k_a)(1 - 1/k_a\mu_0)}\, t(-1/k_a) \qquad (a = \pm 1, \ldots, \pm n). \tag{39}$$

Comparing equations (38) and (39), we conclude that

$$s(1/k_a) = e^{k_a\tau_1} \frac{P(-1/k_a)}{P(+1/k_a)}\, t(-1/k_a) \qquad (a = \pm 1, \ldots, \pm n). \tag{40}$$

Re-writing this equation separately for the positive and the negative values of a, we have

$$s(1/k_a) = e^{k_a\tau_1} \frac{P(-1/k_a)}{P(+1/k_a)}\, t(-1/k_a) \qquad (a = 1, \ldots, n) \tag{41}$$

and

$$t(1/k_a) = e^{k_a\tau_1} \frac{P(-1/k_a)}{P(+1/k_a)}\, s(-1/k_a) \qquad (a = 1, \ldots, n). \tag{42}$$

An immediate consequence of equations (41) and (42) is

$$s(1/k_a)\, s(-1/k_a) = t(1/k_a)\, t(-1/k_a) \qquad (a = \pm 1, \ldots, \pm n). \tag{43}$$

From this equation it follows that

$$s(\mu)\, s(-\mu) - t(\mu)\, t(-\mu) \equiv \text{constant}\; W(\mu), \tag{44}$$

since the quantity on the left-hand side is a polynomial of degree $2n$ in μ and vanishes for $\mu = \pm 1/k_a (a = 1, \ldots, n)$.

Next, writing

$$F(\mu) = s(\mu) + t(\mu) \qquad \text{and} \qquad G(\mu) = s(\mu) - t(\mu), \tag{45}$$

we find, from equations (41) and (42),

$$F(1/k_a) = + e^{k_a\tau_1} \frac{P(-1/k_a)}{P(+1/k_a)}\, F(-1/k_a) \qquad (a = 1, \ldots, n) \tag{46}$$

and

$$G(1/k_a) = - e^{k_a\tau_1} \frac{P(-1/k_a)}{P(+1/k_a)}\, G(-1/k_a) \qquad (a = 1, \ldots, n). \tag{47}$$

In § 5 we shall show how equations (46) and (47), together with equations (34) and (35), just suffice to determine the polynomials $F(\mu)$ and $G(\mu)$ uniquely. The problem, as we shall see, is essentially one in the theory of interpolation.

A more symmetrical way of writing equations (46) and (47) is

$$F(1/k_a) = +\lambda_a F(-1/k_a) \qquad (a = 1, \ldots, n) \quad (48)$$

and

$$G(1/k_a) = -\lambda_a G(-1/k_a) \qquad (a = 1, \ldots, n), \quad (49)$$

where

$$\lambda_a = e^{k_a \tau_1} \frac{P(-1/k_a)}{P(+1/k_a)}. \quad (50)$$

4. *The solution of the basic mathematical problem.*—The mathematical problem to which we reduced the solution of $S(\mu)$ and $T(\mu)$ in § 3 can be formulated as follows:

To determine two polynomials $\mathrm{F}(\mu)$ *and* $\mathrm{G}(\mu)$ *of degree* n *in* μ *such that*

$$F(x_a) = +\lambda_a F(-x_a) \qquad (a = 1, \ldots, n), \quad (51)$$

and

$$G(x_a) = -\lambda_a G(-x_a) \qquad (a = 1, \ldots, n), \quad (52)$$

where x_a, $a = 1, \ldots, \mathrm{n}$ *are* n *distinct values of the argument and* λ_a, $a = 1, \ldots, \mathrm{n}$, *are* n *assigned numbers, all different from one another.*

As we have already remarked, this problem is essentially one in the theory of interpolation. It does not, however, seem to have been considered in literature before. But it will appear that the problem is closely associated with the method of solution, in a finite approximation, of a class of simultaneous pairs of functional equations of which equations (119) and (120) of Paper XVII are typical. The problem would therefore appear to merit a closer investigation than we can afford in this paper. We shall, however, give explicit solutions for $F(\mu)$ and $G(\mu)$ which satisfy the required conditions.

First, it may be noted that $F(\mu)$ and $G(\mu)$ are related by the identity (cf. eq. [44])

$$F(\mu)\,G(-\mu) + F(-\mu)\,G(\mu) \equiv \text{constant} \prod_{a=1}^{n} (x_a^2 - \mu^2), \quad (53)$$

since the quantity on the right-hand side is a polynomial of degree $2n$ in μ and vanishes for $\mu = \pm x_a (a = 1, \ldots, n)$.

Next it should be observed that in general *the conditions stated determine* $\mathrm{F}(\mu)$ *and* $\mathrm{G}(\mu)$ *uniquely, apart from a constant factor of proportionality.* That this is the case can be seen by writing $F(\mu)$ (for example) in the form

$$F(\mu) = \sum_{m=0}^{n} a_m \mu^m \quad (54)$$

and noting that the conditions of the problem (eq. [51]) require that

$$\sum_{m=0}^{n} a_m \left[1 + (-1)^{m+1} \lambda_a\right] x_a^m = 0 \qquad (a = 1, \ldots, n). \quad (55)$$

The $n + 1$ coefficients, $a_m (m = 0, \ldots, n)$, therefore satisfy a system of homogeneous linear equations of order n. Moreover, if the x_a's are all distinct and none of the λ_a's are equal to each other (as we have, indeed, assumed), the rank of the system (55) is also n. Consequently, the coefficients a_m are all uniquely determined apart from a constant

factor of proportionality. The polynomial $F(\mu)$ is therefore also determined apart from a constant factor of proportionality. Similar remarks clearly apply to $G(\mu)$ also.

The arguments of the preceding paragraph further establish that *n is the lowest degree of a polynomial (not identically zero) which will satisfy* n *conditions of the form* (51) *or* (52). On the other hand, polynomials of degree higher than n can be readily constructed in terms of $F(\mu)$ and $G(\mu)$ which will satisfy conditions (51) or (52). For example,

$$a_0F(\mu) + a_1\mu G(\mu), \tag{56}$$

where a_0 and a_1 are two arbitrary constants, is the most general polynomial of degree $(n+1)$ in μ which will satisfy the n conditions (51); for, according to equations (51) and (52),

$$\left.\begin{aligned} a_0F(x_\alpha) + a_1x_\alpha G(x_\alpha) &= a_0\lambda_\alpha F(-x_\alpha) - a_1x_\alpha\lambda_\alpha G(-x_\alpha) \\ &= \lambda_\alpha [a_0F(\mu) + a_1\mu G(\mu)]_{\mu=-x_\alpha} \qquad (\alpha = 1, \ldots, n). \end{aligned}\right\} \tag{57}$$

Similarly,

$$b_0G(\mu) + b_1\mu F(\mu), \tag{58}$$

where b_0 and b_1 are two arbitrary constants, is the most general polynomial of degree $(n+1)$ in μ which will satisfy conditions (52).

The foregoing observations can be readily extended to construct polynomials of any degree higher than n which will satisfy condition (51) or (52). We shall state the result in the form of the following theorem:

Theorem 1.—*The most general polynomials* $\mathrm{F}^{(n+m)}(\mu)$ *and* $\mathrm{G}^{(n+m)}(\mu)$ *of degree* (n + m) *in* μ, (m > 0), *which will satisfy the conditions*

$$F^{(n+m)}(x_\alpha) = +\lambda_\alpha F^{(n+m)}(-x_\alpha) \qquad (\alpha = 1, \ldots, n) \tag{59}$$

and

$$G^{(n+m)}(x_\alpha) = -\lambda_\alpha G^{(n+m)}(-x_\alpha) \qquad (\alpha = 1, \ldots, n), \tag{60}$$

are

$$F^{(n+m)}(\mu) = \sum_{l=0}^{m} a_l\mu^l [\epsilon_{l,\,\mathrm{even}} F(\mu) + \epsilon_{l,\,\mathrm{odd}} G(\mu)] \tag{61}$$

and

$$G^{(n+m)}(\mu) = \sum_{l=0}^{m} b_l\mu^l [\epsilon_{l,\,\mathrm{odd}} F(\mu) + \epsilon_{l,\,\mathrm{even}} G(\mu)], \tag{62}$$

where $\mathrm{a_l}$ *and* $\mathrm{b_l}(\mathrm{l} = 0, \ldots, \mathrm{n})$ *are arbitrary constants and*

$$\left.\begin{aligned} \epsilon_{l,\,\mathrm{even}} &= 1 \text{ if } l \text{ is even} \\ &= 0 \text{ if } l \text{ is odd} \end{aligned}\right\} \text{ and } \left.\begin{aligned} \epsilon_{l,\,\mathrm{odd}} &= 1 \text{ if } l \text{ is odd} \\ &= 0 \text{ if } l \text{ is even} \end{aligned}\right\}, \tag{63}$$

and $\mathrm{F}(\mu)$ *and* $\mathrm{G}(\mu)$ *are polynomials of degree* n *in* μ *which satisfy the same conditions as* $\mathrm{F}^{(n+m)}(\mu)$ *and* $\mathrm{G}^{(n+m)}(\mu)$, *respectively.*

This theorem suggests that *the polynomials* $\mathrm{F}(\mu)$ *and* $\mathrm{G}(\mu)$ *can be constructed by a process of induction;* for, if polynomials $F^{(n-1)}(\mu)$ and $G^{(n-1)}(\mu)$ of degree $(n-1)$ in μ which satisfy the $(n-1)$ conditions

$$F^{(n-1)}(x_\alpha) = +\lambda_\alpha F^{(n-1)}(-x_\alpha) \qquad (\alpha = 1, \ldots, n-1) \tag{64}$$

and

$$G^{(n-1)}(x_\alpha) = -\lambda_\alpha G^{(n-1)}(-x_\alpha) \qquad (\alpha = 1, \ldots, n-1) \tag{65}$$

are assumed known, then polynomials $F^{(n)}(\mu)$ and $G^{(n)}(\mu)$ of one higher degree satisfying conditions (51) and (52) appropriate to polynomials of degree n can be constructed. Thus, according to theorem 1,

$$F^{(n)}(\mu) = F^{(n-1)}(\mu) + a_1 \mu G^{(n-1)}(\mu), \tag{66}$$

where a_1 is an arbitrary constant, will satisfy all the conditions (64) that are satisfied by $F^{(n-1)}(\mu)$. We therefore need to satisfy only the one additional condition,

$$F^{(n)}(x_n) = \lambda_n F^{(n)}(-x_n). \tag{67}$$

This condition can be used to determine a_1. In this manner we find that, with the choice of

$$a_1 = -\frac{F^{(n-1)}(x_n) - \lambda_n F^{(n-1)}(-x_n)}{x_n [G^{(n-1)}(x_n) + \lambda_n G^{(n-1)}(-x_n)]}, \tag{68}$$

$F^{(n)}(\mu)$ defined as in equation (66) will satisfy all the required conditions. Similarly,

$$G^{(n)}(\mu) = G^{(n-1)}(\mu) + b_1 \mu F^{(n-1)}(\mu), \tag{69}$$

where

$$b_1 = -\frac{G^{(n-1)}(x_n) + \lambda_n G^{(n-1)}(-x_n)}{x_n [F^{(n-1)}(x_n) - \lambda_n F^{(n-1)}(-x_n)]}, \tag{70}$$

will satisfy the n conditions (52). Thus polynomials of degree n satisfying the required number of conditions can be constructed if polynomials of one lower degree, each satisfying one less condition, are assumed known. On the other hand,

$$F^{(1)}(\mu) = (x_1 - \mu) + \lambda_1 (x_1 + \mu) \tag{71}$$

and

$$G^{(1)}(\mu) = (x_1 - \mu) - \lambda_1 (x_1 + \mu) \tag{72}$$

clearly satisfy the conditions appropriate to polynomials of degree 1. With this we have established that the solution to our problem can, in fact, be found by a process of induction.

While the construction by induction which we have outlined above solves our problem in principle, it is still unsatisfactory, in that the solution obtained by following the construction literally will be excessively complicated. This apparent complexity must, in part, be attributed to the fact that the manner of construction destroys the essential symmetry of the problem in the x_a's and the λ_a's. It would therefore seem that the construction of the polynomials $F(\mu)$ and $G(\mu)$ by a straightforward process of induction is not a significant approach to the problem. The method was therefore abandoned; and the somewhat indirect method that we shall now describe has at least the merit of providing explicit formulae for the functions $F(\mu)$ and $G(\mu)$ which preserve the symmetries of the problem.

From the form of the solution for the case $n = 2$, it appeared that $F(\mu)$ and $G(\mu)$ must be expressible as linear combinations of the 2^n polynomials of the form

$$\prod_{a=1}^{n} (x_a \pm \mu), \tag{73}$$

where in each of the n factors we have either a plus or a minus sign in the parenthesis. Moreover, after some consideration, it also appeared that the coefficient of the term

$$\prod_{i=1}^{l} (x_{r_i} + \mu) \prod_{m=1}^{n-l} (x_{s_m} - \mu), \tag{74}$$

where $r_1, \ldots, r_l$ and $s_1, \ldots, s_{n-l}$ are selections of l, respectively $n-l$, distinct integers from the set $(1, 2, \ldots, n)$, must be

$$\pm \lambda_{r_1} \ldots \lambda_{r_l} \frac{\prod_{m=1}^{n-l} \prod_{i=1}^{l} (x_{s_m} + x_{r_i})}{\prod_{m=1}^{n-l} \prod_{i=1}^{l} (x_{s_m} - x_{r_i})}. \tag{75}$$

But the decision regarding the sign turned out to be a rather more delicate matter. We shall, therefore, describe the method by which the decision was reached, as it will establish at the same time that the expression which we shall obtain does represent the solution to our problem.

According to our remarks in the preceding paragraph, we shall write

$$\left.\begin{aligned} F(\mu) = \sum_{2^n \text{ terms}} \epsilon_{r_1 \ldots r_l} \lambda_{r_1} \ldots \lambda_{r_l} \\ \times \frac{\prod_{m=1}^{n-l} \prod_{i=1}^{l} (x_{s_m} + x_{r_i})}{\prod_{m=1}^{n-l} \prod_{i=1}^{l} (x_{s_m} - x_{r_i})} \prod_{i=1}^{l} (x_{r_i} + \mu) \prod_{m=1}^{n-l} (x_{s_m} - \mu), \end{aligned}\right\} \tag{76}$$

where

$$\epsilon^2_{r_1 \ldots r_l} = 1 \tag{77}$$

but is unspecified, otherwise, for the present.

It should be particularly noted that, in the summation on the right-hand side of equation (76), terms with the various factors $\lambda_{r_1} \ldots \lambda_{r_l}$ occur just exactly once.

Now if $F(\mu)$, as given by equation (76), represents a polynomial which satisfies the conditions of our problem, then we must have

$$F(x_{r_j}) = \lambda_{r_j} F(-x_{r_j}). \tag{78}$$

According to equation (76), in $F(x_{r_j})$, there is *one and only one term* which occurs with the factor

$$\lambda_{r_1} \ldots \lambda_{r_j} \ldots \lambda_{r_l}, \tag{79}$$

and this arises, in fact, from the term

$$\left.\begin{aligned} \epsilon_{r_1 \ldots r_j \ldots r_l} \lambda_{r_1} \ldots \lambda_{r_j} \ldots \lambda_{r_l} \frac{\prod_{m=1}^{n-l} \prod_{i=1}^{l} (x_{s_m} + x_{r_i})}{\prod_{m=1}^{n-l} \prod_{i=1}^{l} (x_{s_m} - x_{r_i})} \\ \times \prod_{i=1}^{l} (x_{r_i} + \mu) \prod_{m=1}^{n-l} (x_{s_m} - \mu), \end{aligned}\right\} \tag{80}$$

on the right-hand side of equation (76). The validity of equation (78) therefore requires that the term in $F(x_{r_j})$ arising from equation (80) must cancel the term in $F(-x_{r_j})$ which occurs with the factor

$$\lambda_{r_1} \ldots . \lambda_{r_{j-1}} \lambda_{r_{j+1}} \ldots . \lambda_{r_l} ; \tag{81}$$

and the only term on the right-hand side of equation (76) which occurs with this factor is

$$\left.\begin{aligned} &\epsilon_{r_1 \ldots . r_{j-1} r_{j+1} \ldots . r_l} \lambda_{r_1} \ldots . \lambda_{r_{j-1}} \lambda_{r_{j+1}} \ldots . \lambda_{r_l} \\ &\times \frac{\prod_{m=1}^{n-l} \prod_{\substack{i=1 \\ i \neq j}}^{l} (x_{s_m} + x_{r_i}) \prod_{\substack{i=1 \\ i \neq j}}^{l} (x_{r_j} + x_{r_i})}{\prod_{m=1}^{n-l} \prod_{\substack{i=1 \\ i \neq j}}^{l} (x_{s_m} - x_{r_i}) \prod_{\substack{i=1 \\ i \neq j}}^{l} (x_{r_j} - x_{r_i})} \prod_{\substack{i=1 \\ i \neq j}}^{l} (x_{r_i} + \mu) \prod_{m=1}^{n-l} (x_{s_m} - \mu)(x_{r_j} - \mu). \end{aligned}\right\} \tag{82}$$

Putting $\mu = x_{r_j}$ in equation (80) and $\mu = -x_{r_j}$ in equation (82), we have, respectively,

$$\epsilon_{r_1 \ldots . r_j \ldots . r_l} \lambda_{r_1} \ldots . \lambda_{r_j} \ldots . \lambda_{r_l} \frac{\prod_{m=1}^{n-l} \prod_{i=1}^{l} (x_{s_m} + x_{r_i})}{\prod_{m=1}^{n-l} \prod_{\substack{i=1 \\ i \neq j}}^{l} (x_{s_m} - x_{r_i})} \prod_{i=1}^{l} (x_{r_i} + x_{r_j}) \tag{83}$$

and

$$\left.\begin{aligned} &\epsilon_{r_1 \ldots . r_{j-1} r_{j+1} \ldots . r_l} \lambda_{r_1} \ldots . \lambda_{r_{j-1}} \lambda_{r_{j+1}} \ldots . \lambda_{r_l} \\ &\times \frac{\prod_{m=1}^{n-l} \prod_{\substack{i=1 \\ i \neq j}}^{l} (x_{s_m} + x_{r_i}) \prod_{\substack{i=1 \\ i \neq j}}^{l} (x_{r_j} + x_{r_i})}{\prod_{m=1}^{n-l} \prod_{\substack{i=1 \\ i \neq j}}^{l} (x_{s_m} - x_{r_i}) \prod_{\substack{i=1 \\ i \neq j}}^{l} (x_{r_j} - x_{r_i})} \prod_{\substack{i=1 \\ i \neq j}}^{l} (x_{r_i} - x_{r_j}) \prod_{m=1}^{n-l} (x_{s_m} + x_{r_j})(x_{r_j} + x_{r_j}) \\ &= \epsilon_{r_1 \ldots . r_{j-1} r_{j+1} \ldots . r_l} \lambda_{r_1} \ldots . \lambda_{r_{j-1}} \lambda_{r_{j+1}} \ldots . \lambda_{r_l} (-1)^{l-1} \\ &\times \frac{\prod_{m=1}^{n-l} \prod_{i=1}^{l} (x_{s_m} + x_{r_i})}{\prod_{m=1}^{n-l} \prod_{\substack{i=1 \\ i \neq j}}^{l} (x_{s_m} - x_{r_i})} \prod_{i=1}^{l} (x_{r_i} + x_{r_j}). \end{aligned}\right\} \tag{84}$$

Comparing (83) and (84), we observe that the validity of equation (78) requires only that

$$\epsilon_{r_1 \ldots . r_l} = \epsilon_{r_1 \ldots . r_{j-1} r_{j+1} \ldots . r_l} (-1)^{l-1} . \tag{85}$$

Hence,

$$\epsilon_{r_1 \ldots . r_l} = \epsilon_l = (-1)^{l-1} \epsilon_{l-1} . \tag{86}$$

Letting $\epsilon_n = 1$, we conclude from equation (86) that

$$\epsilon_n = +1 , \quad \epsilon_{n-1} = (-1)^{n-1} , \quad \epsilon_{n-2} = -1 , \quad \epsilon_{n-3} = (-1)^n , \quad \epsilon_{n-4} = +1 , \text{ etc.} \tag{87}$$

The ϵ's which occur in equation (76) can therefore be arranged in a sequence which we shall denote by $\epsilon_l^{(e)}$. With this choice of the ϵ's, equation (77) does, in fact, represent a solution for $F(\mu)$. (Any constant multiple of $F(\mu)$ will, of course, also be a solution.)

The solution for $G(\mu)$ can be constructed along similar lines. Thus $G(\mu)$ is also a linear combination of the 2^n polynomials (73), with, in fact, the same coefficients as $F(\mu)$ except for the ϵ-factor. And it can be verified that again ϵ depends only on the number of factors, l, in (73) which occurs with the positive sign in the parenthesis. However, in view of the minus sign in the conditions (52), we must now require that (cf. eq. [86])

$$\epsilon_l = \epsilon_{l-1} (-1)^l . \tag{88}$$

The ϵ's in the expansion for $G(\mu)$ therefore form the sequence

$$\epsilon_n = +1 . \quad \epsilon_{n-1} = (-1)^n , \quad \epsilon_{n-2} = -1 , \quad \epsilon_{n-3} = (-1)^{n-1} . \quad \epsilon_{n-4} = +1 , \text{ etc.,} \tag{89}$$

which we shall denote by $\epsilon_l^{(o)}$. We have thus established the following basic theorem:

Theorem 2.—The polynomials

$$F(\mu) = \sum_{2^n \text{ terms}} \epsilon_l^{(e)} \frac{\prod_{m=1}^{n-l} \prod_{i=1}^{l} (x_{s_m} + x_{r_i})}{\prod_{m=1}^{n-l} \prod_{i=1}^{l} (x_{s_m} - x_{r_i})} \prod_{i=1}^{l} \lambda_{r_i} (x_{r_i} + \mu) \prod_{m=1}^{n-l} (x_{s_m} - \mu) \tag{90}$$

and

$$G(\mu) = \sum_{2^n \text{ terms}} \epsilon_l^{(o)} \frac{\prod_{m=1}^{n-l} \prod_{i=1}^{l} (x_{s_m} + x_{r_i})}{\prod_{m=1}^{n-l} \prod_{i=1}^{l} (x_{s_m} - x_{r_i})} \prod_{i=1}^{l} \lambda_{r_i} (x_{r_i} + \mu) \prod_{m=1}^{n-l} (x_{s_m} - \mu) , \tag{91}$$

where $\epsilon_l^{(e)}$ and $\epsilon_l^{(o)}$ denote the sequences

$$\epsilon_l^{(e)} = +1 , \ (-1)^{n-1} , \ -1 , \ (-1)^n , \ +1 , \ (-1)^{n-1} , \ -1 , \ (-1)^n , \ldots . , \tag{92}$$

and

$$\epsilon_l^{(o)} = +1 , \ (-1)^n , \ -1 , \ (-1)^{n-1} , \ +1 , \ (-1)^n , \ -1 , \ (-1)^{n-1} , \ldots . , \tag{93}$$

satisfy the conditions

$$F(x_a) = \lambda_a F(-x_a) \quad \text{and} \quad G(x_a) = -\lambda_a G(-x_a) \qquad (a = 1 , \ldots . , n) , \tag{94}$$

where x_α, $\alpha = 1, \ldots, n$, *are* n *distinct values of the argument and* λ_α, $\alpha = 1, \ldots, n$, *are* n *assigned numbers all different from one another. Any other polynomial of degree n which satisfies either of these conditions must be a simple numerical multiple of* $F(\mu)$ *or* $G(\mu)$ *as defined.*

By writing

$$x_\alpha = \frac{1}{k_\alpha} \qquad (\alpha = 1, \ldots, n), \quad (95)$$

we can express the solutions (90) and (91) for $F(\mu)$ and $G(\mu)$ alternatively in the forms

$$F(\mu) = \sum_{2^n \text{ terms}} \epsilon_l^{(e)} \frac{\prod_{i=1}^{l}\prod_{m=1}^{n-l}(k_{r_i}+k_{s_m})}{\prod_{i=1}^{l}\prod_{m=1}^{n-l}(k_{r_i}-k_{s_m})} \prod_{i=1}^{l}(1+k_{r_i}\mu) \prod_{m=1}^{n-l}\frac{1}{\lambda_{s_m}}(1-k_{s_m}\mu) \quad (96)$$

and

$$G(\mu) = \sum_{2^n \text{ terms}} \epsilon_l^{(o)} \frac{\prod_{i=1}^{l}\prod_{m=1}^{n-l}(k_{r_i}+k_{s_m})}{\prod_{i=1}^{l}\prod_{m=1}^{n-l}(k_{r_i}-k_{s_m})} \prod_{i=1}^{l}(1+k_{r_i}\mu) \prod_{m=1}^{n-l}\frac{1}{\lambda_{s_m}}(1-k_{s_m}\mu). \quad (97)$$

Now, examining the sequences (92) and (93), we observe that the terms n, $n-2$, etc., agree, while the terms $n-1$, $n-3$, etc., are of opposite signs. We can, therefore, express $F(\mu)$ and $G(\mu)$ in the forms

$$F(\mu) = C_0(\mu) + C_1(\mu) \quad (98)$$

and

$$G(\mu) = C_0(\mu) - C_1(\mu), \quad (99)$$

where

$$C_0(\mu) = \sum_{2^{n-1} \text{ terms}}^{l=n, n-2, \ldots} \epsilon_l^{(0)} \frac{\prod_{i=1}^{l}\prod_{m=1}^{n-l}(k_{r_i}+k_{s_m})}{\prod_{i=1}^{l}\prod_{m=1}^{n-l}(k_{r_i}-k_{s_m})} \prod_{i=1}^{l}(1+k_{r_i}\mu) \prod_{m=1}^{n-l}\frac{1}{\lambda_{s_m}}(1-k_{s_m}\mu) \quad (100)$$

and

$$C_1(\mu) = (-1)^{n-1} \sum_{2^{n-1} \text{ term}}^{l=n-1, n-3, \ldots} \epsilon_l^{(1)} \frac{\prod_{i=1}^{l}\prod_{m=1}^{n-l}(k_{r_i}+k_{s_m})}{\prod_{i=1}^{l}\prod_{m=1}^{n-l}(k_{r_i}-k_{s_m})} \prod_{i=1}^{l}(1+k_{r_i}\mu) \prod_{m=1}^{n-l}\frac{1}{\lambda_{s_m}}(1-k_{s_m}\mu), \quad (101)$$

where

$$\left.\begin{aligned} \epsilon_l^{(0)} &= +1 \text{ for integers of the form } n-4l \\ &= -1 \text{ for integers of the form } n-4l-2 \\ &= 0 \text{ otherwise} \end{aligned}\right\} \quad (102)$$

and

$$\left.\begin{aligned}\epsilon_l^{(1)} &= +1 \text{ for integers of the form } n-4l-1\\ &= -1 \text{ for integers of the form } n-4l-3\\ &= 0 \text{ otherwise}\end{aligned}\right\}\ . \qquad (103)$$

In our future work we shall adopt equations (96)–(103) as our standard definitions of the various functions, and it will always have to be assumed that functions defined in this manner are meant unless something explicitly to the contrary is stated.

Finally, some properties of the functions $C_0(\mu)$ and $C_1(\mu)$ may be noted:

By virtue of equations (98) and (99), the identity (53) between $F(\mu)$ and $G(\mu)$ becomes, in our present notation (cf. eq. [25])

$$\left.\begin{aligned}C_0(\mu)\,C_0(-\mu)\,-C_1(\mu)\,C_1(-\mu) &= \text{constant}\prod_{\alpha=1}^{n}(1-k_\alpha^2\mu^2)\\ &= \text{constant}\ W(\mu)\,.\end{aligned}\right\} \qquad (104)$$

Since $W(0) = 1$, we can re-write equation (104) in the form

$$C_0(\mu)\,C_0(-\mu)\,-C_1(\mu)\,C_1(-\mu) = [C_0^2(0)\,-C_1^2(0)\,]\,W(\mu)\,, \qquad (105)$$

a relation which we shall find very useful in our further work.

Again, according to equations (51) and (52),

$$F(x_\alpha)\,+G(x_\alpha) = \lambda_\alpha\,[F(-x_\alpha)\,-G(-x_\alpha)\,]\,, \qquad (106)$$

and

$$F(x_\alpha)\,-G(x_\alpha) = \lambda_\alpha\,[F(-x_\alpha)\,+G(-x_\alpha)\,]\,. \qquad (107)$$

Expressing F and G as in equations (98) and (99), we find that the foregoing equations are equivalent, in our present notation, to

$$C_0(1/k_\alpha) = \lambda_\alpha C_1(-1/k_\alpha) \qquad (\alpha = 1\,,\ldots.\,,n) \qquad (108)$$

and

$$C_1(1/k_\alpha) = \lambda_\alpha C_0(-1/k_\alpha) \qquad (\alpha = 1\,,\ldots.\,,n)\,. \qquad (109)$$

Equations (108) and (109) will be formally equivalent to each other if (again formally!)

$$\lambda_\alpha = \frac{1}{\lambda_{-\alpha}}\,. \qquad (110)$$

For λ_α defined as in equation (50), this is *actually* the case.

5. *Completion of the solutions for* s(μ) *and* t(μ).—Returning, now, to the solution for $s(\mu)$ and $t(\mu)$ at the point where we left it in § 3, we conclude that $s(\mu) + t(\mu)$ and $s(\mu) - t(\mu)$ must be proportional, respectively, to $F(\mu)$ and $G(\mu)$ as we have defined them in equations (96) and (97), with λ_α having the particular value given by equation (50). Expressing $F(\mu)$ and $G(\mu)$ in terms of $C_0(\mu)$ and $C_1(\mu)$, as in equations (100) and (101), we can therefore write

$$s(\mu) = q_0C_0(\mu) + q_1C_1(\mu) \qquad (111)$$

and

$$t(\mu) = q_1C_0(\mu) + q_0C_1(\mu)\,, \qquad (112)$$

where q_0 and q_1 are two constants. To determine these constants we make use of equations (34) and (35), which require that

$$s(\mu_0) = q_0 C_0(\mu_0) + q_1 C_1(\mu_0) = P(-\mu_0) \tag{113}$$

and

$$t(-\mu_0) = q_0 C_1(-\mu_0) + q_1 C_0(-\mu_0) = P(\mu_0)\, e^{-\tau_1/\mu_0}. \tag{114}$$

Solving these equations for q_0 and q_1, we find

$$q_0 = \frac{P(-\mu_0)\, C_0(-\mu_0) - e^{-\tau_1/\mu_0} P(\mu_0)\, C_1(\mu_0)}{C_0(\mu_0)\, C_0(-\mu_0) - C_1(\mu_0)\, C_1(-\mu_0)} \tag{115}$$

and

$$q_1 = \frac{e^{-\tau_1/\mu_0} P(\mu_0)\, C_0(\mu_0) - P(-\mu_0)\, C_1(-\mu_0)}{C_0(\mu_0)\, C_0(-\mu_0) - C_1(\mu_0)\, C_1(-\mu_0)}. \tag{116}$$

The denominator in equations (115) and (116) can be simplified by using equation (105). We thus find that

$$q_0 = \frac{1}{[C_0^2(0) - C_1^2(0)]\, W(\mu_0)} [P(-\mu_0)\, C_0(-\mu_0) - e^{-\tau_1/\mu_0} P(\mu_0)\, C_1(\mu_0)] \tag{117}$$

and

$$q_1 = \frac{1}{[C_0^2(0) - C_1^2(0)]\, W(\mu_0)} [e^{-\tau_1/\mu_0} P(\mu_0)\, C_0(\mu_0) - P(-\mu_0)\, C_1(-\mu_0)]. \tag{118}$$

With this determination of the constants q_0 and q_1, we have completed the formal solution of our problem.

6. *The solution for the reflected and the transmitted radiations.*—With $s(\mu)$ and $t(\mu)$ given by equations (111) and (112), equations (30) and (31) for $S(\mu)$ and $T(\mu)$ take the forms

$$S(\mu) = \frac{1}{\mu_1^2 \ldots \mu_n^2} \frac{P(\mu)}{W(\mu)} \frac{\mu_0}{\mu_0 - \mu} [q_0 C_0(\mu) + q_1 C_1(\mu)] \tag{119}$$

and

$$T(\mu) = \frac{1}{\mu_1^2 \ldots \mu_n^2} \frac{P(\mu)}{W(\mu)} \frac{\mu_0}{\mu_0 + \mu} [q_1 C_0(\mu) + q_0 C_1(\mu)]. \tag{120}$$

Substituting for $S(\mu)$ and $T(\mu)$ from the foregoing equations in equations (22) and (23), we obtain, after some minor rearranging of the terms, the following expressions for the reflected and the transmitted intensities:

$$\left.\begin{aligned} I(0, \mu) = \frac{1}{4} \frac{\varpi_0 F}{\mu_1^2 \ldots \mu_n^2} \frac{1}{W(\mu)} [\, & q_0 \{P(-\mu)\, C_0(-\mu) - e^{-\tau_1/\mu} P(\mu)\, C_1(\mu)\} \\ & - q_1 \{e^{-\tau_1/\mu} P(\mu)\, C_0(\mu) - P(-\mu)\, C_1(-\mu)\}] \frac{\mu_0}{\mu_0 + \mu} \end{aligned}\right\} \tag{121}$$

and

$$\left.\begin{aligned} I(\tau_1, -\mu) = \frac{1}{4} \frac{\varpi_0 F}{\mu_1^2 \ldots \mu_n^2} \frac{1}{W(\mu)} [\, & q_1 \{P(-\mu) C_0(-\mu) - e^{-\tau_1/\mu} P(\mu) C_1(\mu)\} \\ & - q_0 \{e^{-\tau_1/\mu} P(\mu) C_0(\mu) - P(-\mu) C_1(-\mu)\}] \frac{\mu_0}{\mu_0 - \mu}. \end{aligned}\right\} \tag{122}$$

Substituting, next, for q_0 and q_1 according to equations (117) and (118), we have

$$I(0,\mu)=\frac{1}{4}\frac{\varpi_0 F}{\mu_1^2\ldots.\,\mu_n^2}\frac{1}{[C_0^2(0)-C_1^2(0)]}\frac{1}{W(\mu)W(\mu_0)}\frac{\mu_0}{\mu_0+\mu}$$
$$\times[\{P(-\mu)C_0(-\mu)-e^{-\tau_1/\mu}P(\mu)C_1(\mu)\}\{P(-\mu_0)C_0(-\mu_0)-e^{-\tau_1/\mu_0}P(\mu_0)C_1(\mu_0)\}$$
$$-\{e^{-\tau_1/\mu}P(\mu)C_0(\mu)-P(-\mu)C_1(-\mu)\}\{e^{-\tau_1/\mu_0}P(\mu_0)C_0(\mu_0)-P(-\mu_0)C_1(-\mu_0)\}] \quad (123)$$

and

$$I(\tau_1,-\mu)=\frac{1}{4}\frac{\varpi_0 F}{\mu_1^2\ldots.\,\mu_n^2}\frac{1}{[C_0^2(0)-C_1^2(0)]}\frac{1}{W(\mu)W(\mu_0)}\frac{\mu_0}{\mu_0-\mu}$$
$$\times[\{P(-\mu)C_0(-\mu)-e^{-\tau_1/\mu}P(\mu)C_1(\mu)\}\{e^{-\tau_1/\mu_0}P(\mu_0)C_0(\mu_0)-P(-\mu_0)C_1(-\mu_0)\}$$
$$-\{e^{-\tau_1/\mu}P(\mu)C_0(\mu)-P(-\mu)C_1(-\mu)\}\{P(-\mu_0)C_0(-\mu_0)-e^{-\tau_1/\mu_0}P(\mu_0)C_1(\mu_0)\}]. \quad (124)$$

Now let

$$X(\mu)=\frac{(-1)^n}{\mu_1\ldots.\,\mu_n}\frac{1}{[C_0^2(0)-C_1^2(0)]^{\frac{1}{2}}}\frac{1}{W(\mu)}[P(-\mu)C_0(-\mu)-e^{-\tau_1/\mu}P(\mu)C_1(\mu)] \quad (125)$$

and

$$Y(\mu)=\frac{(-1)^n}{\mu_1\ldots.\,\mu_n}\frac{1}{[C_0^2(0)-C_1^2(0)]^{\frac{1}{2}}}\frac{1}{W(\mu)}[e^{-\tau_1/\mu}P(\mu)C_0(\mu)-P(-\mu)C_1(-\mu)]. \quad (126)$$

It will appear that functions $X(\mu)$ and $Y(\mu)$, defined in this manner, play the same fundamental role in the theory of atmospheres of finite optical thicknesses as the function $H(\mu)$ did in the theory of semi-infinite atmospheres.

In terms of the functions $X(\mu)$ and $Y(\mu)$, equations (123) and (124) for the reflected and the transmitted intensities take the following simple forms:

$$I(0,\mu)=\tfrac{1}{4}\varpi_0 F\frac{\mu_0}{\mu_0+\mu}[X(\mu)X(\mu_0)-Y(\mu)Y(\mu_0)] \quad (127)$$

and

$$I(\tau_1,-\mu)=\tfrac{1}{4}\varpi_0 F\frac{\mu_0}{\mu_0-\mu}[X(\mu)Y(\mu_0)-Y(\mu)X(\mu_0)]. \quad (128)$$

It will be seen that the solutions for $I(0,\mu)$ and $I(\tau_1,-\mu)$ given by equations (127) and (128) are of exactly the forms required by the functional equations satisfied by the scattering and the transmission functions (Paper XVII, § 6); they further bring into evidence Helmholtz' principle of reciprocity.

Finally, attention should be drawn to the fact that there is nothing in the analysis of the preceding sections which has depended on the k_α's being the roots of the particular characteristic equation (2) except that it has $2n$ roots which occur in pairs (i.e., $k_\alpha=-k_{-\alpha}$). The method of solution and the reduction to the basic problem considered in § 4 has depended only on the single circumstance of the solution for the intensities being of the form given by equations (1) and (3). Conversely, it follows that the expressions for the reflected and the transmitted radiations can always be brought to the forms (127) and (128), provided only that the intensities I_i at the points of the Gaussian division are given by equations of the general form of (1) and (3) and the k_α's are the roots of an equation of the form

$$1=2\sum_{j=1}^{n}\frac{a_j\Psi(\mu_j)}{1-k^2\mu_j^2}, \quad (129)$$

where the characteristic function, $\Psi(\mu)$, is an even polynomial, satisfying the condition

$$\int_0^1 \Psi(\mu)\, d\mu < \tfrac{1}{2}\,. \tag{130}$$ [11]

An obvious corollary of this observation is that for all equations of transfer of the form considered in Paper IX, § 4, the solution for the reflected and the transmitted intensities can be reduced to the forms given by equations (127) and (128), in which the functions $X(\mu)$ and $Y(\mu)$ are defined according to equations (24), (25), (100), (101), (125), and (126).

II. ISOTROPIC SCATTERING WITH UNIT ALBEDO

7. *The reduction for the case* $\varpi_0 = 1$.—The solution for the case of isotropic scattering with unit albedo cannot be obtained by simply letting $\varpi_0 = 1$ in the equations of the preceding sections (§§ 5 and 6); for, in this case, the various functions become indeterminate because two of the characteristic roots become zero. While there can, of course, be no difficulty of principle in properly passing to the limit $\varpi_0 = 1$ with due regard to the indeterminateness we have mentioned, it appears simpler to treat this case separately.

When $\varpi_0 = 1$, the solution for the intensities I_i at the points of the Gaussian division is (cf. Paper VIII)

$$\left.\begin{aligned} I_i = \tfrac{1}{4}F\Big[\sum_{a=-n+1}^{+n-1} \frac{L_a e^{-k_a\tau}}{1+k_a\mu_i} + L_0(\tau+\mu_i) + L_n + \frac{\gamma e^{-\tau/\mu_0}}{1+\mu_i/\mu_0}\Big] \\ (i = \pm 1, \ldots, \pm n)\,, \end{aligned}\right\} \tag{131}$$

where the k_a's ($a = \pm 1, \ldots, \pm n \mp 1$, and $k_{+a} = -k_{-a}$) are the $(2n-2)$ distinct nonvanishing roots of the characteristic equation

$$1 = \sum_{j=1}^{n} \frac{a_j}{1-k^2\mu_j^2} \tag{132}$$

and the L_a's ($a = 0, \pm 1, \ldots, \pm n \mp 1, n$) are the $2n$ constants of integration and

$$\gamma = H(\mu_0)\, H(-\mu_0) = \frac{1}{\mu_1^2 \ldots \mu_n^2} \frac{P(\mu_0)\, P(-\mu_0)}{W(\mu_0)}\,. \tag{133}$$

In terms of the functions

$$S(\mu) = \sum_{a=-n+1}^{+n-1} \frac{L_a}{1-k_a\mu} - L_0\mu + L_n + \frac{\gamma}{1-\mu/\mu_0} \tag{134}$$

and

$$T(\mu) = \sum_{a=-n+1}^{+n-1} \frac{L_a e^{-k_a\tau_1}}{1+k_a\mu} + L_0(\tau_1+\mu) + L_n + \frac{\gamma e^{-\tau_1/\mu_0}}{1+\mu/\mu_0}, \tag{135}$$

the boundary conditions requiring

$$I_{-i} = 0 \text{ at } \tau = 0 \quad \text{and} \quad I_{+i} = 0 \text{ at } \tau = \tau_1 \quad \text{for} \quad i = 1, \ldots, n\,, \tag{136}$$

can be written as

$$S(\mu_i) = T(\mu_i) = 0 \qquad (i = 1, \ldots, n)\,. \tag{137}$$

[11] Notice the exclusion of the equality sign here. This means that we exclude conservative cases from this discussion (see Sec. II below).

And, as in the case $\varpi_0 < 1$ (§ 2), it can be shown that, in this case also, the reflected and the transmitted intensities can be expressed in the forms (cf. eqs. [22] and [23])

$$I(0, \mu) = \tfrac{1}{4}F[S(-\mu) - e^{-\tau_1/\mu}T(\mu)] \tag{138}$$

and

$$I(\tau_1, -\mu) = \tfrac{1}{4}F[T(-\mu) - e^{-\tau_1/\mu}S(\mu)]. \tag{139}$$

Returning to equations (134) and (135), we observe that, since the μ_i's ($i = 1, \ldots, n$) are zeros of $S(\mu)$ and $T(\mu)$, we can write (cf. eqs. [30], [31], and n. 10)

$$S(\mu) = \frac{1}{\mu_1^2 \ldots \mu_n^2} \frac{P(\mu)}{W(\mu)} \frac{1}{1 - \mu/\mu_0} s(\mu) \tag{140}$$

and

$$T(\mu) = \frac{1}{\mu_1^2 \ldots \mu_n^2} \frac{P(\mu)}{W(\mu)} \frac{1}{1 + \mu/\mu_0} t(\mu), \tag{141}$$

where $s(\mu)$ and $t(\mu)$ are polynomials of degree n in μ.

From equations (133)–(135), (140), and (141), it readily follows that (cf. eqs. [32]–[35])

$$s(\mu_0) = P(-\mu_0) \qquad \text{and} \qquad t(-\mu_0) = e^{-\tau_1/\mu_0}P(\mu_0). \tag{142}$$

But we now have only $(2n - 2)$ relations of the form (cf. eq. [40])

$$s(1/k_a) = e^{k_a\tau_1}\frac{P(-1/k_a)}{P(+1/k_a)}t(-1/k_a) \qquad (a = \pm 1, \ldots, \pm n \mp 1). \tag{143}$$

Consequently, $s(\mu) + t(\mu)$ and $s(\mu) - t(\mu)$ satisfy only $(n - 1)$ (instead of n) relations of the forms (46) and (47), respectively. In accordance with theorems 1 and 2 (§ 4), we therefore conclude that, in the present case, $s(\mu) + t(\mu)$ must be a linear combination of $F(\mu)$ and $\mu G(\mu)$ with numerical coefficients, where $F(\mu)$ and $G(\mu)$ are polynomials of degree $n - 1$, defined in the manner of equations (50), (96), and (97) in terms of the $n - 1$ positive nonvanishing roots of equation (132).[12] Similarly, $s(\mu) - t(\mu)$ must be a linear combination of $G(\mu)$ and $\mu F(\mu)$ with numerical coefficients. We can therefore write (cf. eqs. [98] and [99])

$$s(\mu) = (p_0 + q_0\mu)C_0(\mu) + (p_1 - q_1\mu)C_1(\mu) \tag{144}$$

and

$$t(\mu) = (p_1 + q_1\mu)C_0(\mu) + (p_0 - q_0\mu)C_1(\mu), \tag{145}$$

where p_0, q_0, p_1, and q_1 are certain constants. Equations (142) provide two relations between these four constants. Two further relations can be obtained in the following manner:

According to equations (134), (135), (140), and (141), we have

$$\left.\begin{aligned} \frac{1}{\mu_1^2 \ldots \mu_n^2} P(\mu)\, s(\mu) &= \left(1 - \frac{\mu}{\mu_0}\right) W(\mu)\, S(\mu) \\ &= (-1)^{n-1}k_1^2 \ldots k_{n-1}^2 \left[\frac{L_0}{\mu_0}\mu^{2n} - \left(L_0 + \frac{L_n}{\mu_0}\right)\mu^{2n-1} + \ldots\right] \end{aligned}\right\} \tag{146}$$

[12] We shall adopt this convention throughout. It is therefore always to be understood that W, W_a, F, G, C_0, C_1, X, and Y signify the functions defined as in eqs. (25), (26), (50), (96)–(103), (125), and (126) in terms of the positive nonvanishing roots of the particular characteristic equation which is appropriate in the context.

and

$$\left.\begin{aligned}\frac{1}{\mu_1 \ldots \mu_n^2} P(\mu)\, t(\mu) &= \left(1+\frac{\mu}{\mu_0}\right) W(\mu)\, T(\mu) \\ &= (-1)^{n-1} k_1^2 \ldots k_{n-1}^2 \left[\frac{L_0}{\mu_0}\mu^{2n} + \left(L_0 + \frac{L_n}{\mu_0} + \frac{L_0\tau_1}{\mu_0}\right)\mu^{2n-1} + \ldots .\right].\end{aligned}\right\} \quad (147)$$

From equations (146) and (147) it is apparent that the coefficients of μ^n in $s(\mu)$ and $t(\mu)$ are the same. This requires that in equations (144) and (145)

$$q_0 = q_1 = a \text{ (say)} . \quad (148)$$

We can therefore write

$$s(\mu) = (p_0 + a\mu)\, C_0(\mu) + (p_1 - a\mu)\, C_1(\mu) \quad (149)$$

and

$$t(\mu) = (p_1 + a\mu)\, C_0(\mu) + (p_0 - a\mu)\, C_1(\mu) . \quad (150)$$

With the foregoing forms for $s(\mu)$ and $t(\mu)$, it is readily verified that

$$\left.\begin{aligned}P(\mu)\, s(\mu) = \mu^{2n}\{a[c_0^{(n-1)} - c_1^{(n-1)}]\} + \mu^{2n-1}\Big\{a[c_0^{(n-2)} - c_1^{(n-2)}] \\ + p_0 c_0^{(n-1)} + p_1 c_1^{(n-1)} - \Big(\sum_{i=1}^{n}\mu_i\Big) a[c_0^{(n-1)} - c_1^{(n-1)}]\Big\} + \ldots .\end{aligned}\right\} \quad (151)$$

and

$$\left.\begin{aligned}P(\mu)\, t(\mu) = \mu^{2n}\{a[c_0^{(n-1)} - c_1^{(n-1)}]\} + \mu^{2n-1}\Big\{a[c_0^{(n-2)} - c_1^{(n-2)}] \\ + p_1 c_0^{(n-1)} + p_0 c_1^{(n-1)} - \Big(\sum_{i=1}^{n}\mu_i\Big) a[c_0^{(n-1)} - c_1^{(n-1)}]\Big\} + \ldots ,\end{aligned}\right\} \quad (152)$$

where $c_0^{(n-1)}$, $c_0^{(n-2)}$ and $c_1^{(n-1)}$, $c_1^{(n-2)}$ are the coefficients of the highest and the next highest powers of μ in $C_0(\mu)$ and $C_1(\mu)$, respectively.

Comparing equations (146) and (147) with (151) and (152), we conclude that

$$\left.\begin{aligned}\frac{1}{c_0^{(n-1)} - c_1^{(n-1)}}\Big\{c_0^{(n-2)} - c_1^{(n-2)} + \frac{1}{a}[p_0 c_0^{(n-1)} + p_1 c_1^{(n-1)}]\Big\} - \sum_{i=1}^{n}\mu_i \\ = -\left(\mu_0 + \frac{L_n}{L_0}\right)\end{aligned}\right\} \quad (153)$$

and

$$\left.\begin{aligned}\frac{1}{c_0^{(n-1)} - c_1^{(n-1)}}\Big\{c_0^{(n-2)} - c_1^{(n-2)} + \frac{1}{a}[p_1 c_0^{(n-1)} + p_0 c_1^{(n-1)}]\Big\} - \sum_{i=1}^{n}\mu_i \\ = +\left(\mu_0 + \frac{L_n}{L_0} + \tau_1\right).\end{aligned}\right\} \quad (154)$$

Adding equations (153) and (154), we obtain

$$\frac{1}{c_0^{(n-1)} - c_1^{(n-1)}}\Big\{2[c_0^{(n-2)} - c_1^{(n-2)}] + \frac{p_0 + p_1}{a}[c_0^{(n-1)} + c_1^{(n-1)}]\Big\} - 2\sum_{i=1}^{n}\mu_i = \tau_1 . \quad (155)$$

Hence

$$a = Q(p_0 + p_1), \tag{156}$$

where

$$Q = \frac{c_0^{(n-1)} + c_1^{(n-1)}}{\left(\tau_1 + 2\sum_{i=1}^{n} \mu_i\right)[c_0^{(n-1)} - c_1^{(n-1)}] - 2[c_0^{(n-2)} - c_1^{(n-2)}]}. \tag{157}$$

Now, from equations (142), (149), and (150) we have

$$(p_0 + a\mu_0) C_0(\mu_0) + (p_1 - a\mu_0) C_1(\mu_0) = P(-\mu_0) \tag{158}$$

and

$$(p_0 + a\mu_0) C_1(-\mu_0) + (p_1 - a\mu_0) C_0(-\mu_0) = e^{-\tau_1/\mu_0} P(\mu_0). \tag{159}$$

Solving these equations for $(p_0 + a\mu_0)$ and $(p_1 - a\mu_0)$, we have (cf. eqs. [113]–[118])

$$p_0 + a\mu_0 = \frac{1}{[C_0^2(0) - C_1^2(0)]W(\mu_0)}[P(-\mu_0)C_0(-\mu_0) - e^{-\tau_1/\mu_0}P(\mu_0)C_1(\mu_0)] \tag{160}$$

and

$$p_1 - a\mu_0 = \frac{1}{[C_0^2(0) - C_1^2(0)]W(\mu_0)}[e^{-\tau_1/\mu_0}P(\mu_0)C_0(\mu_0) - P(-\mu_0)C_1(-\mu_0)]. \tag{161}$$

And, finally, according to equations (156), (160), and (161)

$$\left.\begin{aligned} a = \frac{Q}{[C_0^2(0) - C_1^2(0)]W(\mu_0)}[&P(-\mu_0)C_0(-\mu_0) - e^{-\tau_1/\mu_0}P(\mu_0)C_1(\mu_0) \\ &+ e^{-\tau_1/\mu_0}P(\mu_0)C_0(\mu_0) - P(-\mu_0)C_1(-\mu_0)]. \end{aligned}\right\} \tag{162}$$

With this determination of the various constants, the solution of the formal problem is completed.

8. *The solution for the reflected and the transmitted radiations.*—The angular distributions of the reflected and the transmitted radiations are given by

$$I(0, \mu) = \frac{1}{4}\frac{F}{\mu_1^2 \cdots \mu_n^2}\frac{1}{W(\mu)}[P(-\mu)\, s(-\mu) - e^{-\tau_1/\mu}P(\mu)\, t(\mu)]\frac{\mu_0}{\mu_0 + \mu} \tag{163}$$

and

$$I(\tau_1, -\mu) = \frac{1}{4}\frac{F}{\mu_1^2 \cdots \mu_n^2}\frac{1}{W(\mu)}[P(-\mu)t(-\mu) - e^{-\tau_1/\mu}P(\mu)\, s(\mu)]\frac{\mu_0}{\mu_0 - \mu}. \tag{164}$$

On the other hand, according to equations (149) and (150),

$$\left.\begin{aligned} &P(-\mu)\, s(-\mu) - e^{-\tau_1/\mu}P(\mu)\, t(\mu) \\ &\quad = (p_0 - a\mu)[P(-\mu)C_0(-\mu) - e^{-\tau_1/\mu}P(\mu)C_1(\mu)] \\ &\qquad - (p_1 + a\mu)[e^{-\tau_1/\mu}P(\mu)C_0(\mu) - P(-\mu)C_1(-\mu)] \\ &\quad = (p_0 + a\mu_0)[P(-\mu)C_0(-\mu) - e^{-\tau_1/\mu}P(\mu)C_1(\mu)] \\ &\qquad - (p_1 - a\mu_0)[e^{-\tau_1/\mu}P(\mu)C_0(\mu) - P(-\mu)C_1(-\mu)] \\ &\qquad - a(\mu_0 + \mu)[P(-\mu)C_0(-\mu) - e^{-\tau_1/\mu}P(\mu)C_1(\mu) \\ &\qquad\qquad + e^{-\tau_1/\mu}P(\mu)C_0(\mu) - P(-\mu)C_1(-\mu)]. \end{aligned}\right\} \tag{165}$$

Similarly,

$$\left.\begin{aligned} P(-\mu)\,t(-\mu) - e^{-\tau_1/\mu}P(\mu)\,s(\mu) &\\ = (p_1 - a\mu_0)\,[P(-\mu)\,C_0(-\mu) - e^{-\tau_1/\mu}P(\mu)\,C_1(\mu)] &\\ - (p_0 + a\mu_0)\,[e^{-\tau_1/\mu}P(\mu)\,C_0(\mu) - P(-\mu)\,C_1(-\mu)] &\\ + a(\mu_0 - \mu)\,[P(-\mu)\,C_0(-\mu) - e^{-\tau_1/\mu}P(\mu)\,C_1(\mu) &\\ + e^{-\tau_1/\mu}P(\mu)\,C_0(\mu) - P(-\mu)\,C_1(-\mu)]. & \end{aligned}\right\} \quad (166)$$

In the foregoing equations we can now substitute for $(p_0 + a\mu_0)$, $(p_1 - a\mu_0)$, and a in accordance with equations (160)–(162). In this manner we find

$$\left.\begin{aligned} I(0,\mu) = \tfrac{1}{4}F\frac{\mu_0}{\mu_0+\mu}\{X(\mu)\,X(\mu_0) - Y(\mu)\,Y(\mu_0) &\\ - Q(\mu_0+\mu)\,[X(\mu) + Y(\mu)]\,[X(\mu_0) + Y(\mu_0)]\} & \end{aligned}\right\} \quad (167)$$

and

$$\left.\begin{aligned} I(\tau_1,-\mu) = \tfrac{1}{4}F\frac{\mu_0}{\mu_0-\mu}\{X(\mu)\,Y(\mu_0) - Y(\mu)\,X(\mu_0) &\\ + Q(\mu_0-\mu)\,[X(\mu) + Y(\mu)]\,[X(\mu_0) + Y(\mu_0)]\}. & \end{aligned}\right\} \quad (168)$$

Equations (167) and (168) can be brought into forms analogous to solutions (127) and (128) for the case $\varpi_0 < 1$, if we introduce the functions

$$\psi(\mu) = X(\mu) - Q\mu\,[X(\mu) + Y(\mu)] \quad (169)$$

and

$$\phi(\mu) = Y(\mu) + Q\mu\,[X(\mu) + Y(\mu)]. \quad (170)$$

In terms of these functions, the angular distributions of the reflected and the transmitted radiations take the required forms:

$$I(0,\mu) = \tfrac{1}{4}F\frac{\mu_0}{\mu_0+\mu}[\psi(\mu)\,\psi(\mu_0) - \phi(\mu)\,\phi(\mu_0)] \quad (171)$$

and

$$I(\tau_1,-\mu) = \tfrac{1}{4}F\frac{\mu_0}{\mu_0-\mu}[\psi(\mu)\,\phi(\mu_0) - \phi(\mu)\,\psi(\mu_0)]. \quad (172)$$

III. SCATTERING IN ACCORDANCE WITH RAYLEIGH'S PHASE FUNCTION

9. *The azimuth independent term. The reduction of the solution.*—In solving the equation of transfer appropriately for the problem of diffuse reflection and transmission by a plane-parallel atmosphere scattering radiation in accordance with Rayleigh's phase function, we must distinguish three terms in the radiation field: an azimuth independent term, a term proportional to $\cos(\varphi - \varphi_0)$, and a term proportional to $\cos 2(\varphi - \varphi_0)$ (cf. Paper IX, eq. [152]). Considering, first, the azimuth independent term, we have the solution (cf. Papers III and IX, Sec. II)

$$\left.\begin{aligned} I_i = \tfrac{3}{32}F\Big[(3-\mu_i^2)\sum_{a=-n+1}^{+n-1}\frac{L_a e^{-k_a\tau}}{1+k_a\mu_i} + L_0(\tau+\mu_i) + L_n &\\ + (3-\mu_i^2)\frac{\gamma e^{-\tau/\mu_0}}{1+\mu_i/\mu_0}\Big] \qquad (i = \pm 1, \ldots, \pm n), & \end{aligned}\right\} \quad (173)$$

where the k_a's ($a = \pm 1, \ldots, \pm n \mp 1$ and $k_{+a} = -k_{-a}$) are the $(2n-2)$ distinct nonvanishing roots of the characteristic equation

$$1 = \frac{3}{8} \sum_{j=1}^{n} \frac{a_j (3 - \mu_j^2)}{1 - k^2 \mu_j^2}, \tag{174}$$

$$\gamma = H(\mu_0)\, H(-\mu_0), \tag{175}$$

and the rest of the symbols have their usual meanings.

In terms of the functions

$$S(\mu) = (3-\mu^2) \sum_{a=-n+1}^{+n-1} \frac{L_a}{1 - k_a \mu} - L_0 \mu + L_n + (3-\mu^2) \frac{\gamma}{1 - \mu/\mu_0} \tag{176}$$

and

$$T(\mu) = (3-\mu^2) \sum_{a=-n+1}^{+n-1} \frac{L_a e^{-k_a \tau_1}}{1 + k_a \mu} + L_0 (\tau_1 + \mu) + L_n + (3-\mu^2) \frac{\gamma e^{-\tau_1/\mu_0}}{1 + \mu/\mu_0}, \tag{177}$$

the boundary conditions determining the constants of integration and the equations governing the reflected and the transmitted radiations can be written in the following forms:

$$S(\mu_i) = T(\mu_i) = 0 \qquad (i = 1, \ldots, n), \tag{178}$$

$$I(0, \mu) = \tfrac{3}{32} F [S(-\mu) - e^{-\tau_1/\mu} T(\mu)], \tag{179}$$

and

$$I(\tau_1, -\mu) = \tfrac{3}{32} F [T(-\mu) - e^{-\tau_1/\mu} S(\mu)]. \tag{180}$$

By virtue of the boundary conditions (eq. [178]), we can write

$$S(\mu) = \frac{1}{\mu_1^2 \ldots \mu_n^2} \frac{P(\mu)}{W(\mu)} \frac{1}{1 - \mu/\mu_0}\, s(\mu) \tag{181}$$

an

$$T(\mu) = \frac{1}{\mu_1^2 \ldots \mu_n^2} \frac{P(\mu)}{W(\mu)} \frac{1}{1 + \mu/\mu_0}\, t(\mu), \tag{182}$$

where $s(\mu)$ and $t(\mu)$ are polynomials of degree n in μ.

From equations (175)–(177), (181), and (182), it now follows that

$$s(\mu_0) = (3 - \mu_0^2) P(-\mu_0) \tag{183}$$

and

$$t(-\mu_0) = (3 - \mu_0^2)\, e^{-\tau_1/\mu_0} P(\mu_0). \tag{184}$$

And again from equations (176), (177), (181), and (182) we have

$$\left(3 - \frac{1}{k_a^2}\right) L_a = \frac{1}{\mu_1^2 \ldots \mu_n^2} \frac{P(+1/k_a)}{W_a(1/k_a)} \frac{1}{1 - 1/k_a \mu_0}\, s(1/k_a) \qquad (a = \pm 1, \ldots, \pm n \mp 1) \tag{185}$$

and

$$\left(3-\frac{1}{k_a^2}\right)L_a\,e^{-k_a\tau_1}=\frac{1}{\mu_1^2\,.\,.\,.\,.\,\mu_n^2}\,\frac{P(-1/k_a)}{W_a(1/k_a)}\,\frac{1}{1-1/k_a\mu_0}\,t(-1/k_a)\qquad(a=\pm 1\,,\,.\,.\,.\,.\,,\pm n\mp 1)\,. \tag{186}$$

We therefore have the $2n-2$ relations

$$s(1/k_a)=e^{k_a\tau_1}\,\frac{P(-1/k_a)}{P(+1/k_a)}\,t(-1/k_a)\qquad(a=\pm 1\,,\,.\,.\,.\,.\,,\pm n\mp 1)\,. \tag{187}$$

Since, however, $s(\mu)$ and $t(\mu)$ are polynomials of degree n in μ, we conclude, in accordance with theorems 1 and 2 (§ 4), that $s(\mu)$ and $t(\mu)$ must be expressible in the forms (cf. eqs. [144] and [145])

$$s(\mu)=(p_0+q_0\mu)\,C_0(\mu)+(p_1-q_1\mu)\,C_1(\mu) \tag{188}$$

and

$$t(\mu)=(p_1+q_1\mu)\,C_0(\mu)+(p_0-q_0\mu)\,C_1(\mu)\,, \tag{189}$$

where p_0, q_0, p_1, and q_1 are certain constants to be determined and $C_0(\mu)$ and $C_1(\mu)$ are polynomials of degree $n-1$ in μ defined in the manner of equations (100) and (101) in terms of the $(n-1)$ positive nonvanishing roots of the equation (174) (see n. 12).

From equations (183), (184), (188), and (189) we now have

$$(p_0+q_0\mu_0)\,C_0(\mu_0)+(p_1-q_1\mu_0)\,C_1(\mu_0)=(3-\mu_0^2)\,P(-\mu_0) \tag{190}$$

and

$$(p_0+q_0\mu_0)\,C_1(-\mu_0)+(p_1-q_1\mu_0)\,C_0(-\mu_0)=(3-\mu_0^2)\,e^{-\tau_1/\mu_0}P(\mu_0)\,. \tag{191}$$

Solving these equations for $p_0+q_0\mu_0$ and $p_1-q_1\mu_0$, we have

$$p_0+q_0\mu_0=\frac{3-\mu_0^2}{[C_0^2(0)-C_1^2(0)]W(\mu_0)}\,[P(-\mu_0)C_0(-\mu_0)-e^{-\tau_1/\mu_0}P(\mu_0)C_1(\mu_0)] \tag{192}$$

and

$$p_1-q_1\mu_0=\frac{3-\mu_0^2}{[C_0^2(0)-C_1^2(0)]W(\mu_0)}\,[e^{-\tau_1/\mu_0}P(\mu_0)C_0(\mu_0)-P(-\mu_0)C_1(-\mu_0)]. \tag{193}$$

Next, combining equations (179)–(182), (188), and (189), we find, after some rearranging of the terms, that the reflected and the transmitted intensities can be expressed in the forms

$$\begin{aligned}I(0,\mu)=\tfrac{3}{32}\,\frac{F}{\mu_1^2\,.\,.\,.\,.\,\mu_n^2}\,\frac{1}{W(\mu)}\{&(p_0+q_0\mu_0)\,[P(-\mu)\,C_0(-\mu)-e^{-\tau_1/\mu}P(\mu)\,C_1(\mu)]\\&-(p_1-q_1\mu_0)\,[e^{-\tau_1/\mu}P(\mu)\,C_0(\mu)-P(-\mu)\,C_1(-\mu)]\\&-q_0(\mu_0+\mu)\,[P(-\mu)\,C_0(-\mu)-e^{-\tau_1/\mu}P(\mu)\,C_1(\mu)]\\&-q_1(\mu_0+\mu)\,[e^{-\tau_1/\mu}P(\mu)\,C_0(\mu)-P(-\mu)\,C_1(-\mu)]\}\,\frac{\mu_0}{\mu_0+\mu}\end{aligned} \tag{194}$$

and

$$I(\tau_1,-\mu)=\tfrac{3}{32}\frac{F}{\mu_1^2\cdot\cdots\cdot\mu_n^2}\frac{1}{W(\mu)}\{(p_1-q_1\mu_0)[P(-\mu)C_0(-\mu)-e^{-\tau_1/\mu}P(\mu)C_1(\mu)]$$
$$-(p_0+q_0\mu_0)[e^{-\tau_1/\mu}P(\mu)C_0(\mu)-P(-\mu)C_1(-\mu)]$$
$$+q_1(\mu_0-\mu)[P(-\mu)C_0(-\mu)-e^{-\tau_1/\mu}P(\mu)C_1(\mu)]$$
$$+q_0(\mu_0-\mu)[e^{-\tau_1/\mu}P(\mu)C_0(\mu)-P(-\mu)C_1(-\mu)]\}\frac{\mu_0}{\mu_0-\mu}. \qquad (195)$$

It remains to determine the constants q_0 and q_1.

10. *The determination of the constants* q_0 *and* q_1.—Putting $\mu=+\sqrt{3}$, respectively, $-\sqrt{3}$, in equations (176), (177), (181), and (182) we have

$$\frac{1}{\mu_1^2\cdot\cdots\cdot\mu_n^2}\frac{P(\pm\sqrt{3})}{W(\sqrt{3})}\frac{s(\pm\sqrt{3})}{1\mp\frac{\sqrt{3}}{\mu_0}}=S(\pm\sqrt{3})$$
$$=\mp\sqrt{3}L_0+L_n \qquad (196)$$

and

$$\frac{1}{\mu_1^2\cdot\cdots\cdot\mu_n^2}\frac{P(\pm\sqrt{3})}{W(\sqrt{3})}\frac{t(\pm\sqrt{3})}{1\pm\frac{\sqrt{3}}{\mu_0}}=T(\pm\sqrt{3})$$
$$=(\tau_1\pm\sqrt{3})L_0+L_n. \qquad (197)$$

The foregoing equations can be simplified by using the relation (Paper XIV, eq. [267])

$$\frac{1}{\mu_1^2\cdot\cdots\cdot\mu_n^2}\frac{P(+\sqrt{3})P(-\sqrt{3})}{W(\sqrt{3})}=-8. \qquad (198)$$

We find

$$-\frac{8}{1\mp\frac{\sqrt{3}}{\mu_0}}\frac{s(\pm\sqrt{3})}{P(\mp\sqrt{3})}=\mp\sqrt{3}L_0+L_n \qquad (199)$$

and

$$-\frac{8}{1\pm\frac{\sqrt{3}}{\mu_0}}\frac{t(\pm\sqrt{3})}{P(\mp\sqrt{3})}=(\tau_1\pm\sqrt{3})L_0+L_n. \qquad (200)$$

From equations (199) and (200) we obtain the following set of equations:

$$\frac{8}{1\mp\frac{\sqrt{3}}{\mu_0}}\left[\frac{s(\pm\sqrt{3})}{P(\mp\sqrt{3})}-\frac{t(\mp\sqrt{3})}{P(\pm\sqrt{3})}\right]=L_0\tau_1, \qquad (201)$$

$$-\frac{8}{1+\frac{\sqrt{3}}{\mu_0}}\frac{t(+\sqrt{3})}{P(-\sqrt{3})}+\frac{8}{1-\frac{\sqrt{3}}{\mu_0}}\frac{t(-\sqrt{3})}{P(+\sqrt{3})}=2\sqrt{3}L_0, \qquad (202)$$

and

$$-\frac{8}{1+\frac{\sqrt{3}}{\mu_0}}\frac{s(-\sqrt{3})}{P(+\sqrt{3})}+\frac{8}{1-\frac{\sqrt{3}}{\mu_0}}\frac{s(+\sqrt{3})}{P(-\sqrt{3})}=2\sqrt{3}L_0. \qquad (203)$$

Now, eliminating L_0 from equations (201)–(203), we obtain the equations

$$\left(1+\frac{\sqrt{3}}{\mu_0}\right)\left[\frac{s(+\sqrt{3})}{P(-\sqrt{3})}-\frac{t(-\sqrt{3})}{(P+\sqrt{3})}\right]=\left(1-\frac{\sqrt{3}}{\mu_0}\right)\left[\frac{s(-\sqrt{3})}{P(+\sqrt{3})}-\frac{t(+\sqrt{3})}{P(-\sqrt{3})}\right] \tag{204}$$

and

$$\left.\begin{aligned}2\sqrt{3}\left\{\left(1+\frac{\sqrt{3}}{\mu_0}\right)\left[\frac{s(+\sqrt{3})}{P(-\sqrt{3})}-\frac{t(-\sqrt{3})}{P(+\sqrt{3})}\right]+\left(1-\frac{\sqrt{3}}{\mu_0}\right)\left[\frac{s(-\sqrt{3})}{P(+\sqrt{3})}-\frac{t(+\sqrt{3})}{P(-\sqrt{3})}\right]\right\}\\ =\tau_1\left\{\left(1+\frac{\sqrt{3}}{\mu_0}\right)\left[\frac{s(+\sqrt{3})}{P(-\sqrt{3})}+\frac{t(-\sqrt{3})}{P(+\sqrt{3})}\right]-\left(1-\frac{\sqrt{3}}{\mu_0}\right)\left[\frac{s(-\sqrt{3})}{P(+\sqrt{3})}+\frac{t(+\sqrt{3})}{P(-\sqrt{3})}\right]\right\}\\ =\frac{\sqrt{3}}{2}\left(1-\frac{3}{\mu_0^2}\right)L_0\tau_1.\end{aligned}\right\} \tag{205}$$

These equations can be further reduced to the forms

$$\left.\begin{aligned}(\sqrt{3}+\mu_0)\,[\,s\,(+\sqrt{3})\,P\,(+\sqrt{3})\,-t\,(-\sqrt{3})\,P\,(-\sqrt{3})\,]\\ +\,(\sqrt{3}-\mu_0)\,[\,s\,(-\sqrt{3})\,P\,(-\sqrt{3})\,-t\,(+\sqrt{3})\,P\,(+\sqrt{3})\,]=0\end{aligned}\right\} \tag{206}$$

and

$$\left.\begin{aligned}2\sqrt{3}\,\{(\sqrt{3}+\mu_0)\,[\,s(+\sqrt{3})P(+\sqrt{3})-t(-\sqrt{3})P(-\sqrt{3})\,]-(\sqrt{3}-\mu_0)\\ \times[\,s(-\sqrt{3})P(-\sqrt{3})-t(+\sqrt{3})P(+\sqrt{3})\,]\}=\tau_1\{(\sqrt{3}+\mu_0)\,[\,s(+\sqrt{3})P(+\sqrt{3})\\ +t(-\sqrt{3})P(-\sqrt{3})\,]+(\sqrt{3}-\mu_0)\,[\,s(-\sqrt{3})P(-\sqrt{3})+t(+\sqrt{3})P(+\sqrt{3})\,]\}.\end{aligned}\right\} \tag{207}$$

We now have to substitute for $s(\pm\sqrt{3})$ and $t(\pm\sqrt{3})$ in equations (206) and (207) according to equations (188) and (189). For this purpose, it is convenient to write $s(\pm\sqrt{3})$ and $t(\pm\sqrt{3})$ in the forms

$$\left.\begin{aligned}s\,(\pm\sqrt{3})\;=\;(p_0+q_0\mu_0)\,C_0\,(\pm\sqrt{3})\;+\;(p_1-q_1\mu_0)\,C_1\,(\pm\sqrt{3})\\ +\;(\sqrt{3}\mp\mu_0)\,[\,\pm\,q_0C_0\,(\pm\sqrt{3})\;\mp\,q_1C_1\,(\pm\sqrt{3})\,]\end{aligned}\right\} \tag{208}$$

and

$$\left.\begin{aligned}t\,(\pm\sqrt{3})\;=\;(p_0+q_0\mu_0)\,C_1\,(\pm\sqrt{3})\;+\;(p_1-q_1\mu_0)\,C_0\,(\pm\sqrt{3})\\ +\;(\sqrt{3}\pm\mu_0)\,[\,\mp\,q_0C_1\,(\pm\sqrt{3})\;\pm\,q_1C_0\,(\pm\sqrt{3})\,].\end{aligned}\right\} \tag{209}$$

Substituting for $s(\pm\sqrt{3})$ and $t(\pm\sqrt{3})$ from equations (208) and (209) in equations (206) and (207), we find, after some lengthy but straightforward reductions, that

$$\left.\begin{aligned}(p_0+q_0\mu_0)\,(\sqrt{3}w_1+w_2\mu_0)\;+\;(p_1-q_1\mu_0)\,(-\sqrt{3}w_1+w_2\mu_0)\\ +\;(3-\mu_0^2)\,w_2\,(q_0-q_1)\;=0\end{aligned}\right\} \tag{210}$$

and

$$\left.\begin{aligned}2\sqrt{3}\,\{\,(p_0+q_0\mu_0)\,(\sqrt{3}w_2+w_1\mu_0)\;+\;(p_1-q_1\mu_0)\,(\sqrt{3}w_2-w_1\mu_0)\\ +\;(3-\mu_0^2)\,w_1\,(q_0+q_1)\,\}\;=\tau_1\{\,(p_0+q_0\mu_0)\,(\sqrt{3}w_4+w_3\mu_0)\\ +\;(p_1-q_1\mu_0)\,(\sqrt{3}w_4-w_3\mu_0)\;+\;(3-\mu_0^2)\,w_3\,(q_0+q_1)\,\},\end{aligned}\right\} \tag{211}$$

where, for the sake of brevity, we have written

$$\left.\begin{aligned} w_1 &= C_0(\sqrt{3})P(\sqrt{3}) - C_1(\sqrt{3})P(\sqrt{3}) + C_0(-\sqrt{3})P(-\sqrt{3}) - C_1(-\sqrt{3})P(-\sqrt{3}), \\ w_2 &= C_0(\sqrt{3})P(\sqrt{3}) + C_1(\sqrt{3})P(\sqrt{3}) - C_0(-\sqrt{3})P(-\sqrt{3}) - C_1(-\sqrt{3})P(-\sqrt{3}), \\ w_3 &= C_0(\sqrt{3})P(\sqrt{3}) - C_1(\sqrt{3})P(\sqrt{3}) - C_0(-\sqrt{3})P(-\sqrt{3}) + C_1(-\sqrt{3})P(-\sqrt{3}), \\ w_4 &= C_0(\sqrt{3})P(\sqrt{3}) + C_1(\sqrt{3})P(\sqrt{3}) + C_0(-\sqrt{3})P(-\sqrt{3}) + C_1(-\sqrt{3})P(-\sqrt{3}). \end{aligned}\right\} \quad (212)$$

Equations (210) and (211) can be re-written in the forms

$$\left.\begin{aligned} (3-\mu_0^2)(q_0 - q_1) + (p_0 + q_0\mu_0)\left(\mu_0 + \sqrt{3}\,\frac{w_1}{w_2}\right) \\ + (p_1 - q_1\mu_0)\left(\mu_0 - \sqrt{3}\,\frac{w_1}{w_2}\right) = 0 \end{aligned}\right\} \quad (213)$$

and

$$\left.\begin{aligned} (3-\mu_0^2)(q_0 + q_1) + (p_0 + q_0\mu_0)\left[\sqrt{3}\,\frac{w_4\tau_1 - 2\sqrt{3}w_2}{w_3\tau_1 - 2\sqrt{3}w_1} + \mu_0\right] \\ + (p_1 - q_1\mu_0)\left[\sqrt{3}\,\frac{w_4\tau_1 - 2\sqrt{3}w_2}{w_3\tau_1 - 2\sqrt{3}w_1} - \mu_0\right] = 0. \end{aligned}\right\} \quad (214)$$

Solving these equations for q_0 and q_1, we have

$$(3-\mu_0^2)\,q_0 = -[(c_1+\mu_0)(p_0 + q_0\mu_0) + c_2(p_1 - q_1\mu_0)] \quad (215)$$

and

$$(3-\mu_0^2)\,q_1 = -[c_2(p_0 + q_0\mu_0) + (c_1 - \mu_0)(p_1 - q_1\mu_0)], \quad (216)$$

where

$$c_1 = \frac{\sqrt{3}}{2}\left[\frac{w_4\tau_1 - 2\sqrt{3}w_2}{w_3\tau_1 - 2\sqrt{3}w_1} + \frac{w_1}{w_2}\right] \quad (217)$$

and

$$c_2 = \frac{\sqrt{3}}{2}\left[\frac{w_4\tau_1 - 2\sqrt{3}w_2}{w_3\tau_1 - 2\sqrt{3}w_1} - \frac{w_1}{w_2}\right]. \quad (218)$$

Since $(p_0 + q_0\mu_0)$ and $(p_1 - q_1\mu_0)$ have already been determined (eqs. [192] and [193]), the foregoing equations complete the formal solution for $S(\mu)$ and $T(\mu)$.

11. *The solution for the reflected and the transmitted radiations.*—Now, substituting for $(p_0 + q_0\mu_0)$, $(p_1 - q_1\mu_0)$, q_0, and q_1 according to equations (192), (193), (215), and (216) in equations (194) and (195) and introducing the functions $X(\mu)$ and $Y(\mu)$, defined as in equations (125) and (126), we have

$$\left.\begin{aligned} I(0,\mu) = \tfrac{3}{32}F\,\frac{\mu_0}{\mu_0+\mu}\{(3-\mu_0^2)[X(\mu)X(\mu_0) - Y(\mu)Y(\mu_0)] \\ + (\mu_0+\mu)X(\mu)[(c_1+\mu_0)X(\mu_0) + c_2Y(\mu_0)] \\ + (\mu_0+\mu)Y(\mu)[c_2X(\mu_0) + (c_1-\mu_0)Y(\mu_0)]\} \end{aligned}\right\} \quad (219)$$

and

$$\left.\begin{aligned} I(\tau_1,-\mu) = \tfrac{3}{32}F\,\frac{\mu_0}{\mu_0-\mu}\{(3-\mu_0^2)[X(\mu)Y(\mu_0) - Y(\mu)X(\mu_0)] \\ - (\mu_0-\mu)X(\mu)[c_2X(\mu_0) + (c_1-\mu_0)Y(\mu_0)] \\ - (\mu_0-\mu)Y(\mu)[(c_1+\mu_0)X(\mu_0) + c_2Y(\mu_0)]\}. \end{aligned}\right\} \quad (220)$$

After some rearranging, equations (219) and (220) can be brought to the forms

$$\left.\begin{aligned} I^{(0)}(0,\mu) = \tfrac{3}{32}F\frac{\mu_0}{\mu_0+\mu}\{ & X^{(0)}(\mu)\,X^{(0)}(\mu_0)\,[3+c_1(\mu_0+\mu)+\mu\mu_0] \\ & - Y^{(0)}(\mu)\,Y^{(0)}(\mu_0)\,[3-c_1(\mu_0+\mu)+\mu\mu_0] \\ & + c_2(\mu_0+\mu)\,[X^{(0)}(\mu)\,Y^{(0)}(\mu_0)+Y^{(0)}(\mu)\,X^{(0)}(\mu_0)]\}\end{aligned}\right\} \quad (221)$$

and

$$\left.\begin{aligned} I^{(0)}(\tau_1,-\mu) = \tfrac{3}{32}F\frac{\mu_0}{\mu_0-\mu}\{ & X^{(0)}(\mu)\,Y^{(0)}(\mu_0)\,[3-c_1(\mu_0-\mu)-\mu\mu_0] \\ & - Y^{(0)}(\mu)\,X^{(0)}(\mu_0)\,[3+c_1(\mu_0-\mu)-\mu\mu_0] \\ & - c_2(\mu_0-\mu)\,[X^{(0)}(\mu)\,X^{(0)}(\mu_0)+Y^{(0)}(\mu)\,Y^{(0)}(\mu_0)]\}.\end{aligned}\right\} \quad (222)$$

In equations (221) and (222) we have inserted a superscript "0" with the various functions to emphasize the fact that these equations represent only the solutions for the azimuth independent terms in the reflected and the transmitted intensities.

To complete the solution we need to find the remaining terms in the reflected and the transmitted intensities which are proportional to $\cos(\varphi-\varphi_0)$ and $\cos 2(\varphi-\varphi_0)$. The determination of these terms presents no difficulty, since the equations satisfied by $I^{(1)}(\tau,\mu)$ and $I^{(2)}(\tau,\mu)$ (cf. Paper IX, eqs. [154] and [155]) are of the standard form considered in Paper IX, § 4, and the analysis of Section I applies without any modifications. We can, therefore, write (cf. Paper IX, eqs. [190] and [194])

$$\left.\begin{aligned} I^{(1)}(0,\mu) &= -\tfrac{3}{8}F\mu\mu_0(1-\mu^2)^{\frac{1}{2}}(1-\mu_0^2)^{\frac{1}{2}}\frac{\mu_0}{\mu_0+\mu} \\ &\quad\times[X^{(1)}(\mu)\,X^{(1)}(\mu_0)-Y^{(1)}(\mu)\,Y^{(1)}(\mu_0)], \\ I^{(1)}(\tau_1,-\mu) &= +\tfrac{3}{8}F\mu\mu_0(1-\mu^2)^{\frac{1}{2}}(1-\mu_0^2)^{\frac{1}{2}}\frac{\mu_0}{\mu_0-\mu} \\ &\quad\times[X^{(1)}(\mu)\,Y^{(1)}(\mu_0)-Y^{(1)}(\mu)\,X^{(1)}(\mu_0)],\end{aligned}\right\} \quad (223)$$

and

$$\left.\begin{aligned} I^{(2)}(0,\mu) &= \tfrac{3}{32}F(1-\mu^2)(1-\mu_0^2)\frac{\mu_0}{\mu_0+\mu} \\ &\quad\times[X^{(2)}(\mu)\,X^{(2)}(\mu_0)-Y^{(2)}(\mu)\,Y^{(2)}(\mu_0)], \\ I^{(2)}(\tau_1,-\mu) &= \tfrac{3}{32}F(1-\mu^2)(1-\mu_0^2)\frac{\mu_0}{\mu_0-\mu} \\ &\quad\times[X^{(2)}(\mu)\,Y^{(2)}(\mu_0)-Y^{(2)}(\mu)\,X^{(2)}(\mu_0)],\end{aligned}\right\} \quad (224)$$

where $X^{(1)}$, $Y^{(1)}$ and $X^{(2)}$, $Y^{(2)}$ are defined in terms of the characteristic functions

$$\Psi^{(1)}(\mu) = \tfrac{3}{8}\mu^2(1-\mu^2) \qquad \text{and} \qquad \Psi^{(2)}(\mu) = \tfrac{3}{32}(1-\mu^2)^2. \quad (225)$$

In terms of the foregoing solutions (eqs. [221]–[224]), the reflected and the transmitted intensities are given by

$$\left.\begin{aligned} I(0,\mu,\varphi;\mu_0,\varphi_0) = I^{(0)}(0,\mu) &+ I^{(1)}(0,\mu)\cos(\varphi-\varphi_0) \\ &+ I^{(2)}(0,\mu)\cos 2(\varphi-\varphi_0)\end{aligned}\right\} \quad (226)$$

and

$$I(\tau_1,-\mu,\varphi;\ \mu_0,\varphi_0) = I^{(0)}(\tau_1,-\mu) + I^{(1)}(\tau_1,-\mu)\cos(\varphi-\varphi_0) + I^{(2)}(\tau_1,-\mu)\cos 2(\varphi-\varphi_0)\,. \tag{227}$$

IV. SCATTERING IN ACCORDANCE WITH THE PHASE FUNCTION $\lambda(1 + x\cos\Theta)$

12. *The azimuth independent term.*—In the problem of diffuse reflection and transmission by a plane-parallel atmosphere scattering radiation in accordance with the phase function $\lambda(1 + x\cos\Theta)$ ($\lambda < 1$, $1 \geqslant x \geqslant -1$), we must distinguish between two terms in the radiation field: an azimuth independent term and a term proportional to $\cos(\varphi - \varphi_0)$ (cf. Paper IX, eq. [6]). Considering, first, the azimuth independent term, we can express the reflected and the transmitted radiations in terms of the functions

$$S(\mu) = \sum_{a=-n}^{+n} \frac{L_a[1 + x(1-\lambda)\mu/k_a]}{1 - k_a\mu} + \gamma\frac{[1 + x(1-\lambda)\mu\mu_0]}{1 - \mu/\mu_0} \tag{228}$$

and

$$T(\mu) = \sum_{a=-n}^{+n} \frac{L_a[1 - x(1-\lambda)\mu/k_a]}{1 + k_a\mu}\, e^{-k_a\tau_1} + \gamma\, e^{-\tau_1/\mu_0}\frac{[1 - x(1-\lambda)\mu\mu_0]}{1 + \mu/\mu_0}, \tag{229}$$

where the k_a's ($a = \pm 1, \ldots, \pm n$ and $k_{+a} = -k_{-a}$) are the $2n$ roots of the characteristic equation

$$1 = \lambda\sum_{j=1}^{n} \frac{a_j[1 + x(1-\lambda)\mu_j^2]}{1 - k^2\mu_j^2}, \tag{230}$$

$$\gamma = H(\mu_0)\,H(-\mu_0)\,, \tag{231}$$

and the rest of the symbols have their usual meanings. We have

$$I(0,\mu) = \tfrac{1}{4}\lambda F[S(-\mu) - e^{-\tau_1/\mu}T(\mu)] \tag{232}$$

and

$$I(\tau_1,-\mu) = \tfrac{1}{4}\lambda F[T(-\mu) - e^{-\tau_1/\mu}S(\mu)]\,. \tag{233}$$

Moreover, the boundary conditions at $\tau = 0$ and $\tau = \tau_1$ require that

$$S(\mu_i) = T(\mu_i) = 0 \qquad (i = 1, \ldots, n)\,. \tag{234}$$

In view of these boundary conditions, we can write

$$S(\mu) = \frac{1}{\mu_1^2 \cdots \mu_n^2}\frac{P(\mu)}{W(\mu)}\frac{1}{1 - \mu/\mu_0}\,s(\mu) \tag{235}$$

and

$$T(\mu) = \frac{1}{\mu_1^2 \cdots \mu_n^2}\frac{P(\mu)}{W(\mu)}\frac{1}{1 + \mu/\mu_0}\,t(\mu)\,, \tag{236}$$

where $s(\mu)$ and $t(\mu)$ are polynomials of degree $n + 1$ in μ.

From equations (228), (229), (231), (235), and (236) it follows that

$$s(\mu_0) = [1 + x(1-\lambda)\mu_0^2]\, P(-\mu_0) \tag{237}$$

and

$$t(-\mu_0) = [1 + x(1-\lambda)\mu_0^2]\, e^{-\tau_1/\mu_0} P(\mu_0)\,. \tag{238}$$

And again, from equations (228), (229), (235), and (236), we have

$$L_a = \frac{1}{\mu_1^2 \cdot \cdots \cdot \mu_n^2} \frac{P(1/k_a)}{W_a(1/k_a)} \frac{1}{1 - 1/k_a\mu_0} \frac{s(1/k_a)}{1 + x(1-\lambda)/k_a^2} \qquad (a = \pm 1, \ldots, \pm n) \tag{239}$$

and

$$L_a e^{-k_a\tau_1} = \frac{1}{\mu_1^2 \cdot \cdots \cdot \mu_n^2} \frac{P(-1/k_a)}{W_a(1/k_a)} \frac{1}{1 - 1/k_a\mu_0} \frac{t(-1/k_a)}{1 + x(1-\lambda)/k_a^2} \qquad (a = \pm 1, \ldots, \pm n)\,. \tag{240}$$

We therefore have the $2n$ relations

$$s(1/k_a) = e^{k_a\tau_1} \frac{P(-1/k_a)}{P(+1/k_a)}\, t(-1/k_a) \qquad (a = \pm 1, \ldots, \pm n)\,. \tag{241}$$

However, since $s(\mu)$ and $t(\mu)$ are polynomials of degree $(n+1)$ in μ, we conclude, in accordance with theorems 1 and 2 (§ 4), that $s(\mu)$ and $t(\mu)$ must be expressible in the forms

$$s(\mu) = (p_0 + q_0\mu) C_0(\mu) + (p_1 - q_1\mu) C_1(\mu) \tag{242}$$

and

$$t(\mu) = (p_1 + q_1\mu) C_0(\mu) + (p_0 - q_0\mu) C_1(\mu)\,, \tag{243}$$

where p_0, q_0, p_1, and q_1 are certain constants and $C_0(\mu)$ and $C_1(\mu)$ are defined as in equations (50), (100), and (101) in terms of the n positive roots of equation (230).

From equations (237), (238), (242), and (243) it now follows that

$$p_0 + q_0\mu_0 = \frac{1 + x(1-\lambda)\mu_0^2}{[C_0^2(0) - C_1^2(0)]\, W(\mu_0)} [P(-\mu_0) C_0(-\mu_0) - e^{-\tau_1/\mu_0} P(\mu_0) C_1(\mu_0)] \tag{244}$$

and

$$p_1 - q_1\mu_0 = \frac{1 + x(1-\lambda)\mu_0^2}{[C_0^2(0) - C_1^2(0)]\, W(\mu_0)} [e^{-\tau_1/\mu_0} P(\mu_0) C_0(\mu_0) - P(-\mu_0) C_1(-\mu_0)]\,. \tag{245}$$

It remains to determine the constants q_0 and q_1.

13. *The determination of the constants* q_0 *and* q_1.—Putting $\mu = 0$ in equations (228), (229), (235), and (236), we obtain

$$S(0) = \sum_{a=-n}^{+n} L_a + \gamma = \frac{(-1)^n}{\mu_1 \cdot \cdots \cdot \mu_n}\, s(0) \tag{246}$$

and

$$T(0) = \sum_{a=-n}^{+n} L_a e^{-k_a\tau_1} + \gamma e^{-\tau_1/\mu_0} = \frac{(-1)^n}{\mu_1 \cdot \cdots \cdot \mu_n}\, t(0)\,. \tag{247}$$

Now, according to equation (239),

$$\left.\begin{aligned}\sum_{\alpha=-n}^{+n} L_\alpha &= \frac{1}{\mu_1^2 \cdot \cdots \cdot \mu_n^2} \sum_{\alpha=-n}^{+n} \frac{P(1/k_\alpha)\, s(1/k_\alpha)}{W_\alpha(1/k_\alpha)(1-1/k_\alpha\mu_0)[1+x(1-\lambda)/k_\alpha^2]} \\ &= -\frac{\mu_0}{\mu_1^2 \cdot \cdots \cdot \mu_n^2 W(\mu_0)} \sum_{\alpha=-n}^{+n} \frac{k_\alpha P(1/k_\alpha)\, s(1/k_\alpha)}{W_\alpha(1/k_\alpha)[1+x(1-\lambda)/k_\alpha^2]} W_\alpha(\mu_0)\,.\end{aligned}\right\} \quad (248)$$

To evaluate the sum on the right-hand side, we introduce the function

$$f(z) = \sum_{\alpha=-n}^{+n} \frac{k_\alpha P(1/k_\alpha)\, s(1/k_\alpha)}{W_\alpha(1/k_\alpha)[1+x(1-\lambda)/k_\alpha^2]} W_\alpha(z) \quad (249)$$

and express ΣL_α in terms of it. Thus

$$\sum_{\alpha=-n}^{+n} L_\alpha = -\frac{\mu_0}{\mu_1^2 \cdot \cdots \cdot \mu_n^2} \frac{f(\mu_0)}{W(\mu_0)}\,. \quad (250)$$

As defined in equation (249), $f(z)$ is a polynomial of degree $(2n-1)$ in z and takes the values

$$\frac{k_\alpha P(1/k_\alpha)\, s(1/k_\alpha)}{1+x(1-\lambda)/k_\alpha^2} \quad (251)$$

for $z = 1/k_\alpha$ ($\alpha = \pm 1, \ldots, \pm n$). In other words,

$$z[1+x(1-\lambda)z^2] f(z) - P(z)\, s(z) = 0 \quad \text{for} \quad z = 1/k_\alpha \quad \text{and} \quad \alpha = \pm 1, \ldots, \pm n\,. \quad (252)$$

Hence there must exist a relation of the form

$$z[1+x(1-\lambda)z^2] f(z) = P(z)\, s(z) + W(z)[Az^2 + Bz + D] \quad (253)$$

where A, B, and D are certain constants to be determined.

Putting $z = 0$ in equation (253), we determine at once that

$$D = -(-1)^n \mu_1 \cdots \mu_n s(0)\,. \quad (254)$$

Next, putting $z = \pm i/\sqrt{x(1-\lambda)}$ in equation (253), we find

$$P(\pm i\zeta)\, s(\pm i\zeta) + W(i\zeta)[-A\zeta^2 \pm iB\zeta + D] = 0\,, \quad (255)$$

where, for the sake of brevity, we have written

$$\zeta = \frac{1}{\sqrt{x(1-\lambda)}}\,, \quad (256)$$

Solving equations (255) for A and B, we find

$$A = \frac{D}{\zeta^2} + \frac{1}{2\zeta^2 W(i\zeta)}[P(i\zeta)\, s(i\zeta) + P(-i\zeta)\, s(-i\zeta)] \quad (257)$$

and

$$B = \frac{i}{2\zeta W(i\zeta)}[P(i\zeta)\, s(i\zeta) - P(-i\zeta)\, s(-i\zeta)]\,. \quad (258)$$

Returning to equation (253) and setting $z = \mu_0$ and remembering that

$$s(\mu_0) = \left(1 + \frac{\mu_0^2}{\zeta^2}\right) P(-\mu_0) \tag{259}$$

we obtain

$$f(\mu_0) = \frac{1}{\mu_0} P(\mu_0) P(-\mu_0) + \frac{W(\mu_0)}{\mu_0 [1 + x(1-\lambda)\mu_0^2]} [A\mu_0^2 + B\mu_0 + D) . \tag{260}$$

Using the foregoing expression for $f(\mu_0)$ in equation (250) and inserting for A, B, and D their values given by equations (254), (257), and (258), we find, after some reductions, that

$$\left.\begin{aligned}\sum_{a=-n}^{+n} L_a = -\gamma + \frac{(-1)^n}{\mu_1 \ldots . \mu_n} s(0) \\ - \frac{x(1-\lambda)\mu_0}{2\mu_1^2 \ldots . \mu_n^2 [1 + x(1-\lambda)\mu_0^2] W(i\zeta)} [\mu_0 \{P(i\zeta) s(i\zeta) + P(-i\zeta) s(-i\zeta)\} \\ + i\zeta \{P(i\zeta) s(i\zeta) - P(-i\zeta) s(-i\zeta)\}] .\end{aligned}\right\} \tag{261}$$

Similarly,

$$\left.\begin{aligned}\sum_{a=-n}^{+n} L_a e^{-k_a \tau_1} = -\gamma e^{-\tau_1/\mu_0} + \frac{(-1)^n}{\mu_1 \ldots . \mu_n} t(0) \\ + \frac{x(1-\lambda)\mu_0}{2\mu_1^2 \ldots . \mu_n^2 [1 + x(1-\lambda)\mu_0^2] W(i\zeta)} [-\mu_0 \{P(i\zeta) t(i\zeta) + P(-i\zeta) t(-i\zeta)\} \\ + i\zeta \{P(i\zeta) t(i\zeta) - P(-i\zeta) t(-i\zeta)\}] .\end{aligned}\right\} \tag{262}$$

Equations (261) and (262) evaluate the required sums.

According to equations (246), (247), (261), and (262), we clearly have

$$(\mu_0 + i\zeta) P(i\zeta) s(i\zeta) + (\mu_0 - i\zeta) P(-i\zeta) s(-i\zeta) = 0 \tag{263}$$

and

$$(\mu_0 - i\zeta) P(i\zeta) t(i\zeta) + (\mu_0 + i\zeta) P(-i\zeta) t(-i\zeta) = 0 . \tag{264}$$

We now have to substitute for $s(\pm i\zeta)$ and $t(\pm i\zeta)$ in equations (263) and (264) according to equations (242) and (243). For this purpose it is convenient to write $s(\pm i\zeta)$ and $t(\pm i\zeta)$ in the forms

$$\left.\begin{aligned}s(\pm i\zeta) = (p_0 + q_0\mu_0) C_0(\pm i\zeta) + (p_1 - q_1\mu_0) C_1(\pm i\zeta) \\ + (\mu_0 \mp i\zeta)[-q_0 C_0(\pm i\zeta) + q_1 C_1(\pm i\zeta)]\end{aligned}\right\} \tag{265}$$

and

$$\left.\begin{aligned}t(\pm i\zeta) = (p_0 + q_0\mu_0) C_1(\pm i\zeta) + (p_1 - q_1\mu_0) C_0(\pm i\zeta) \\ + (\mu_0 \pm i\zeta)[-q_0 C_1(\pm i\zeta) + q_1 C_0(\pm i\zeta)] .\end{aligned}\right\} \tag{266}$$

Substituting from equations (265) and (266) in equations (263) and (264), we find, after some minor reductions, that

$$\left.\begin{aligned}(\mu_0^2 + \zeta^2)(q_0\alpha_0 - q_1\alpha_1) = (p_0 + q_0\mu_0)(\alpha_0\mu_0 + \beta_0\zeta) \\ + (p_1 - q_1\mu_0)(\alpha_1\mu_0 + \beta_1\zeta)\end{aligned}\right\} \tag{267}$$

and

$$\left.\begin{aligned}(\mu_0^2+\zeta^2)\,(q_0\alpha_1-q_1\alpha_0) &= (p_0+q_0\mu_0)\,(\alpha_1\mu_0-\beta_1\zeta)\\ &\quad+(p_1-q_1\mu_0)\,(\alpha_0\mu_0-\beta_0\zeta)\,,\end{aligned}\right\} \tag{268}$$

where

$$\left.\begin{aligned}\alpha_0 &= P(i\zeta)\,C_0(i\zeta)+P(-i\zeta)\,C_0(-i\zeta)\,,\\ \alpha_1 &= P(i\zeta)\,C_1(i\zeta)+P(-i\zeta)\,C_1(-i\zeta)\,,\\ \beta_0 &= i\,[P(i\zeta)\,C_0(i\zeta)-P(-i\zeta)\,C_0(-i\zeta)]\,,\\ \beta_1 &= i\,[P(i\zeta)\,C_1(i\zeta)-P(-i\zeta)\,C_1(-i\zeta)]\,.\end{aligned}\right\} \tag{269}$$

Defined in this manner, α_0, α_1, β_0, and β_1 are all real constants.

Solving equations (267) and (268) for q_0 and q_1, we find

$$q_0=\frac{x\,(1-\lambda)}{1+x\,(1-\lambda)\,\mu_0^2}\,[\,(c_1+\mu_0)\,(p_0+q_0\mu_0)+c_2\,(p_1-q_1\mu_0)\,] \tag{270}$$

and

$$q_1=\frac{x\,(1-\lambda)}{1+x\,(1-\lambda)\,\mu_0^2}\,[\,c_2\,(p_0+q_0\mu_0)+(c_1-\mu_0)\,(p_1-q_1\mu_0)\,]\,, \tag{271}$$

where

$$c_1=\frac{1}{\sqrt{x\,(1-\lambda)}}\,\frac{\alpha_0\beta_0+\alpha_1\beta_1}{\alpha_0^2-\alpha_1^2} \tag{272}$$

and

$$c_2=\frac{1}{\sqrt{x\,(1-\lambda)}}\,\frac{\alpha_0\beta_1+\alpha_1\beta_0}{\alpha_0^2-\alpha_1^2}\,. \tag{273}$$

With this, the determination of the constants is completed.

14. *The solutions for the reflected and the transmitted radiations.*—It is apparent that for $s(\mu)$ and $t(\mu)$ given by equations (242) and (243), the equations governing the angular distributions of the reflected and the transmitted radiations can be reduced to the forms (194) and (195) with $\lambda/4$ replacing "3/32." With the expressions for $(p_0+q_0\mu_0)$, $(p_1-q_1\mu_0)$, q_0, and q_1 given by equations (244), (245), (270), and (271), we therefore have

$$\left.\begin{aligned}I(0,\mu) &= \tfrac{1}{4}\lambda F\{\,[1+x\,(1-\lambda)\,\mu_0^2]\,[X(\mu)\,X(\mu_0)-Y(\mu)\,Y(\mu_0)]\\ &\quad-x\,(1-\lambda)\,(\mu_0+\mu)\,X(\mu)\,[\,(c_1+\mu_0)\,X(\mu_0)+c_2\,Y(\mu_0)]\\ &\quad-x\,(1-\lambda)\,(\mu_0+\mu)\,Y(\mu)\,[\,c_2X(\mu_0)+(c_1-\mu_0)\,Y(\mu_0)]\,\}\,\frac{\mu_0}{\mu_0+\mu}\end{aligned}\right\} \tag{274}$$

and

$$\left.\begin{aligned}I(\tau_1,-\mu) &= \tfrac{1}{4}\lambda F\{\,[1+x\,(1-\lambda)\,\mu_0^2]\,[X(\mu)\,Y(\mu_0)-Y(\mu)\,X(\mu_0)]\\ &\quad+x\,(1-\lambda)\,(\mu_0-\mu)\,X(\mu)\,[\,c_2X(\mu_0)+(c_1-\mu_0)\,Y(\mu_0)]\\ &\quad+x\,(1-\lambda)\,(\mu_0-\mu)\,Y(\mu)\,[\,(c_1+\mu_0)\,X(\mu_0)+c_2\,Y(\mu_0)]\,\}\,\frac{\mu_0}{\mu_0-\mu}\,.\end{aligned}\right\} \tag{275}$$

After some rearranging, equations (274) and (275) can be brought to the forms

$$\left.\begin{aligned} I^{(0)}(0,\mu) = \tfrac{1}{4}\lambda F\{ & X^{(0)}(\mu)\,X^{(0)}(\mu_0)\,[1-x(1-\lambda)\,c_1(\mu_0+\mu)-x(1-\lambda)\,\mu\mu_0] \\ & - Y^{(0)}(\mu)\,Y^{(0)}(\mu_0)\,[1+x(1-\lambda)\,c_1(\mu_0+\mu)-x(1-\lambda)\,\mu\mu_0] \\ & - x(1-\lambda)\,c_2(\mu_0+\mu)\,[X^{(0)}(\mu)\,Y^{(0)}(\mu_0)+Y^{(0)}(\mu)\,X^{(0)}(\mu_0)]\}\frac{\mu_0}{\mu_0+\mu} \end{aligned}\right\} \quad (276)$$

and

$$\left.\begin{aligned} I^{(0)}(\tau_1,-\mu) = \tfrac{1}{4}\lambda F\{ & X^{(0)}(\mu)\,Y^{(0)}(\mu_0)\,[1+x(1-\lambda)\,c_1(\mu_0-\mu)+x(1-\lambda)\,\mu\mu_0] \\ & - Y^{(0)}(\mu)\,X^{(0)}(\mu_0)\,[1-x(1-\lambda)\,c_1(\mu_0-\mu)+x(1-\lambda)\,\mu\mu_0] \\ & + x(1-\lambda)\,c_2(\mu_0-\mu)\,[X^{(0)}(\mu)\,X^{(0)}(\mu_0)+Y^{(0)}(\mu)\,Y^{(0)}(\mu_0)]\}\frac{\mu_0}{\mu_0-\mu}. \end{aligned}\right\} \quad (277)$$

In equations (276) and (277) we have inserted a superscript "0" to the various functions to emphasize the fact that these equations represent only the solutions for the azimuth independent terms in the reflected and the transmitted radiations.

To complete the solution we must find the remaining term in the reflected and the transmitted intensities which is proportional to cos $(\varphi - \varphi_0)$. The determination of this term presents no difficulty, since the equation satisfied by $I^{(1)}(\tau, \mu)$ (Paper IX, eq. [8]) is of the form for which the analysis of Section I is applicable without modifications. We therefore have

$$\left.\begin{aligned} I^{(1)}(0,\mu) = {} & \tfrac{1}{4}x\lambda F\,(1-\mu^2)^{\frac{1}{2}}\,(1-\mu_0^2)^{\frac{1}{2}}\,\frac{\mu_0}{\mu_0+\mu} \\ & \times [X^{(1)}(\mu)\,X^{(1)}(\mu_0) - Y^{(1)}(\mu)\,Y^{(1)}(\mu_0)] \end{aligned}\right\} \quad (278)$$

and

$$\left.\begin{aligned} I^{(1)}(\tau_1,-\mu) = {} & \tfrac{1}{4}x\lambda F\,(1-\mu^2)^{\frac{1}{2}}\,(1-\mu_0^2)^{\frac{1}{2}}\,\frac{\mu_0}{\mu_0-\mu} \\ & \times [X^{(1)}(\mu)\,Y^{(1)}(\mu_0) - Y^{(1)}(\mu)\,X^{(1)}(\mu_0)], \end{aligned}\right\} \quad (279)$$

where $X^{(1)}(\mu)$ and $Y^{(1)}(\mu)$ are defined in terms of the characteristic function

$$\Psi^{(1)}(\mu) = \tfrac{1}{4}x\lambda\,(1-\mu^2). \quad (280)$$

In terms of the foregoing solution, the reflected and the transmitted intensities are given by

$$I(0,\mu,\varphi;\,\mu_0,\varphi_0) = I^{(0)}(0,\mu) + I^{(1)}(0,\mu)\cos(\varphi-\varphi_0) \quad (281)$$

and

$$I(\tau_1,-\mu,\varphi;\,\mu_0;\,\varphi_0) = I^{(0)}(\tau_1,-\mu) + I^{(1)}(\tau_1,-\mu)\cos(\varphi-\varphi_0). \quad (282)$$

V. RAYLEIGH SCATTERING

15. *The formulation of the problem.*—In a proper treatment of problems involving multiple scattering we should take into account the fact that after the first scattering even natural light becomes partially polarized. In formulating the equations of transfer we must, therefore, include the polarization characteristics of the radiation and allow for the dependence of the scattered light on these characteristics. As we have shown in the earlier papers[13] of this series, this can best be accomplished by considering the in-

[13] See esp. Papers XI, XIII, XIV, and XV (*Ap. J.*, **104**, 110, 1946; **105**, 151, 424, 1947).

tensities I_l and I_r in two directions at right angles to each other in the plane of the electric and the magnetic vectors and the further quantities

$$U = (I_l - I_r) \tan 2\chi \quad \text{and} \quad V = (I_l - I_r) \sec 2\chi \tan 2\beta , \tag{283}$$

where χ denotes the inclination of the plane of polarization to the direction to which l refers and $-\pi/2 \leqslant \beta \leqslant +\pi/2$ is an angle whose tangent is equal to the ratio of the axes of the ellipse which characterizes the state of polarization. (The sign of β depends on whether the polarization is right-handed or left-handed.)

For the case of Rayleigh scattering, the equations of transfer for I_l, I_r,[14] U, and V have been explicitly formulated[15] and exactly solved[16] for transfer problems in semi-infinite plane-parallel atmospheres. In this Section we shall be concerned with the solutions of these same equations for the problem of diffuse reflection and transmission by a plane-parallel atmosphere of finite optical thickness.

16. *The solution for* V *and the azimuth dependent terms.*—Considering the general case of incidence of a parallel beam of partially elliptically polarized light on a plane-parallel atmosphere in the direction $(-\mu_0, \varphi_0)$, we may recall that the equations of transfer break up into seven independent sets of equations[17] when the intensities I_l, I_r, U, and V are expressed in the forms[18]

$$\left.\begin{aligned} I_l(\tau, \mu, \varphi) = {} & I_l^{(0)}(\tau, \mu) + I_l^{(1)}(\tau, \mu) \cos(\varphi - \varphi_0) + I_l^{(-1)}(\tau, \mu) \sin(\varphi - \varphi_0) \\ & + I_l^{(2)}(\tau, \mu) \cos 2(\varphi - \varphi_0) + I_l^{(-2)}(\tau, \mu) \sin 2(\varphi - \varphi_0) , \end{aligned}\right\} \tag{284}$$

$$I_r(\tau, \mu, \varphi) = I_r^{(0)}(\tau, \mu) + I_r^{(2)}(\tau, \mu) \cos 2(\varphi - \varphi_0) + I_r^{(-2)}(\tau, \mu) \sin 2(\varphi - \varphi_0), \tag{285}$$

$$\left.\begin{aligned} U(\tau, \mu, \varphi) = {} & U^{(1)}(\tau, \mu) \sin(\varphi - \varphi_0) + U^{(-1)}(\tau, \mu) \cos(\varphi - \varphi_0) \\ & + U^{(2)}(\tau, \mu) \sin 2(\varphi - \varphi_0) + U^{(-2)}(\tau, \mu) \cos 2(\varphi - \varphi_0) , \end{aligned}\right\} \tag{286}$$

and

$$V(\tau, \mu, \varphi) = V^{(0)}(\tau, \mu) + V^{(1)}(\tau, \mu) \cos(\varphi - \varphi_0) . \tag{287}$$

Of the seven systems of equations which arise in this manner, the only one which requires any detailed consideration is the first, which governs the azimuth independent terms, $I_l^{(0)}(\tau, \mu)$ and $I_r^{(0)}(\tau, \mu)$. The other systems present no difficulties. Thus, Systems II–V (Paper XIII, pp. 154–55) governing the various azimuth dependent terms in I_l, I_r, and U admit the first integrals

$$I_l^{(1)}(\tau, \mu) = \mu U^{(1)}(\tau, \mu) ; \qquad I_l^{(-1)}(\tau, \mu) = -\mu U^{(-1)}(\tau, \mu) , \tag{288}$$

and

$$\left.\begin{aligned} I_l^{(2)}(\tau, \mu) &= -\mu^2 I_r^{(2)}(\tau, \mu) = +\tfrac{1}{2}\mu U^{(2)}(\tau, \mu) , \\ I_l^{(-2)}(\tau, \mu) &= -\mu^2 I_r^{(-2)}(\tau, \mu) = -\tfrac{1}{2}\mu U^{(-2)}(\tau, \mu) . \end{aligned}\right\} \tag{289}$$

Moreover, the resulting equations for $U^{(1)}(\tau, \mu)$, $U^{(-1)}(\tau, \mu)$, $I_r^{(2)}(\tau, \mu)$, and $I_r^{(-2)}(\tau, \mu)$ are all such that the analysis of Section I applies without any modifications. Conse-

[14] The symbols l and r now refer to the directions in the meridian plane and at right angles to it, respectively.

[15] See Papers XI (§ 5), XIII (§ 2), XIV (§ 2), and XV (eq. [74]).

[16] Cf. Paper XVI (*Ap. J.*, **105**, 425, 1947), where the functions and constants representing the exact solutions are tabulated.

[17] Paper XIII, Systems I–V (pp. 153–54) and Paper XV, eqs. (78) and (79).

[18] Paper XIII, eqs. (4)–(6) and Paper XV, eq. (77).

quently, we can write down at once the solutions for the corresponding reflected and transmitted intensities. We have (cf. Paper XIII, eqs. [47]–[50])

$$\left.\begin{aligned} I_l^{(1)}(0,\mu) &= +\mu U^{(1)}(0,\mu) \\ &= -\tfrac{3}{4}F_l\mu\mu_0(1-\mu^2)^{\frac{1}{2}}(1-\mu_0^2)^{\frac{1}{2}}[X^{(1)}(\mu)\,X^{(1)}(\mu_0)-Y^{(1)}(\mu)\,Y^{(1)}(\mu_0)]\frac{\mu_0}{\mu_0+\mu}, \end{aligned}\right\} \quad (290)$$

$$\left.\begin{aligned} I_l^{(-1)}(0,\mu) &= -\mu U^{(-1)}(0,\mu) \\ &= -\tfrac{3}{8}U_0\mu(1-\mu^2)^{\frac{1}{2}}(1-\mu_0^2)^{\frac{1}{2}}[X^{(1)}(\mu)\,X^{(1)}(\mu_0)-Y^{(1)}(\mu)\,Y^{(1)}(\mu_0)]\frac{\mu_0}{\mu_0+\mu}, \end{aligned}\right\} \quad (291)$$

$$\left.\begin{aligned} I_l^{(2)}(0,\mu) &= -\mu^2 I_r^{(2)}(0,\mu) = +\tfrac{1}{2}\mu U^{(2)}(0,\mu) \\ &= \tfrac{3}{16}(F_l\mu_0^2-F_r)\,\mu^2[X^{(2)}(\mu)\,X^{(2)}(\mu_0)-Y^{(2)}(\mu)\,Y^{(2)}(\mu_0)]\frac{\mu_0}{\mu_0+\mu}, \end{aligned}\right\} \quad (292)$$

$$\left.\begin{aligned} I_l^{(-2)}(0,\mu) &= -\mu^2 I_r^{(-2)}(0,\mu) = -\tfrac{1}{2}\mu U^{(-2)}(0,\mu) \\ &= \tfrac{3}{16}U_0\mu^2\mu_0[X^{(2)}(\mu)\,X^{(2)}(\mu_0)-Y^{(2)}(\mu)\,Y^{(2)}(\mu_0)]\frac{\mu_0}{\mu_0+\mu}, \end{aligned}\right\} \quad (293)$$

$$\left.\begin{aligned} I_l^{(1)}(\tau_1,-\mu) &= -\mu U^{(1)}(\tau_1,-\mu) \\ &= \tfrac{3}{4}F_l\mu\mu_0(1-\mu^2)^{\frac{1}{2}}(1-\mu_0^2)^{\frac{1}{2}}[X^{(1)}(\mu)\,Y^{(1)}(\mu_0)-Y^{(1)}(\mu)\,X^{(1)}(\mu_0)]\frac{\mu_0}{\mu_0-\mu}, \end{aligned}\right\} \quad (294)$$

$$\left.\begin{aligned} I_l^{(-1)}(\tau_1,-\mu) &= +\mu U^{(-1)}(\tau_1,-\mu) \\ &= \tfrac{3}{8}U_0\mu(1-\mu^2)^{\frac{1}{2}}(1-\mu_0^2)^{\frac{1}{2}}[X^{(1)}(\mu)\,Y^{(1)}(\mu_0)-Y^{(1)}(\mu)\,X^{(1)}(\mu_0)]\frac{\mu_0}{\mu_0-\mu}, \end{aligned}\right\} \quad (295)$$

$$\left.\begin{aligned} I_l^{(2)}(\tau_1,-\mu) &= -\mu^2 I_r^{(2)}(\tau_1,-\mu) = -\tfrac{1}{2}\mu U^{(2)}(\tau_1,-\mu) \\ &= \tfrac{3}{16}(F_l\mu_0^2-F_r)\,\mu^2[X^{(2)}(\mu)\,Y^{(2)}(\mu_0)-Y^{(2)}(\mu)\,X^{(2)}(\mu_0)]\frac{\mu_0}{\mu_0-\mu}, \end{aligned}\right\} \quad (296)$$

and

$$\left.\begin{aligned} I_l^{(-2)}(\tau_1,-\mu) &= -\mu^2 I_r^{(-2)}(\tau_1,-\mu) = +\tfrac{1}{2}\mu U^{(-2)}(\tau_1,-\mu) \\ &= \tfrac{3}{16}U_0\mu^2\mu_0[X^{(2)}(\mu)\,Y^{(2)}(\mu_0)-Y^{(2)}(\mu)\,X^{(2)}(\mu_0)]\frac{\mu_0}{\mu_0-\mu}, \end{aligned}\right\} \quad (297)$$

where $X^{(1)}(\mu)$, $Y^{(1)}(\mu)$, and $X^{(2)}(\mu)$, $Y^{(2)}(\mu)$, are defined as in equations (50), (100), (101), (125), and (126) in terms of the characteristic functions

$$\Psi^{(1)}(\mu) = \tfrac{3}{8}(1-\mu^2)(1+2\mu^2) \qquad \text{and} \qquad \Psi^{(2)}(\mu) = \tfrac{3}{16}(1+\mu^2)^2, \quad (298)$$

respectively.

Similarly, the equations for $V^{(0)}(\tau, \mu)$ and $V^{(1)}(\tau, \mu)$ also do not require any special consideration. The solutions for the reflected and the transmitted intensities are of standard form, and we have

$$V^{(0)}(0, \mu) = -\tfrac{3}{8} V_0 \mu\mu_0 [X_v(\mu) X_v(\mu_0) - Y_v(\mu) Y_v(\mu_0)] \frac{\mu_0}{\mu_0 + \mu}, \quad (299)$$

$$V^{(1)}(0, \mu) = +\tfrac{3}{8} V_0 (1-\mu^2)^{\frac{1}{2}} (1-\mu_0^2)^{\frac{1}{2}} [X_r(\mu) X_r(\mu_0) - Y_r(\mu) Y_r(\mu_0)] \frac{\mu_0}{\mu_0 + \mu}, \quad (300)$$

$$V^{(0)}(\tau_1, -\mu) = \tfrac{3}{8} V_0 \mu\mu_0 [X_v(\mu) Y_v(\mu_0) - Y_v(\mu) X_v(\mu_0)] \frac{\mu_0}{\mu_0 - \mu}, \quad (301)$$

and

$$V^{(1)}(\tau_1, -\mu) = \tfrac{3}{8} V_0 (1-\mu^2)^{\frac{1}{2}} (1-\mu_0^2)^{\frac{1}{2}} [X_r(\mu) Y_r(\mu_0) - Y_r(\mu) X_r(\mu_0)] \frac{\mu_0}{\mu_0 - \mu}, \quad (302)$$

where $X_r(\mu)$, $Y_r(\mu)$ and $X_v(\mu)$, $Y_v(\mu)$ are defined in terms of the characteristic functions

$$\Psi_r(\mu) = \tfrac{3}{8}(1-\mu^2) \qquad \text{and} \qquad \Psi_v(\mu) = \tfrac{3}{4}\mu^2. \quad (303)$$

Finally, it may be noted that in equations (290)–(297) and (299)–(302) πF_l, πF_r, πU_0, and πV_0 represent the fluxes in the four components of the incident beam.

17. *The azimuth independent terms proportional to* F_l.—In the preceding section we have given the solutions for V and the various azimuth dependent terms in the expansions (eqs. [284]–[286]) for I_l, I_r, and U. The azimuth independent terms, $I_l^{(0)}$ and $I_r^{(0)}$, remain to be considered.

Now in the equations (Paper XIII, System I) governing $I_l^{(0)}$ and $I_r^{(0)}$, the inhomogeneous parts consist of two terms proportional, respectively, to F_l and F_r. The solutions for $I_l^{(0)}$ and $I_r^{(0)}$ can therefore be expressed in the forms

$$\left.\begin{aligned} I_l^{(0)}(\tau, \mu) &= I_{ll}^{(0)}(\tau, \mu) + I_{lr}^{(0)}(\tau, \mu) \\ \text{and} \quad I_r^{(0)}(\tau, \mu) &= I_{rl}^{(0)}(\tau, \mu) + I_{rr}^{(0)}(\tau, \mu), \end{aligned}\right\} \quad (304)$$

where $I_{ll}^{(0)}$ and $I_{rl}^{(0)}$ are proportional to F_l and $I_{lr}^{(0)}$ and $I_{rr}^{(0)}$ are proportional to F_r. Considering, first, the terms proportional to F_l, we can express the corresponding terms in the reflected and the transmitted intensities in the following forms:

$$\left.\begin{aligned} I_{ll}^{(0)}(0, \mu) &= \tfrac{3}{16} [S_{ll}(-\mu) - e^{-\tau_1/\mu} T_{ll}(\mu)] F_l, \\ I_{ll}^{(0)}(\tau_1, -\mu) &= \tfrac{3}{16} [T_{ll}(-\mu) - e^{-\tau_1/\mu} S_{ll}(\mu)] F_l, \\ I_{rl}^{(0)}(0, \mu) &= \tfrac{3}{16} [S_{rl}(-\mu) - e^{-\tau_1/\mu} T_{rl}(\mu)] F_l, \\ \text{and} \quad I_{rl}^{(0)}(\tau_1, -\mu) &= \tfrac{3}{16} [T_{rl}(-\mu) - e^{-\tau_1/\mu} S_{rl}(\mu)] F_l, \end{aligned}\right\} \quad (305)$$

where (cf. Paper XIII, eqs. [12] and [13])

$$\left.\begin{aligned} S_{ll}(\mu) = (1-\mu^2)\sum_{\beta=-n+1}^{+n-1}\frac{L_\beta}{1-\kappa_\beta\mu} - L_0\mu + L_n \\ + \sum_{a=-n}^{+n} M_a(1+k_a\mu) + 2(1-\mu^2)\frac{\Gamma}{1-\mu/\mu_0}, \end{aligned}\right\} \tag{306}$$

$$\left.\begin{aligned} T_{ll}(\mu) = (1-\mu^2)\sum_{\beta=-n+1}^{+n-1}\frac{L_\beta e^{-\kappa_\beta\tau_1}}{1+\kappa_\beta\mu} + L_0(\tau_1+\mu) + L_n \\ + \sum_{a=-n}^{+n} M_a(1-k_a\mu)\, e^{-k_a\tau_1} + 2(1-\mu^2)\frac{\Gamma e^{-\tau_1/\mu_0}}{1+\mu/\mu_0}, \end{aligned}\right\} \tag{307}$$

$$S_{rl}(\mu) = -L_0\mu + L_n - \sum_{a=-n}^{+n}\frac{M_a(k_a^2-1)}{1-k_a\mu}, \tag{308}$$

and

$$T_{rl}(\mu) = L_0(\tau_1+\mu) + L_n - \sum_{a=-n}^{+n}\frac{M_a(k_a^2-1)\, e^{-k_a\tau_1}}{1+k_a\mu}. \tag{309}$$

In the foregoing equations the κ_β's ($\beta = \pm 1, \ldots, \pm n \mp 1$) and k_a's ($a = \pm 1, \ldots, \pm n$) are the distinct nonvanishing roots of the characteristic equations

$$1 = \frac{3}{2}\sum_{j=1}^{n}\frac{a_j(1-\mu_j^2)}{1-\kappa^2\mu_j^2} \tag{310}$$

and

$$1 = \frac{3}{4}\sum_{j=1}^{n}\frac{a_j(1-\mu_j^2)}{1-k^2\mu_j^2}, \tag{311}$$

respectively, and

$$\Gamma = H_l(\mu_0)\, H_l(-\mu_0) = \frac{1}{\mu_1^2 \ldots \mu_n^2}\frac{P(\mu_0)\, P(-\mu_0)}{\Omega(\mu_0)}, \tag{312}$$

$$\Omega(\mu) = \prod_{\beta=-n+1}^{+n-1}(1-\kappa_\beta\mu) = \prod_{\beta=1}^{n-1}(1-\kappa_\beta^2\mu^2), \tag{313}$$

and the rest of the symbols have their usual meanings.

The boundary conditions at $\tau = 0$ and $\tau = \tau_1$ require that

$$S_{ll}(\mu_i) = T_{ll}(\mu_i) = S_{rl}(\mu_i) = T_{rl}(\mu_i) = 0 \qquad (i = 1, \ldots, n). \tag{314}$$

By virtue of these boundary conditions we can write

$$S_{ll}(\mu) = \frac{1}{\mu_1^2 \ldots . \mu_n^2} \frac{P(\mu)}{\Omega(\mu)} \frac{1}{1-\mu/\mu_0} s_{ll}(\mu), \tag{315}$$

$$T_{ll}(\mu) = \frac{1}{\mu_1^2 \ldots . \mu_n^2} \frac{P(\mu)}{\Omega(\mu)} \frac{1}{1+\mu/\mu_0} t_{ll}(\mu), \tag{316}$$

$$S_{rl}(\mu) = \frac{1}{\mu_1^2 \ldots . \mu_n^2} \frac{P(\mu)}{W(\mu)} s_{rl}(\mu), \tag{317}$$

and

$$T_{rl}(\mu) = \frac{1}{\mu_1^2 \ldots . \mu_n^2} \frac{P(\mu)}{W(\mu)} t_{rl}(\mu), \tag{318}$$

where $s_{ll}(\mu)$ and $t_{ll}(\mu)$ are polynomials of degree n in μ and $s_{rl}(\mu)$ and $t_{rl}(\mu)$ are polynomials of degree $(n+1)$ in μ.

From equations (305), (306), (312), (315), and (316) it now follows that

$$s_{ll}(\mu_0) = 2(1-\mu_0^2) P(-\mu_0) \quad \text{and} \quad t_{ll}(-\mu_0) = 2(1-\mu_0^2)\, e^{-\tau_1/\mu_0} P(\mu_0). \tag{319}$$

And again from equations (305), (306), (315), and (316) we have

$$\left(1-\frac{1}{\kappa_\beta^2}\right) L_\beta = \frac{1}{\mu_1^2 \ldots . \mu_n^2} \frac{P(1/\kappa_\beta)}{\Omega_\beta(1/\kappa_\beta)} \frac{1}{1-1/\kappa_\beta\mu_0} s_{ll}(1/\kappa_\beta) \quad (\beta = \pm 1, \ldots . , \pm n \mp 1) \tag{320}$$

and

$$\left(1-\frac{1}{\kappa_\beta^2}\right) L_\beta e^{-\kappa_\beta \tau_1} = \frac{1}{\mu_1^2 \ldots . \mu_n^2} \frac{P(-1/\kappa_\beta)}{\Omega_\beta(1/\kappa_\beta)} \frac{1}{1-1/\kappa_\beta\mu_0} t_{ll}(-1/\kappa_\beta) \quad (\beta = \pm 1, \ldots . , \pm n \mp 1). \tag{321}$$

We therefore have $(2n-2)$ relations of the form

$$s_{ll}(1/\kappa_\beta) = e^{\kappa_\beta \tau_1} \frac{P(-1/\kappa_\beta)}{P(+1/\kappa_\beta)} t_{ll}(-1/\kappa_\beta) \qquad (\beta = \pm 1, \ldots . , \pm n \mp 1). \tag{322}$$

However, since $s_{ll}(\mu)$ and $t_{ll}(\mu)$ are polynomials of degree n in μ, we conclude in accordance with theorems 1 and 2 (§ 4) that (cf. eqs. [144] and [145])

$$s_{ll}(\mu) = (\varpi_0 + \chi_0\mu) C_{0,l}(\mu) + (\varpi_1 - \chi_1\mu) C_{1,l}(\mu) \tag{323}$$

and

$$t_{ll}(\mu) = (\varpi_1 + \chi_1\mu) C_{0,l}(\mu) + (\varpi_0 - \chi_0\mu) C_{1,l}(\mu) \tag{324}$$

where ϖ_0, ϖ_1, χ_0, and χ_1 are constants and $C_{0,l}$ and $C_{1,l}$ are polynomials of degree $(n-1)$ in μ defined in the manner of equations (50), (100), (101), (125), and (126) in terms of the roots κ_β $(\beta = 1, \ldots . , n-1)$ of equation (310).

From equations (319), (323), and (324) we now obtain

$$\varpi_0 + \chi_0\mu_0 = \frac{2(1-\mu_0^2)}{[C_{0,l}^2(0) - C_{1,l}^2(0)]\,\Omega(\mu_0)} \times [P(-\mu_0) C_{0,l}(-\mu_0) - e^{-\tau_1/\mu_0} P(\mu_0) C_{1,l}(\mu_0)] \tag{325}$$

and

$$\left.\begin{aligned}\varpi_1 - \chi_1\mu_0 = \frac{2\,(1-\mu_0^2)}{[C_{0,\,l}^2(0) - C_{1,\,l}^2(0)]\,\Omega(\mu_0)} \\ \times\,[\,e^{-\tau_1/\mu_0}P(\mu_0)\,C_{0,\,l}(\mu_0) - P(-\mu_0)\,C_{1,\,l}(-\mu_0)]\,.\end{aligned}\right\} \quad (326)$$

Considering, next, equations (308), (309), (317), and (318), we have

$$M_a = -\frac{1}{\mu_1^2 \ldots . \mu_n^2}\frac{P(1/k_a)}{W_a(1/k_a)(k_a^2-1)}\,s_{rl}(1/k_a) \quad (327)$$

and

$$M_a e^{-k_a\tau_1} = -\frac{1}{\mu_1^2 \ldots . \mu_n^2}\frac{P(-1/k_a)}{W_a(1/k_a)(k_a^2-1)}\,t_{rl}(-1/k_a)\,. \quad (328)$$

We therefore have $2n$ relations of the form

$$s_{rl}(1/k_a) = e^{k_a\tau_1}\frac{P(-1/k_a)}{P(+1/k_a)}\,t_{rl}(-1/k_a) \qquad (a = \pm 1\,,\ldots.,\pm n)\,. \quad (329)$$

It will be recalled that $s_{rl}(\mu)$ and $t_{rl}(\mu)$ are polynomials of degree $(n+1)$ in μ. However, it can be shown that $s_{rl}(\mu) + t_{rl}(\mu)$ is only of degree n; for, according to equations (308), (309), (317), and (318), we have

$$\left.\begin{aligned}\frac{1}{\mu_1^2 \ldots . \mu_n^2}P(\mu)\,s_{rl}(\mu) &= W(\mu)\,S_{rl}(\mu) \\ &= (-1)^n k_1^2 \ldots . k_n^2\,[-L_0\mu^{2n+1} + L_n\mu^{2n} + \ldots .]\end{aligned}\right\} \quad (330)$$

and

$$\left.\begin{aligned}\frac{1}{\mu_1^2 \ldots . \mu_n^2}P(\mu)\,t_{rl}(\mu) &= W(\mu)\,T_{rl}(\mu) \\ &= (-1)^n k_1^2 \ldots . k_n^2\,[+L_0\mu^{2n+1} + (L_0\tau_1 + L_n)\,\mu^{2n} + \ldots .]\,.\end{aligned}\right\} \quad (331)$$

And it is apparent from these equations that the coefficients of μ^{n+1} in $s_{rl}(\mu)$ and $t_{rl}(\mu)$ are of opposite signs. We may therefore write

$$s_{rl}(\mu) = (p_0 + a\mu)\,C_{0,\,r}(\mu) + (p_1 + a\mu)\,C_{1,\,r}(\mu) \quad (332)$$

and

$$t_{rl}(\mu) = (p_1 - a\mu)\,C_{0,\,r}(\mu) + (p_0 - a\mu)\,C_{1,\,r}(\mu)\,, \quad (333)$$

where p_0, p_1, and a are constants and $C_{0,\,r}$ and $C_{1,\,r}$ are defined in terms of the roots of equation (311).

With the forms (332) and (333) for $s_{rl}(\mu)$ and $t_{rl}(\mu)$ we can readily verify that

$$\left.\begin{aligned}P(\mu)\,s_{rl}(\mu) &= +a\,[c_{0,\,r}^{(n)} + c_{1,\,r}^{(n)}]\,\mu^{2n+1} + \Big\{a\,[c_{0,\,r}^{(n-1)} + c_{1,\,r}^{(n-1)}] \\ &\quad + p_0 c_{0,\,r}^{(n)} + p_1 c_{1,\,r}^{(n)} - \Big(\sum_{i=1}^{n}\mu_i\Big)\,a\,[c_{0,\,r}^{(n)} + c_{1,\,r}^{(n)}]\Big\}\mu^{2n} + \ldots .\end{aligned}\right\} \quad (334)$$

and

$$P(\mu)\, t_{rl}(\mu) = -a\,[c^{(n)}_{0,r} + c^{(n)}_{1,r}]\,\mu^{2n+1} + \Big\{ -a\,[c^{(n-1)}_{0,r} + c^{(n-1)}_{1,r}] + p_1 c^{(n)}_{0,r} + p_0 c^{(n)}_{1,r} + \Big(\sum_{i=1}^{n} \mu_i\Big)\, a\,[c^{(n)}_{0,r} + c^{(n)}_{1,r}] \Big\} \mu^{2n} + \ldots\ldots, \tag{335}$$

where $c^{(n)}_{0,r}$, $c^{(n)}_{1,r}$ and $c^{(n-1)}_{0,r}$, $c^{(n-1)}_{1,r}$ are the coefficients of the highest and the next highest powers of μ in $C_{0,r}$ and $C_{1,r}$.

From a comparison of equations (330) and (331) and (334) and (335) we now conclude that

$$-\sum_{i=1}^{n} \mu_i + \frac{1}{c^{(n)}_{0,r} + c^{(n)}_{1,r}} \Big\{ c^{(n-1)}_{0,r} + c^{(n-1)}_{1,r} + \frac{1}{a}\,[p_0 c^{(n)}_{0,r} + p_1 c^{(n)}_{1,r}] \Big\} = -\frac{L_n}{L_0} \tag{336}$$

and

$$-\sum_{i=1}^{n} \mu_i + \frac{1}{c^{(n)}_{0,r} + c^{(n)}_{1,r}} \Big\{ c^{(n-1)}_{0,r} + c^{(n-1)}_{1,r} - \frac{1}{a}\,[p_1 c^{(n)}_{0,r} + p_0 c^{(n)}_{1,r}] \Big\} = \frac{L_n}{L_0} + \tau_1 . \tag{337}$$

From equations (336) and (337) we readily find that

$$a = Q\,(p_0 - p_1)\,, \tag{338}$$

where

$$Q = \frac{c^{(n)}_{0,r} - c^{(n)}_{1,r}}{\Big(\tau_1 + 2\sum_{i=1}^{n} \mu_i\Big)\,[c^{(n)}_{0,r} + c^{(n)}_{1,r}] - 2\,[c^{(n-1)}_{0,r} + c^{(n-1)}_{1,r}]}\,. \tag{339}$$

It will be observed that among the seven constants—ϖ_0, ϖ_1, χ_0, χ_1, p_0, p_1, and a—which occur in the solutions (323), (324), (332), and (333) for s_{ll}, t_{ll}, s_{rl}, and t_{rl}, we have so far obtained only three relations (eqs. [325], [326], and [338]). We therefore require four more relations to make the problem determinate. To obtain these additional relations we proceed in the following manner:

Putting $\mu = +1$, respectively, -1 in equations (306) and (307), we have

$$S_{ll}(\pm 1) = \mp L_0 + L_n + \sum_{a=-n}^{+n} M_a\,(1 \pm k_a) \tag{340}$$

and

$$T_{ll}(\pm 1) = L_0\,(\tau_1 \pm 1) + L_n + \sum_{a=-n}^{+n} M_a\,(1 \mp k_a)\; e^{-k_a \tau_1}\,. \tag{341}$$

Similarly, putting $\mu = 0$ in equations (308) and (309), we have

$$S_{rl}(0) = L_n - \sum_{a=-n}^{+n} M_a\,(k_a^2 - 1) \tag{342}$$

and

$$T_{rl}(0) = L_0 \tau_1 + L_n - \sum_{a=-n}^{+n} M_a\,(k_a^2 - 1)\; e^{-k_a \tau_1}\,. \tag{343}$$

Combining equations (340)–(343) appropriately, we obtain the following relations:

$$\tfrac{1}{2}\,[S_{ll}(+1) + S_{ll}(-1)] - S_{rl}(0) = \sum_{a=-n}^{+n} M_a k_a^2, \tag{344}$$

$$\tfrac{1}{2}\,[T_{ll}(+1) + T_{ll}(-1)] - T_{rl}(0) = \sum_{a=-n}^{+n} M_a k_a^2 e^{-k_a\tau_1}, \tag{345}$$

$$\left.\begin{aligned} \tfrac{1}{2}\,[S_{ll}(+1) - S_{ll}(-1)] + \tfrac{1}{2}\,[T_{ll}(+1) - T_{ll}(-1)] \\ = \sum_{a=-n}^{+n} M_a k_a - \sum_{a=-n}^{+n} M_a k_a e^{-k_a\tau_1}, \end{aligned}\right\} \tag{346}$$

and

$$\left.\begin{aligned} \tau_1\Big\{\tfrac{1}{2}\,[S_{ll}(+1) - S_{ll}(-1)] - \tfrac{1}{2}\,[T_{ll}(+1) - T_{ll}(-1)] \\ - \sum_{a=-n}^{+n} M_a k_a - \sum_{a=-n}^{+n} M_a k_a e^{-k_a\tau_1}\Big\} = 2\Big\{\tfrac{1}{2}\,[S_{ll}(+1) + S_{ll}(-1)] \\ - \tfrac{1}{2}\,[T_{ll}(+1) + T_{ll}(-1)] - \sum_{a=-n}^{+n} M_a + \sum_{a=-n}^{+n} M_a e^{-k_a\tau_1}\Big\} = -2L_0\tau_1. \end{aligned}\right\} \tag{347}$$

We shall now show how the foregoing equations provide the required additional relations between the constants ϖ_0, ϖ_1, χ_0, χ_1, p_0, p_1, and a. However, we must first evaluate the summations

$$\sum_{a=-n}^{+n} M_a k_a^m \quad \text{and} \quad \sum_{a=-n}^{+n} M_a k_a^m e^{-k_a\tau_1} \qquad (m = 0,\ 1,\ 2), \tag{348}$$

which occur in these equations.

Considering the summation $\Sigma M_a k_a^m$, for example, we have (cf. eq. [327])

$$\sum_{a=-n}^{+n} M_a k_a^m = -\frac{1}{\mu_1^2 \ldots \mu_n^2} \sum_{a=-n}^{+n} \frac{P(1/k_a)\, s_{rl}(1/k_a)}{k_a^{2-m}(1-k_a^{-2})\, W_a(1/k_a)}. \tag{349}$$

In terms of the function

$$f_m(x) = \sum_{a=-n}^{+n} \frac{P(1/k_a)\, s_{rl}(1/k_a)}{k_a^{2-m}(1-k_a^{-2})\, W_a(1/k_a)}\, W_a(x), \tag{350}$$

we can therefore express $\Sigma M_a k_a^m$ as

$$\sum_{a=-n}^{+n} M_a k_a^m = -\frac{1}{\mu_1^2 \ldots \mu_n^2}\, f_m(0). \tag{351}$$

Now $f_m(x)$ is a polynomial of degree $(2n-1)$ in x, which takes the values

$$\frac{P(1/k_a)\, s_{rl}(1/k_a)}{k_a^{2-m}(1-k_a^{-2})} \tag{352}$$

for $x = 1/k_a$ ($a = \pm 1, \ldots, \pm n$). There must, accordingly, exist a relation of the form

$$(1 - x^2)\, f_m(x) - x^{2-m} P(x)\, s_{rl}(x) = W(x)\, g_m(x) \qquad (m = 0, 1, 2), \quad (353)$$

where $g_m(x)$ is a polynomial of degree $3 - m$ in x. To determine $g_m(x)$ more explicitly, we must consider each case separately. We shall illustrate the procedure by considering the case $m = 0$.

For $m = 0$, equation (353) becomes

$$(1 - x^2)\, f_0(x) - x^2 P(x)\, s_{rl}(x) = W(x)\,(A x^3 + B x^2 + D x + E), \quad (354)$$

where A, B, D, and E are certain constants to be determined. The constants A and B follow directly from a comparison of the coefficients of x^{2n+3} and x^{2n+2} on either side of equation (354). We find (cf. eq. [334])

$$A = (-1)^{n+1} \frac{a\,[c_{0,r}^{(n)} + c_{1,r}^{(n)}]}{k_1^2 \ldots k_n^2} \quad (355)$$

and

$$B = \frac{(-1)^{n+1}}{k_1^2 \ldots k_n^2} \left\{ a\,[c_{0,r}^{(n-1)} + c_{1,r}^{(n-1)}] + p_0 c_{0,r}^{(n)} + p_1 c_{1,r}^{(n)} - \left(\sum_{i=1}^{n} \mu_i \right) a\,[c_{0,r}^{(n)} + c_{1,r}^{(n)}] \right\}. \quad (356)$$

Next, putting $x = 1$, respectively -1, in equation (354), we have

$$-P(\pm 1)\, s_{rl}(\pm 1) = W(1)\,(\pm A + B \pm D + E). \quad (357)$$

From this equation it follows that

$$B + E = -\frac{1}{2W(1)} [P(+1)\, s_{rl}(+1) + P(-1)\, s_{rl}(-1)]. \quad (358)$$

Hence

$$f_0(0) = \frac{(-1)^n}{k_1^2 \ldots k_n^2} \left\{ a\,[c_{0,r}^{(n-1)} + c_{1,r}^{(n-1)}] + p_0 c_{0,r}^{(n)} + p_1 c_{1,r}^{(n)} - \left(\sum_{i=1}^{n} \mu_i \right) \times a\,[c_{0,r}^{(n)} + c_{1,r}^{(n)}] \right\} - \frac{1}{2W(1)} [P(+1)\, s_{rl}(+1) + P(-1)\, s_{rl}(-1)]. \quad (359)$$

Inserting this value of $f_0(0)$ in equation (351) and making use of the relations (cf. Paper X, eq. [143] and Paper XI, n. 16)

$$k_1^2 \ldots k_n^2 \mu_1^2 \ldots \mu_n^2 = \tfrac{1}{2} \quad (360)$$

and

$$\frac{1}{\mu_1^2 \ldots \mu_n^2} \frac{P(+1) P(-1)}{W(1)} = 4, \quad (361)$$

we obtain

$$\sum_{a=-n}^{+n} M_a = (-1)^{n+1} 2 \left\{ a\,[c_{0,r}^{(n-1)} + c_{1,r}^{(n-1)}] + p_0 c_{0,r}^{(n)} + p_1 c_{1,r}^{(n)} - \left(\sum_{i=1}^{n} \mu_i \right) a\,[c_{0,r}^{(n)} + c_{1,r}^{(n)}] \right\} + 2 \left[\frac{s_{rl}(+1)}{P(-1)} + \frac{s_{rl}(-1)}{P(+1)} \right]. \quad (362)$$

The other summations can be similarly evaluated. We find

$$\sum_{\alpha=-n}^{+n} M_\alpha k_\alpha = (-1)^{n+1} 2a\,[c^{(n)}_{0,r} + c^{(n)}_{1,r}] + 2\left[\frac{s_{rl}(+1)}{P(-1)} - \frac{s_{rl}(-1)}{P(+1)}\right], \quad (363)$$

$$\sum_{\alpha=-n}^{+n} M_\alpha k_\alpha^2 = (-1)^{n+1} \frac{s_{rl}(0)}{\mu_1 \cdot \cdots \cdot \mu_n} + 2\left[\frac{s_{rl}(+1)}{P(-1)} + \frac{s_{rl}(-1)}{P(+1)}\right], \quad (364)$$

$$\left.\begin{aligned}\sum_{\alpha=-n}^{+n} M_\alpha e^{-k_\alpha \tau_1} = (-1)^{n+1} 2 \Big\{ &- a\,[c^{(n-1)}_{0,r} + c^{(n-1)}_{1,r}] + p_1 c^{(n)}_{0,r} + p_0 c^{(n)}_{1,r} \\ &+ \Big(\sum_{i=1}^{n} \mu_i\Big) a\,[c^{(n)}_{0,r} + c^{(n)}_{1,r}] \Big\} + 2\left[\frac{t_{rl}(+1)}{P(-1)} + \frac{t_{rl}(-1)}{P(+1)}\right],\end{aligned}\right\} \quad (365)$$

$$\sum_{\alpha=-n}^{+n} M_\alpha k_\alpha e^{-k_\alpha \tau_1} = (-1)^{n+1} 2a\,[c^{(n)}_{0,r} + c^{(n)}_{1,r}] - 2\left[\frac{t_{rl}(+1)}{P(-1)} - \frac{t_{rl}(-1)}{P(+1)}\right], \quad (366)$$

and

$$\sum_{\alpha=-n}^{+n} M_\alpha k_\alpha^2 e^{-k_\alpha \tau_1} = (-1)^{n+1} \frac{t_{rl}(0)}{\mu_1 \cdot \cdots \cdot \mu_n} + 2\left[\frac{t_{rl}(+1)}{P(-1)} + \frac{t_{rl}(-1)}{P(+1)}\right]. \quad (367)$$

A relation which follows from equations (362) and (365) may be noted here. We have

$$\left.\begin{aligned}\sum_{\alpha=-n}^{+n} M_\alpha - \sum_{\alpha=-n}^{+n} M_\alpha e^{-k_\alpha \tau_1} = 2\left[\frac{s_{rl}(+1)}{P(-1)} + \frac{s_{rl}(-1)}{P(+1)}\right] - 2\left[\frac{t_{rl}(+1)}{P(-1)} + \frac{t_{rl}(-1)}{P(+1)}\right] \\ + (-1)^{n+1} 2 \Big\{ 2a\,[c^{(n-1)}_{0,r} + c^{(n-1)}_{1,r}] + (p_0 - p_1)\,[c^{(n)}_{0,r} - c^{(n)}_{1,r}] - 2\Big(\sum_{i=1}^{n} \mu_i\Big) a\,[c^{(n)}_{0,r} + c^{(n)}_{1,r}] \Big\},\end{aligned}\right\} \quad (368)$$

or, substituting for $(p_0 - p_1)$ according to equations (338) and (339), we have

$$\left.\begin{aligned}\sum_{\alpha=-n}^{+n} M_\alpha - \sum_{\alpha=-n}^{+n} M_\alpha e^{-k_\alpha \tau_1} = (-1)^{n+1} 2a\,[c^{(n)}_{0,r} + c^{(n)}_{1,r}]\,\tau_1 \\ + 2\left[\frac{s_{rl}(+1)}{P(-1)} + \frac{s_{rl}(-1)}{P(+1)}\right] - 2\left[\frac{t_{rl}(+1)}{P(-1)} + \frac{t_{rl}(-1)}{P(+1)}\right].\end{aligned}\right\} \quad (369)$$

Returning to equations (344)–(347), we first observe that (cf. eqs. [317] and [318])

$$S_{rl}(0) = \frac{(-1)^n}{\mu_1 \cdot \cdots \cdot \mu_n}\, s_{rl}(0) \qquad \text{and} \qquad T_{rl}(0) = \frac{(-1)^n}{\mu_1 \cdot \cdots \cdot \mu_n}\, t_{rl}(0). \quad (370)$$

From equations (344), (345), (364), (367), and (370) it now follows that

$$\tfrac{1}{2}\,[S_{ll}(+1) + S_{ll}(-1)] = 2\left[\frac{s_{rl}(+1)}{P(-1)} + \frac{s_{rl}(-1)}{P(+1)}\right] \quad (371)$$

and

$$\tfrac{1}{2}\,[T_{ll}(+1) + T_{ll}(-1)] = 2\left[\frac{t_{rl}(+1)}{P(-1)} + \frac{t_{rl}(-1)}{P(+1)}\right]. \quad (372)$$

Similarly, from equations (346), (363), and (366) we have

$$\left.\begin{aligned}&\tfrac{1}{2}\,[S_{II}(+1)-S_{II}(-1)]+\tfrac{1}{2}\,[T_{II}(+1)-T_{II}(-1)]\\&\qquad=2\left[\frac{s_{rI}(+1)}{P(-1)}-\frac{s_{rI}(-1)}{P(+1)}\right]+2\left[\frac{t_{rI}(+1)}{P(-1)}-\frac{t_{rI}(-1)}{P(+1)}\right].\end{aligned}\right\}\tag{373}$$

And, finally, from equations (347), (363), (366), and (369) we have

$$\left.\begin{aligned}&\tau_1\left\{\tfrac{1}{2}[S_{II}(+1)-S_{II}(-1)]-\tfrac{1}{2}[T_{II}(+1)-T_{II}(-1)]-2\left[\frac{s_{rI}(+1)}{P(-1)}-\frac{s_{rI}(-1)}{P(+1)}\right]\right.\\&\left.+2\left[\frac{t_{rI}(+1)}{P(-1)}-\frac{t_{rI}(-1)}{P(+1)}\right]\right\}=2\left\{\tfrac{1}{2}[S_{II}(+1)+S_{II}(-1)]-\tfrac{1}{2}[T_{II}(+1)+T_{II}(-1)]\right.\\&\left.\qquad-2\left[\frac{s_{rI}(+1)}{P(-1)}+\frac{s_{rI}(-1)}{P(+1)}\right]+2\left[\frac{t_{rI}(+1)}{P(-1)}+\frac{t_{rI}(-1)}{P(+1)}\right]\right\}.\end{aligned}\right\}\tag{374}$$

But, according to equations (371) and (372), the right-hand side of equation (374) vanishes ($\tau_1 \neq 0$). Hence

$$\left.\begin{aligned}&\tfrac{1}{2}\,[S_{II}(+1)-S_{II}(-1)]-\tfrac{1}{2}\,[T_{II}(+1)-T_{II}(-1)]\\&\qquad=2\left[\frac{s_{rI}(+1)}{P(-1)}-\frac{s_{rI}(-1)}{P(+1)}\right]-2\left[\frac{t_{rI}(+1)}{P(-1)}-\frac{t_{rI}(-1)}{P(+1)}\right].\end{aligned}\right\}\tag{375}$$

From equations (371), (372), (373), and (375) it is now apparent that

$$S_{II}(\pm 1)=4\,\frac{s_{rI}(\pm 1)}{P(\mp 1)}\qquad\text{and}\qquad T_{II}(\pm 1)=4\,\frac{t_{rI}(\pm 1)}{P(\mp 1)}.\tag{376}$$

On the other hand, according to equations (315) and (316),

$$\left.\begin{aligned}S_{II}(\pm 1)&=\frac{1}{\mu_1^2\cdot\cdots\cdot\mu_n^2}\,\frac{P(\pm 1)}{\Omega(1)}\,\frac{1}{1\mp\dfrac{1}{\mu_0}}\,s_{II}(\pm 1),\\ \text{and}\qquad T_{II}(\pm 1)&=\frac{1}{\mu_1^2\cdot\cdots\cdot\mu_n^2}\,\frac{P(\pm 1)}{\Omega(1)}\,\frac{1}{1\pm\dfrac{1}{\mu_0}}\,t_{II}(\pm 1).\end{aligned}\right\}\tag{377}$$

The foregoing equations can be simplified by making use of the relation (Paper XI, n. 16)

$$\frac{1}{\mu_1^2\cdot\cdots\cdot\mu_n^2}\,\frac{P(+1)P(-1)}{\Omega(1)}=-2.\tag{378}$$

We thus find

$$S_{II}(\pm 1)=-\frac{2}{1\mp\dfrac{1}{\mu_0}}\,\frac{s_{II}(\pm 1)}{P(\mp 1)}=4\,\frac{s_{rI}(\pm 1)}{P(\mp 1)}\tag{379}$$

and

$$T_{II}(\pm 1)=-\frac{2}{1\pm\dfrac{1}{\mu_0}}\,\frac{t_{II}(\pm 1)}{P(\mp 1)}=4\,\frac{t_{rI}(\pm 1)}{P(\mp 1)}.\tag{380}$$

Hence

$$\mu_0 s_{ll}(\pm 1) = \pm 2(1 \mp \mu_0)\, s_{rl}(\pm 1), \tag{381}$$

and

$$\mu_0 t_{ll}(\pm 1) = \mp 2(1 \pm \mu_0)\, t_{rl}(\pm 1), \tag{382}$$

or, alternatively,

$$(1 \pm \mu_0)\, s_{ll}(\pm 1) = \pm \frac{2}{\mu_0}(1 - \mu_0^2)\, s_{rl}(\pm 1), \tag{383}$$

and

$$(1 \mp \mu_0)\, t_{ll}(\pm 1) = \mp \frac{2}{\mu_0}(1 - \mu_0^2)\, t_{rl}(\pm 1). \tag{384}$$

We shall find it convenient to combine equations (383) and (384) in the following forms:

$$+(1+\mu_0)\, s_{ll}(+1) \mp (1-\mu_0)\, t_{ll}(+1) = \frac{2}{\mu_0}(1-\mu_0^2)\,[\, s_{rl}(+1) \pm t_{rl}(+1)\,] \tag{385}$$

and

$$-(1-\mu_0)\, s_{ll}(-1) \pm (1+\mu_0)\, t_{ll}(-1) = \frac{2}{\mu_0}(1-\mu_0^2)\,[\, s_{rl}(-1) \pm t_{rl}(-1)\,]. \tag{386}$$

We now have to substitute for $s_{ll}(\pm 1)$, $t_{ll}(\pm 1)$, $s_{rl}(\pm 1)$, and $t_{rl}(\pm 1)$ according to equations (323), (324), (332), and (333). For this purpose, we shall write these quantities in the following forms:

$$\left.\begin{aligned} s_{ll}(\pm 1) = {} & (\varpi_0 + \chi_0\mu_0)\, C_{0,\,l}(\pm 1) + (\varpi_1 - \chi_1\mu_0)\, C_{1,\,l}(\pm 1) \\ & + (1 \mp \mu_0)\,[\, \pm \chi_0 C_{0,\,l}(\pm 1) \mp \chi_1 C_{1,\,l}(\pm 1)\,], \end{aligned}\right\} \tag{387}$$

$$\left.\begin{aligned} t_{ll}(\pm 1) = {} & (\varpi_0 + \chi_0\mu_0)\, C_{1,\,l}(\pm 1) + (\varpi_1 - \chi_1\mu_0)\, C_{0,\,l}(\pm 1) \\ & + (1 \pm \mu_0)\,[\, \mp \chi_0 C_{1,\,l}(\pm 1) \pm \chi_1 C_{0,\,l}(\pm 1)\,], \end{aligned}\right\} \tag{388}$$

$$s_{rl}(\pm 1) = p_0 C_{0,\,r}(\pm 1) + p_1 C_{1,\,r}(\pm 1) \pm a\,[C_{0,\,r}(\pm 1) + C_{1,\,r}(\pm 1)\,], \tag{389}$$

and

$$t_{rl}(\pm 1) = p_0 C_{1,\,r}(\pm 1) + p_1 C_{0,\,r}(\pm 1) \mp a\,[C_{0,\,r}(\pm 1) + C_{1,\,r}(\pm 1)\,]. \tag{390}$$

Substituting from equations (387)–(390) in equations (385) and (386), we find, after some lengthy, but straightforward, reductions, that

$$\left.\begin{aligned} \frac{2}{\mu_0}(1-\mu_0^2)\, c_1(p_0+p_1) = {} & \mathfrak{A}_l(\gamma_2 + \gamma_1\mu_0) + \mathfrak{B}_l(-\gamma_2 + \gamma_1\mu_0) \\ & + (1-\mu_0^2)\,\gamma_1(\chi_0 - \chi_1), \end{aligned}\right\} \tag{391}$$

$$\left.\begin{aligned} \frac{2}{\mu_0}(1-\mu_0^2)\, c_3(p_0+p_1) = {} & \mathfrak{A}_l(-\gamma_4 + \gamma_3\mu_0) + \mathfrak{B}_l(\gamma_4 + \gamma_3\mu_0) \\ & + (1-\mu_0^2)\,\gamma_3(\chi_0 - \chi_1), \end{aligned}\right\} \tag{392}$$

$$\left.\begin{aligned} \frac{2}{\mu_0}(1-\mu_0^2)\,[\, c_2(p_0 - p_1) + 2a\, c_1] = {} & \frac{2}{\mu_0}(1-\mu_0^2)\,(c_2 + 2\, c_1 Q)\,(p_0 - p_1) \\ = {} & \mathfrak{A}_l(\gamma_1 + \gamma_2\mu_0) + \mathfrak{B}_l(\gamma_1 - \gamma_2\mu_0) + (1-\mu_0^2)\,\gamma_2(\chi_0 + \chi_1), \end{aligned}\right\} \tag{393}$$

and

$$\left.\begin{aligned}\frac{2}{\mu_0}(1-\mu_0^2)\,[c_4(p_0-p_1)-2ac_3] &= \frac{2}{\mu_0}(1-\mu_0^2)(c_4-2c_3Q)(p_0-p_1)\\ &= \mathfrak{A}_l(-\gamma_3+\gamma_4\mu_0)+\mathfrak{B}_l(-\gamma_3-\gamma_4\mu_0)+(1-\mu_0^2)\gamma_4(\chi_0+\chi_1),\end{aligned}\right\} \tag{394}$$

where we have used the following abbreviations:

$$\mathfrak{A}_l=\varpi_0+\chi_0\mu_0 \quad \text{and} \quad \mathfrak{B}_l=\varpi_1-\chi_1\mu_0\,, \tag{395}$$

and

$$\left.\begin{aligned}\gamma_1&=C_{0,\,l}(+1)+C_{1,\,l}(+1); & c_1&=C_{0,\,r}(+1)+C_{1,\,r}(+1),\\ \gamma_2&=C_{0,\,l}(+1)-C_{1,\,l}(+1); & c_2&=C_{0,\,r}(+1)-C_{1,\,r}(+1),\\ \gamma_3&=C_{0,\,l}(-1)+C_{1,\,l}(-1); & c_3&=C_{0,\,r}(-1)+C_{1,\,r}(-1),\\ \gamma_4&=C_{0,\,l}(-1)-C_{1,\,l}(-1); & c_4&=C_{0,\,r}(-1)-C_{1,\,r}(-1).\end{aligned}\right\} \tag{396}$$

Eliminating $(\chi_0-\chi_1)$ from equations (391) and (392) and $(\chi_0+\chi_1)$ from equations (393) and (394), we find

$$\frac{2}{\mu_0}(1-\mu_0^2)(p_0+p_1)=\frac{\gamma_1\gamma_4+\gamma_2\gamma_3}{c_3\gamma_1-c_1\gamma_3}(\mathfrak{B}_l-\mathfrak{A}_l) \tag{397}$$

and

$$\frac{2}{\mu_0}(1-\mu_0^2)(p_0-p_1)=\frac{\gamma_1\gamma_4+\gamma_2\gamma_3}{(c_2\gamma_4-c_4\gamma_2)+2Q(c_1\gamma_4+c_3\gamma_2)}(\mathfrak{B}_l+\mathfrak{A}_l)\,. \tag{398}$$

Similarly, eliminating (p_0+p_1) from equations (391) and (392) and (p_0-p_1) from equations (393) and (394), we find

$$(1-\mu_0^2)(\chi_1-\chi_0)=\mathfrak{A}_l\left[\mu_0+\frac{c_3\gamma_2+c_1\gamma_4}{c_3\gamma_1-c_1\gamma_3}\right]+\mathfrak{B}_l\left[\mu_0-\frac{c_3\gamma_2+c_1\gamma_4}{c_3\gamma_1-c_1\gamma_3}\right] \tag{399}$$

and

$$\left.\begin{aligned}(1-\mu_0^2)(\chi_1+\chi_0)=\mathfrak{A}_l&\left[-\mu_0+\frac{c_4\gamma_1+c_2\gamma_3-2Q(c_3\gamma_1-c_1\gamma_3)}{c_2\gamma_4-c_4\gamma_2+2Q(c_1\gamma_4+c_3\gamma_2)}\right]\\ &+\mathfrak{B}_l\left[\mu_0+\frac{c_4\gamma_1+c_2\gamma_3-2Q(c_3\gamma_1-c_1\gamma_3)}{c_2\gamma_4-c_4\gamma_2+2Q(c_1\gamma_4+c_3\gamma_2)}\right].\end{aligned}\right\} \tag{400}$$

Finally, solving equations (397) and (398) for p_0 and p_1 and equations (399) and (400) for χ_0 and χ_1, we find that these constants can be expressed in the following forms:

$$\frac{2}{\mu_0}(1-\mu_0^2)\,p_0=-\nu_2(\varpi_0+\chi_0\mu_0)+\nu_1(\varpi_1-\chi_1\mu_0)\,, \tag{401}$$

$$\frac{2}{\mu_0}(1-\mu_0^2)\,p_1=-\nu_1(\varpi_0+\chi_0\mu_0)+\nu_2(\varpi_1-\chi_1\mu_0)\,, \tag{402}$$

$$(1-\mu_0^2)\,\chi_0=-(\mu_0+\nu_4)(\varpi_0+\chi_0\mu_0)+\nu_3(\varpi_1-\chi_1\mu_0)\,, \tag{403}$$

and

$$(1-\mu_0^2)\,\chi_1=+\nu_3(\varpi_0+\chi_0\mu_0)+(\mu_0-\nu_4)(\varpi_1-\chi_1\mu_0)\,, \tag{404}$$

where

$$\nu_1 = \tfrac{1}{2}(\gamma_1\gamma_4 + \gamma_2\gamma_3)\left[\frac{1}{c_3\gamma_1 - c_1\gamma_3} + \frac{1}{c_2\gamma_4 - c_4\gamma_2 + 2Q(c_1\gamma_4 + c_3\gamma_2)}\right], \quad (405)$$

$$\nu_2 = \tfrac{1}{2}(\gamma_1\gamma_4 + \gamma_2\gamma_3)\left[\frac{1}{c_3\gamma_1 - c_1\gamma_3} - \frac{1}{c_2\gamma_4 - c_4\gamma_2 + 2Q(c_1\gamma_4 + c_3\gamma_2)}\right], \quad (406)$$

$$\nu_3 = \frac{1}{2}\left[\frac{c_3\gamma_2 + c_1\gamma_4}{c_3\gamma_1 - c_1\gamma_3} + \frac{c_4\gamma_1 + c_2\gamma_3 - 2Q(c_3\gamma_1 - c_1\gamma_3)}{c_2\gamma_4 - c_4\gamma_2 + 2Q(c_1\gamma_4 + c_3\gamma_2)}\right], \quad (407)$$

and

$$\nu_4 = \frac{1}{2}\left[\frac{c_3\gamma_2 + c_1\gamma_4}{c_3\gamma_1 - c_1\gamma_3} - \frac{c_4\gamma_1 + c_2\gamma_3 - 2Q(c_3\gamma_1 - c_1\gamma_3)}{c_2\gamma_4 - c_4\gamma_2 + 2Q(c_1\gamma_4 + c_3\gamma_2)}\right]. \quad (408)$$

Also, according to equations (338), (401), and (402) (or more directly from eq. [398]), we have

$$\frac{2}{\mu_0}(1 - \mu_0^2)\, a = Q(\nu_1 - \nu_2)\left[(\varpi_0 + \chi_0\mu_0) + (\varpi_1 - \chi_1\mu_0)\right]. \quad (409)$$

Since $(\varpi_0 + \chi_0\mu_0)$ and $(\varpi_1 - \chi_1\mu_0)$ are already known (eqs. [325] and [326]), the foregoing equations complete the solution of the formal problem.

Returning to equations (305) we first observe that, for $s_{ll}(\mu)$ and $t_{ll}(\mu)$ given by equations (323) and (324), the constants $\varpi_0 + \chi_0\mu_0$, $\varpi_1 - \chi_1\mu_0$, χ_0, and χ_1 must enter the equations governing the angular distributions of the reflected and the transmitted radiations in the component l in the manner of $p_0 + q_0\mu_0$, $p_1 - q_1\mu_0$, q_0, and q_1 in equations (194) and (195). With the expressions for $\varpi_0 + \chi_0\mu_0$, $\varpi_1 - \chi_1\mu_0$, χ_0, and χ_1 given by equations (325), (326), (403), and (404), we therefore have

$$\left.\begin{aligned} I_{ll}(0, \mu) = \tfrac{3}{16}F_l\frac{2\mu_0}{\mu_0 + \mu}\{ &(1 - \mu_0^2)\left[X_l(\mu)\, X_l(\mu_0) - Y_l(\mu)\, Y_l(\mu_0)\right] \\ &- (\mu_0 + \mu)\, X_l(\mu)\left[-(\mu_0 + \nu_4)\, X_l(\mu_0) + \nu_3 Y_l(\mu_0)\right] \\ &- (\mu_0 + \mu)\, Y_l(\mu)\left[\nu_3 X_l(\mu_0) + (\mu_0 - \nu_4)\, Y_l(\mu_0)\right]\} \end{aligned}\right\} \quad (410)$$

and

$$\left.\begin{aligned} I_{ll}(\tau_1, -\mu) = \tfrac{3}{16}F_l\frac{2\mu_0}{\mu_0 - \mu}\{ &(1 - \mu_0^2)\left[X_l(\mu)\, Y_l(\mu_0) - Y_l(\mu)\, X_l(\mu_0)\right] \\ &+ (\mu_0 - \mu)\, X_l(\mu)\left[\nu_3 X_l(\mu_0) + (\mu_0 - \nu_4)\, Y_l(\mu_0)\right] \\ &+ (\mu_0 - \mu)\, Y_l(\mu)\left[-(\mu_0 + \nu_4)\, X_l(\mu_0) + \nu_3 Y_l(\mu_0)\right]\}, \end{aligned}\right\} \quad (411)$$

where $X_l(\mu)$ amd $Y_l(\mu)$ are defined in terms of $C_{0,l}(\mu)$ and $C_{1,l}(\mu)$ (cf. eqs. [125] and [126]). Equations (410) and (411) can be reduced to the forms

$$\left.\begin{aligned} I_{ll}(0, \mu) = \tfrac{3}{16}F_l\frac{2\mu_0}{\mu_0 + \mu}\{ &X_l(\mu)\, X_l(\mu_0)\left[1 + \nu_4(\mu_0 + \mu) + \mu\mu_0\right] \\ &- Y_l(\mu)\, Y_l(\mu_0)\left[1 - \nu_4(\mu_0 + \mu) + \mu\mu_0\right] \\ &- \nu_3(\mu_0 + \mu)\left[X_l(\mu)\, Y_l(\mu_0) + Y_l(\mu)\, X_l(\mu_0)\right]\} \end{aligned}\right\} \quad (412)$$

and

$$\left.\begin{aligned} I_{ll}(\tau_1, -\mu) = \tfrac{3}{16}F_l\frac{2\mu_0}{\mu_0 - \mu}\{ &X_l(\mu)\, Y_l(\mu_0)\left[1 - \nu_4(\mu_0 - \mu) - \mu\mu_0\right] \\ &- Y_l(\mu)\, X_l(\mu_0)\left[1 + \nu_4(\mu_0 - \mu) - \mu\mu_0\right] \\ &+ \nu_3(\mu_0 - \mu)\left[X_l(\mu)\, X_l(\mu_0) + Y_l(\mu)\, Y_l(\mu_0)\right]\}. \end{aligned}\right\} \quad (413)$$

Turning, next, to the reflected and the transmitted intensities in the component r, we have (cf. eqs. [305], [332], and [333])

$$\left.\begin{aligned} I_{rl}(0,\mu) = \tfrac{3}{16}F_l \frac{(-1)^n}{\mu_1 \cdots \mu_n}[C^2_{0,r}(0) - C^2_{1,r}(0)]^{\frac{1}{2}} \\ \times [(p_0 - a\mu)\, X_r(\mu) - (p_1 - a\mu)\, Y_r(\mu)] \end{aligned}\right\} \quad (414)$$

and

$$\left.\begin{aligned} I_{rl}(\tau_1,-\mu) = \tfrac{3}{16}F_l \frac{(-1)^n}{\mu_1 \cdots \mu_n}[C^2_{0,r}(0) - C^2_{1,r}(0)]^{\frac{1}{2}} \\ \times [(p_1 + a\mu)\, X_r(\mu) - (p_0 + a\mu)\, Y_r(\mu)], \end{aligned}\right\} \quad (415)$$

where $X_r(\mu)$ and $Y_r(\mu)$ are defined in terms of $C_{0,r}(\mu)$ and $C_{1,r}(\mu)$. Substituting for p_0, p_1, and a from equations (401), (402), and (409) in the foregoing equations, we find, after some minor rearrangement of the terms,

$$\left.\begin{aligned} I_{rl}(0,\mu) = \tfrac{3}{16}F_l\left[\frac{C^2_{0,r}(0) - C^2_{1,r}(0)}{C^2_{0,l}(0) - C^2_{1,l}(0)}\right]^{\frac{1}{2}} \mu_0 \{\nu_1 [X_r(\mu)\, Y_l(\mu_0) + Y_r(\mu)\, X_l(\mu_0)] \\ - \nu_2 [X_r(\mu)\, X_l(\mu_0) + Y_r(\mu)\, Y_l(\mu_0)] \\ - Q(\nu_1 - \nu_2)\,\mu [X_r(\mu) - Y_r(\mu)][X_l(\mu_0) + Y_l(\mu_0)]\} \end{aligned}\right\} \quad (416)$$

and

$$\left.\begin{aligned} I_{rl}(\tau_1,-\mu) = \tfrac{3}{16}F_l\left[\frac{C^2_{0,r}(0) - C^2_{1,r}(0)}{C^2_{0,l}(0) - C^2_{1,l}(0)}\right]^{\frac{1}{2}} \mu_0 \{\nu_2 [X_r(\mu)\, Y_l(\mu_0) + Y_r(\mu)\, X_l(\mu_0)] \\ - \nu_1 [X_r(\mu)\, X_l(\mu_0) + Y_r(\mu)\, Y_l(\mu_0)] \\ + Q(\nu_1 - \nu_2)\,\mu [X_r(\mu) - Y_r(\mu)][X_l(\mu_0) + Y_l(\mu_0)]\}. \end{aligned}\right\} \quad (417)$$

18. *The azimuth independent terms proportional to* F_r.—In the preceding section we completed the solution for the azimuth independent terms in the reflected and transmitted intensities which are proportional to F_l. We shall now consider the terms proportional to F_r.

The azimuth independent terms proportional to F_r in the reflected and transmitted intensities can be expressed in the forms

$$\left.\begin{aligned} I^{(0)}_{lr}(0,\mu) &= \tfrac{3}{16}[S_{lr}(-\mu) - e^{-\tau_1/\mu}T_{lr}(\mu)]F_r, \\ I^{(0)}_{lr}(\tau_1,-\mu) &= \tfrac{3}{16}[T_{lr}(-\mu) - e^{-\tau_1/\mu}S_{lr}(\mu)]F_r, \\ I^{(0)}_{rr}(0,\mu) &= \tfrac{3}{16}[S_{rr}(-\mu) - e^{-\tau_1/\mu}T_{rr}(\mu)]F_r, \\ \text{and} \\ I^{(0)}_{rr}(\tau_1,-\mu) &= \tfrac{3}{16}[T_{rr}(-\mu) - e^{-\tau_1/\mu}S_{rr}(\mu)]F_r, \end{aligned}\right\} \quad (418)$$

where (cf. Paper XIII, eqs. [33] and [34])

$$S_{lr}(\mu) = (1-\mu^2)\sum_{\beta=-n+1}^{n-1}\frac{\mathfrak{L}_\beta}{1-\kappa_\beta\mu} - \mathfrak{L}_0\mu + \mathfrak{L}_n + \sum_{\alpha=-n}^{+n}\mathfrak{M}_\alpha(1+k_\alpha\mu) - C\left(1+\frac{\mu}{\mu_0}\right)\mu_0^2, \tag{419}$$

$$T_{lr}(\mu) = (1-\mu^2)\sum_{\beta=-n+1}^{n-1}\frac{\mathfrak{L}_\beta e^{-\kappa_\beta\tau_1}}{1+\kappa_\beta\mu} + \mathfrak{L}_0(\tau_1+\mu) + \mathfrak{L}_n + \sum_{\alpha=-n}^{+n}\mathfrak{M}_\alpha(1-k_\alpha\mu)\,e^{-k_\alpha\tau_1} - C\left(1-\frac{\mu}{\mu_0}\right)\mu_0^2 e^{-\tau_1/\mu_0}, \tag{420}$$

$$S_{rr}(\mu) = -\mathfrak{L}_0\mu + \mathfrak{L}_n - \sum_{\alpha=-n}^{+n}\frac{\mathfrak{M}_\alpha(k_\alpha^2-1)}{1-k_\alpha\mu} + \frac{C(1-\mu_0^2)}{1+\mu/\mu_0}, \tag{421}$$

and

$$T_{rr}(\mu) = \mathfrak{L}_0(\tau_1+\mu) + \mathfrak{L}_n - \sum_{\alpha=-n}^{+n}\frac{\mathfrak{M}_\alpha(k_\alpha^2-1)\,e^{-k_\alpha\tau_1}}{1+k_\alpha\mu} + \frac{C(1-\mu_0^2)\,e^{-\tau_1/\mu_0}}{1+\mu/\mu_0}. \tag{422}$$

In the foregoing equations κ_β and k_α have the same meanings as in § 18,

$$C = H_r(\mu_0)\,H_r(-\mu_0) = \frac{1}{\mu_1^2\ldots\mu_n^2}\frac{P(\mu_0)\,P(-\mu_0)}{W(\mu_0)}; \tag{423}$$

further, we have used $\mathfrak{L}_\beta(\beta = 0, \pm1, \ldots, \pm n \mp 1, n)$ and $\mathfrak{M}_\alpha$ $(\alpha = \pm1, \ldots, \pm n)$ to denote the constants of integration to distinguish them from the L_β's and M_α's of the preceding section.

The boundary conditions, as usual, require that

$$S_{lr}(\mu_i) = T_{lr}(\mu_i) = S_{rr}(\mu_i) = T_{rr}(\mu_i) = 0 \qquad (i = 1, \ldots, n). \tag{424}$$

By virtue of these boundary conditions we can write

$$S_{lr}(\mu) = \frac{1}{\mu_1^2\ldots\mu_n^2}\frac{P(\mu)}{\Omega(\mu)}\,s_{lr}(\mu), \tag{425}$$

$$T_{lr}(\mu) = \frac{1}{\mu_1^2\ldots\mu_n^2}\frac{P(\mu)}{\Omega(\mu)}\,t_{lr}(\mu), \tag{426}$$

$$S_{rr}(\mu) = \frac{1}{\mu_1^2\ldots\mu_n^2}\frac{P(\mu)}{W(\mu)}\frac{1}{1-\mu/\mu_0}\,s_{rr}(\mu), \tag{427}$$

and

$$T_{rr}(\mu) = \frac{1}{\mu_1^2\ldots\mu_n^2}\frac{P(\mu)}{W(\mu)}\frac{1}{1+\mu/\mu_0}\,t_{rr}(\mu), \tag{428}$$

where $s_{lr}(\mu)$ and $t_{lr}(\mu)$ are polynomials of degree $n-1$ in μ and $s_{rr}(\mu)$ and $t_{rr}(\mu)$ are polynomials of degree $n+2$ in μ.

From equations (421), (422), (423), (427), and (428) it follows that

$$s_{rr}(\mu_0) = (1-\mu_0^2)\,P(-\mu_0) \qquad \text{and} \qquad t_{rr}(-\mu_0) = (1-\mu_0^2)\,e^{-\tau_1/\mu_0}P(\mu_0)\,. \quad (429)$$

From equations (419), (420), (425), and (426) we now have

$$\left(1-\frac{1}{\kappa_\beta^2}\right)\mathfrak{L}_\beta = \frac{1}{\mu_1^2\,.\,.\,.\,.\,\mu_n^2}\,\frac{P(1/\kappa_\beta)}{\Omega_\beta(1/\kappa_\beta)}\,s_{lr}(1/\kappa_\beta) \quad (430)$$

and

$$\left(1-\frac{1}{\kappa_\beta^2}\right)\mathfrak{L}_\beta e^{-\kappa_\beta\tau_1} = \frac{1}{\mu_1^2\,.\,.\,.\,.\,\mu_n^2}\,\frac{P(-1/\kappa_\beta)}{\Omega_\beta(1/\kappa_\beta)}\,t_{lr}(-1/\kappa_\beta)\,. \quad (431)$$

We therefore have $(2n-2)$ relations of the form

$$s_{lr}(1/\kappa_\beta) = e^{\kappa_\beta\tau_1}\,\frac{P(-1/\kappa_\beta)}{P(+1/\kappa_\beta)}\,t_{lr}(-1/\kappa_\beta) \qquad (\beta = \pm 1\,,\,.\,.\,.\,.\,,\pm n \mp 1)\,. \quad (432)$$

Since, however, $s_{lr}(\mu)$ and $t_{lr}(\mu)$ are polynomials of degree only $n-1$, we can conclude, in accordance with theorem 2, § 4, that

$$s_{lr}(\mu) = \varpi_0^* C_{0,\,l}(\mu) + \varpi_1^* C_{1,\,l}(\mu) \quad (433)$$

and

$$t_{lr}(\mu) = \varpi_1^* C_{0,\,l}(\mu) + \varpi_0^* C_{1,\,l}(\mu)\,, \quad (434)$$

where ϖ_0^* and ϖ_1^* are constants and $C_{0,l}(\mu)$ and $C_{1,l}(\mu)$ have the same meanings as in § 17.

Turning, next, to equations (421), (422), (425), and (426), we have

$$\left.\begin{aligned}\mathfrak{M}_a = -\frac{1}{\mu_1^2\,.\,.\,.\,.\,\mu_n^2}\,\frac{P(1/k_a)}{W_a(1/k_a)\,(k_a^2-1)}\,\frac{1}{1-1/k_a\mu_0}\,s_{rr}(1/k_a)\\ (a = \pm 1\,,\,.\,.\,.\,.\,,\pm n)\end{aligned}\right\} \quad (435)$$

and

$$\left.\begin{aligned}\mathfrak{M}_a e^{-k_a\tau_1} = -\frac{1}{\mu_1^2\,.\,.\,.\,.\,\mu_n^2}\,\frac{P(-1/k_a)}{W_a(1/k_a)\,(k_a^2-1)}\,\frac{1}{1-1/k_a\mu_0}\,t_{rr}(-1/k_a)\\ (a = \pm 1\,,\,.\,.\,.\,.\,,\pm n)\,.\end{aligned}\right\} \quad (436)$$

We therefore have $2n$ relations of the form

$$s_{rr}(1/k_a) = e^{k_a\tau_1}\,\frac{P(-1/k_a)}{P(+1/\kappa_a)}\,t_{rr}(-1/k_a) \qquad (a = \pm 1\,,\,.\,.\,.\,.\,,\pm n)\,. \quad (437)$$

It will be recalled that $s_{rr}(\mu)$ and $t_{rr}(\mu)$ are polynomials of degree $(n+2)$ in μ. However, it can be shown that $s_{rr}(\mu) - t_{rr}(\mu)$ is only of degree $n+1$; for, according to equations (421), (422), (427), and (428),

$$\left.\begin{aligned}\frac{1}{\mu_1^2\,.\,.\,.\,.\,\mu_n^2}\,P(\mu)\,s_{rr}(\mu) &= \left(1-\frac{\mu}{\mu_0}\right)W(\mu)\,S_{rr}(\mu)\\ &= (-1)^n k_1^2\,.\,.\,.\,.\,k_n^2\left[\frac{\mathfrak{L}_0}{\mu_0}\,\mu^{2n+2} - \left(\mathfrak{L}_0+\frac{\mathfrak{L}_n}{\mu_0}\right)\mu^{2n+1}+.\,.\,.\,.\right]\end{aligned}\right\} \quad (438)$$

and

$$\left.\begin{aligned}\frac{1}{\mu_1^2 \ldots . \mu_n^2} P(\mu)\, t_{rr}(\mu) &= \left(1+\frac{\mu}{\mu_0}\right) W(\mu) T_{rr}(\mu) \\ &= (-1)^n k_1^2 \ldots . k_n^2 \left[\frac{\varrho_0}{\mu_0}\mu^{2n+2} + \left(\varrho_0 + \frac{\varrho_n + \varrho_0 \tau_1}{\mu_0}\right)\mu^{n+1} + \ldots .\right].\end{aligned}\right\} \quad (439)$$

And it is apparent from these equations that the coefficients of μ^{n+2} in $s_{rr}(\mu)$ and $t_{rr}(\mu)$ are the same. We may therefore write

$$s_{rr}(\mu) = (p_0^* + q_0^*\mu + a^*\mu^2) C_{0,r}(\mu) + (p_1^* - q_1^*\mu + a^*\mu^2) C_{1,r}(\mu) \quad (440)$$

and

$$t_{rr}(\mu) = (p_1^* + q_1^*\mu + a^*\mu^2) C_{0,r}(\mu) + (p_0^* - q_0^*\mu + a^*\mu^2) C_{1,r}(\mu)\,, \quad (441)$$

where p_0^*, p_1^*, q_0^*, q_1^*, and a^* are constants and $C_{0,r}(\mu)$ and $C_{1,r}(\mu)$ again have the same meanings as in § 17.

For $s_{rr}(\mu)$ and $t_{rr}(\mu)$ given by equations (440) and (441) we can verify that

$$\left.\begin{aligned}P(\mu)\, s_{rr}(\mu) &= a^* [c_{0,r}^{(n)} + c_{1,r}^{(n)}]\mu^{2n+2} + \left\{ a^* [c_{0,r}^{(n-1)} + c_{1,r}^{(n-1)}] \right. \\ &\quad \left. + q_0^* c_{0,r}^{(n)} - q_1^* c_{1,r}^{(n)} - \left(\sum_{i=1}^{n} \mu_i\right) a^* [c_{0,r}^{(n)} + c_{1,r}^{(n)}] \right\} \mu^{2n+1} + \ldots .\end{aligned}\right\} \quad (442)$$

and

$$\left.\begin{aligned}P(\mu)\, t_{rr}(\mu) &= a^* [c_{0,r}^{(n)} + c_{1,r}^{(n)}]\mu^{2n+2} + \left\{ a^* [c_{0,r}^{(n-1)} + c_{1,r}^{(n-1)}] \right. \\ &\quad \left. + q_1^* c_{0,r}^{(n)} - q_0^* c_{1,r}^{(n)} - \left(\sum_{i=1}^{n} \mu_i\right) a^* [c_{0,r}^{(n)} + c_{1,r}^{(n)}] \right\} \mu^{2n+1} + \ldots ,\end{aligned}\right\} \quad (443)$$

where $c_{0,r}^{(n)}$, $c_{1,r}^{(n)}$ and $c_{0,r}^{(n-1)}$, $c_{1,r}^{(n-1)}$ are the coefficients of the highest and the next highest powers of μ in $C_{0,r}$ and $C_{1,r}$.

From a comparison of equations (438) and (439) and (442) and (443), we conclude that

$$\left.\begin{aligned}-\sum_{i=1}^{n} \mu_i + \frac{1}{c_{0,r}^{(n)} + c_{1,r}^{(n)}} \left\{ c_{0,r}^{(n-1)} + c_{1,r}^{(n-1)} + \frac{1}{a^*} [q_0^* c_{0,r}^{(n)} - q_1^* c_{1,r}^{(n)}] \right\} \\ = -\left(\mu_0 + \frac{\varrho_n}{\varrho_0}\right)\end{aligned}\right\} \quad (444)$$

and

$$\left.\begin{aligned}-\sum_{i=1}^{n} \mu_i + \frac{1}{c_{0,r}^{(n)} + c_{1,r}^{(n)}} \left\{ c_{0,r}^{(n-1)} + c_{1,r}^{(n-1)} + \frac{1}{a^*} [q_1^* c_{0,r}^{(n)} - q_0^* c_{1,r}^{(n)}] \right\} \\ = +\left(\mu_0 + \frac{\varrho_n}{\varrho_0} + \tau_1\right).\end{aligned}\right\} \quad (445)$$

From equations (444) and (445) we readily find that

$$a^* = Q(q_0^* + q_1^*)\,, \quad (446)$$

where Q has the same meaning as in § 17 (eq. [339]).

Finally, from equations (429), (440), and (441), we find

$$\left.\begin{aligned} p_0^* + q_0^*\mu_0 + a^*\mu_0^2 = {} & \frac{(1-\mu_0^2)}{[C_{0,\,r}^2(0) - C_{1,\,r}^2(0)]W(\mu_0)} \\ & \times [P(-\mu_0)C_{0,\,r}(-\mu_0) - e^{-\tau_1/\mu_0}P(\mu_0)C_{1,\,r}(\mu_0)] \end{aligned}\right\} \quad (447)$$

and

$$\left.\begin{aligned} p_1^* - q_1^*\mu_0 + a^*\mu_0^2 = {} & \frac{(1-\mu_0^2)}{[C_{0,\,r}^2(0) - C_{1,\,r}^2(0)]W(\mu_0)} \\ & \times [e^{-\tau_1/\mu_0}P(\mu_0)C_{0,\,r}(\mu_0) - P(-\mu_0)C_{1,\,r}(-\mu_0)]. \end{aligned}\right\} \quad (448)$$

Now it will be observed that, among the seven constants ϖ_0^*, ϖ_1^*, p_0^*, p_1^*, q_0^*, q_1^*, and a^* which we have introduced in the solutions for s_{lr}, t_{lr}, s_{rr}, and t_{rr}, we have so far only three relations (eqs. [446]–[448]). To obtain the four additional relations we proceed in the following manner:

Putting $\mu = +1$, respectively -1, in equations (419) and (420), we have

$$S_{lr}(\pm 1) = \mp \mathfrak{L}_0 + \mathfrak{L}_n + \sum_{a=-n}^{+n} \mathfrak{M}_a(1 \pm k_a) - C(\mu_0^2 \pm \mu_0) \quad (449)$$

and

$$T_{lr}(\pm 1) = \mathfrak{L}_0(\tau_1 \pm 1) + \mathfrak{L}_n + \sum_{a=-n}^{+n} \mathfrak{M}_a(1 \mp k_a)\, e^{-k_a\tau_1} - C(\mu_0^2 \mp \mu_0)\, e^{-\tau_1/\mu_0}. \quad (450)$$

Similarly, putting $\mu = 0$ in equations (421) and (422), we have

$$S_{rr}(0) = \mathfrak{L}_n - \sum_{a=-n}^{+n} \mathfrak{M}_a(k_a^2 - 1) + (1-\mu_0^2)C \quad (451)$$

and

$$T_{rr}(0) = \mathfrak{L}_0\tau_1 + \mathfrak{L}_n - \sum_{a=-n}^{+n} \mathfrak{M}_a(k_a^2 - 1)\, e^{-k_a\tau_1} + (1-\mu_0^2)C\, e^{-\tau_1/\mu_0}. \quad (452)$$

Combining equations (449)–(452) appropriately, we obtain the following relations:

$$\tfrac{1}{2}[S_{lr}(+1) + S_{lr}(-1)] - S_{rr}(0) = \sum_{a=-n}^{+n} \mathfrak{M}_a k_a^2 - C, \quad (453)$$

$$\tfrac{1}{2}[T_{lr}(+1) + T_{lr}(-1)] - T_{rr}(0) = \sum_{a=-n}^{+n} \mathfrak{M}_a k_a^2 e^{-k_a\tau_1} - C\, e^{-\tau_1/\mu_0}, \quad (454)$$

$$\left.\begin{aligned} & \tfrac{1}{2}[S_{lr}(+1) - S_{lr}(-1)] + \tfrac{1}{2}[T_{lr}(+1) - T_{lr}(-1)] \\ & \qquad = \sum_{a=-n}^{+n} \mathfrak{M}_a k_a - \sum_{a=-n}^{+n} \mathfrak{M}_a k_a\, e^{-k_a\tau_1} - C\mu_0(1 - e^{-\tau_1/\mu_0}), \end{aligned}\right\} \quad (455)$$

and

$$\left.\begin{aligned}\tau_1\Big\{\tfrac{1}{2}\,[S_{lr}(+1)-S_{lr}(-1)]-\tfrac{1}{2}\,[T_{lr}(+1)-T_{lr}(-1)]-\sum_{a=-n}^{+n}\mathfrak{M}_a k_a \\ -\sum_{a=-n}^{+n}\mathfrak{M}_a k_a e^{-k_a\tau_1}+C\mu_0(1+e^{-\tau_1/\mu_0})\Big\}=2\Big\{\tfrac{1}{2}\,[S_{lr}(+1)+S_{lr}(-1)] \\ -\tfrac{1}{2}\,[T_{lr}(+1)+T_{lr}(-1)]-\sum_{a=-n}^{+n}\mathfrak{M}_a+\sum_{a=-n}^{+n}\mathfrak{M}_a e^{-k_a\tau_1}+C\mu_0^2(1-e^{-\tau_1/\mu_0})\Big\} \\ =-2\mathfrak{L}_0\tau_1\,.\end{aligned}\right\}\quad(456)$$

We shall now indicate how the various summations which occur in the foregoing equations can be evaluated. Considering the summation $\Sigma\mathfrak{M}_a k_a^m$, for example, we have (cf. eq. [435])

$$\left.\begin{aligned}\sum_{a=-n}^{+n}\mathfrak{M}_a k_a^m&=\frac{\mu_0}{\mu_1^2\,\ldots\,\mu_n^2}\sum_{a=-n}^{+n}\frac{k_a^{m-1}P(1/k_a)\,s_{rr}(1/k_a)}{W_a(1/k_a)(1-k_a^{-2})(1-k_a\mu_0)} \\ &=\frac{\mu_0}{\mu_1^2\,\ldots\,\mu_n^2 W(\mu_0)}\sum_{a=-n}^{+n}\frac{k_a^{m-1}P(1/k_a)\,s_{rr}(1/k_a)}{W_a(1/k_a)(1-k_a^{-2})}\,W_a(\mu_0)\,,\end{aligned}\right\}\quad(457)$$

or, in terms of the function

$$f_m(x)=\sum_{a=-n}^{+n}\frac{k_a^{m-1}P(1/k_a)\,s_{rr}(1/k_a)}{W_a(1/k_a)(1-k_a^{-2})}\,W_a(x)\,,\qquad(458)$$

$$\sum_{a=-n}^{+n}\mathfrak{M}_a k_a^m=\frac{\mu_0}{\mu_1^2\,\ldots\,\mu_n^2 W(\mu_0)}\,f_m(\mu_0)\,.\qquad(459)$$

Now $f_m(x)$ is a polynomial of degree $(2n-1)$ in x, which takes the values

$$\frac{k_a^{m-1}}{(1-k_a^{-2})}\,P(1/k_a)\,s_{rr}(1/k_a)\qquad(460)$$

for $x=1/k_a$ $(a=\pm1,\ldots,\pm n)$. In other words, $(1-x^2)f_m(x)-x^{1-m}P(x)s_{rr}(x)$ vanishes for $x=1/k_a$ $(a=\pm1,\ldots,\pm n)$; it must accordingly divide $W(x)$. This fact enables us to determine $f_m(x)$. To illustrate this, we shall consider the case $m=0$. In this case, there must exist a relation of the form

$$(1-x^2)\,f_0(x)=xP(x)\,s_{rr}(x)+W(x)\,(Ax^3+Bx^2+Dx+E)\,,\qquad(461)$$

where A, B, D, and E are certain constants to be determined. The constants A and B follow from the fact that the coefficients of x^{2n+3} and x^{2n+2} on the right-hand side of equation (461) must vanish. We find (cf. eq. [442])

$$A=\frac{(-1)^{n+1}}{k_1^2\,\ldots\,k_n^2}\,a^*\,[c_{0,r}^{(n)}+c_{1,r}^{(n)}]\qquad(462)$$

and

$$B=\frac{(-1)^{n+1}}{k_1^2\cdot\cdots\cdot k_n^2}\left\{a^*\left[c_{0,\,r}^{(n-1)}+c_{1,\,r}^{(n-1)}\right]+q_0^*\,c_{0,\,r}^{(n)}-q_1^*\,c_{1,\,r}^{(n)}\right.$$
$$\left.-\left(\sum_{i=1}^{n}\mu_i\right)a^*\left[c_{0,\,r}^{(n)}+c_{1,\,r}^{(n)}\right]\right\}. \tag{463}$$

Next, putting $x=+1$, respectively -1, in equation (461), we have

$$\pm P(\pm 1)\,s_{rr}(\pm 1)+W(1)(\pm A+B\pm D+E)=0\,. \tag{464}$$

From this equation it readily follows that

$$B+E=-\frac{1}{2W(1)}\left[P(+1)\,s_{rr}(+1)-P(-1)\,s_{rr}(-1)\right] \tag{465}$$

and

$$A+D=-\frac{1}{2W(1)}\left[P(+1)\,s_{rr}(+1)+P(-1)\,s_{rr}(-1)\right]. \tag{466}$$

Returning to equation (461) and setting $x=\mu_0$ and remembering that

$$s_{rr}(\mu_0)=(1-\mu_0^2)\,P(-\mu_0)\,, \tag{467}$$

we have

$$f_0(\mu_0)=\mu_0 P(\mu_0)\,P(-\mu_0)-W(\mu_0)\left\{A\mu_0+B-\frac{(A+D)\,\mu_0+B+E}{1-\mu_0^2}\right\}. \tag{468}$$

Substituting for $f_0(\mu_0)$ according to equation (468) in equation (459) and making use of the relations (360), (361), (465), and (466), we obtain

$$\sum_{a=-n}^{+n}\mathfrak{M}_a=C\mu_0^2+2(-1)^n\left\{a^*\left[c_{0,\,r}^{(n)}+c_{1,\,r}^{(n)}\right]\mu_0^2+\left[a^*\left[c_{0,\,r}^{(n-1)}+c_{1,\,r}^{(n-1)}\right]\right.\right.$$
$$\left.+q_0^*\,c_{0,\,r}^{(n)}-q_1^*\,c_{1,\,r}^{(n)}-\left(\sum_{i=1}^{n}\mu_i\right)a^*\left[c_{0,\,r}^{(n)}+c_{1,\,r}^{(n)}\right]\right]\mu_0\Big\}$$
$$\left.-\frac{2\mu_0}{1-\mu_0^2}\left\{\left[\frac{s_{rr}(+1)}{P(-1)}+\frac{s_{rr}(-1)}{P(+1)}\right]\mu_0+\left[\frac{s_{rr}(+1)}{P(-1)}-\frac{s_{rr}(-1)}{P(+1)}\right]\right\}\right. \tag{469}$$

The other summations can be similarly evaluated, and we find

$$\sum_{a=-n}^{+n}\mathfrak{M}_a k_a^2=C+\frac{(-1)^{n+1}}{\mu_1\cdot\cdots\cdot\mu_n}\,s_{rr}(0)-\frac{2\mu_0}{1-\mu_0^2}(\xi_1\mu_0+\xi_2)\,, \tag{470}$$

$$\sum_{a=-n}^{+n}\mathfrak{M}_a k_a^2 e^{-k_a\tau_1}=C\,e^{-\tau_1/\mu_0}+\frac{(-1)^{n+1}}{\mu_1\cdot\cdots\cdot\mu_n}\,t_{rr}(0)-\frac{2\mu_0}{1-\mu_0^2}(\eta_1\mu_0-\eta_2)\,, \tag{471}$$

$$\sum_{a=-n}^{+n}\mathfrak{M}_a k_a=C\mu_0+2(-1)^n a^*\left[c_{0,\,r}^{(n)}+c_{1,\,r}^{(n)}\right]\mu_0-\frac{2\mu_0}{1-\mu_0^2}(\xi_2\mu_0+\xi_1)\,, \tag{472}$$

$$\sum_{a=-n}^{+n} \mathfrak{M}_a k_a e^{-k_a\tau_1} = C\mu_0 e^{-\tau_1/\mu_0} + 2(-1)^n a^* [c_{0,r}^{(n)} + c_{1,r}^{(n)}]\mu_0 + \frac{2\mu_0}{1-\mu_0^2}(\eta_2\mu_0 - \eta_1), \tag{473}$$

$$\sum_{a=-n}^{+n} \mathfrak{M}_a = C\mu_0^2 + 2(-1)^n \Big\{ a^* [c_{0,r}^{(n)} + c_{1,r}^{(n)}]\mu_0^2 + \Big[a^* [c_{0,r}^{(n-1)} + c_{1,r}^{(n-1)}] + q_0^* c_{0,r}^{(n)} - q_1^* c_{1,r}^{(n)} - \Big(\sum_{i=1}^{n} \mu_i\Big) a^* [c_{0,r}^{(n)} + c_{1,r}^{(n)}] \Big]\mu_0 \Big\} - \frac{2\mu_0}{1-\mu_0^2}(\xi_1\mu_0 + \xi_2), \tag{474}$$

and

$$\sum_{a=-n}^{+n} \mathfrak{M}_a e^{-k_a\tau_1} = C\mu_0^2 e^{-\tau_1/\mu_0} + 2(-1)^n \Big\{ a^* [c_{0,r}^{(n)} + c_{1,r}^{(n)}]\mu_0^2 - \Big[a^* [c_{0,r}^{(n-1)} + c_{1,r}^{(n-1)}] + q_1^* c_{0,r}^{(n)} - q_0^* c_{1,r}^{(n)} - \Big(\sum_{i=1}^{n} \mu_i\Big) a^* [c_{0,r}^{(n)} + c_{1,r}^{(n)}] \Big]\mu_0 \Big\} - \frac{2\mu_0}{1-\mu_0^2}(\eta_1\mu_0 - \eta_2), \tag{475}$$

where we have used the abbreviations

$$\xi_1 = \frac{s_{rr}(+1)}{P(-1)} + \frac{s_{rr}(-1)}{P(+1)}; \qquad \xi_2 = \frac{s_{rr}(+1)}{P(-1)} - \frac{s_{rr}(-1)}{P(+1)}$$

and

$$\eta_1 = \frac{t_{rr}(+1)}{P(-1)} + \frac{t_{rr}(-1)}{P(+1)}; \qquad \eta_2 = \frac{t_{rr}(+1)}{P(-1)} - \frac{t_{rr}(-1)}{P(+1)}. \tag{476}$$

A relation which follows from equations (474) and (475) may be noted here. We have

$$\sum_{a=-n}^{+n} \mathfrak{M}_a - \sum_{a=-n}^{+n} \mathfrak{M}_a e^{-k_a\tau_1} - C\mu_0^2(1 - e^{-\tau_1/\mu_0}) = 2(-1)^n \Big\{ 2a^* [c_{0,r}^{(n-1)} + c_{1,r}^{(n-1)}] + (q_0^* + q_1^*)[c_{0,r}^{(n)} - c_{1,r}^{(n)}] - 2\Big(\sum_{i=1}^{n} \mu_i\Big) a^* [c_{0,r}^{(n)} + c_{1,r}^{(n)}] \Big\}\mu_0 - \frac{2\mu_0}{1-\mu_0^2}[(\xi_1\mu_0 + \xi_2) - (\eta_1\mu_0 - \eta_2)]; \tag{477}$$

or, substituting for $q_0^* + q_1^*$ according to equations (339) and (446), we have

$$\sum_{a=-n}^{+n} \mathfrak{M}_a - \sum_{a=-n}^{+n} \mathfrak{M}_a e^{-k_a\tau_1} - C\mu_0^2(1 - e^{-\tau_1/\mu_0}) = 2(-1)^n a^* \tau_1 [c_{0,r}^{(n)} + c_{1,r}^{(n)}]\mu_0 - \frac{2\mu_0}{1-\mu_0^2}[(\xi_1\mu_0 + \xi_2) - (\eta_1\mu_0 - \eta_2)]. \tag{478}$$

Returning to equations (453)–(456), we first observe that (cf. eqs. [427] and [428])

$$S_{rr}(0) = \frac{(-1)^n}{\mu_1 \ldots \mu_n} s_{rr}(0) \qquad \text{and} \qquad T_{rr}(0) = \frac{(-1)^n}{\mu_1 \ldots \mu_n} t_{rr}(0). \tag{479}$$

From equations (453), (454), (470), (471), and (479) it now follows that

$$\tfrac{1}{2}\,[S_{lr}(+1)+S_{lr}(-1)] = -\frac{2\mu_0}{1-\mu_0^2}(\xi_1\mu_0+\xi_2) \tag{480}$$

and

$$\tfrac{1}{2}\,[T_{lr}(+1)+T_{lr}(-1)] = -\frac{2\mu_0}{1-\mu_0^2}(\eta_1\mu_0-\eta_2)\,. \tag{481}$$

Similarly, from equations (455), (472), and (473) we have

$$\left.\begin{aligned}\tfrac{1}{2}\,[S_{lr}(+1)-S_{lr'}(-1)]+\tfrac{1}{2}\,[T_{lr}(+1)-T_{lr}(-1)]\\ = -\frac{2\mu_0}{1-\mu_0^2}[(\xi_2\mu_0+\xi_1)+(\eta_2\mu_0-\eta_1)]\,.\end{aligned}\right\} \tag{482}$$

And, finally, from equations (456), (472), (473), and (478) we have

$$\left.\begin{aligned}\tau_1\Big\{\tfrac{1}{2}\,[S_{lr}(+1)-S_{lr}(-1)]-\tfrac{1}{2}\,[T_{lr}(+1)-T_{lr}(-1)]\\ +\frac{2\mu_0}{1-\mu_0^2}[(\xi_2\mu_0+\xi_1)-(\eta_2\mu_0-\eta_1)]\Big\} = 2\Big\{\tfrac{1}{2}\,[S_{lr}(+1)+S_{lr}(-1)]\\ -\tfrac{1}{2}\,[T_{lr}(+1)+T_{lr}(-1)]+\frac{2\mu_0}{1-\mu_0^2}[(\xi_1\mu_0+\xi_2)-(\eta_1\mu_0-\eta_2)]\Big\}\,.\end{aligned}\right\} \tag{483}$$

But, according to equations (480) and (481), the right-hand side of the foregoing equation vanishes. Hence

$$\left.\begin{aligned}\tfrac{1}{2}\,[S_{lr}(+1)+S_{lr}(-1)]-\tfrac{1}{2}\,[T_{lr}(+1)+T_{lr}(-1)]\\ = -\frac{2\mu_0}{1-\mu_0^2}[(\xi_2\mu_0+\xi_1)-(\eta_2\mu_0-\eta_1)]\,.\end{aligned}\right\} \tag{484}$$

From equations (480), (481), (482), and (484) it readily follows that

$$S_{lr}(+1) = -\frac{2\mu_0}{1-\mu_0^2}(\xi_1+\xi_2)(\mu_0+1) = -\frac{4\mu_0}{1-\mu_0}\frac{s_{rr}(+1)}{P(-1)}\,, \tag{485}$$

$$S_{lr}(-1) = -\frac{2\mu_0}{1-\mu_0^2}(\xi_1-\xi_2)(\mu_0-1) = +\frac{4\mu_0}{1+\mu_0}\frac{s_{rr}(-1)}{P(+1)}\,, \tag{486}$$

$$T_{lr}(+1) = -\frac{2\mu_0}{1-\mu_0^2}(\eta_1+\eta_2)(\mu_0-1) = +\frac{4\mu_0}{1+\mu_0}\frac{t_{rr}(+1)}{P(-1)}\,, \tag{487}$$

and

$$T_{lr}(-1) = -\frac{2\mu_0}{1-\mu_0^2}(\eta_1-\eta_2)(\mu_0+1) = -\frac{4\mu_0}{1-\mu_0}\frac{t_{rr}(-1)}{P(+1)}\,. \tag{488}$$

On the other hand, according to equations (378), (425), and (426),

$$S_{lr}(\pm 1) = \frac{1}{\mu_1^2 \ldots . \mu_n^2} \frac{P(\pm 1)}{\Omega(1)} s_{lr}(\pm 1) = -2 \frac{s_{lr}(\pm 1)}{P(\mp 1)}, \tag{489}$$

and

$$T_{lr}(\pm 1) = \frac{1}{\mu_1^2 \ldots . \mu_n^2} \frac{P(\pm 1)}{\Omega(1)} t_{lr}(\pm 1) = -2 \frac{t_{lr}(\pm 1)}{P(\mp 1)}. \tag{490}$$

We thus find

$$s_{lr}(\pm 1) = \pm \frac{2\mu_0}{1-\mu_0^2}(1 \pm \mu_0)\, s_{rr}(\pm 1) \tag{491}$$

and

$$t_{lr}(\pm 1) = \mp \frac{2\mu_0}{1-\mu_0^2}(1 \mp \mu_0)\, t_{rr}(\pm 1). \tag{492}$$

We now have to substitute for $s_{lr}(\pm 1)$, $t_{lr}(\pm 1)$, $s_{rr}(\pm 1)$, and $t_{rr}(\pm 1)$ according to equations (433), (434), (440), and (441). For this purpose it is convenient to write $s_{rr}(\pm 1)$ and $t_{rr}(\pm 1)$ in the forms

$$\left.\begin{aligned} s_{rr}(\pm 1) &= (p_0^* + q_0^* \mu_0 + a^* \mu_0^2) C_{0,\,r}(\pm 1) + (p_1^* - q_1^* \mu_0 + a^* \mu_0^2) C_{1,\,r}(\pm 1) \\ &+ (1 \mp \mu_0)[\pm q_0^* C_{0,\,r}(\pm 1) \mp q_1^* C_{1,\,r}(\pm 1)] + a^*(1-\mu_0^2)[C_{0,\,r}(\pm 1) + C_{1,\,r}(\pm 1)] \end{aligned}\right\} \tag{49}$$

and

$$\left.\begin{aligned} t_{rr}(\pm 1) &= (p_0^* + q_0^* \mu_0 + a^* \mu_0^2) C_{1,\,r}(\pm 1) + (p_1^* - q_1^* \mu_0 + a^* \mu_0^2) C_{0,\,r}(\pm 1) \\ &+ (1 \pm \mu_0)[\mp q_0^* C_{1,\,r}(\pm 1) \pm q_1^* C_{0,\,r}(\pm 1)] + a^*(1-\mu_0^2)[C_{0,\,r}(\pm 1) + C_{1,\,r}(\pm 1)]. \end{aligned}\right\} \tag{49}$$

We also have

$$s_{lr}(\pm 1) = \varpi_0^* C_{0,\,l}(\pm 1) + \varpi_1^* C_{1,\,l}(\pm 1) \tag{495}$$

and

$$t_{lr}(\pm 1) = \varpi_0^* C_{1,\,l}(\pm 1) + \varpi_1^* C_{0,\,l}(\pm 1). \tag{496}$$

Substituting from equations (493)–(496) in equations (491) and (492), we find, after some lengthy but straightforward reductions, that (cf. eq. [446])

$$\left.\begin{aligned} (\varpi_0^* + \varpi_1^*)\gamma_1 = \frac{2\mu_0}{1-\mu_0^2}[&\mathfrak{A}_r(\mu_0 c_1 + c_2) + \mathfrak{B}_r(\mu_0 c_1 - c_2) \\ &+ c_1(1-\mu_0^2)\{(q_0^* - q_1^*) + 2Q(q_0^* + q_1^*)\mu_0\}], \end{aligned}\right\} \tag{497}$$

$$\left.\begin{aligned} (\varpi_0^* + \varpi_1^*)\gamma_3 = \frac{2\mu_0}{1-\mu_0^2}[&\mathfrak{A}_r(\mu_0 c_3 - c_4) + \mathfrak{B}_r(\mu_0 c_3 + c_4) \\ &+ c_3(1-\mu_0^2)\{(q_0^* - q_1^*) + 2Q(q_0^* + q_1^*)\mu_0\}], \end{aligned}\right\} \tag{498}$$

$$\left.\begin{aligned} (\varpi_0^* - \varpi_1^*)\gamma_2 = \frac{2\mu_0}{1-\mu_0^2}[&\mathfrak{A}_r(\mu_0 c_2 + c_1) + \mathfrak{B}_r(-\mu_0 c_2 + c_1) \\ &+ (1-\mu_0^2)(c_2 + 2c_1 Q)(q_0^* + q_1^*)], \end{aligned}\right\} \tag{499}$$

and

$$(\varpi_0^* - \varpi_1^*)\,\gamma_4 = \frac{2\mu_0}{1-\mu_0^2}\,[\,\mathfrak{A}_r(\mu_0 c_4 - c_3) - \mathfrak{B}_r(\mu_0 c_4 + c_3) + (1-\mu_0^2)(c_4 - 2c_3 Q)(q_0^* + q_1^*)\,]\,, \tag{500}$$

where γ_1, γ_2, γ_3, γ_4, and c_1, c_2, c_3, c_4, have the same meanings as in equations (396) and

$$\mathfrak{A}_r = p_0^* + q_0^*\mu_0 + a^*\mu_0^2 \qquad \text{and} \qquad \mathfrak{B}_r = p_1^* - q_1^*\mu_0 + a^*\mu_0^2\,. \tag{501}$$

Eliminating $[(q_0^* - q_1^*) + 2Q(q_0^* + q_1^*)]$ from equations (497) and (498) and $(q_0^* + q_1^*)$ from equations (499) and (500), we find

$$\varpi_1^* + \varpi_0^* = \frac{2\mu_0}{1-\mu_0^2}\,\frac{c_1c_4 + c_2c_3}{c_3\gamma_1 - c_1\gamma_3}\,(\mathfrak{A}_r - \mathfrak{B}_r) \tag{502}$$

and

$$\varpi_1^* - \varpi_0^* = \frac{2\mu_0}{1-\mu_0^2}\,\frac{c_1c_4 + c_2c_3}{(c_2\gamma_4 - c_4\gamma_2) + 2Q(c_1\gamma_4 + c_3\gamma_2)}\,[\,\mathfrak{A}_r(1-2Q\mu_0) + \mathfrak{B}_r(1+2Q\mu_0)\,]\,. \tag{503}$$

Similarly, eliminating $(\varpi_0^* + \varpi_1^*)$ from equations (497) and (498) and $(\varpi_0^* - \varpi_1^*)$ from equations (499) and (500), we find

$$(1-\mu_0^2)\,[(q_0^* - q_1^*) + 2Q(q_0^* + q_1^*)\,\mu_0] = \mathfrak{A}_r\left(\frac{c_2\gamma_3 + c_4\gamma_1}{c_3\gamma_1 - c_1\gamma_3} - \mu_0\right) - \mathfrak{B}_r\left(\frac{c_2\gamma_3 + c_4\gamma_1}{c_3\gamma_1 - c_1\gamma_3} + \mu_0\right) \tag{504}$$

and

$$(1-\mu_0^2)\left(1 + 2Q\,\frac{c_1\gamma_4 + c_3\gamma_2}{c_2\gamma_4 - c_4\gamma_2}\right)(q_0^* + q_1^*) = -\,\mathfrak{A}_r\left(\frac{c_1\gamma_4 + c_3\gamma_2}{c_2\gamma_4 - c_4\gamma_2} + \mu_0\right) - \mathfrak{B}_r\left(\frac{c_1\gamma_4 + c_3\gamma_2}{c_2\gamma_4 - c_4\gamma_2} - \mu_0\right). \tag{505}$$

Finally, solving equations (502) and (503) for ϖ_0^* and ϖ_1^* and equations (504) and (505) for q_0^* and q_1^*, we find that these constants can be expressed in the forms

$$\varpi_0^* = \frac{\mu_0}{1-\mu_0^2}\{\,\mathfrak{A}_r[u_2 + Q(u_1 - u_2)\,\mu_0] - \mathfrak{B}_r[u_1 + Q(u_1 - u_2)\,\mu_0]\,\}\,, \tag{506}$$

$$\varpi_1^* = \frac{\mu_0}{1-\mu_0^2}\{\,\mathfrak{A}_r[u_1 - Q(u_1 - u_2)\,\mu_0] - \mathfrak{B}_r[u_2 - Q(u_1 - u_2)\,\mu_0]\,\}\,, \tag{507}$$

$$(1-\mu_0^2)\,q_0^* = \mathfrak{A}_r(u_4 + u_5\mu_0 + u_6\mu_0^2) - \mathfrak{B}_r(u_3 + u_6\mu_0^2)\,, \tag{508}$$

and

$$(1-\mu_0^2)\,q_1^* = -\,\mathfrak{A}_r(u_3 + u_6\mu_0^2) + \mathfrak{B}_r(u_4 + u_5\mu_0 + u_6\mu_0^2)\,, \tag{509}$$

where

$$u_1 = (c_1c_4 + c_2c_3)\left[\frac{1}{c_3\gamma_1 - c_1\gamma_3} + \frac{1}{c_2\gamma_4 - c_4\gamma_2 + 2Q(c_1\gamma_4 + c_3\gamma_2)}\right], \quad (510)$$

$$u_2 = (c_1c_4 + c_2c_3)\left[\frac{1}{c_3\gamma_1 - c_1\gamma_3} - \frac{1}{c_2\gamma_4 - c_4\gamma_2 + 2Q(c_1\gamma_4 + c_3\gamma_2)}\right], \quad (511)$$

$$u_3 = \frac{1}{2}\left[\frac{c_2\gamma_3 + c_4\gamma_1}{c_3\gamma_1 - c_1\gamma_3} + \frac{c_1\gamma_4 + c_3\gamma_2}{c_2\gamma_4 - c_4\gamma_2 + 2Q(c_1\gamma_4 + c_3\gamma_2)}\right], \quad (512)$$

$$u_4 = \frac{1}{2}\left[\frac{c_2\gamma_3 + c_4\gamma_1}{c_3\gamma_1 - c_1\gamma_3} - \frac{c_1\gamma_4 + c_3\gamma_2}{c_2\gamma_4 - c_4\gamma_2 + 2Q(c_1\gamma_4 + c_3\gamma_2)}\right], \quad (513)$$

$$u_5 = \frac{c_2\gamma_4 - c_4\gamma_2}{c_2\gamma_4 - c_4\gamma_2 + 2Q(c_1\gamma_4 + c_3\gamma_2)}, \quad (514)$$

and

$$u_6 = Qu_5 . \quad (515)$$

Also, according to equations (446), (505), (514), and (515), we have

$$(1 - \mu_0^2)\, a^* = -u_6\left[\mathfrak{A}_r\left(\frac{c_1\gamma_4 + c_3\gamma_2}{c_2\gamma_4 - c_4\gamma_2} + \mu_0\right) + \mathfrak{B}_r\left(\frac{c_1\gamma_4 + c_3\gamma_2}{c_2\gamma_4 - c_4\gamma_2} - \mu_0\right)\right]. \quad (516)$$

It may be recalled that $\mathfrak{A}_r$ and $\mathfrak{B}_r$, which occur in the foregoing solution for the constants, are defined in equation (501). According to equations (447) and (448) we may, therefore, write

$$\mathfrak{A}_r = p_0^* + q_0^*\mu_0 + a^*\mu_0^2 = (-1)^n \mu_1 \ldots\ldots \mu_n \frac{(1 - \mu_0^2)\, X_r(\mu_0)}{[C_{0,r}^2(0) - C_{1,r}^2(0)]^{\frac{1}{2}}} \quad (517)$$

and

$$\mathfrak{B}_r = p_1^* - q_1^*\mu_0 + a^*\mu_0^2 = (-1)^n \mu_1 \ldots\ldots \mu_n \frac{(1 - \mu_0^2)\, Y_r(\mu_0)}{[C_{0,r}^2(0) - C_{1,r}^2(0)]^{\frac{1}{2}}}. \quad (518)$$

With this determination of the constants we have completed the solution of the formal problem.

We now return to equations (418) and the angular distributions of the reflected and the transmitted radiations.

It is first apparent that for $s_{lr}(\mu)$ and $t_{lr}(\mu)$ given by equations (433) and (434) the reflected and the transmitted intensities in the component l are of the forms

$$I_{lr}(0, \mu) = \tfrac{3}{16}F_r \frac{(-1)^n}{\mu_1 \ldots\ldots \mu_n}[C_{0,l}^2(0) - C_{1,l}^2(0)]^{\frac{1}{2}}[\varpi_0^* X_l(\mu) - \varpi_1^* Y_l(\mu)] \quad (519)$$

and

$$I_{lr}(\tau_1, -\mu) = \tfrac{3}{16}F_r \frac{(-1)^n}{\mu_1 \ldots\ldots \mu_n}[C_{0,l}^2(0) - C_{1,l}^2(0)]^{\frac{1}{2}}[\varpi_1^* X_l(\mu) - \varpi_0^* Y_l(\mu)]. \quad (520)$$

Substituting for ϖ_0^* and ϖ_1^* according to equations (506), (507), (517), and (518), we have

$$\left.\begin{aligned} I_{lr}(0, \mu) &= \tfrac{3}{16}F_r\left[\frac{C_{0,l}^2(0) - C_{1,l}^2(0)}{C_{0,r}^2(0) - C_{1,r}^2(0)}\right]^{\frac{1}{2}} \mu_0 \\ &\times \{X_l(\mu)[X_r(\mu_0)[\![u_2 + Q(u_1 - u_2)\mu_0]\!] - Y_r(\mu_0)[\![u_1 + Q(u_1 - u_2)\mu_0]\!]] \\ &- Y_l(\mu)[X_r(\mu_0)[\![u_1 - Q(u_1 - u_2)\mu_0]\!] - Y_r(\mu_0)[\![u_2 - Q(u_1 - u_2)\mu_0]\!]]\} \end{aligned}\right\} \quad (521)$$

and

$$\left.\begin{aligned} I_{lr}(\tau_1, -\mu) &= \tfrac{3}{16} F_r \left[\frac{C^2_{0,\,l}(0) - C^2_{1,\,l}(0)}{C^2_{0,\,r}(0) - C^2_{1,\,r}(0)}\right]^{\frac{1}{2}} \mu_0 \\ &\times \{ X_l(\mu) [X_r(\mu_0) [\![u_1 - Q(u_1 - u_2)\,\mu_0]\!] - Y_r(\mu_0) [\![u_2 - Q(u_1 - u_2)\,\mu_0]\!]] \\ &- Y_l(\mu) [X_r(\mu_0) [\![u_2 + Q(u_1 - u_2)\,\mu_0]\!] - Y_r(\mu_0) [\![u_1 + Q(u_1 - u_2)\,\mu_0]\!]] \}. \end{aligned}\right\} \quad (522)$$

After some minor rearranging of the terms, equations (521) and (522) can be brought to the forms

$$\left.\begin{aligned} I_{lr}(0, \mu) &= \tfrac{3}{16} F_r \left[\frac{C^2_{0,\,l}(0) - C^2_{1,\,l}(0)}{C^2_{0,\,r}(0) - C^2_{1,\,r}(0)}\right]^{\frac{1}{2}} \mu_0 \\ &\times \{ -u_1 [X_l(\mu)\, Y_r(\mu_0) + Y_l(\mu)\, X_r(\mu_0)] \\ &+ u_2 [X_l(\mu)\, X_r(\mu_0) + Y_l(\mu)\, Y_r(\mu_0)] \\ &+ Q(u_1 - u_2)\,\mu_0 [X_l(\mu) + Y_l(\mu)] [X_r(\mu_0) - Y_r(\mu_0)] \} \end{aligned}\right\} \quad (523)$$

and

$$\left.\begin{aligned} I_{lr}(\tau_1, -\mu) &= \tfrac{3}{16} F_r \left[\frac{C^2_{0,\,l}(0) - C^2_{1,\,l}(0)}{C^2_{0,\,r}(0) - C^2_{1,\,r}(0)}\right]^{\frac{1}{2}} \mu_0 \\ &\times \{ -u_2 [X_l(\mu)\, Y_r(\mu_0) + Y_l(\mu)\, X_r(\mu_0)] \\ &+ u_1 [X_l(\mu)\, X_r(\mu_0) + Y_l(\mu)\, Y_r(\mu_0)] \\ &- Q(u_1 - u_2)\,\mu_0 [X_l(\mu) + Y_l(\mu)] [X_r(\mu_0) - Y_r(\mu_0)] \}. \end{aligned}\right\} \quad (524)$$

Turning, next, to the reflected and the transmitted intensities in the component r, we have (cf. eqs. [418], [427], [428], [440], and [441])

$$\left.\begin{aligned} I_{rr}(0, \mu) &= \tfrac{3}{16} F_r \frac{(-1)^n}{\mu_1 \cdots \mu_n} [C^2_{0,\,r}(0) - C^2_{1,\,r}(0)]^{\frac{1}{2}} \frac{\mu_0}{\mu_0 + \mu} \\ &\times \{ (p_0^* - q_0^* \mu + a^* \mu^2)\, X_r(\mu) - (p_1^* + q_1^* \mu + a^* \mu^2)\, Y_r(\mu) \} \end{aligned}\right\} \quad (525)$$

and

$$\left.\begin{aligned} I_{rr}(\tau_1, -\mu) &= \tfrac{3}{16} F_r \frac{(-1)^n}{\mu_1 \cdots \mu_n} [C^2_{0,\,r}(0) - C^2_{1,\,r}(0)]^{\frac{1}{2}} \frac{\mu_0}{\mu_0 - \mu} \\ &\times \{ (p_1^* - q_1^* \mu + a^* \mu^2)\, X_r(\mu) - (p_0^* + q_0^* \mu + a^* \mu^2)\, Y_r(\mu) \}. \end{aligned}\right\} \quad (526)$$

We can re-write equations (525) and (526) in the forms

$$\left.\begin{aligned} I_{rr}(0, \mu) &= \tfrac{3}{16} F_r \frac{(-1)^n}{\mu_1 \cdots \mu_n} [C^2_{0,\,r}(0) - C^2_{1,\,r}(0)]^{\frac{1}{2}} \frac{\mu_0}{\mu_0 + \mu} \\ &\times \{ (p_0^* + q_0^* \mu_0 + a^* \mu_0^2)\, X_r(\mu) - (p_1^* - q_1^* \mu_0 + a^* \mu_0^2)\, Y_r(\mu) \\ &- q_0^* (\mu_0 + \mu)\, X_r(\mu) - q_1^* (\mu_0 + \mu)\, Y_r(\mu) - a^* (\mu_0^2 - \mu^2) [X_r(\mu) - Y_r(\mu)] \} \end{aligned}\right\} \quad (527)$$

and

$$\left.\begin{aligned} I_{rr}(\tau_1,-\mu) = \tfrac{3}{16}F_r\frac{(-1)^n}{\mu_1\ldots\mu_n}(C^2_{0,r}(0)-C^2_{1,r}(0))^{\frac{1}{2}}\frac{\mu_0}{\mu_0-\mu} \\ \times\{(p_1^*-q_1^*\mu_0+a^*\mu_0^2)X_r(\mu)-(p_0^*+q_0^*\mu_0+a^*\mu_0^2)Y_r(\mu) \\ +q_1^*(\mu_0-\mu)X_r(\mu)+q_0^*(\mu_0-\mu)Y_r(\mu)-a^*(\mu_0^2-\mu^2)[X_r(\mu)-Y_r(\mu)]\}. \end{aligned}\right\} \quad (528)$$

Substituting for q_0^*, q_1^*, a^*, p_0^*, $+\ q_0^*\mu_0+a^*\mu_0^2$ and $p_1^*-q_1^*\mu_0+a^*\mu_0^2$ in accordance with equations (508), (509), and (516)–(518) in equations (527) and (528), we obtain

$$\left.\begin{aligned} I_{rr}(0,\mu) = \tfrac{3}{16}F_r\frac{\mu_0}{\mu_0+\mu}\Big\{(1-\mu_0^2)[X_r(\mu)X_r(\mu_0)-Y_r(\mu)Y_r(\mu_0)] \\ -(\mu_0+\mu)X_r(\mu)[X_r(\mu_0)(u_4-u_5\mu_0+u_6\mu_0^2)-Y_r(\mu_0)(u_3+u_6\mu_0^2)] \\ -(\mu_0+\mu)Y_r(\mu)[-X_r(\mu_0)(u_3+u_6\mu_0^2)+Y_r(\mu_0)(u_4+u_5\mu_0+u_6\mu_0^2)] \\ -u_6(\mu_0^2-\mu^2)\Big[-X_r(\mu_0)\Big(\mu_0+\frac{c_1\gamma_4+c_3\gamma_2}{c_2\gamma_4-c_4\gamma_2}\Big)+Y_r(\mu_0)\Big(\mu_0-\frac{c_1\gamma_4+c_3\gamma_2}{c_2\gamma_4-c_4\gamma_2}\Big)\Big] \\ \times[X_r(\mu)-Y_r(\mu)]\Big\}. \end{aligned}\right\} \quad (529)$$

and

$$\left.\begin{aligned} I_{rr}(\tau_1,-\mu) = \tfrac{3}{16}F_r\frac{\mu_0}{\mu_0-\mu}\Big\{(1-\mu_0^2)[X_r(\mu)Y_r(\mu_0)-Y_r(\mu)X_r(\mu_0)] \\ +(\mu_0-\mu)X_r(\mu)[-X_r(\mu_0)(u_3+u_6\mu_0^2)+Y_r(\mu_0)(u_4+u_5\mu_0+u_6\mu_0^2)] \\ +(\mu_0-\mu)Y_r(\mu)[X_r(\mu_0)(u_4-u_5\mu_0+u_6\mu_0^2)-Y_r(\mu_0)(u_3+u_6\mu_0^2)] \\ -u_6(\mu_0^2-\mu^2)\Big[-X_r(\mu_0)\Big(\mu_0+\frac{c_1\gamma_4+c_3\gamma_2}{c_2\gamma_4-c_4\gamma_2}\Big)+Y_r(\mu_0)\Big(\mu_0-\frac{c_1\gamma_4+c_3\gamma_2}{c_2\gamma_4-c_4\gamma_2}\Big)\Big] \\ \times[X_r(\mu)-Y_r(\mu)]\Big\}. \end{aligned}\right\} \quad (530)$$

After some lengthy reductions, the foregoing equations can be brought to the forms

$$\left.\begin{aligned} I_{rr}(0,\mu) = \tfrac{3}{16}F_r\frac{\mu_0}{\mu_0+\mu}\{X_r(\mu)X_r(\mu_0)[1-u_4(\mu_0+\mu)+u_5\mu\mu_0] \\ -Y_r(\mu)Y_r(\mu_0)[1+u_4(\mu_0+\mu)+u_5\mu\mu_0] \\ +u_3(\mu_0+\mu)[X_r(\mu)Y_r(\mu_0)+Y_r(\mu)X_r(\mu_0)] \\ -Qu_5\mu\mu_0(\mu_0+\mu)[X_r(\mu)-Y_r(\mu)][X_r(\mu_0)-Y_r(\mu_0)] \\ -Q(u_3-u_4)\mu^2[X_r(\mu)-Y_r(\mu)][X_r(\mu_0)+Y_r(\mu_0)] \\ -Q(u_3-u_4)\mu_0^2[X_r(\mu)+Y_r(\mu)][X_r(\mu_0)-Y_r(\mu_0)]\}. \end{aligned}\right\} \quad (531)$$

and

$$\left.\begin{aligned} I_{rr}(\tau_1, -\mu) = \tfrac{3}{16}F_r \frac{\mu_0}{\mu_0-\mu}\{ & X_r(\mu)\, Y_r(\mu_0)[1+u_4(\mu_0+\mu)-u_5\mu\mu_0] \\ & - Y_r(\mu)\, X_r(\mu_0)[1-u_4(\mu_0-\mu)-u_5\mu\mu_0] \\ & - u_3(\mu_0-\mu)[X_r(\mu)\, X_r(\mu_0)+Y_r(\mu)\, Y_r(\mu_0)] \\ & + Qu_5\mu\mu_0(\mu_0-\mu)[X_r(\mu)-Y_r(\mu)][X_r(\mu_0)-Y_r(\mu_0)] \\ & - Q(u_3-u_4)\mu^2[X_r(\mu)-Y_r(\mu)][X_r(\mu_0)+Y_r(\mu_0)] \\ & + Q(u_3-u_4)\mu_0^2[X_r(\mu)+Y_r(\mu)][X_r(\mu_0)-Y_r(\mu_0)]\}. \end{aligned}\right\} \quad (532)$$

19. *The scattering and the transmission matrices. The reciprocity principle.*—The solutions for the various terms given in the preceding sections can be combined to give the complete distribution of the reflected and the transmitted radiations. The resulting laws of diffuse reflection and transmission can be expressed in terms of a scattering ($\boldsymbol{S}$) and a transmission ($\boldsymbol{T}$) matrix in the forms (cf. Paper XIII, § 4; Paper XIV, § 2; and Paper XVI, Sec. II)

$$\boldsymbol{I}(0; \mu, \varphi; \mu_0, \varphi_0) = \frac{3}{16\mu}\boldsymbol{Q}\boldsymbol{S}(\mu, \varphi; \mu_0, \varphi_0)\boldsymbol{F} \quad (533)$$

and

$$\boldsymbol{I}(\tau_1; -\mu, \varphi; \mu_0, \varphi_0) = \frac{3}{16\mu}\boldsymbol{Q}\boldsymbol{T}(\mu, \varphi; \mu_0, \varphi_0)\boldsymbol{F}, \quad (534)$$

where

$$\boldsymbol{I} = (I_l, I_r, U) \quad \text{and} \quad \boldsymbol{F} = (F_l, F_r, U_0) \quad (535)$$

and

$$\boldsymbol{Q} = \begin{pmatrix} 1 & 0 & 0 \\ 0 & 1 & 0 \\ 0 & 0 & 2 \end{pmatrix}. \quad (536)$$

In accordance with equations (284)–(287) and the solutions obtained in the preceding sections, we can write

$$\left.\begin{aligned} \boldsymbol{S}(\mu, \varphi; \mu_0, \varphi_0) = {} & \boldsymbol{S}^{(0)}(\mu; \mu_0) + (1-\mu^2)^{\frac{1}{2}}(1-\mu_0^2)^{\frac{1}{2}}\boldsymbol{S}^{(1)}(\mu, \varphi; \mu_0, \varphi_0) \\ & + \boldsymbol{S}^{(2)}(\mu, \varphi; \mu_0, \varphi_0) \end{aligned}\right\} \quad (537)$$

and

$$\left.\begin{aligned} \boldsymbol{T}(\mu, \varphi; \mu_0, \varphi_0) = {} & \boldsymbol{T}^{(0)}(\mu; \mu_0) + (1-\mu^2)^{\frac{1}{2}}(1-\mu_0^2)^{\frac{1}{2}}\boldsymbol{T}^{(1)}(\mu, \varphi; \mu_0, \varphi_0) \\ & + \boldsymbol{T}^{(2)}(\mu, \varphi; \mu_0, \varphi_0), \end{aligned}\right\} \quad (538)$$

where

$$\left.\begin{aligned} \left(\frac{1}{\mu}+\frac{1}{\mu_0}\right)S_{11}^{(0)}(\mu; \mu_0) = 2\{ & X_l(\mu)\, X_l(\mu_0)[1+\nu_4(\mu_0+\mu)+\mu\mu_0] \\ & - Y_l(\mu)\, Y_l(\mu_0)[1-\nu_4(\mu_0+\mu)+\mu\mu_0] \\ & - \nu_3(\mu_0+\mu)[X_l(\mu)\, Y_l(\mu_0)+Y_l(\mu)\, X_l(\mu_0)]\}, \end{aligned}\right\} \quad (539)$$

$$\left(\frac{1}{\mu}+\frac{1}{\mu_0}\right)S_{12}^{(0)}(\mu;\,\mu_0)=\left[\frac{C_{0,\,l}^2(0)-C_{1,\,l}^2(0)}{C_{0,\,r}^2(0)-C_{1,\,r}^2(0)}\right]^{\frac{1}{2}}(\mu_0+\mu)$$
$$\times\{-u_1[X_l(\mu)\,Y_r(\mu_0)+Y_l(\mu)\,X_r(\mu_0)]$$
$$+u_2[X_l(\mu)\,X_r(\mu_0)+Y_l(\mu)\,Y_r(\mu_0)]$$
$$+Q(u_1-u_2)\,\mu_0[X_l(\mu)+Y_l(\mu)][X_r(\mu_0)-Y_r(\mu_0)]\},\tag{540}$$

$$\left(\frac{1}{\mu}+\frac{1}{\mu_0}\right)S_{21}^{(0)}(\mu;\,\mu_0)=\left[\frac{C_{0,\,r}^2(0)-C_{1,\,r}^2(0)}{C_{0,\,l}^2(0)-C_{1,\,l}^2(0)}\right]^{\frac{1}{2}}(\mu_0+\mu)$$
$$\times\{\nu_1[X_r(\mu)\,Y_l(\mu_0)+Y_r(\mu)\,X_l(\mu_0)]$$
$$-\nu_2[X_r(\mu)\,X_l(\mu_0)+Y_r(\mu)\,Y_l(\mu_0)]$$
$$-Q(\nu_1-\nu_2)\,\mu[X_r(\mu)-Y_r(\mu)][X_l(\mu_0)+Y_l(\mu_0)]\},\tag{541}$$

$$\left(\frac{1}{\mu}+\frac{1}{\mu_0}\right)S_{22}^{(0)}(\mu;\,\mu_0)=X_r(\mu)\,X_r(\mu_0)[1-u_4(\mu_0+\mu)+u_5\mu\mu_0]$$
$$-Y_r(\mu)\,Y_r(\mu_0)[1+u_4(\mu_0+\mu)+u_5\mu\mu_0]$$
$$+u_3(\mu_0+\mu)[X_r(\mu)\,Y_r(\mu_0)+Y_r(\mu)\,X_r(\mu_0)]$$
$$-Qu_5\mu\mu_0(\mu_0+\mu)[X_r(\mu)-Y_r(\mu)][X_r(\mu_0)-Y_r(\mu_0)]$$
$$-Q(u_3-u_4)\{\mu^2[X_r(\mu)-Y_r(\mu)][X_r(\mu_0)+Y_r(\mu_0)]$$
$$+\mu_0^2[X_r(\mu)+Y_r(\mu)][X_r(\mu_0)-Y_r(\mu_0)]\};\tag{542}$$

$$\left(\frac{1}{\mu}-\frac{1}{\mu_0}\right)T_{11}^{(0)}(\mu;\,\mu_0)=2\{X_l(\mu)\,Y_l(\mu_0)[1-\nu_4(\mu_0-\mu)-\mu\mu_0]$$
$$-Y_l(\mu)\,X_l(\mu_0)[1+\nu_4(\mu_0-\mu)-\mu\mu_0]$$
$$+\nu_3(\mu_0-\mu)[X_l(\mu)\,X_l(\mu_0)+Y_l(\mu)\,Y_l(\mu_0)]\},\tag{543}$$

$$\left(\frac{1}{\mu}-\frac{1}{\mu_0}\right)T_{12}^{(0)}(\mu;\,\mu_0)=\left[\frac{C_{0,\,l}^2(0)-C_{1,\,l}^2(0)}{C_{0,\,r}^2(0)-C_{1,\,r}^2(0)}\right]^{\frac{1}{2}}(\mu_0-\mu)$$
$$\times\{-u_2[X_l(\mu)\,Y_r(\mu_0)+Y_l(\mu)\,X_r(\mu_0)]$$
$$+u_1[X_l(\mu)\,X_r(\mu_0)+Y_l(\mu)\,Y_r(\mu_0)]$$
$$-Q(u_1-u_2)\,\mu_0[X_l(\mu)+Y_l(\mu)][X_r(\mu_0)-Y_r(\mu_0)]\},\tag{544}$$

$$\left(\frac{1}{\mu}-\frac{1}{\mu_0}\right)T_{21}^{(0)}(\mu;\,\mu_0)=\left[\frac{C_{0,\,r}^2(0)-C_{1,\,r}^2(0)}{C_{0,\,l}^2(0)-C_{1,\,l}^2(0)}\right]^{\frac{1}{2}}(\mu_0-\mu)$$
$$\times\{\nu_2[X_r(\mu)\,Y_l(\mu_0)+Y_r(\mu)\,X_l(\mu_0)]$$
$$-\nu_1[X_r(\mu)\,X_l(\mu_0)+Y_r(\mu)\,Y_l(\mu_0)]$$
$$+Q(\nu_1-\nu_2)\,\mu[X_r(\mu)-Y_r(\mu)][X_l(\mu_0)+Y_l(\mu_0)]\},\tag{545}$$

$$\left(\frac{1}{\mu}-\frac{1}{\mu_0}\right)T_{22}^{(0)}(\mu;\,\mu_0) = X_r(\mu)\,Y_r(\mu_0)\,[1+u_4(\mu_0-\mu)-u_5\mu\mu_0]$$
$$-Y_r(\mu)\,X_r(\mu_0)\,[1-u_4(\mu_0-\mu)-u_5\mu\mu_0]$$
$$-u_3(\mu_0-\mu)\,[X_r(\mu)\,X_r(\mu_0)+Y_r(\mu)\,Y_r(\mu_0)]$$
$$+Qu_5\mu\mu_0(\mu_0-\mu)\,[X_r(\mu)-Y_r(\mu)]\,[X_r(\mu_0)-Y_r(\mu_0)]$$
$$-Q(u_3-u_4)\,\{\mu^2[X_r(\mu)-Y_r(\mu)]\,[X_r(\mu_0)+Y_r(\mu_0)]$$
$$-\mu_0^2[X_r(\mu)+Y_r(\mu)]\,[X_r(\mu_0)-Y_r(\mu_0)]\}; \qquad (546)$$

$$S_{31}^{(0)}=S_{13}^{(0)}=S_{32}^{(0)}=S_{23}^{(0)}=S_{33}^{(0)}=0\,,$$
$$T_{31}^{(0)}=T_{13}^{(0)}=T_{32}^{(0)}=T_{23}^{(0)}=T_{33}^{(0)}=0\,; \qquad (547)$$

$$\left(\frac{1}{\mu}+\frac{1}{\mu_0}\right)\boldsymbol{S}^{(1)}(\mu,\varphi;\,\mu_0,\varphi_0) = [X^{(1)}(\mu)\,X^{(1)}(\mu_0)-Y^{(1)}(\mu)\,Y^{(1)}(\mu_0)]$$
$$\times\begin{pmatrix}-4\mu\mu_0\cos(\varphi-\varphi_0) & 0 & -2\mu\sin(\varphi-\varphi_0)\\ 0 & 0 & 0\\ -2\mu_0\sin(\varphi-\varphi_0) & 0 & \cos(\varphi-\varphi_0)\end{pmatrix}; \qquad (548)$$

$$\left(\frac{1}{\mu}-\frac{1}{\mu_0}\right)\boldsymbol{T}^{(1)}(\mu,\varphi;\,\mu_0,\varphi_0) = [X^{(1)}(\mu)\,Y^{(1)}(\mu_0)-Y^{(1)}(\mu)\,X^{(1)}(\mu_0)]$$
$$\times\begin{pmatrix}4\mu\mu_0\cos(\varphi-\varphi_0) & 0 & 2\mu\sin(\varphi-\varphi_0)\\ 0 & 0 & 0\\ -2\mu_0\sin(\varphi-\varphi_0) & 0 & \cos(\varphi-\varphi_0)\end{pmatrix}; \qquad (549)$$

$$\left(\frac{1}{\mu}+\frac{1}{\mu_0}\right)\boldsymbol{S}^{(2)}(\mu,\varphi;\,\mu_0,\varphi_0) = [X^{(2)}(\mu)\,X^{(2)}(\mu_0)-Y^{(2)}(\mu)\,Y^{(2)}(\mu_0)]$$
$$\times\begin{pmatrix}\mu^2\mu_0^2\cos 2(\varphi-\varphi_0) & -\mu^2\cos 2(\varphi-\varphi_0) & \mu^2\mu_0\sin 2(\varphi-\varphi_0)\\ -\mu_0^2\cos 2(\varphi-\varphi_0) & \cos 2(\varphi-\varphi_0) & -\mu_0\sin 2(\varphi-\varphi_0)\\ \mu\mu_0^2\sin 2(\varphi-\varphi_0) & -\mu\sin 2(\varphi-\varphi_0) & -\mu\mu_0\cos 2(\varphi-\varphi_0)\end{pmatrix}; \qquad (550)$$

and

$$\left(\frac{1}{\mu}-\frac{1}{\mu_0}\right)\boldsymbol{T}^{(2)}(\mu,\varphi;\,\mu_0,\varphi_0) = [X^{(2)}(\mu)\,Y^{(2)}(\mu_0)-Y^{(2)}(\mu)\,X^{(2)}(\mu_0)]$$
$$\times\begin{pmatrix}\mu^2\mu_0^2\cos 2(\varphi-\varphi_0) & -\mu^2\cos 2(\varphi-\varphi_0) & \mu^2\mu_0\sin 2(\varphi-\varphi_0)\\ -\mu_0^2\cos 2(\varphi-\varphi_0) & \cos 2(\varphi-\varphi_0) & -\mu_0\sin 2(\varphi-\varphi_0)\\ -\mu\mu_0^2\sin 2(\varphi-\varphi_0) & \mu\sin 2(\varphi-\varphi_0) & \mu\mu_0\cos 2(\varphi-\varphi_0)\end{pmatrix}. \qquad (551)$$

Now, Helmholtz' principle of reciprocity as reformulated in Paper XIII (§ 4) requires that the scattering and the transmission matrices have the following property for transposition:

$$\left.\begin{aligned} \boldsymbol{S}(\mu, \varphi; \mu_0, \varphi_0) &= \tilde{\boldsymbol{S}}(\mu_0, \varphi; \mu, \varphi_0) \\ \text{and} \qquad \boldsymbol{T}(\mu, \varphi; \mu_0, \varphi_0) &= \tilde{\boldsymbol{T}}(\mu_0, \varphi_0; \mu, \varphi)\,. \end{aligned}\right\} \tag{552}$$

From equations (548)–(551) it is evident that the matrices $\boldsymbol{S}^{(1)}$, $\boldsymbol{S}^{(2)}$, $\boldsymbol{T}^{(1)}$, and $\boldsymbol{T}^{(2)}$ have the required symmetries. But it is not at once apparent that the matrices $\boldsymbol{S}^{(0)}$ and $\boldsymbol{T}^{(0)}$ are in conformity with the reciprocity principle; for, though the diagonal elements of $\boldsymbol{S}^{(0)}$ and $\boldsymbol{T}^{(0)}$ clearly satisfy the necessary conditions, for the nondiagonal elements the validity of the principle requires that (cf. eqs. [540] and [541] or [543] and [544])

$$\left[\frac{C^2_{0,\,r}(0) - C^2_{1,\,r}(0)}{C^2_{0,\,l}(0) - C^2_{1,\,l}(0)}\right]^{\frac{1}{2}} \nu_i = -\left[\frac{C^2_{0,\,l}(0) - C^2_{1,\,l}(0)}{C^2_{0,\,r}(0) - C^2_{1,\,r}(0)}\right]^{\frac{1}{2}} u_i \qquad (i = 1, 2)\,. \tag{553}$$

From equations (405), (406), (510), and (511) defining the constants ν_i amd u_i, it is seen that the condition (553) is equivalent to

$$\frac{1}{2}\left[\frac{C^2_{0,\,r}(0) - C^2_{1,\,r}(0)}{C^2_{0,\,l}(0) - C^2_{1,\,l}(0)}\right]^{\frac{1}{2}} (\gamma_1\gamma_4 + \gamma_2\gamma_3) = -\left[\frac{C^2_{0,\,l}(0) - C^2_{1,\,l}(0)}{C^2_{0,\,r}(0) - C^2_{1,\,r}(0)}\right]^{\frac{1}{2}} (c_1c_4 + c_2c_3) \tag{554}$$

or

$$\frac{\gamma_1\gamma_4 + \gamma_2\gamma_3}{c_1c_4 + c_2c_3} = -2\,\frac{C^2_{0,\,l}(0) - C^2_{1,\,l}(0)}{C^2_{0,\,r}(0) - C^2_{1,\,r}(0)}\,. \tag{555}$$

On the other hand, from the definitions of the various constants γ_i (eq. [396]), it readily follows that

$$\gamma_1\gamma_4 + \gamma_2\gamma_3 = 2\,[C_{0,\,l}(+1)\,C_{0,\,l}(-1) - C_{1,\,l}(+1)\,C_{1,\,l}(-1)]\,; \tag{556}$$

or, using the identity (105) satisfied by the C-functions in general, we have

$$\gamma_1\gamma_4 + \gamma_2\gamma_3 = 2\,[C^2_{0,\,l}(0) - C^2_{1,\,l}(0)]\,\Omega(1)\,. \tag{557}$$

Similarly,

$$c_1c_4 + c_2c_3 = 2\,[C^2_{0,\,r}(0) - C^2_{1,\,r}(0)]\,W(1)\,. \tag{558}$$

Hence (cf. Paper XI, eq. [133]),

$$\frac{\gamma_1\gamma_4 + \gamma_2\gamma_3}{c_1c_4 + c_2c_3} = \frac{C^2_{0,\,l}(0) - C^2_{1,\,l}(0)}{C^2_{0,\,r}(0) - C^2_{1,\,r}(0)}\,\frac{\Omega(1)}{W(1)} = -2\,\frac{C^2_{0,\,l}(0) - C^2_{1,\,l}(0)}{C^2_{0,\,r}(0) - C^2_{1,\,r}(0)}\,, \tag{559}$$

in agreement with equation (555). Thus our solution for $\boldsymbol{S}$ and $\boldsymbol{T}$ is in conformity with the requirements of the reciprocity principle.

MODEL SOLAR ATMOSPHERES

GUIDO MÜNCH
Observatorio de Tacubaya
Received May 1, 1947

ABSTRACT

In this paper the model solar atmospheres considered earlier by Strömgren have been revised, using the recent determination of the continuous absorption coefficient of H^- by Chandrasekhar and Breen. The mean absorption coefficients have been obtained in the manner pointed out by Chandrasekhar and with the temperature distribution of a gray atmosphere. The values of the opacity per gram, $\bar{\kappa}$, the total pressure, p, and the electron pressure, p_e, at a number of depths in the range $0.01 \leqslant \tau \leqslant 1.4$, are tabulated for the different values of the hydrogen-metal ratio considered. It is found that the values of p and p_e are systematically lower than those given by Strömgren, while the values of $\bar{\kappa}$ are higher by factors of the order of 1.2 for layers with $\tau > 0.02$.

1. *Introduction.*—The work of Bengt Strömgren on model solar atmospheres[1] provides, at the present time, the most accurate foundation for the theoretical analysis of the outer layers of stars with spectral types between A5 and G2.[2] However, after this important work was published, there appeared two investigations which contain certain developments that may modify to some extent the results of his calculations. The first of these investigations by S. Chandrasekhar,[3] deals with the radiative equilibrium of a nongray atmosphere, and the second, by Chandrasekhar and Breen,[4] contains values for the continuous absorption coefficient of the negative ion of hydrogen, which are much more accurate than those used earlier. Preliminary results of these recent developments have been pointed out by Chandrasekhar and Münch[5] and have been shown to be highly satisfactory. The object of the present work is to compute, on the basis of the same developments, the model solar atmospheres and to compare them with those obtained by Strömgren.

In order to specify our models, we shall keep most of the simplifying assumptions made by Strömgren. We shall suppose, accordingly, that the structure of the solar atmosphere is defined by the effective temperature, $T_e = 5713°$, the specific gravity, $g = 2.740$ cm/sec^2, and the chemical composition. Furthermore, we shall suppose that only H^- and neutral H contribute appreciably to the opacity. Our problem is then to determine the temperature, T, the total pressure, p, the electron pressure, p_e, and the opacity, $\bar{\kappa}$, as functions of depth.

2. *The mean absorption coefficients of* H^- *and* H.—It has been shown by Chandrasekhar in Radiative Equilibrium VII, that the temperature distribution in a nongray atmosphere in radiative equilibrium, in a first approximation, is given by the expression

$$T^4 = \tfrac{3}{4} T_e^4 [\tau + q(\tau)] , \qquad (1)$$

where $q(\tau)$ is a certain monotonic increasing function of the optical depth τ, provided that we measure τ in terms of a mean absorption coefficient, $\bar{\kappa}$, defined as a straight mean of the monochromatic absorption coefficient weighted according to the fluxes $F_\nu^{(1)}$ of a gray atmosphere of the same effective temperature, T_e, as the actual one considered.

[1] *Pub. mind. Med. Kobenhavns Obs.*, No. 138, 1944. This paper will be referred to hereafter as "Tables."

[2] Cf. B. Strömgren, *Festschrift für Elis Strömgren* (Copenhagen, 1940), p. 218.

[3] *Ap. J.*, **101**, 238, 1945. This paper will be referred to as "Radiative Equilibrium VII."

[4] *Ap. J.*, **104**, 429, 1946.

[5] *Ap. J.*, **104**, 446, 1946.

Accordingly, if x_H denotes the degree of ionization of hydrogen and m_H the mass of the hydrogen atom, the opacity per gram of stellar material, on account of the large abundance of hydrogen, can be written as

$$\bar{\kappa}(\tau) = \frac{1 - x_H}{m_H} [p_e a_\tau(H^-) + a_\tau(H)] , \tag{2}$$

where

$$a_\tau(H^-) = \frac{1}{F}\int_0^\infty \kappa'_\nu F_\nu^{(1)}(\tau)\, d\nu \tag{3}$$

and

$$a_\tau(H) = \frac{1}{F}\int_0^\infty k'_\nu F_\nu^{(1)}(\tau)\, d\nu . \tag{4}$$

In equation (3) κ'_ν denotes the monochromatic absorption coefficient of H^-, per neutral hydrogen atom and per unit electron pressure, after allowing for the stimulated emission factor; this coefficient has been tabulated by Chandrasekhar and Breen[6] as a function

TABLE 1

THE MEAN ABSORPTION COEFFICIENTS $a_\tau(H^-)$ AND $a_\tau(H)$

τ	θ_τ	$a_\tau(H^-)$	$a_\tau(H)$	$a_\tau(H^-)/\phi(\theta)$
		$\times 10^{-26}$	$\times 10^{-26}$	$\times 10^{-17}$
0.00	1.088	11.74	.....	3.490
0.01	1.080	11.41	.....	3.498
0.02	1.074	11.14	.....	3.505
0.04	1.062	10.64	.....	3.517
0.06	1.051	10.19	.....	3.529
0.08	1.041	9.797	.....	3.540
0.10	1.031	9.447	.....	3.551
0.12	1.022	9.133	.....	3.561
0.14	1.014	8.845	.....	3.570
0.16	1.006	8.576	.....	3.578
0.18	0.998	8.318	0.03	3.585
0.20	0.991	8.082	0.05	3.592
0.24	0.977	7.650	0.07	3.604
0.28	0.965	7.251	0.10	3.615
0.32	0.953	6.922	0.13	3.624
0.36	0.942	6.618	0.17	3.630
0.40	0.933	6.342	0.22	3.632
0.50	0.910	5.725	0.42	3.628
0.60	0.891	5.235	0.70	3.620
0.70	0.874	4.824	1.07	3.608
0.80	0.858	4.470	1.69	3.594
0.90	0.844	4.164	2.43	3.578
1.00	0.831	3.901	3.48	3.561
1.2	0.808	3.460	6.42	3.525
1.4	0.787	3.109	11.2	3.486

of wave length and reciprocal temperature θ ($=5040°/T$). Similarly, under the integral sign of equation (4), k'_ν stands for the continuous absorption coefficient of one neutral hydrogen atom. These latter coefficients are given in a convenient numerical form in Strömgren's Tables.

In Table 1 the reciprocal temperatures, θ_τ, computed from equation (1), using the "fourth approximation"[7] for $q(\tau)$, are given. In this same table the values of $a_\tau(H^-)$ and

[6] *Op. cit.*, Table 7.

[7] S. Chandrasekhar, *Ap. J.*, **100**, 76, Table 1, 1944.

$a_\tau(H)$, computed from equations (3) and (4) by graphical integration, are also given. In the last column of Table 1 we have written the values $a_\tau(H^-)/\phi(\theta)$, where

$$\phi(\theta) = 4.158 \times 10^{-10}\theta^{5/2} e^{1.726\theta} \tag{5}$$

represents the number of H^- ions per neutral hydrogen atom and unit electron pressure. The values of the opacity of one H^- ion at different layers thus obtained should be compared with the constant value $Cm_H = 2.51 \times 10^{-17}$ adopted by Strömgren in his calculations.

3. *The calculation of the models.*—Once $\bar{\kappa}$ has been found as a function of τ and p_e, the next step in the calculation of a model stellar atmosphere is to establish a relation between p_e and p which characterizes the degree of ionization of the particular mixture of elements considered. This mixture is specified by one variable parameter $A (A \gg 1)$, which represents the ratio of the number of hydrogen atoms (and ions) and the corresponding number for all metals taken together. Adopting the metal mixture adopted by Strömgren, as well as his calculations of the mean degree of ionization x_M of this mixture, we can write for the number of electrons N_e per unit volume

$$N_e = N_H x_H + \frac{N_H}{A} x_M , \tag{6}$$

where N_H is the number of hydrogen atoms (and ions) per unit volume. The total number of particles per unit volume, on the other hand, is practically

$$N = N_H (1 + x_H) . \tag{7}$$

Therefore, the relation between p_e and p is

$$\frac{p_e}{p} = \frac{x_H}{1 + x_H} + \frac{1}{A} \frac{x_M}{1 + x_H} = \psi (p_e, \tau) . \tag{8}$$

The numerical determination of p_e/p is much simplified by the use of Strömgren's Tables 5, 6, and 7.[8]

The complete determination of p, p_e, and $\bar{\kappa}$ as functions of τ follows from considering simultaneously equations (2) and (8), together with the equation of mechanical equilibrium, written in the form

$$\frac{dp}{d\tau} = \frac{g}{\bar{\kappa}} . \tag{9}$$

Strömgren has solved these three equations by introducing log p as the independent variable. However, in our case, as $\bar{\kappa}$ depends explicitly on τ (by the manner in which the mean absorption coefficients are taken), besides depending on θ_τ through the ionization equation, it may be simpler to carry out the following iteration process. First, we neglect the term $a_\tau(H)$ in equation (2)[9] and write

$$\bar{\kappa}^{(0)} = \frac{1 - x_H}{m_H} p_e^{(0)} a_\tau (H^-) . \tag{10}$$

Introducing equations (10) and (8) in equation (9) we readily obtain

$$p^{(0)} = (g m_H)^{1/2} \left[2 \int_0^\tau \frac{d\tau}{(1 - x_H) \psi (p_e^{(0)}, \tau) a_\tau (H^-)} \right]^{1/2} , \tag{11}$$

[8] *Op. cit.*

[9] It can readily be seen from the results of the calculations that the contribution of neutral H to κ is, at most, 5 per cent that of H^-, in the range of depths considered.

as p and τ vanish simultaneously. A first approximation to $\psi(p_e, \tau)$ is obtained, by taking

$$\psi\,(p_e^{(0)},\ \tau) = \frac{1}{A}; \tag{12}$$

and using this value we may compute $\bar{\kappa}^{(0)}$, $p^{(0)}$, and $p_e^{(0)}$ from equations (10), (11), and (8). With an average of the values of $p_e^{(0)}$ thus obtained, we compute $\psi(p_e^{(0)}, \tau)$ and introduce it again in equation (11) for the calculation of a new set of values $p^{(0)}$, $p_e^{(0)}$, and $\bar{\kappa}^{(0)}$. The process is repeated as many times as are necessary until we find values of the variables which satisfy simultaneously the relations (11), (10), and (8) within the desired degree of accuracy. In order to give an idea of the convergence of such an iteration process, we give the values obtained for log (p/p_e) in the successive iterations for the most unfavorable case (that with log $A = 4.2$), at some values of τ (Table 2).

TABLE 2*

VALUES OF LOG $\psi(p_e^{(0)}, \tau)$ AT SUCCESSIVE ITERATIONS

τ	I	II	III	IV	V	VI
0.01	4.2	4.28	4.26	4.25	4.25	4.25
0.20	4.2	4.22	4.22	4.22	4.22	4.22
1.4	4.2	2.71	3.29	3.37	3.34	3.34

* The Roman numerals refer to the order of the iteration.

Finally, in order to take into account the contribution of the term $a_\tau(H)$ to the opacity, we introduce equation (2) in equation (9) and obtain

$$p\frac{dp}{d\tau}\psi\,(p_e^{(0)},\ \tau)\,a_\tau(H^-) + a_\tau(H)\frac{dp^{(0)}}{d\tau} = \frac{g m_H}{1 - x_H}. \tag{13}$$

From equation (13) it follows that

$$p = (g m_H)^{1/2}\left[2\int_0^\tau \frac{1 - a_\tau(H)\,/\,m_H\bar{\kappa}^{(0)}}{(1 - x_H)\,\psi\,(d_e^{(0)},\ \tau)\,a_\tau(H^-)}\,d\tau\right]^{1/2}. \tag{14}$$

With the values of p obtained from this formula we recompute $\bar{\kappa}$ and p_e by means of equations (8) and (2). The final values thus obtained are very close to those of $p^{(0)}$, $p_e^{(0)}$, and $\bar{\kappa}^{(0)}$. It was found, for example, that the maximum correction introduced into log $\bar{\kappa}^{(0)}$ is only 0.02, which is of the same order of magnitude as the computational uncertainties.

In Table 3 we have collected the results of the integrations for the values of log A used by Strömgren. In this table we have reproduced, for comparison, the values tabulated by Strömgren.

4. *Concluding remarks.*—An inspection of Table 3 shows immediately that our model solar atmospheres differ from those of Strömgren in two main features. (*a*) As a consequence of the more accurate values of the absorption cross-sections of H^- now available, the opacity per gram turns out to be larger by factors of the order of 1.2, except in the extreme outer layers ($\tau < 0.02$). At the same time the total pressure and the electron pressure come out systematically lower. (*b*) The much steeper temperature gradient predicted by equation (1), when compared with the constant gradient used by Strömgren, gives steeper gradients for log p, log p_e, and log $\bar{\kappa}$. With respect to the latter point, we may recall that an earlier discussion by the author[10] has shown that the effect of the

[10] *Ap. J.*, **104**, 87, 1946.

TABLE 3

MODEL SOLAR ATMOSPHERES

τ	FINAL VALUES			STRÖMGREN'S VALUES		
	log p	log p_e	log $\bar{\kappa}$	log p	log p_e	log $\bar{\kappa}$
	log $A=3.0$					
0.01	3.38	0.22	9.05	3.66	0.52	9.10
0.02	3.65	0.44	9.27	3.81	0.64	9.22
0.04	3.88	0.62	9.42	3.96	0.78	9.35
0.06	3.95	0.72	9.51	4.06	0.87	9.43
0.08	4.02	0.80	9.56	4.12	0.93	9.48
0.10	4.08	0.86	9.61	4.18	1.00	9.52
0.12	4.12	0.92	9.65	.....	.....	.....
0.14	4.15	0.96	9.69	.....	.....	.....
0.16	4.18	1.00	9.72	.....	.....	.....
0.18	4.21	1.04	9.74	.....	.....	.....
0.20	4.24	1.08	9.76	4.34	1.20	9.64
0.24	4.29	1.13	9.79	.....	.....	.....
0.28	4.32	1.18	9.82	.....	.....	.....
0.32	4.35	1.22	9.84	.....	.....	.....
0.36	4.38	1.26	9.86	.....	.....	.....
0.40	4.42	1.30	9.88	4.51	1.39	9.78
0.50	4.46	1.37	9.91	4.57	1.47	9.82
0.60	4.51	1.44	9.94	4.61	1.53	9.85
0.70	4.55	1.50	9.96	4.65	1.59	9.87
0.80	4.58	1.55	9.98	4.68	1.64	9.90
0.90	4.62	1.60	0.00	4.71	1.69	9.91
1.0	4.65	1.66	0.03	4.74	1.74	9.94
1.2	4.69	1.75	0.07	4.78	1.83	9.98
1.4	4.73	1.85	0.11	4.82	1.92	0.05
	log $A=3.4$					
0.01	3.56	0.04	8.88	3.84	0.33	8.91
0.02	3.83	0.26	9.09	4.00	0.47	9.05
0.04	3.98	0.44	9.24	4.15	0.60	9.17
0.06	4.10	0.54	9.32	4.24	0.69	9.25
0.08	4.19	0.62	9.38	4.31	0.76	9.31
0.10	4.25	0.68	9.43	4.36	0.82	9.35
0.12	4.29	0.73	9.47	.....	.....	.....
0.14	4.33	0.78	9.50	.....	.....	.....
0.16	4.36	0.82	9.53	.....	.....	.....
0.18	4.39	0.86	9.55	.....	.....	.....
0.20	4.43	0.89	9.58	4.52	1.00	9.47
0.24	4.46	0.95	9.61	.....	.....	.....
0.28	4.50	1.00	9.64	.....	.....	.....
0.32	4.53	1.04	9.66	.....	.....	.....
0.36	4.56	1.08	9.68	.....	.....	.....
0.40	4.59	1.12	9.70	4.69	1.22	9.61

TABLE 3—*Continued*

τ	Final Values			Strömgren's Values		
	log p	log p_e	log $\bar{\kappa}$	log p	log p_e	log $\bar{\kappa}$
	log A =3.4—*Continued*					
0.50	4.64	1.20	9.74	4.75	1.30	9.65
0.60	4.69	1.27	9.77	4.79	1.38	9.68
0.70	4.72	1.34	9.80	4.83	1.44	9.71
0.80	4.76	1.41	9.84	4.86	1.50	9.74
0.90	4.78	1.47	9.87	4.89	1.56	9.79
1.0	4.81	1.54	9.91	4.91	1.62	9.82
1.2	4.87	1.68	9.99	4.95	1.74	9.90
1.4	4.91	1.80	0.07	4.98	1.86	9.98
	log A =3.8					
0.01	3.74	9.85	8.69	4.02	0.15	8.74
0.02	4.01	0.09	8.92	4.17	0.28	8.86
0.04	4.19	0.27	9.06	4.33	0.43	8.99
0.06	4.30	0.36	9.15	4.42	0.52	9.08
0.08	4.38	0.44	9.21	4.49	0.59	9.13
0.10	4.43	0.50	9.25	4.54	0.64	9.17
0.12	4.46	0.56	9.29	.....	.....	.....
0.14	4.51	0.61	9.32	.....	.....	.....
0.16	4.54	0.64	9.35	.....	.....	.....
0.18	4.57	0.68	9.38	.....	.....	.....
0.20	4.60	0.71	9.40	4.70	0.82	9.30
0.24	4.64	0.77	9.43	.....	.....	.....
0.28	4.68	0.82	9.46	.....	.....	.....
0.32	4.71	0.87	9.49	.....	.....	.....
0.36	4.74	0.92	9.51	.....	.....	.....
0.40	4.77	0.96	9.54	4.86	1.05	9.44
0.50	4.82	1.06	9.60	4.92	1.15	9.50
0.60	4.86	1.15	9.65	4.96	1.24	9.55
0.70	4.89	1.24	9.70	4.99	1.32	9.60
0.80	4.91	1.32	9.75	5.02	1.40	9.66
0.90	4.93	1.40	9.81	5.04	1.48	9.70
1.0	4.94	1.48	9.86	5.06	1.56	9.77
1.2	4.97	1.64	9.96	5.09	1.71	9.87
1.4	4.99	1.78	9.06	5.11	1.85	9.97
	log A =4.2					
0.01	3.92	9.67	8.51	4.23	0.01	8.60
0.02	4.19	9.92	8.75	4.37	0.13	8.71
0.04	4.37	0.09	8.89	4.51	0.26	8.83
0.06	4.48	0.19	8.97	4.61	0.36	8.92
0.08	4.55	0.26	9.03	4.66	0.42	8.96
0.10	4.60	0.33	9.08	4.72	0.48	9.01

TABLE 3—*Continued*

τ	Final Values			Strömgren's Values		
	log p	log p_e	log $\bar{\kappa}$	log p	log p_e	log $\bar{\kappa}$
	log $A = 4.2$—*Continued*					
0.12	4.65	0.38	9.12	.....	.....	.....
0.14	4.69	0.43	9.16	.....	.....	.....
0.16	4.72	0.47	9.18	.....	.....	.....
0.18	4.75	0.51	9.21	.....	.....	.....
0.20	4.77	0.55	9.23	4.87	0.67	9.14
0.24	4.81	0.62	9.28	.....	.....	.....
0.28	4.85	0.67	9.31	.....	.....	.....
0.32	4.88	0.73	9.35	.....	.....	.....
0.36	4.90	0.79	9.39	.....	.....	.....
0.40	4.93	0.84	9.42	5.04	0.95	9.34
0.50	4.97	0.96	9.50	5.08	1.06	9.41
0.60	5.01	1.08	9.58	5.11	1.17	9.48
0.70	5.04	1.19	9.65	5.14	1.28	9.55
0.80	5.06	1.29	9.73	5.16	1.37	9.62
0.90	5.08	1.39	9.79	5.18	1.46	9.69
1.0	5.09	1.48	9.86	5.20	1.56	9.77
1.2	5.11	1.65	9.97	5.22	1.72	9.88
1.4	5.13	1.79	0.08	5.24	1.87	0.00

Fraunhofer lines on the temperature distribution is such that the temperature gradient predicted by equation (1) is not likely to be higher than the actual one and that the boundary temperature given by the same equation is also close to the actual one.[11] It must be noticed, however, that for layers with $\tau > 0.2$, our values of p, p_e, and $\bar{\kappa}$ run sensibly parallel to those given by Strömgren, for this fact implies that the upper limit of the hydrogen convection zone determined earlier[12] remains essentially unchanged.

From the discussion of the preceding paragraph we may conclude that the differences between the model solar atmospheres here presented and those computed by Strömgren are most significant in the layers relevant to the formation of absorption lines. Therefore, it might be important to use these new models when a rediscussion of the problems related to the absorption lines in the solar spectrum is undertaken.

It is again a pleasure to record my indebtedness to Dr. S. Chandrasekhar for his advice and encouragement in connection with the present work.

[11] It should be remembered that, according to the ideas of Radiative Equilibrium VII, it is still necessary to analyze how the temperature distribution given by equation (1) is altered by the nongrayness of the solar atmosphere. It is our intention to come back to this question in a later paper.

[12] Cf. M. Rudkjøbing, *Zs. f. Ap.*, **21**, 254, 1942.

THE SOLAR CURVE OF GROWTH FOR LINES OF *V* I*

R. B. KING AND K. O. WRIGHT
Mount Wilson Observatory and Dominion Astrophysical Observatory†
Received June 9, 1947

ABSTRACT

Curves of growth for solar lines of *V* I are constructed for lines of different excitation potential by plotting solar equivalent widths against laboratory *gf*-values. The displacements of these curves yield an adopted excitation temperature of 5400° ± 200° K, which is higher than the temperatures found for lines of *Ti* I and *Fe* I. Shapes of the transition portions of the empirical curves of growth are systematically different. If this is interpreted as due to varying turbulence in the atmosphere, the effect is the same as that observed by Wright in the spectra of F-type stars: the turbulence increases with decreasing excitation potential. Other tests made for the existence of turbulence are inconclusive.

Several investigations of the solar spectrum have been made in the past, in which a general relationship has been established between the *total absorption* or *equivalent width* of absorption lines and the relative numbers of atoms active in producing these lines. This relationship, called the "curve of growth," has been derived by plotting observed equivalent widths against numbers of active atoms derived from (*a*) the Adams-Russell calibration of the Rowland intensity scale,[1] (*b*) theoretical line intensities,[2,3] and (*c*) laboratory measurements of true relative line intensities (*gf*-values).[4] Because theoretical line intensities calculated for LS coupling are not always accurate for complex spectra and because these spectra with large numbers of lines in the solar spectrum usually offer the best observational material for construction of a curve of growth, the use of laboratory intensity data is desirable when such data are available.

The construction of a curve of growth for a star involves the determination of an excitation temperature for the atom whose lines are considered; it may also lead to discoveries of effects such as that which has been commonly ascribed to turbulence in stellar atmospheres. Moreover, if the solar and laboratory data are precise enough, small systematic differences in these quantities may be revealed. For example, solar lines of *Ti* I yield an excitation temperature of about 4400° K when a solar curve of growth is constructed from either laboratory[4,5] or theoretical[3] intensity data, whereas solar lines of *Fe* I in conjunction with laboratory intensities yield an excitation temperature in the neighborhood of 4900° K.[4,6] Thus, further studies of curves of growth for other atoms seem desirable in order to verify possible differences in the excitation temperatures. The present paper, based on recent laboratory measurements of intensities in the spectrum of *V* I by one of the authors,[7] is a contribution to this end.

The larger problem, namely, the effect of the new data on the form of the solar curve of growth as a whole, will be discussed by one of us (Wright) in a paper now in preparation.

* *Contributions from the Mount Wilson Observatory, Carnegie Institution of Washington*, No. 736.

† Surveys and Engineering Branch, Department of Mines and Resources, Canada.

[1] Minnaert and Mulders, *Zs. f. Ap.*, **2**, 165, 1931.

[2] C. W. Allen, *Mem. Commonwealth Solar Obs.*, Vol. 1, No. 5, 1934; Vol. **2**, No. 6, 1938.

[3] Menzel, Baker, and Goldberg, *Ap. J.*, **87**, 81, 1938.

[4] K. O. Wright, *Ap. J.*, **99**, 249, 1944.

[5] R. B. King, *Ap. J.*, **87**, 40, 1938.

[6] R. B. King, *Mt. W. Contr.*, No. 656; *Ap. J.*, **95**, 82, 1942.

[7] R. B. King, *Mt. W. Contr.*, No. 731; *Ap. J.*, **105**, 376, 1947.

Observations.—All solar lines of neutral vanadium for which laboratory intensity measures are available were examined in the *Revision of Rowland's Table of Solar Wave-Lengths*[8] and in the Utrecht *Photometric Atlas of the Solar Spectrum*.[9] Wherever the vanadium line seemed to be a major contributor to a solar line and where some estimate of the effect of other components could be made, the intensity in the *Atlas* was measured, usually by both authors. As there seems to be little or no systematic difference between the *Atlas* measures and equivalent widths given by Allen,[2] the mean of all three measures was adopted as the solar equivalent width of a line; it was given weight 3, 2, or 1 depending on the relative blending and the strength of the line. In this way the equivalent widths were obtained for a total of 169 *V* I lines between λ 3376 and λ 6766 for which laboratory *gf*-values are available. The estimated probable error for both solar and laboratory intensities is about 10 per cent.

Curves of growth.—Following the usual procedure in deriving excitation temperatures and curves of growth, the lines were separated into groups with approximately the same excitation potential. For each group, log W/λ was plotted against log X_f. Here W is the equivalent width of the line, λ its wave length, and X_f is a quantity proportional to the number of atoms active in absorbing the line. For our purpose, since we are concerned at present only with relative members of absorbing atoms and the construction of empirical curves of growth, log X_f may be defined as[4]

$$\log X_f = \log gf + \log \lambda - \frac{5040}{T} \cdot E_i , \qquad (1)$$

where gf is the laboratory gf-value for the line, T the absolute temperature, and E_i the excitation potential of the lower level of the line, expressed in volts. Values of log X_f were obtained for each line by using for E_i the difference between the excitation potential of the low level for the line and the common excitation potential adopted for its group. For this purpose a temperature of 4400° was first adopted because it was thought that the temperature for vanadium should be approximately the same as that for titanium, since the two elements are adjacent in the periodic table. However, a temperature of about 5200° was indicated for vanadium, and, for simplicity, $T = 5040°$ has been adopted in the further calculations for small ranges in excitation potential. Thus, within each group, all lines were reduced to a common excitation potential for the group by subtracting the differences from log $gf \cdot \lambda$.

Three of the best plots of log W/λ against log X_f are shown in Figure 1 for $E_i = 0.04$, 0.28, and 1.06 volts, corresponding to lines arising from the low terms a^4F, a^6D, and a^4D, respectively. Those for higher excitation potentials contain fewer observations of weaker lines and therefore cannot be considered as reliable. For each plot, all near-by observations were grouped together, and weighted mean values, shown by circled crosses on the diagrams, were calculated. Points which were not included in these means are indicated by crosses. Most of the observations fit so well that it seems probable that those omitted contain other components in the solar spectrum, for which no blending correction was made. Because of the multiplicity of symbols which would be required, it is not practicable to indicate on the diagrams the wave-length region of the points. It should be mentioned, however, that there are some suggestions of systematic differences with respect to wave length. But, since these effects are small and inconsistent and since they may be inherent in either the laboratory or the solar data, a discussion of them does not appear warranted at the present time.

Excitation temperatures.—Since the curves of growth for different groups of lines are plotted for different common excitation potentials, they are displaced along the log X_f-

[8] C. E. St. John *et al.*, *Pub. Carnegie Institution of Washington*, No. 396, 1928.

[9] Minnaert, Mulders, and Houtgast (Amsterdam, 1940).

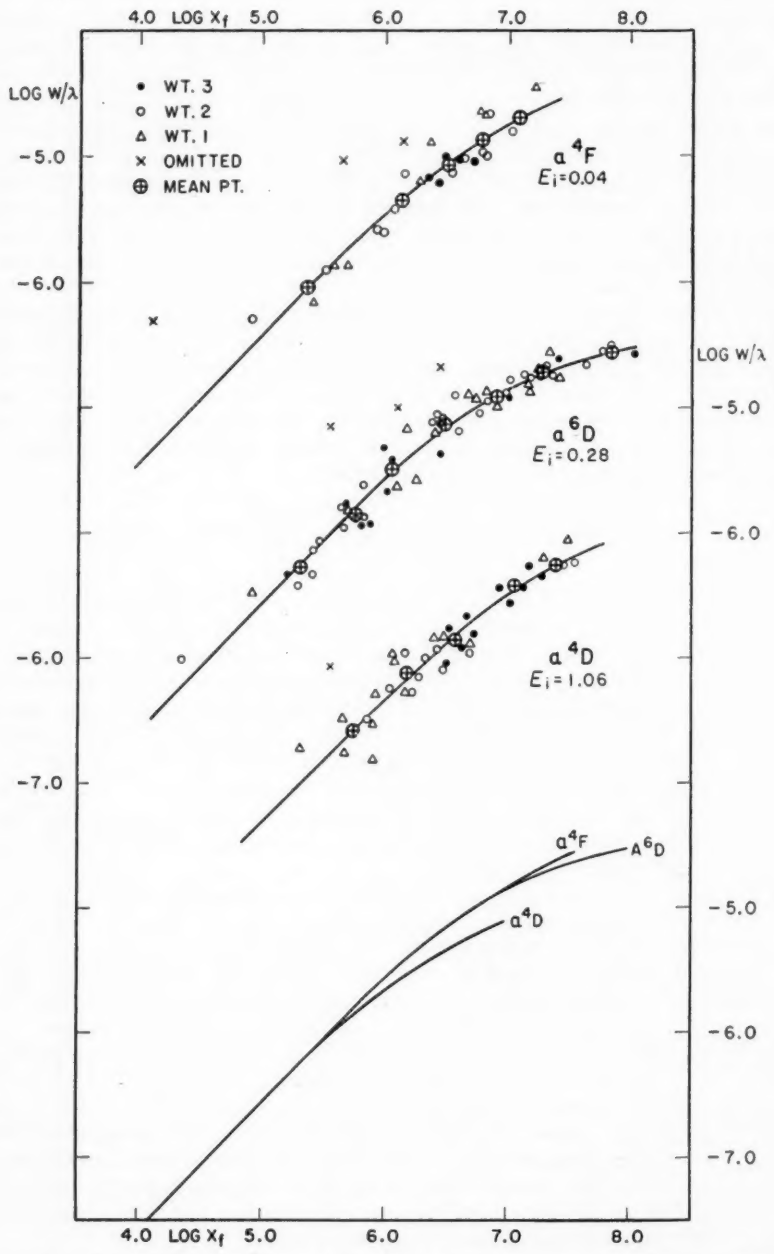

FIG. 1.—*Above:* Curves of growth for *V* I lines arising from a^{4}F, a^{6}D, and a^{4}D terms. *Below:* Mean curves fitted on linear portions.

axis according to excitation potential. To determine the excitation temperature, the best empirical curves were drawn through the mean points for each group of lines, and the several plots for different values of E_i were fitted successively on that for $E_i = 0.28$ volt (a^6D). It was noted (see Fig. 1) that the curved portions of the curves did not agree well; therefore two methods of obtaining a fit were used.

In the first case the graphs were shifted back and forth along the log X_f-axis until the best mean fit for all points was obtained. The displacement of each curve, $\Delta \log X_f$, obtained in this manner from the curve for $E_i = 0.28$ volt, is given in the second column of Table 1, and the plot of $\Delta \log X_f$ against E_i is shown in Figure 2, *a*. The best straight

TABLE 1

DISPLACEMENT OF CURVES OF GROWTH FOR LINES OF DIFFERENT EXCITATION POTENTIALS

E_i	$\Delta \log X_f$	$\Delta' \log X_f$	Wt.	E_i	$\Delta \log X_f$	$\Delta' \log X_f$	Wt.
0.04	−0.15	−0.15	45	1.35	+0.77	+0.75	2
0.28	0.00	0.00	108	1.90	+1.56	+1.49	34
1.06	+0.83	+0.73	70	2.10	+1.75	+1.70	15
1.20	+0.60	+0.55	18	2.35	+2.25	+2.24	8

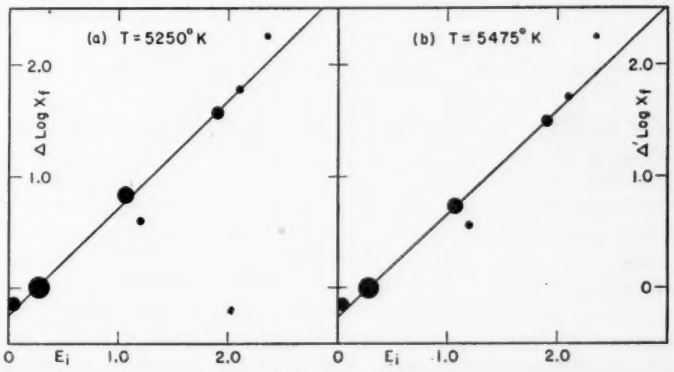

FIG. 2.—Displacements of curves of growth for *V* I lines from various low terms as a function of excitation potential: (*a*) from best fit of all points on curves; (*b*) from best fit of linear portions of curves.

line through these points was determined by least squares; the slope is $5040/T$ and corresponds to a temperature of 5250° ± 225° K.

A second determination of excitation temperature was made by measuring the displacements ($\Delta' \log X_f$) of the straight-line portions of the curves of growth at $\log W/\lambda = -7.00$. These results are given in the third column of Table 1 and Figure 2, *b;* they yield a temperature of 5475° ± 215° K.

Thus either method gives an excitation temperature greater than that found for either *Ti* I or *Fe* I. Moreover, since the linear portions of the curves are less affected by distorting influences, the second method should yield the more reliable value. A mean solar temperature for lines of *V* I may be adopted as 5400° ± 200° K. However, it should be noted from Figure 2 that there is a similar trend in each diagram; if the best smooth curve were drawn through the points, it would be somewhat concave, corresponding to a higher temperature for lines of higher excitation potential. This is a phenomenon

similar to that observed by W. Petrie[10] for flash spectra taken at the 1936 solar eclipse. The observations on the plot for $E_i = 1.20$ volts show rather more scatter than those on other plots; the position of this point in Figure 2 suggests that the intensities might be too large, but a study of the individual lines does not indicate any such trend.

Turbulent velocities.—When the curves of growth were first plotted and preliminary excitation temperatures were derived, it was noted immediately that the curves could not be exactly superposed when shifted along the log X_f-axis. The lines of lowest excitation potential tended to rise above those of higher excitation potential on the transition portion of the curve, as shown in Figure 1. These discrepancies led to the different excitation temperatures derived above and seemed similar to a phenomenon observed by one of us in the spectra of F-type stars.[11] In these F-type stars, curves of growth for lines of neutral iron indicated higher turbulent velocities for low-excitation lines than for those of high excitation potential; further, since this phenomenon was observed in dwarf stars (α Canis Minoris), it was predicted that it might be possible to observe such an effect in the sun.

Accordingly, the plots for different excitation potentials were fitted to theoretical curves of growth which had been calculated according to various stellar models. In theoretical curves both ordinates and abscissae are expressed in terms of units of the Doppler width, which is a function of the kinetic temperature of the absorbing gas and the atomic weight of the element under consideration and which may be expressed as the root-mean-square kinetic velocity (v) of the gas atoms. For example, in D. H. Menzel's theoretical curves,[12] $\log W/\lambda \cdot c/v$ is expressed as a function of $\log X_0$, where X_0, the optical depth at the center of the line, may be defined by

$$X_0 = \frac{\pi e^2}{m c} \cdot \frac{N_a}{\sqrt{\pi}\, b\,(T)} \cdot g f \frac{\lambda}{v} \cdot e^{-E_i/kT}. \qquad (2)$$

In this equation N_a is the total number of atoms of an element in the given stage of ionization, and $b(T)$ is the partition function. In stellar atmospheres, v may be due to a combination of thermal and turbulent motions. For the theoretical curve, the ordinate is $\log W/\lambda \cdot c/v$; for the observations it is $\log W/\lambda$. Therefore, the turbulent velocity may be found from the difference in the ordinates and, if found to vary, will be observed as shifts of different amounts. Such shifts will be readily detected only in the transition portions of the curves. Unfortunately, the lines of V I in the solar spectrum are relatively weak, and few lines reach the transition portion of the curve of growth. Further, the strongest lines are in the violet region and are frequently blended with other lines. Consequently, it is difficult to be certain that such an effect is real. The results of the fit of the observed curves on theoretical curves of growth for the sun are given in Table 2. The theoretical curves used were: (*a*) the curve calculated for the Schuster-Schwarzschild model atmosphere, according to Menzel's formulae[12] which most nearly fitted the empirical curve of growth for the sun determined by Wright;[4] (*b*) the same curve which most nearly agreed with A. Unsöld's calculations;[13] and (*c*) the solar curve of growth calculated by Pannekoek and Van Albada[14] for the Milne-Eddington model of the solar atmosphere. The differences between these curves are small and of the same order as the errors in the observations. In Table 2 are listed the values of $\log W/\lambda = -6.0$, $\log X_f = 0.0$, of the observational curves relative to the theoretical curves for the three models when they are superposed in the position of best fit.

[10] *J.R.A.S. Canada*, **38**, 137, 1944.

[11] K. O. Wright, *J.R.A.S. Canada*, **41**, 49, 1947.

[12] *Ap. J.*, **84**, 462, 1936; *Pop. Astr.*, **47**, 66, 1939.

[13] *Physik der Sternatmosphären* (Berlin: Springer, 1938), p. 264.

[14] *Pub. Amsterdam Astr. Inst.*, No. 6, Part II, 1946.

It is seen that there is considerable scatter in the results for the different curves. Part of this is real, since the theoretical curves do not agree exactly; part of it is accidental, since, even though the results are the mean of two or three fittings, the relatively small curvature of the observed curves makes a definitive fit almost impossible. The curves were superposed at different times, and the close agreement among the results for the same excitation potential seems to indicate that the differences are real. The effect for the sun is the same as that for the stars, namely, that lines of low excitation potential show the best fit with the theoretical curves when shifted to correspond to higher turbulent velocities.

There are two further possible tests of the reality of this effect:

a) If, in equation (2), v varies with E_i in the same manner as X_0, an excitation temperature should be determined from the slope of the straight line drawn through a plot between $\log X_0 \cdot v$ and E_i. For Menzel's curve the mean value of $\log v$ was added to that for $\log X_0$ for each excitation potential, and the sum is given in the fifth column of Table 2. Since it is seen at once that there is not a smooth increase of $\log X_0 v$ with

TABLE 2

TURBULENT VELOCITIES FOR *V* I LINES DETERMINED FROM THEORETICAL CURVES OF GROWTH

THEORETICAL CURVE	(*a*) MENZEL				(*b*) UNSÖLD			(*c*) PANNEKOEK AND VAN ALBADA		
E_i	$\log \frac{W}{\lambda} \cdot \frac{c}{v}$	$\log X_0$	v (Km/Sec)	$\log X_0 v$	$\log \frac{A}{2\Delta\lambda_D}$	$\log \frac{NHf}{\Delta\omega_D}$	v (Km/Sec)	$\log \frac{A}{2b}$	$\log \frac{s_0}{k}$	v (Km/Sec)
0.04	−4.96	6.67	3.3	7.19	−4.57	5.79	4.0	−4.51	6.55	4.6
0.28	5.03	6.72	2.8	7.17	4.68	5.81	3.1	4.64	6.56	3.4
1.06	5.47	7.03	1.0	7.05	5.09	6.14	1.2	5.07	6.86	1.3
1.20	5.70	6.59	0.6	6.37	5.29	5.76	0.8	5.24	6.51	0.9
1.90	5.39	7.87	1.2	7.96	4.97	7.04	1.6	4.89	7.82	1.9
2.10	−5.18	8.30	2.0	8.60	−4.80	7.42	2.4	−4.71	8.22	2.9

E_i, an excitation temperature would have little meaning. This does not, however, preclude the variation of v as some other function of the excitation potential.

b) If there is a real difference in the turbulent velocity for lines of different excitation potential, it should appear in the width of the lines themselves. Because the lines considered in this paper are weak, their true shapes should be determined entirely by the Doppler motions of the atoms; hence a variation might be detectable in their half-widths, defined as[15]

$$2\Delta'\lambda = 1.665 \frac{\lambda}{c} v . \qquad (3)$$

Accordingly, the width ($\Delta\lambda$) of all lines with $\lambda > 4000$ A which seemed free from blends was measured at the point halfway between the central intensity and the continuous spectrum in the Utrecht *Atlas*. The lines were then divided into two groups of $E_i < 0.30$ volts and $1.0 < E_i < 1.3$ volts. Unfortunately, no lines in the second group were strong enough to have central intensities less than 70 per cent of the intensity of the continuous background, and the comparison was on that account confined to the fainter lines whose

[15] Unsöld, *op. cit.*, p. 158.

central intensities were greater than 70 per cent. The two groups contained 23 and 20 lines, respectively. Mean values of $\Delta\lambda/\lambda$, which is proportional to v, were calculated for the two groups of lines and found to be

$$(218 \pm 6) \times 10^{-7} \quad \text{for} \quad E_i < 0.3 \text{ volt}$$

and

$$(200 \pm 6) \times 10^{-7} \quad \text{for} \quad 1.0 < E_i < 1.3 \text{ volts}.$$

For the relatively few strong lines in these groups the behavior is similar, but the differences are greater, suggesting that the lines of low excitation potential may be broader than those of higher excitation potential and that the effect might be more pronounced if stronger lines were available for study.

Thus, although the empirical curves of growth for vanadium lines in the solar spectrum suggest a real variation in the turbulent velocity for lines of different excitation potential, the remaining tests for such variation are inconclusive. As it has not yet been possible to detect such a change in turbulent velocity for lines of iron or titanium,[11] the phenomenon must be considered as possible but not yet conclusively proved for the sun.

However, it seems quite definite that the excitation temperature for vanadium, as determined from curves of growth, is greater than that for either titanium or iron, and therefore it does not appear unreasonable that other differences also may be detected in the future.

ON THE PRESENCE OF POLARIZATION IN THE CONTINUOUS RADIATION OF EARLY-TYPE STARS

W. A. HILTNER
Yerkes Observatory
Received June 26, 1947

ABSTRACT

Observations for detecting the presence of polarization of the continuous spectrum of early-type stars are presented and discussed.

Immediately after Chandrasekhar[1] predicted that the laws of darkening of the continuous radiation from an early-type star were not identical for two planes of polarization (with the component having the electric vector in the meridian plane showing the greater darkening), a program for observing the presence of the polarization was inaugurated at Yerkes Observatory.[2] The method employed was that of placing a Wollaston prism in front of the photographic plate of the 40-inch refractor and then obtaining a series of photographs of an eclipsing binary of suitable character as the eclipse progressed. Since the probable error of a single observation when this technique is employed is of the order of 0.05 mag., it did not seem probable that definitive observations would be obtained. The expected polarization is of the order of only several per cent because of the light from the secondary star.

In November, modifications of the above procedure were introduced, in which the Wollaston prism was placed in front of a microscope objective, which focused the 40-inch objective on a photographic plate. This arrangement gave two images 0.5 mm in diameter and 0.7 mm between their centers. The images were uniform and permitted surface photometry with a transmission photometer. Each photographic plate, which contained as many as 36 pairs of images, was calibrated with a tube photometer.

Three minima of RY Persei at two different position angles of the Wollaston prism were obtained during the past season. This eclipsing system is an especially favorable one because of the early spectral class of the primary star (B4) and because of the rather deep primary minimum (2.0 mag.). The spectral class of the fainter and larger component is F5. An evening's observations consisted of setting the Wollaston prism at a preselected position angle and then obtaining a series of exposures as the eclipse progressed. The exposure time at minimum light was 90 seconds on Eastman 103*a*-O emulsion. The two prism position angles were designated as 1 and 5. Prism position angle No. 1 is such that, if the maximum polarization were observed at this position, the position angle of the plane of the orbit (assuming $i = 90°$) would be 152°. The No. 5 position corresponds to a position angle of 112°.

The individual observations are plotted in Figure 1, and the normal points are recorded in Table 1, along with their internal probable errors and the number of observations in each normal place. The average probable error of a single observation is ± 0.015 mag. and the internal probable error of a normal place is ± 0.003 mag.

The question now arises as to whether or not polarization of the type predicted by Chandrasekhar has been observed. We will first consider the observations of Dec. 2, 1946, $\theta = 112°$. In the course of the night there was a continuous linear change in the observed polarization. Obviously, the polarization is not in the stellar system and must result from an instrumental change. Small systematic errors dependent on hour-angle were anticipated because of flexure in the tube of the 40-inch refractor. However, the

[1] *Ap. J.*, **103**, 365, 1946.

[2] Edith M. Janssen, *Ap. J.*, **103**, 38, 1946.

systematic trend in polarization is independent of hour-angle (see Fig. 1). If we assume that a linear change in polarization resulting from instrumental changes is present, then it is evident that polarization of the light emitted by the star was not observed at this position angle, either before second contact or after third contact.

In considering the observations at $\theta = 152°$, the normal places for the two nights have been combined. The two series agree well. If a straight line best representing the observa-

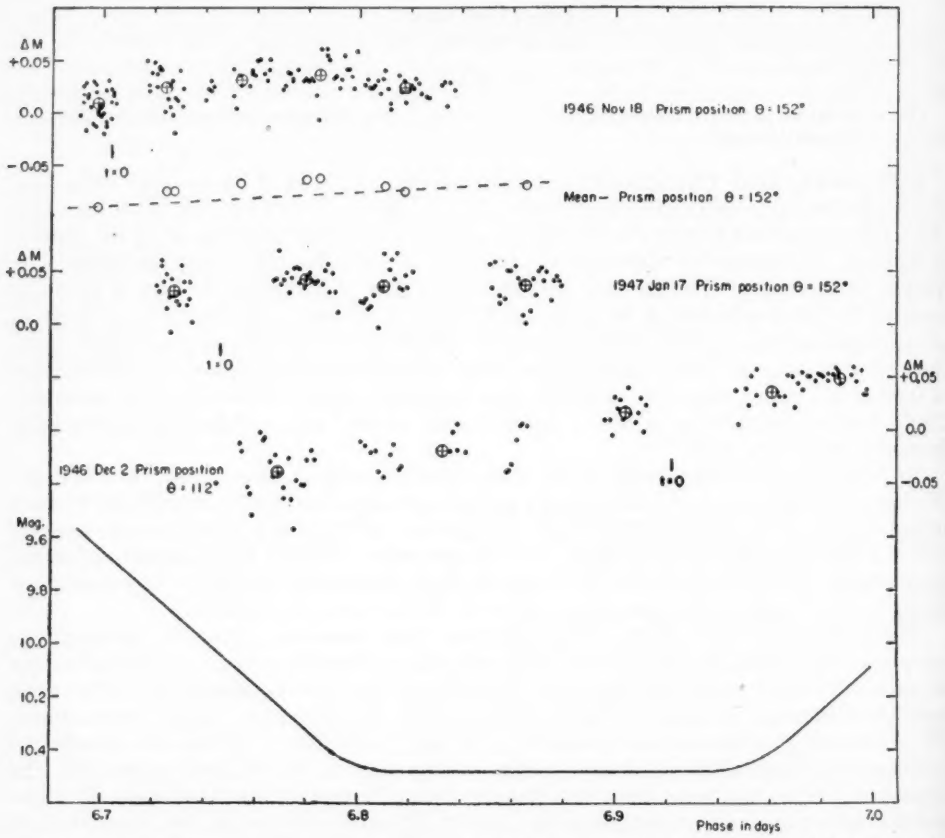

FIG. 1.—Observations for detecting the presence of polarization in the eclipsing variable RY Persei. The small solid dots are individual observations. The large open circles with a cross are normal places. The open circles are the normals for 2 nights when the Wollaston prism had a position angle of 152°. Meridian passage is marked by $t = 0$. The curve at the bottom of the figure is a partial light-curve of RY Persei. NOTE: the date "Jan. 17, 1947" should read "Jan. 19, 1947."

tions is drawn, it is found that four of the normal places fall at least 0.01 mag. from this straight line, a value three times their probable error.

It is apparent that a systematic change in polarization is present and that this systematic trend changes sign through second contact. Furthermore, this systematic trend again reverses sign after second contact. In Figure 1 a straight line has been drawn from the observations during totality to the normal place corresponding to the highest point on the light-curve. The changes in slope of the systematic trend are thus clearly shown.

Thus far there is no information on the magnitude of polarization which one should expect for an eclipsing system like RY Per if electron scattering is important in the

transfer of radiation in the early-type primary star. There are two photographic light-curves of RY Per.[3] The two are not in good agreement, and an average solution was adopted, with $k = 0.55$, $L_1 = 0.20$, and $L_2 = 0.80$. With the aid of tables published by W. Zessewitsch,[4] the difference in intensity of the component polarized with the electric vector in the meridian plane ($\mu_1 = 0.71$) and the component polarized with the electric vector at right angles to the meridian plane ($\mu_1 = 0.63$) was computed. The above coef-

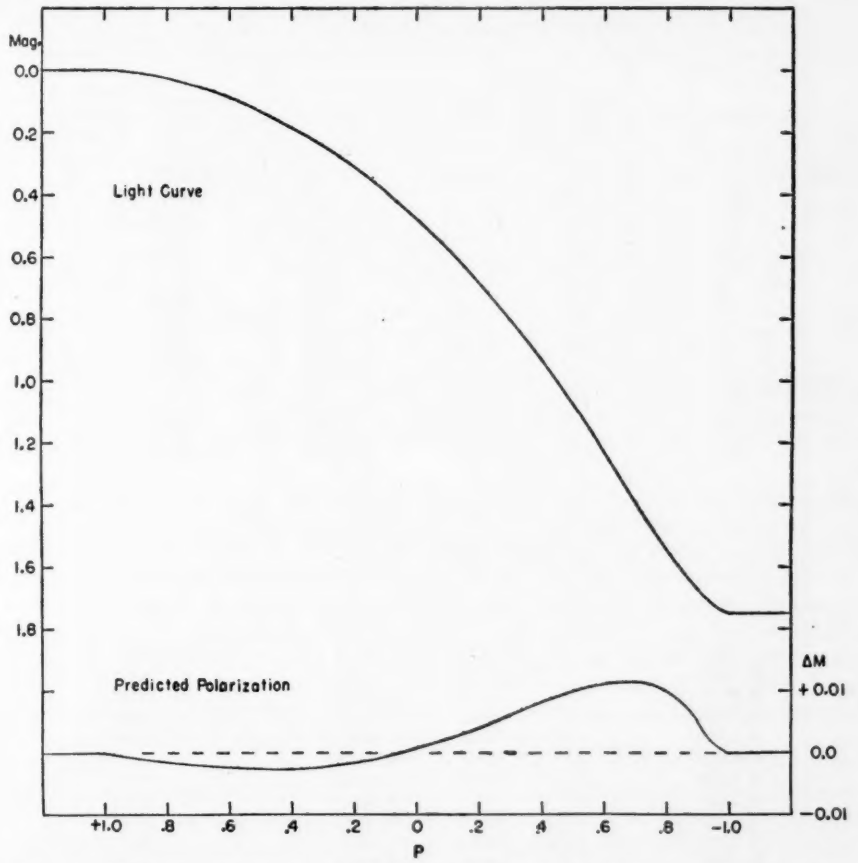

FIG. 2.—Predicted polarization in an eclipsing system similar to RY Persei. Abscissae are in p, where p is the usual symbol for the geometrical depth of the eclipse.

ficients of darkening correspond to the intensities to be expected at the limb. The computations are recorded in Table 2. The small irregularities in the computed values result from the limited accuracy of the tables. Figure 2 shows the predicted polarization and the light-curve of our hypothetical system, which is similar to RY Per. Polarization is present immediately after first contact and changes sign shortly before $p = 0$. Polarization then increases slowly until a maximum effect of 0.015 mag. is attained at $p = -0.7$.

The computed effect is sufficiently large to be observed, and the present observations

[3] Wolbach and Gaposchkin, *Pub. A.A.S.*, **10**, 72, 1940; *Harvard Bull.*, No. 919, p. 24, 1941; Wood, *Contr. Princeton U. Obs.*, No. 21, 1946.

[4] *Bull. Astr., Inst. U.S.S.R. Acad. Sci.*, No. 45, 1939, and No. 50, 1940.

suggest that polarization is present in the primary star of RY Per and that the plane of the orbit of RY Per, assuming $i = 90°$, has a position angle near 152°. However, it is the author's opinion that the present observations should not be accepted as definitive but merely as a progress report. The problem should be attacked with a technique capable of giving results with a precision appreciably greater than that attained here. The technique most likely to give the desired accuracy is a flicker method, which has been successfully employed in the laboratory by the author[5] and on observations on the moon by Öhman.[6] Also, the telescope employed should be one which remains centered throughout the observations, preferably a Cassegrain reflector. Furthermore, the observations should be made rapidly enough so that a neighboring star can be investigated in order to have complete control over the systematic errors.

TABLE 1

NORMAL POINTS

Date	Position Angle	Phase (Days)	ΔM	Probable Error	No. of Observations
1946 Nov. 18	152	6.698	+0.008	±0.0025	31
18	152	6.724	+ .023	.0046	22
18	152	6.754	+ .031	.0024	20
18	152	6.785	+ .035	.0027	28
18	152	6.818	+ .022	.0009	29
Dec. 2	112	6.769	− .040	.0077	23
2	112	6.833	− .020	.0034	22
2	112	6.904	+ .016	.0027	14
2	112	6.961	+ .035	.0036	19
2	112	6.987	+ .049	.0008	19
1947 Jan. 19	152	6.728	+ .031	.0041	21
19	152	6.779	+ .042	.0014	25
19	152	6.810	+ .035	.0056	18
19	152	6.865	+0.036	±0.0032	25

TABLE 2

PREDICTED POLARIZATION

p	ΔM	p	ΔM
−1.000	0.0000	−0.2278	+0.0044
0.9324	+ .0019	−0.1549	+ .0034
0.8950	.0056	−0.0819	+ .0020
0.8640	.0072	−0.0080	+ .0009
0.8366	.0087	+0.0672	− .0001
0.8115	.0093	+0.1445	− .0010
0.7880	.0098	+0.2246	− .0016
0.7659	.0111	+0.3087	− .0024
0.7447	.0115	+0.3982	− .0025
0.7243	.0112	+0.4957	− .0027
0.7045	.0116	+0.6062	− .0033
0.6133	.0114	+0.6560	− .0022
0.5298	.0104	+0.7413	− .0011
0.4510	.0088	+0.8102	− .0013
0.3751	.0078	+1.0000	0.0000
−0.3010	+0.0059		

[5] *Pub. Obs. U. Michigan*, **8**, 45, 1940, and *Ap. J.*, **98**, 43, 1943.

[6] *Ark. f. Mat., Astr., och Fysik*, Vol. **32B**, No. 1, 1945.

SIX-COLOR PHOTOMETRY OF STARS. V. INFRARED RADIATION FROM THE REGION OF THE GALACTIC CENTER*

JOEL STEBBINS AND A. E. WHITFORD
Mount Wilson and Washburn Observatories
Received May 20, 1947

ABSTRACT

A search for the nucleus of our galaxy has been made in a band of infrared radiation at effective wave length 10,300 A. With a photocell and suitable filter on the 60-inch reflector, the sky was allowed to drift with the diurnal motion across the field of a focal diaphragm 8.′6 in diameter. As the intensity along each sweep was recorded, the star clouds and individual stars interfered somewhat, but not entirely, with the penetration to the background. The area of the search extended about 2° on each side of the galactic equator from longitude 321° to 331°, with intensive coverage within 1° of the equator and with supplementary sweeps of greater extent at selected points. The sweeps at successive longitudes usually gave maxima near the galactic circle, outlining a bulge extending about 8° in longitude and 4° or 5° in latitude, with center near 326.°5.

Concurrent sweeps in the red at wave length 7190 A gave a color excess on the red-infrared scale of +1.5 mag., equal to that of the most strongly reddened B stars in the sky. It is shown that the radiation cannot come from a mixture of star clouds and absorbing material like that within 1 or 2 kpc of the sun but must come from a more luminous object behind absorbing material. The light of the bulge, with maximum apparent photographic surface brightness of 25.4 mag/sq sec, adds up, when corrected for absorption, to a total quite comparable with the light of an equal section of the Andromeda nebula. That the observed bulge is probably near the galactic center is shown by its position, form, color, and total light.

Although the idea of using radiation of long wave length to penetrate the interstellar absorbing material in the direction of the galactic center has probably occurred to many investigators, we decided early in 1945 to make the attempt with the means already at hand. The photocell and infrared filter of our six-color system[1] together have an effective wave length of about 10,300 A. On the $1/\lambda$ law this wave length should give less than half the absorption existing for ordinary photographic plates at, say, 4250 A. Estimates of the nature and brightness of a hypothetical galactic nucleus are, of course, purely speculative, but we can derive some rough figures on what to expect. If the galaxy is a spiral of Hubble's class Sb like M31, the chance of detecting the nucleus is better than in a system like M33 of class Sc with a fainter central region.

To estimate the apparent magnitude of the nucleus of M31 at the distance of our galactic center, we assume the distance of the nebula to be 250 kpc and that of the center 10 kpc, and we allow 1 mag/kpc for the photographic absorption. The decreased distance corresponds to an increase of 7 mag. in brightness, which, with 10 mag. of absorption, means that the hypothetical nucleus would be 3 mag. fainter than the observed nucleus of M31. From our measure[2] of M31, $m_{pg} = 9.5$ with a diaphragm of 42″, we then have $m_{pg} = 12.5$ for a circle $25 \times 42'' = 17.'5$ in diameter, or an average surface brightness of 27.3 mag/sq sec, quite beyond the possibility of ordinary photography. Even taking the nucleus alone, which E. Hubble[3] finds to be $m_{pg} = 14$, and diameter 3″, we get $m_{pg} = 17.0$ over a 75″ circle, or 26.1 mag/sq sec, more than 4 mag. fainter than any piece of blank sky in the region of the center.

The red-sensitive plates with which W. Baade[4] has successfully resolved portions of

* *Contributions from the Mount Wilson Observatory, Carnegie Institution of Washington*, No. 734.

[1] *Mt. W. Contr.*, No. 680; *Ap. J.*, **98**, 20, 1943.

[2] *Mt. W. Contr.*, No. 577; *Ap. J.*, **86**, 247, 1937.

[3] *Mt. W. Contr.*, No. 376, p. 52; *Ap. J.*, **69**, 154, 1929.

[4] *Mt. W. Contr.*, No. 696; *Ap. J.*, **100**, 137, 1944.

M31 would, of course, give a great advance in photographing the galactic center. The region of λλ 6000–6700 A might have an interstellar absorption of something like 7 mag. instead of 10, and another magnitude would be picked up with the color index of M31. The infrared will, of course, be still more favorable. The absorption at 10,300 A can be taken as $10 \times 4250/10{,}300 = 4.1$ mag., an improvement of 6 mag. over blue-sensitive plates. With this absorption, M31 would then have $m_i = 6.5$, but this nebula measures 1.8 mag. brighter in the infrared than in the violet of our six-color system. The effective wave length of our violet measures is about the same as that of blue-sensitive plates. Hence we are down to $m_i = 4.7$ for a circle of 17′.5 diameter. The largest diaphragm to be used with the photometer is 8′.6, giving one-quarter the area of 17′.5; hence we have $m_i = 4.7 + 1.5 = 6.2$ for the estimate. With allowance for central concentration, we should expect, then, an infrared magnitude at least as bright as 6.0 for a circle of 8′.6. We shall show that, in terms of galvanometer deflections, this magnitude corresponds to 25 mm, compared with an average sky deflection of something like 150 mm for the same area. As a further comparison, we usually get about 29 mm in the violet from the star NPS 4, $m_{pg} = 5.95$, spectrum A3.

An estimate of the deflection to be expected can be made more directly from our infrared measures of the center of M31. In 1945, with a 4′.1 diaphragm, we obtained a deflection of 60 mm. As before, we allow 3 mag., or a factor of 16, for absorption and distance, and get $16 \times 60 = 960$ mm for a circle $25 \times 4'.1 = 102'$ diameter. The factor for the 8′.6 diaphragm is 1/140; call it 1/100, and we get an expected deflection of $960/100 = 10$ mm, with certainly still more allowance to be made for central condensation.

The comparison with the center of M31 is, of course, pure speculation. If we use M33 for the estimate, we find the central region to be fainter by a factor of 10, and our hoped-for deflection of 25 mm is down to 2 or 3 mm, which would mean no chance of detection. Likewise, the total photographic absorption of 10 mag. between us and the center may be entirely wrong. A few dark clouds absorbing several magnitudes each would bring the figure to 20 mag. instead of 10. The amount of the probable interference of visible star clouds and individual stars in the region of the search can be determined only by trial.

To summarize: If we assume the $1/\lambda$ law and a photographic absorption of 1 mag/kpc, the best to be expected in the infrared is that a central nucleus of our galaxy, like that of M31, could give a galvanometer deflection of 10–25 mm, compared with 100–200 mm from the blank sky or a star cloud. If we knew exactly where to point the 60-inch telescope, such a nucleus could easily be identified even though it was quite out of reach photographically.

The foregoing advance estimates were based conservatively upon the assumption that the $1/\lambda$ law continues linearly out to very long wave lengths and that we would have something like 4 mag. absorption in the infrared. In our study of reddened B stars, however, a slightly curved, rather than a linear, relation with respect to $1/\lambda$ was found.[1] J. L. Greenstein[5] has shown that absorption varying as $\lambda^{-0.56}$ gives the best fit over the observed region but that if the law were continued to long wave lengths a total absorption inadmissible on other grounds would result. In our case the infrared absorption would, on such a law, be 60 per cent of the photographic absorption rather than 40 per cent, as in our preliminary estimate. Greenstein postulated some change in the law beyond 10,300 A. A theoretical curve of this type recently proposed by Oort and Van de Hulst[6] indicates less than 2 mag. absorption at 10,000 A for the same total photographic absorption. This reduction from 4 mag. to 2 mag. in the absorption, or an increase of the expected effective brightness of the center by a factor of 6, seems just too good to be true.

We turn now to the observations with the 60-inch reflector. While for measures of the sky a smaller instrument with the same focal ratio, $f:5$, might serve, for the nucleus itself

[5] *Ap. J.*, **104**, 403, 1946. [6] *B.A.N.*, **10**, 203, 1946.

the advantage would be all with the large reflector if we should happen to hit the right spot. The procedure adopted was to select a point west of the galactic equator and, with the telescope stationary, let the sky drift with the diurnal motion across the field limited by a focal diaphragm of 19 mm or 8.′6 of arc. At declination −30°, the time for a sweep across the field was 40 seconds, long enough to catch any object near the middle of the field, with galvanometer deflections at intervals of 30–15 seconds for full deflection and the same back to zero. With such sweeps at intervals of 6′ in declination, an object crossing in 20 seconds near the edge of the 8.′6 field might be missed, but any detectable nucleus would probably have an appreciable angular diameter.

The tests were begun in July, 1945, necessarily in the dark of the moon. At first, we tried continuous exposures for several minutes between readings for the zero, but this procedure was soon given up because we needed a check on the strong radiation[7] at 10,440 A, which was giving most of the effect and which varies erratically in the course of a night. The brighter *Durchmusterung* stars were identified either at the time or later by comparison with a DM chart. Whereas a late K star of visual magnitude 9.0 might cause a galvanometer jump of 40 mm, an equally bright A star would give only an imperceptible jump of 1 or 2 mm. When several stars in groups or in rapid succession mixed up the record, the general behavior of the region could be established by adjacent sweeps. The method of observation was rather tedious, 30–80 galvanometer readings at 15-second intervals without stop, but perhaps no worse than for long-exposure photography.

In the first season the area of about 1° on each side of the galactic equator was pretty well covered from declination −27°0′ to −30°30′, or galactic longitudes 329.°1 to 324.°9. The ordinary southern limit of the 60-inch is about declination −28°; but, by removing the cover of the mercury trough, the instrument can be pushed to −30°31′ near the meridian, with an additional 6′ available in the double-slide holder at the Newtonian end. In 1946, longer sweeps, extending about 2° each side of the galactic equator, were made at intervals of 30′ in declination. With the 100-inch reflector the search was extended at intervals of 1° down to −34°0′, longitude 320.°7. During this second season a number of much longer sweeps, up to 20 minutes in time, were also taken with the 60-inch on nearby star clouds, as well as various additional duplicate sweeps with a red filter to check the colors.

The procedure is best illustrated by sample traces of the sweeps. In Figure 1 are shown pairs of infrared and red traces for the declinations −29°30′ and −30°30′. The conspicuous radiation at 10,440 A made the infrared deflections five or six times those of the red. The time scale is fixed by the star, HD 160108, $m_v = 6.8$, spectrum K0, which caused the sharp peaks at 0 minutes. Other peaks or "bumps" are likewise synchronous in the two colors. The times of crossing the galactic circle are marked by the vertical lines at −3 and −6 minutes, respectively.

At the outset we note that the HD star is not very red. The deflections are 17.0 and 13.1 mm, giving an uncorrected Δ mag. of R − I = +0.28 mag. We allow −0.06 for differential atmospheric extinction and −0.14 to "normalize" the colors measured that night, and get R − I = +0.08 mag. on the standard system of six colors.[8] This value corresponds to spectrum gG3 or dK1 on the Mount Wilson system; hence the star is probably a dwarf. The giants begin to show space reddening at this low latitude. At both declinations the infrared sweeps show an apparent "bulge" of about 20 mm close to the galactic equator, the smoother one at −30°30′ being 12 to 14 minutes or, say, 3° long.

The bulge in the red is much smaller in each pair. By taking the mean of three to five points near the maximum and the same at 5 or 6 minutes before and after the maximum of each trace, we get the effective deflections corresponding to the bulge. The ratios of these deflections are I/R = 18.2/2.6 and 20.2/3.6, respectively, for dec-

[7] *Mt. W. Contr.*, No. 703; *Ap. J.*, **101**, 39, 1945.

[8] *Mt. W. Contr.*, No. 712; *Ap. J.*, **102**, 318, 1945.

linations $-29°30'$ and $-30°30'$, or Δ mag. = 2.1 and 1.9, with a mean observed R − I = 2.0 mag. Allowing, as before, −0.2 mag. for reduction to standard, we have R − I = +1.8 mag. on the six-color system.

A good sample of the central region of our galaxy is the great star cloud in Sagittarius, which W. Baade[9] has shown to be almost certainly the outer portion of the galactic bulge and to have a stellar population of his type II. We have measured the green and red colors of this cloud in the immediate vicinity of the globular cluster, NGC 6522, at $l = 328°.2$, $b = -3°.9$, and find the G − R index for the cloud and cluster to be the same within 0.01 mag. Hence, assuming the color of the center to be the same as that of unobscured globular clusters, we have from four clusters (unpublished measures) R − I = +0.15 ± 0.02 mag. (p.e.). Another check is with the nuclei of other galaxies; four Sb spirals give R − I = +0.45 ± 0.03 mag. Since these spirals may have some

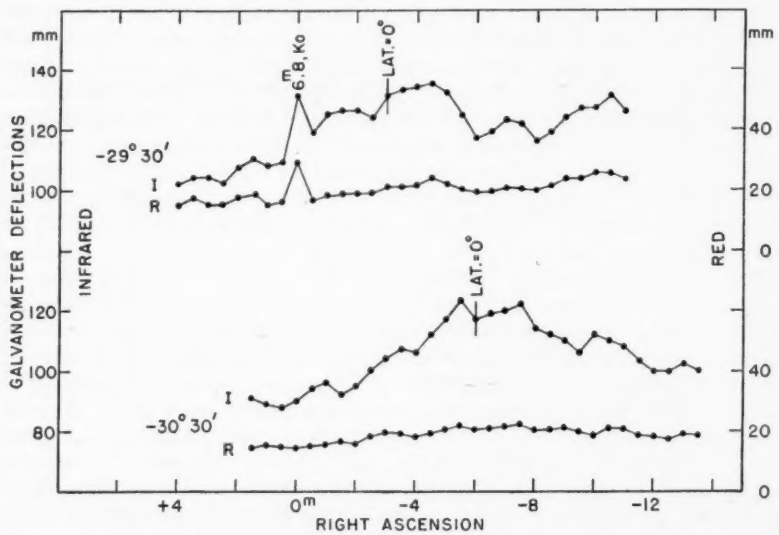

FIG. 1.—Infrared and red sweeps near the galactic center. The times of crossing the galactic equator are marked at −3 minutes and −6 minutes, respectively.

internal space reddening, we really prefer the +0.15 mag. from the star cloud; but, for lack of anything better, we take the rough mean from clusters and spirals, R − I = +0.3 mag., which, combined with the observed +1.8, gives for the color excess of the galactic bulge,

$$E_{r-i} = +1.5 \text{ mag.}$$

This excess indicates strong reddening of the source, whatever it is. We note that the inferred E_{r-i} equals the actual space reddening only if the intrinsic color of the source is uniform along the region of the traces. If the middle is redder, the space reddening is less than E_{r-i}. We can dismiss the possibility that the middle is intrinsically bluer than the margins.

A number of these sweeps are illustrated in Figure 2, in which the diagram is superimposed upon a photograph from the Ross Atlas. The co-ordinates are for 1900. The size of the 8′.6 diaphragm is indicated by the small circle around the bright star at $17^h25^m.6$, $-26°.2$. Since the sweeps were taken at intervals of 6′ in declination and the

[9] *Pub. A.S.P.*, **58**, 249, 1946.

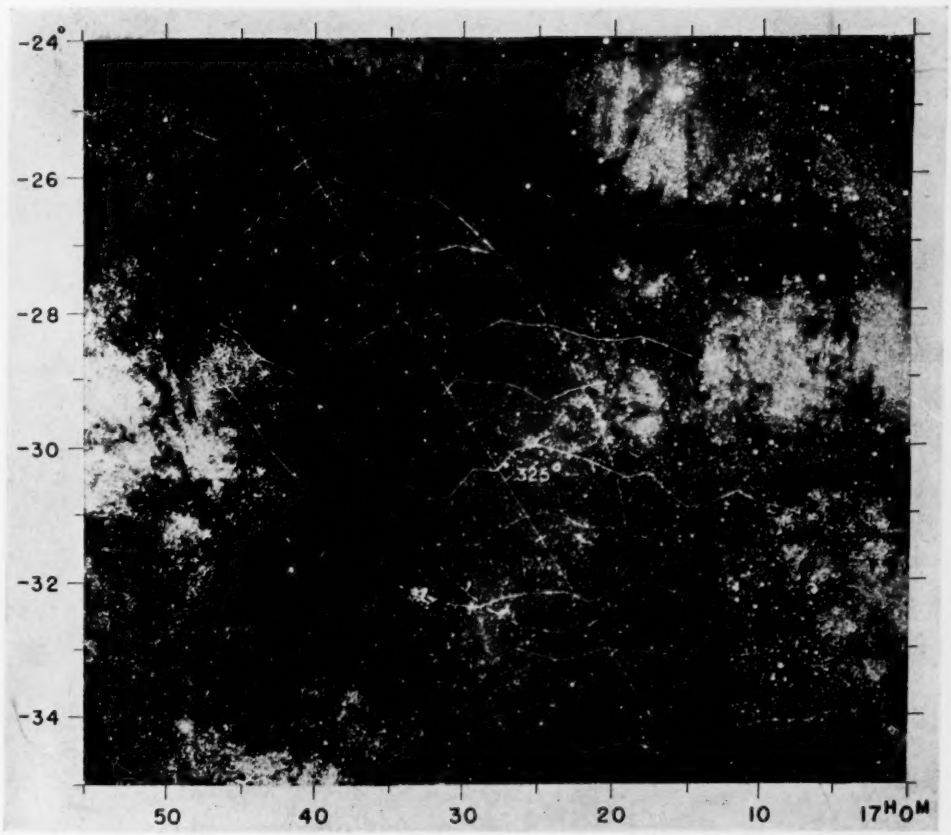

FIG. 2.—Infrared sweeps near the galactic center. The maximum of each curve is placed opposite the corresponding declination. Scale: 20 mm in galvanometer deflections equal 0°.5 in declination.

UNIV. OF MICH.

diagram shows only those on the whole degrees, over much of the region there are nine other sweeps for every one shown. The maximum of each trace is placed opposite the corresponding declination, and the vertical scale for deflections is taken as 20 mm = 0°.5 in declination. The degrees of longitude are marked on the galactic equator of the Lund tables; pole at 12^h40^m, $+28°$ (1900). Note that when a curve goes down, the point measured is not where the curve is but up at the level of the maximum. In general, the plotted points, joined by straight lines, are the means of three observed deflections. When a known *Durchmusterung* star gave a peak in the trace, that point was discarded, but for clouds and unidentified stars the deflections were averaged uniformly, three at a time.

Most of the traces show some sort of maximum near the galactic equator. Consider the longer curves for $-28°$ and $-30°$; these ran for 35–40 minutes and hence were taken in two sections. Each trace shows a minimum to the left of the equator and then a sharp rise at the edge of the great cloud—undoubted evidence that the visible foreground is contributing to the effect. On the other hand, in the trace at $-30°$ the minimum in the obscured region at 10 or 12 minutes to the left of the equator is matched by the intensity at the same distance on the other side in the midst of star clouds. Similarly, at $-28°$ the maximum is in a fairly dark area which measures brighter in the infrared than the apparently much brighter cloud to the right. On the photograph there are many such examples of apparently bright regions which are dark in the infrared, and vice versa. The bulge near the equator seems to be gone at $-34°$; also up at $-25°$ little is left of it.

The oval figure (Fig. 2), some $8° \times 3°.5$ in dimensions, with center at $l = 326°.5$, is drawn not as an isophote to indicate the probable form of a hypothetical bulge, but rather to give a basis of reference. On the left or eastern side this oval curve connects fairly well a series of minima in dark regions running parallel to the equator; but on the other side, in the bright clouds, the same infrared intensities are usually reached, if at all, at greater distances from the equator. Obviously, we should have a series of sweeps in at least two colors, each extending over about an hour in right ascension, but the observational technique will have to be modified to secure them.

In the first summer, rightly or wrongly, we covered quite solidly the area from $l = 325°$–$330°$ within 1° of the equator, on the chance not so much of hitting upon the nucleus itself as of finding a bright central core which would indicate where to intensify the search. When it became evident that something much larger was developing, we extended the limits as shown in the figure and added the red sweeps. Shorter wave lengths, like green and violet, give such small deflections, even for the star clouds, that the accidental errors become predominant.

The photographic surface brightness of the bulge should be close to the computed value for our violet filter. From the 20-mm deflection in the infrared and the reduction of R − I to V − I, allowing for the curved law of reddening, together with check measures on a polar star, we get 25.4 mag/sq sec, in terms of an A0 star at the zenith. When this figure is compared with 21.8 mag/sq sec for the apparently darkest piece of blank sky in the neighborhood, near 17^h24^m, $-26°.2$, we see how little chance there is of photographing such a large faint area with blue-sensitive plates in a field so messed up by star clouds. With infrared plates the situation is, of course, not so unfavorable. It may well be that such plates, if pushed to the limit, will show in greater detail what seems to be indicated in its broad outlines by the photoelectric measures. In particular, if individual stars of known type can be resolved, then photometric distances can be derived and a much better three-dimensional model obtained.

Taken by themselves the traces in Figure 2 may not furnish convincing evidence that they outline something near the galactic center; the minima on the left side of the equator could be simply the effect of a local dark lane. We are well aware of the possibility that to attribute the series of maxima to a galactic bulge may be merely wishful thinking;

but when we change from measures in one color to measures in two colors in that region, the matter appears in a different light. Before making conclusions from the color excess, $E_{r-i} = +1.5$ mag., derived from the traces in Figure 1, we must remember that the space reddening of a cloud of stars mixed in with absorbing material is quite different from the reddening of a cloud or of individual stars all behind such material.

Consider a region of space within a small solid angle centered at the observer. With no absorption and a uniform distribution of stars, each element of volume of thickness dx, on the law of the inverse square, will send the same amount of radiation, call it $\sigma\, dx$, to the center. With absorption corresponding to transmission, p, per unit distance, the total radiation, L, received from the volume out to distance x then becomes

$$L = \int_o^x \sigma p^x dx = \frac{\sigma}{\log p}(p^x - 1)\,. \tag{1}$$

The same reasoning holds whether the observer is in the cloud or is viewing a distant galaxy. In this calculation the contribution of scattered radiation to the received energy is neglected. The reddening of the stellar radiation before it reaches the volume element

TABLE 1

SPACE REDDENING OF A STAR CLOUD

	1/λ Law		Oort and Van de Hulst Law	
	V−I	R−I	V−I	R−I
Δ mag., x=0, 10	0^m97	0^m42	1^m56	0^m59
Δ mag., x=0, ∞	0.99	0.44	1.75	0.75
A/10 kpc	6.0	2.0	8.0	2.0

dx will counteract the bluing effect of the scattering process and give a color for the added contribution to the surface brightness of the element dx which is not very different from that of the stars alone.

For illustration, we apply the relation (1) to our galaxy by assuming a photographic absorption, $A_{pg} = 1$ mag/kpc, the same as for our violet wave length, and also by assuming red and infrared absorptions corresponding to the 1/λ law. Next we try the law of Oort and Van de Hulst,[6] which gives greater transparency for the long wave lengths. Since these guesses on the absorption are merely for illustration, we can adopt the rough figures for red and infrared as 0.60 and 0.40 mag/kpc, respectively, for the first law, and 0.40 and 0.20 mag/kpc for the second. Inserting the proper quantities in equation (1) and converting to magnitudes, we compute the values in Table 1. Considering, first, the figures under the 1/λ law, we see that the Δ mag. for 10 kpc under V − I and R − I, 0.97 and 0.42, respectively, are nearly as large as the 0.99 and 0.44 for infinite distance. As we go outward, the cloud soon becomes practically as red as it will be, owing to the small contribution of the more distant regions. Our observed color excess of the bulge, $E_{r-i} = +1.5$ mag., is not much less than the 2.0 mag. of R − I in the last line of the table, or the total reddening in an optical path of 10 kpc. Therefore, with a photographic absorption of 1 mag/kpc, the reddening we observe cannot come from a few kiloparsecs of a uniform cloud but must be traced to a brighter luminous surface behind the absorbing clouds. This brightening could result from a progressive increase in the ratio of luminous to absorbing material toward the center of the galaxy.

The same remarks apply, though in lesser degree, to the figures under the Oort and Van de Hulst law in Table 1.

From the ratio of the observed to the computed excess in R − I, we have $10 \times 1.5/2.0 = 7.5$ mag. for the minimum photographic absorption at 10 kpc according to either law; the corresponding infrared absorptions are 3.0 and 1.5 mag., respectively. Whether or not these values are plausible depends upon other evidence. Since we have no good direct comparison of our R − I scale with the International scale for space-reddened stars, there is little advantage in attempting to convert E_{r-i} into E_{int} and thence to total photographic absorption for the galactic bulge. The ratio of the scales depends upon the very law of space reddening which is still in doubt. From a dozen bright stars of the North Polar Sequence we have $C_{int}/(R - I) = 1.45$, but this ratio is considerably smaller for space-reddened than for temperature-reddened stars. On the other hand, we do have a good determination of the scales of V − I and R − I for space-reddened B stars, $E_{v-i}/E_{r-i} = 2.91 \pm 0.025$ (p.e.). This value is near that from Table 1 under the $1/\lambda$ law, $6.0/2.0 = 3.0$; hence with the observed $E_{r-i} = 1.5$ we have $E_{v-i} = 3 \times 1.5 = +4.5$. Since this value is 0.75×6.0, the V − I in the table, the total absorption in the violet is 0.75×10; or $A_{pg} = 7.5$ mag. for the total photographic absorption at the center of the bulge.

With this absorption and the apparent maximum surface brightness of 25.4 mag/sq sec, we can estimate the total magnitude of the bulge. From an inspection of Figure 2 we guess that the radiation from the oval area may be represented by that from a rectangle $6° \times 2°$ of intensity corresponding to 10 mm, or about half the maximum deflection. This guess can easily be wrong by a factor of two. The total for this area in square seconds, then, is $25.4 - 19.7 = 5.7$ for the apparent magnitude, or $5.7 - 7.5 = -1.8$ for the unobscured magnitude of the bulge. At the distance of M31 the 8° length of the oval would reduce to 21′, and, changing from modulus 15 for 10 kpc to apparent modulus 22.4,[10] we have $m_{pg} = -1.8 + 7.4 = 5.6$ for the bulge if observed from that distance. By a peculiar coincidence, Whitford's[11] value for M31 with a 24′ diaphragm was also $m_{pg} = 5.6$. This coincidence is, of course, merely the result of a happy combination of numerical values; we could change the figure for the galaxy by a magnitude either way, though on the whole we should prefer to make it brighter rather than fainter. Nevertheless, the brightness of the assumed central region of our system does come out comparable with that of M31, and not vastly different.

We now take up some objections to the conclusion that the light from our so-called "bulge" comes from a source as far away as the center. The two reddest B stars we found in our 1332 list[12] give the following data:

HD 166734, $m_v = 8.8$, Spec. B0, $E_1 = +0.61$, $E_{r-i} = +1.39$.

HD 169034, $m_v = 8.6$, Spec. B0, $E_1 = +0.67$, $E_{r-i} = +1.59$.

The mean E_{r-i} of the two is +1.5, exactly the same as that of the bulge. But, with the allowance of $7E_1$ for absorption and the assumed visual absolute magnitude of −5.5 for supergiants, these stars show distances of only about 1 kpc each. True, they may indicate only a local cloud near longitude 346°, some 20° along the galactic circle from the assumed position of the center; but three or four other B stars within the area of our search have color excesses of about 1.0 mag. in R − I, with distances not more than 2 kpc. Whether this reddening is caused by local clouds or by absorption in a uniform thin layer near the main galactic plane, the chances of getting anything through from a

[10] W. Baade, *Mt. W. Contr.*, No. 697, p. 4; *Ap. J.*, **100**, 150, 1944.

[11] *Mt. W. Contr.*, No. 543, p. 7; *Ap. J.*, **83**, 430, 1936.

[12] *Mt. W. Contr.*, No. 621; *Ap. J.*, **91**, 20, 1940; also *Mt. W. Contr.*, No. 680; *Ap. J.* **98**, 20, 1943.

distance of 10 kpc would seem pretty slim. There are plenty of other reasons for thinking that the center will be difficult to reach; but, since we are dealing with unknown distributions toward the center of both stars and absorbing clouds, as well as with an unknown law of absorption, any conclusion we make can be quickly overturned by further data. Taken at face value, however, the observations here reported seem to suggest that the total absorption toward the galactic center fortunately may not be so great as might have been surmised and that considerable information about this important region of our stellar system may be derived by studying the infrared radiation which it emits. The longer the wave length used, the greater the penetrating power and the better the contrast with the foreground. In the near future we hope to apply a receiver sensitive at 2 μ. Until that is done, further discussion may be held in abeyance.

To summarize: although the space reddening observed in the galactic bulge is equaled in B stars not more than 1 or 2 kpc distant, the location of the bulge, its general outline, and its total light give a strong suspicion that we are actually detecting something near the galactic center. A change in the wave length used, from 1 to 2 μ, would probably settle the question.

We are indebted to Mr. Arundale Vrabec for assistance at the telescope throughout the season of 1945. This investigation was supported in part by the Research Committee of the Graduate School of the University of Wisconsin, from funds supplied by the Wisconsin Alumni Research Foundation.

AN INFRARED STELLAR SPECTROMETER*

G. P. KUIPER, W. WILSON, AND R. J. CASHMAN
Yerkes Observatory and Northwestern University
Received June 23, 1947

ABSTRACT

A stellar spectrometer which was built for the interval $\frac{3}{4}$–3 μ is described. The receiver is a recently developed PbS cell, and the amplifier system was designed for the purpose. Sample spectral records are reproduced.

I. INTRODUCTION

The present paper found its inception during a meeting of the three authors late in 1945. During his work in Germany, Mr. Kuiper had been impressed by the astronomical possibilities opened up by the new PbS cells. The development of these cells in the United States had been carried out by Mr. Cashman, who had also appreciably increased their sensitivity. During the meeting, Mr. Kuiper suggested that a stellar spectrometer be built for the McDonald Observatory; Mr. Cashman offered his co-operation in supplying the cell; and Mr. Wilson agreed to design and build the amplifying system.

The figures on wave-length response of the PbS cell and the modulation frequency were declassified in 1946, when Mr. Cashman presented a paper to the American Optical Society.[1] Further data were announced in a report entitled "Photodetectors for Ultraviolet, Visible, and Infrared Radiation."[2] Cells cooled with dry ice (−78° C) are sensitive for $\lambda < 3\frac{1}{2}$ μ. At the maximum, between 2 and 3 μ, the signal equals the noise for a signal strength on the receiver of about 10^{-12} watt/sec; it is assumed here that the size of the receiver is a few square millimeters. For an uncooled cell the threshold is near 3 μ, and the over-all sensitivity less by a factor of roughly 3 or 5. The most favorable modulation frequency for uncooled cells is near 1000 cps, but the maximum is rather flat. For comparison, the best thermocouples and bolometers will record 10^{-9} watt/sec (signal equals noise).

The spectrometer, exclusive of the amplifier, was designed by Mr. Kuiper, who wishes to acknowledge valuable suggestions from Messrs. Van Biesbroeck and Ridell. The instrument was built by Mr. Ridell in the Yerkes Observatory shop and was completed in November, 1946. The collimator and camera mirrors were made by Mr. Pearson in the optical shop. The prisms were those of the original Bruce spectrograph of the Yerkes Observatory.[3] We used Jena prisms Nos. 1 and 3 after they were found to be satisfactory (0.01-mm definition for 25-cm focal length); prism No. 2 was considerably less satisfactory. The transmission of these prisms up to $2\frac{1}{2}$ μ is fairly good.[4] From $2\frac{1}{2}$ μ to the sensitivity threshold of the cell, astronomical observations are made impossible by the extremely heavy atmospheric band *X* due to water vapor. Since the stellar energy-curves have very little energy beyond 3 μ, the present spectrometer is ideally suited for the investigation of infrared stellar spectra beyond the photographic range.

The co-operation between Northwestern University and the University of Chicago

* *Contributions from the McDonald Observatory, University of Texas*, No. 139.

[1] *Jour. Amer. Opt. Soc.*, **36**, 356, 1946.

[2] R. J. Cashman, *Proceedings* of the National Electronics Conference, Chicago, September, 1946.

[3] E. B. Frost, *Ap. J.*, **15**, 16, 1902.

[4] *Smithsonian Physical Tables* (8th ed.), Table 438, heavy flint, O-469, or O-102.

was further extended by the participation of Mr. Wilson in the observations at the McDonald Observatory for a 10-day period, starting December 16, 1946.

Section III of this paper is written by Mr. Wilson; the rest by Mr. Kuiper.

II. DESCRIPTION OF THE SPECTROMETER

The optical train is shown in Figure 1, which gives a vertical cross-section of the instrument as attached to the telescope. The F ratio at the Cassegrain focus being about 1/14, a 4° beam enters the slit and is reflected by the collimator, consisting of an off-axis paraboloid with focal length of 690 mm. The diameter is 56 mm; the center is 61 mm off-axis. The collimated beam is 50 mm in diameter, passes through two heavy flint prisms (Jena O-102) and is brought to a focus by an off-axis parabolic camera with $F = 250$ mm,

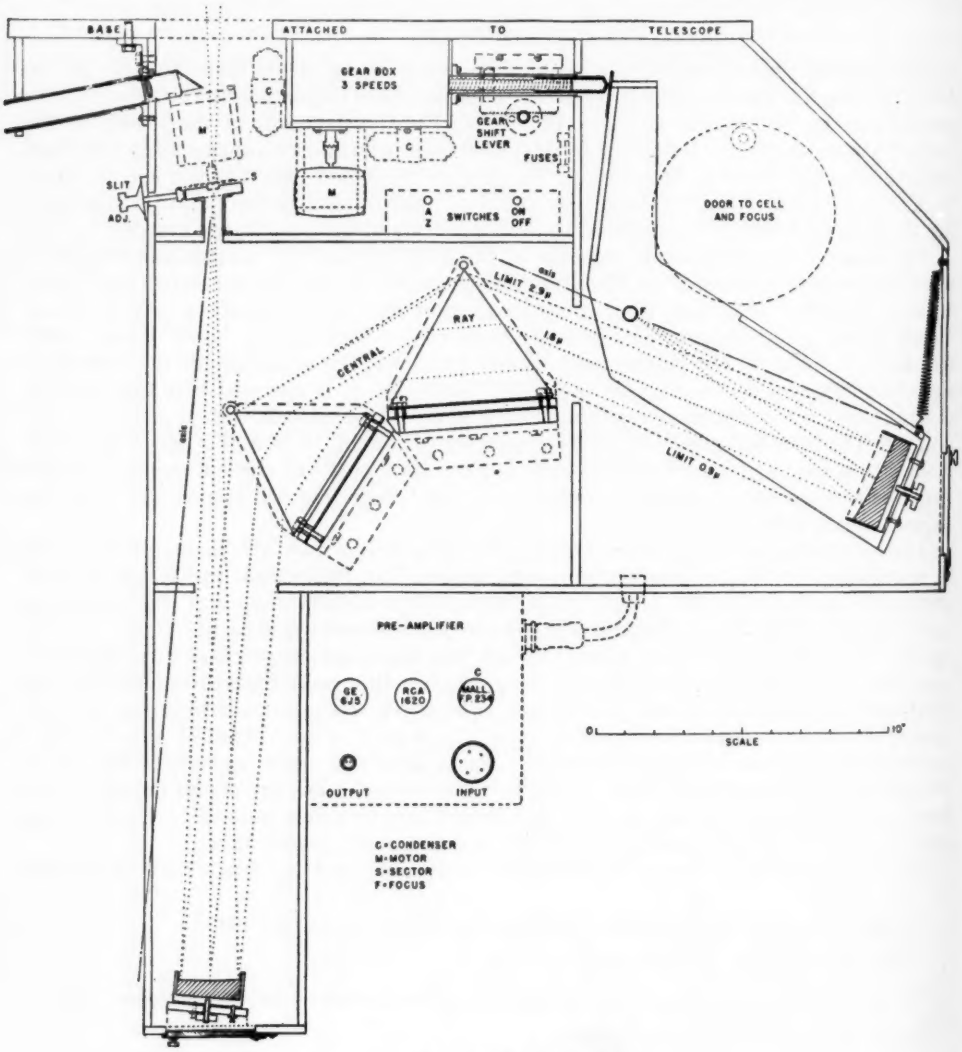

FIG. 1.—Design of spectrometer

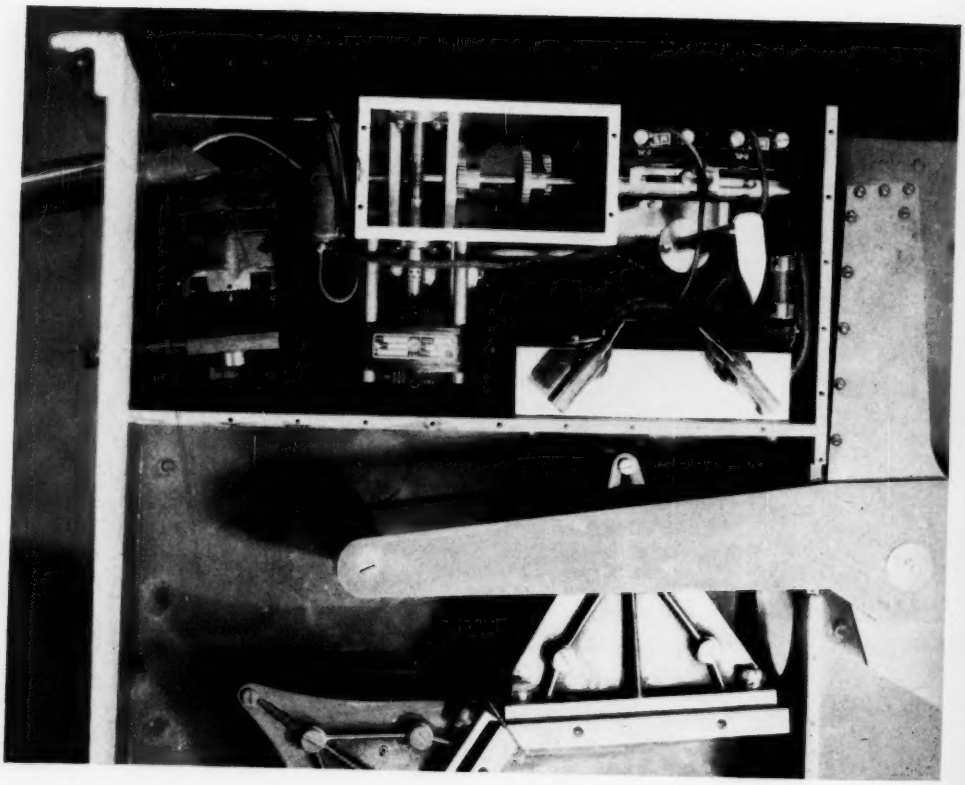

FIG. 2.—Motor compartment of spectrometer

OF
MICH.

aperture 78 mm, and its center 50 mm off-axis. Evidently, the particular wave length leaving the prisms in a direction parallel to the camera axis will be focused without distortion. By rocking the camera about the focus of the paraboloid, all wave lengths are focused successively at that point. The PbS cell is therefore placed with its sensitive strip at the focus of the camera. A scan mechanism is provided, driven by a synchronous motor with three gear shifts for different scanning rates. For the interval 9000–29,000 A the three scan intervals are about 40 seconds, $2\frac{1}{2}$ minutes, and 10 minutes. The length of the spectrum from 9000 to 29,000 A is about 26 mm at the focus; with an effective receiver width of $\frac{1}{4}$ mm, one hundred independent signals are obtained and the approximate resolution, $\lambda/\Delta\lambda$, is 80.

The radiation falling on the slit is interrupted 1080 times per second by means of a rotating sector having 36 teeth, mounted directly on the shaft of an 1800 r.p.m. synchronous motor. The distance between the sector and the slit is about 6 mm, making the diameter of the stellar beam about $\frac{1}{2}$ mm at the place where it is cut. The teeth of the sector are about 3 mm wide and are separated by equal spaces; therefore, the modulation of the admitted radiation is nearly a square wave, which is advantageous. For mechanical reasons it was not possible to bring slit and sector closer together.

The adjustment of the mirrors is made by push-and-pull screws, to which doors in the outer frame of the instrument give access. The adjustment was made by ray-tracing and needed to be made only once. When the instrument is in operation, the sector is kept running while the motion of the scan is controlled by two switches, one *on* and *off* and one *forward* and *backward* (see Fig. 1). When a scan is completed, a microswitch cuts it off automatically. A normal spectral run consists of one scan with increasing wave lengths and one with diminishing wave lengths. If the intensity of the source is unknown beforehand, a trial run is made with the fast scan, in order to give the maximum reflection a suitable value. The guiding microscope is provided with a reticule. The slit can be limited both in length and in width by measured amounts, including a complete cutoff for the dark reading of the cell.

The motor compartment is kept away from camera and cell and is attached directly to the heavy base plate and the telescope itself. This minimizes the transmission of mechanical vibration to the cell, which otherwise might raise the noise level. Another favorable factor is the high modulation frequency of 1080 cps, much higher than the motor frequency of 30 cps (1800 r.p.m.).

The motor compartment is shown in Figure 2. The arm surrounding one prism is a counterweight, not shown in Figure 1, which puts the center of gravity of the camera unit in its axis of rotation. The spring tension is now independent of the orientation of the instrument.

Finally, the several compartments, made of $\frac{1}{4}$-inch aluminum, provide adequate electrical and magnetic shielding. It is found, in fact, that the motors have no effect on the noise level of the cell. Also, the heat of the motors is moved upward by convection through a 4-inch hole in the base plate, leaving the cell unaffected. The whole interior of the instrument is blackened. At first, the mirrors were coated with aluminum, and the observations described below were so obtained; more recently silver has been used for increased infrared reflectivity.

At first, it was planned to use a PbS cell cooled with dry ice ($T = -78°$ C), which would have increased the signal-to-noise ratio by a factor of at least 3, as compared to an uncooled cell. The design made enabled the observer to take the cell mount out of the spectrometer for a periodic refill. Later the plan was temporarily dropped in favor of an uncooled cell which could be left in place. It is hoped that in later work the extra magnitude or more can be recaptured.

The sensitive strip of the cell measures roughly $\frac{1}{3} \times 1\frac{1}{2}$ mm, corresponding roughly to $1 \times 4\frac{1}{2}$ mm, as measured on the slit. By using different slit widths on an extended

source, it was found empirically that no gain in resolution was obtained by diminishing the slit width below 0.7 mm. This corresponds to a stellar image of 5″ in diameter. Since the stellar image, except under conditions of exceptionally poor seeing, is smaller than 5″, the spectrometer may be used in slitless form except under the worst seeing conditions. It was found that for stars a slit width of $1\frac{1}{2}$ or 2 mm was most advantageous. For a narrower slit the very faint extensions of the image, varying with the seeing, would be lost and would give spurious fluctuations of the order of 1 or 2 per cent. The sensitivity of the cell along the strip is not entirely constant, having a broad maximum in the center. A stellar image therefore has to be kept within about 10″, or the signal will suffer some reduction in amplitude.

It is noted that only the radiation entering the slit is modulated and able to produce a signal. The spectral record was found to be remarkably clear; scattered radiation does not appear to exceed 0.001 of the average level of the continuum.

III. THE AMPLIFYING SYSTEM

The function of the amplifier is to provide sufficient gain and selectivity at the modulation frequency of 1080 cps to enable the amplifier output to operate a 1-milliampere Esterline-Angus paper-strip recorder and give the maximum signal-to-noise ratio consistent with desired speed for sweeping across the spectrum from about 0.8 to $2\frac{1}{2}$ μ. The maximum gain is sufficient to show plainly the thermal noise generated by a 1-megohm resistor in the input circuit.

The amplifier system consists of two units, a pre-amplifier, giving a gain of some 300 times, which is located on the spectrometer itself, and a main amplifier containing the regulated power supply. These units and the paper-strip recorder are connected with cables of convenient length.

THE PRE-AMPLIFIER

The circuit diagram of the pre-amplifier is shown in Figure 3. The output of the PbS cell is coupled to the high-gain 1620 pentode by means of a conventional resistance-

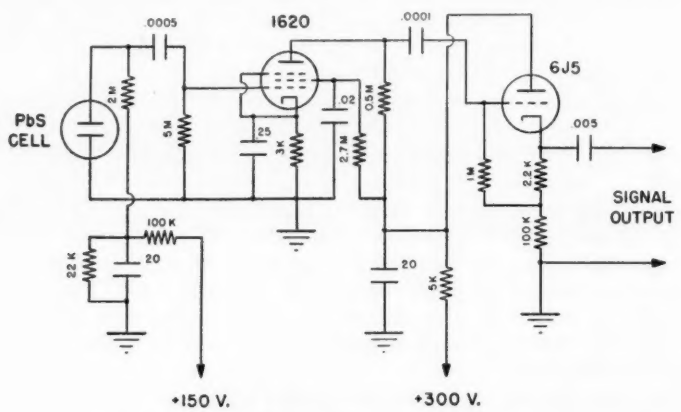

FIG. 3.—Wiring diagram of pre-amplifier

capacitance coupling network, and the potential for operation of the cell is adjusted for maximum signal-to-noise ratio. Inasmuch as PbS cells produce a current-sensitive noise which is in excess of their thermal noise, there is no loss in the signal-to-noise ratio due to this type of input coupling. At all times the amplifier output noise is substantially that originating in the cell itself. A cathode-coupled output stage is employed to enable the

signal to be transmitted without loss over the connecting cable to the main amplifier. The output impedance of the pre-amplifier is about 500 ohms. The voltage gain of the pre-amplifier is 300 times.

THE MAIN AMPLIFIER

The circuit diagram of the main amplifier, together with the regulated power supply, is shown in Figure 4. Following the gain control, a buffer amplifier, consisting of a triode-connected 6SJ7 tube, is employed. This stage has a gain of about 10 times and serves principally to isolate the selective section from the gain control, in order to insure that the selectivity will not be a function of the gain setting.

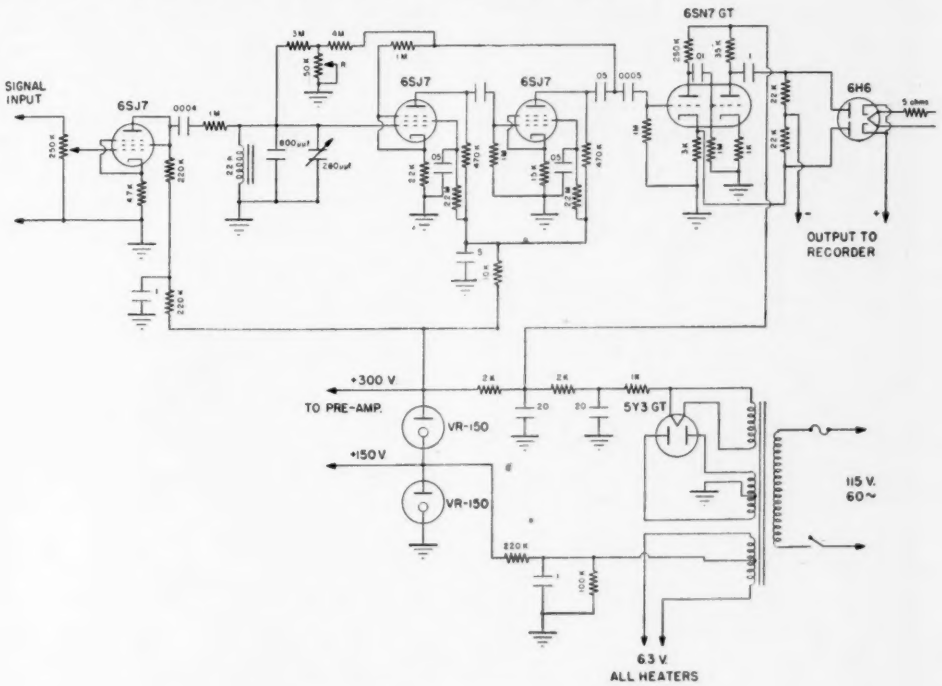

FIG. 4.—Wiring diagram of amplifier

The selective section of the main amplifier consists of the LC circuit and two stages of high-gain pentode-connected 6SJ7 tubes, which are heavily degenerated, for high stability, by means of an inverse feed-back network connected into the 2200-ohm cathode resistor of the first pentode 6SJ7. The LC circuit provides the selectivity, and, by means of the control, R, the Q of this LC circuit can be varied. As R is advanced, positive feed-back is increased across the LC combination. This is equivalent to loading the LC circuit with a controllable negative resistance and thus enables the inherent selectivity of the circuit to be increased. With this arrangement the selectivity can be varied from a band-width about 200 cps wide down to one only 0.5 cps wide. The band-width is measured as the total width when the signal is 6 db down from the peak. At maximum selectivity, the gain of the selective section at 1080 cps is 10^4 times. This provides a total gain from the PbS cell to the output of the selective section of $300 \times 10 \times 10^4 = 3 \times 10^7$ times.

The output of the selective section then feeds a vacuum-tube voltmeter, which is capable of supplying 1 milliampere to the recorder when 2.5 volts alternating current are

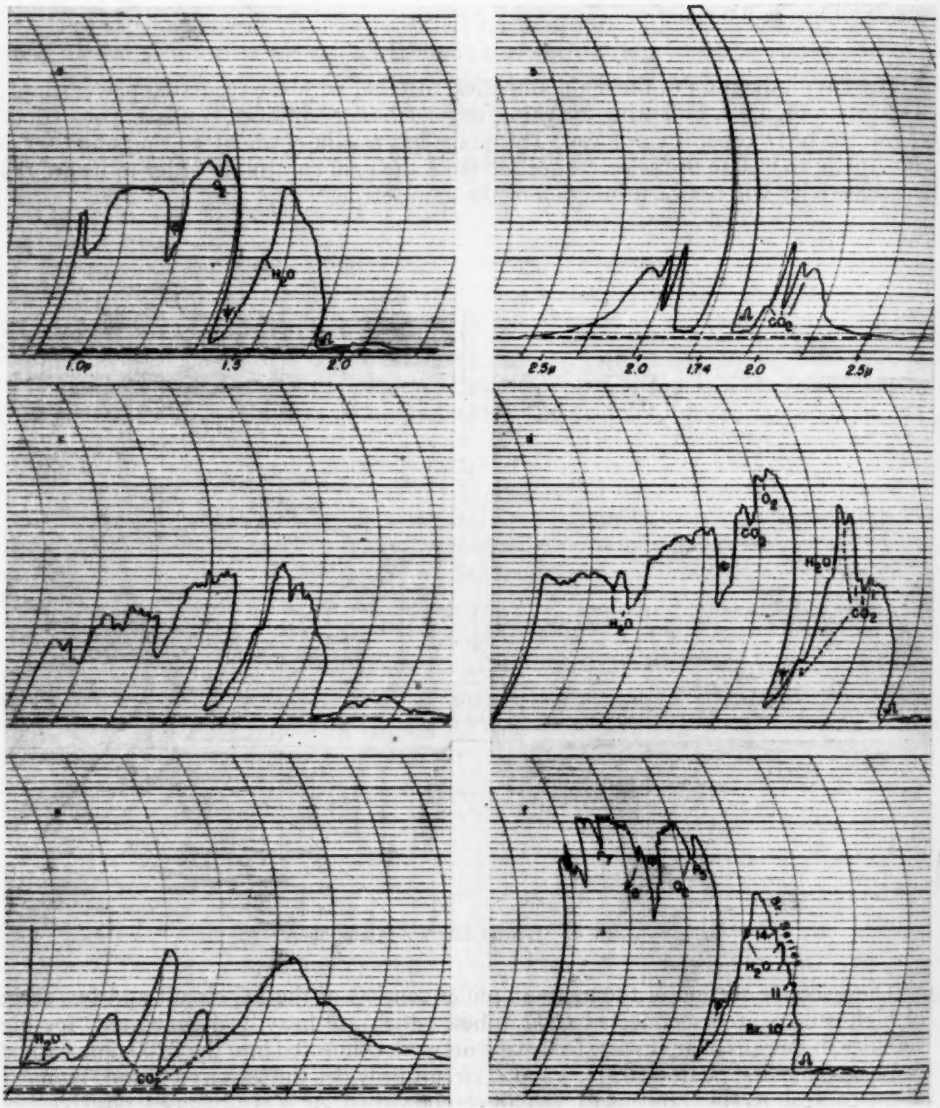

FIG. 5.—*a*, *b*, sun; *c*, Mercury (poor seeing); *d*, *e*, Venus; *f*, Sirius

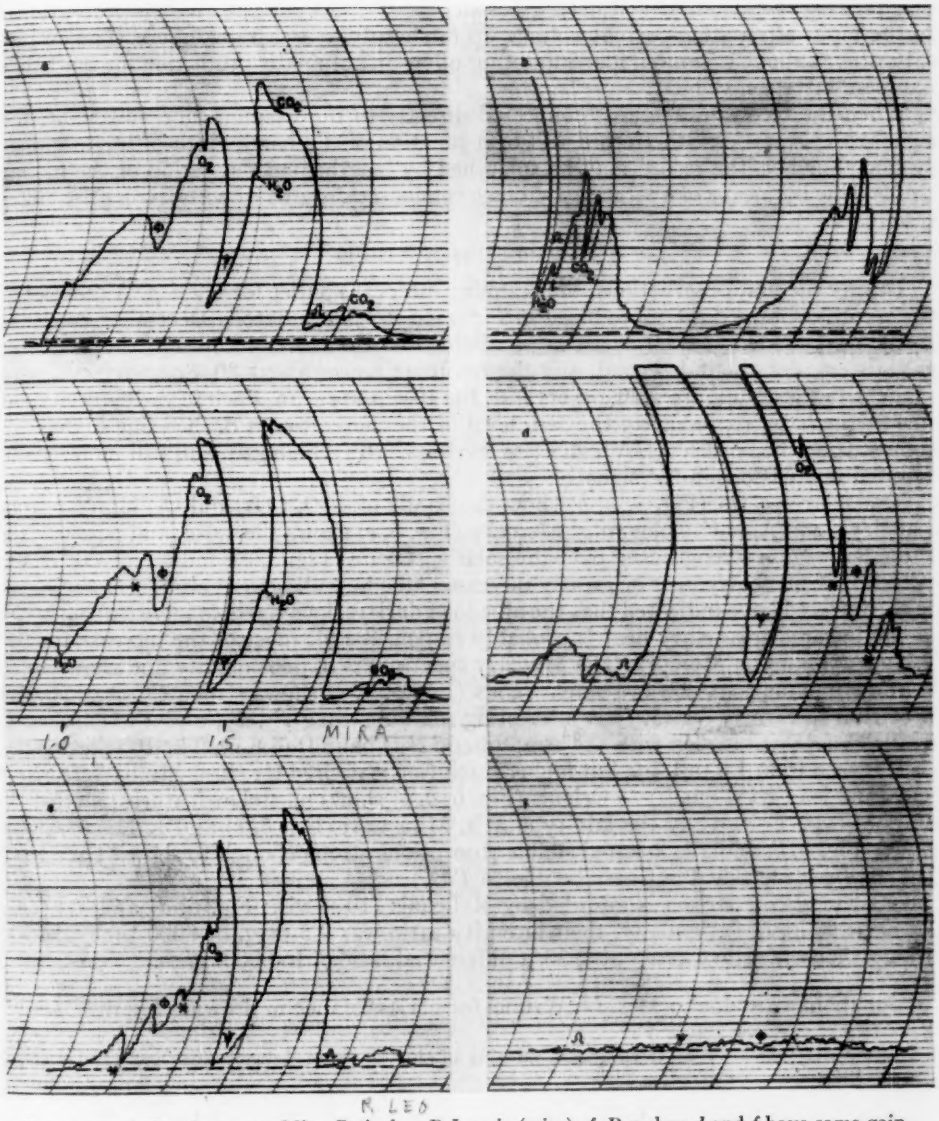

FIG. 6.—*a*, *b*, Betelgeuse; *c*, Mira Ceti; *d*, *e*, R Leonis (min.); *f*, Regulus; *d* and *f* have same gain

applied to its input. The vacuum-tube voltmeter consists of a dual triode 6SN7GT and a full-wave 6H6 rectifier, so connected that about 20 db of negative current feed-back results. This vacuum-tube voltmeter gives an output direct current which is proportional to the input alternating-current voltage up to slightly over 1 milliampere. The output saturates at about 1.5 milliamperes and thus offers an automatic protection for the 1-milliampere meter movement.

When the recording meter is connected directly to the vacuum-tube voltmeter, the signal-to-noise ratio of the record will be a function of the band-width of the amplifier system. Further, the record may be smoothed by lengthening the period of the meter; this is done by means of a large capacitance condenser shunted directly across the meter terminals.

IV. FIRST OBSERVATIONS

During the first observations, the scanning interval was set for 0.9–3 μ. A number of the records obtained are reproduced in Figures 5–6.[5] Their date is December 20, 1946. A 100-mfd condenser was placed in parallel across the meter terminals; the period of the system was about 1 second, and the resolving power about 80. Some records were made with the $2\frac{1}{2}$-minute scan, others with the 10-minute scan. Each record shows a solid line at the base, representing the zero level of the meter, and a dashed line higher up, representing the noise level. A high noise level indicates a high gain and will increase the random fluctuations in the signal.

The solar spectra (Fig. 5, *a*, *b*) show the bands of H_2O, CO_2, and O_2, familiar from Langley's and Abbot's bolograms. Mercury (Fig. 5, *c*) shows the 1.6-μ, and particularly the 2.1-μ, region strengthened over the solar spectrum (Fig. 5, *a*), indicating either the presence of planetary heat or greatly increased albedo. Subsequent studies of the moon in the infrared have indicated that the albedo of dark regions tends to increase somewhat in the infrared; planetary heat is probably responsible for most of the increase for the 2.1-μ maximum on Mercury. The Mercury spectrum is of poor quality and shows some spurious fluctuations due to seeing. Venus (Fig. 5, *d*, *e*) shows strong CO_2 bands. The spectrum of Sirius (Fig. 5, *f*) is interesting for the strong P_7, P_6, and P_5 (Paschen δ, γ, β). P_4 ($P\alpha$) is blended with the atmospheric H_2O band Ω (1.8 μ). The Brackett series of H is seen from 1.6 to 1.7 μ, but higher resolution is desired for closer study. The Sirius spectrum is of good quality. α Orionis (Fig. 6, *a*, *b*) shows no stellar features; neither do stars of type F–K. Only the late-type M's, Mira Ceti (Fig. 6, *c*) and R Leonis, minimum (Fig. 6, *d*, *e*), have infrared stellar absorptions strong enough to show. They have not yet been identified but may be due to *TiO*.

A striking comparison is afforded by R Leonis (10^m8 vis.; Fig. 6, *d*) and α Leonis (1^m3 vis.; Fig. 6, *f*). Visually, their intensity ratio was 9.5 mag. or 8000 times. In the 1.6 μ region the ratio was about 1/20, a differential ratio of 160,000 times.

Our thanks are due to Mrs. N. Wrubel for her assistance in drawing Figures 3–6.

[5] They were exhibited at the Harvard meeting of the American Astronomical Society, December 28–30, 1946.

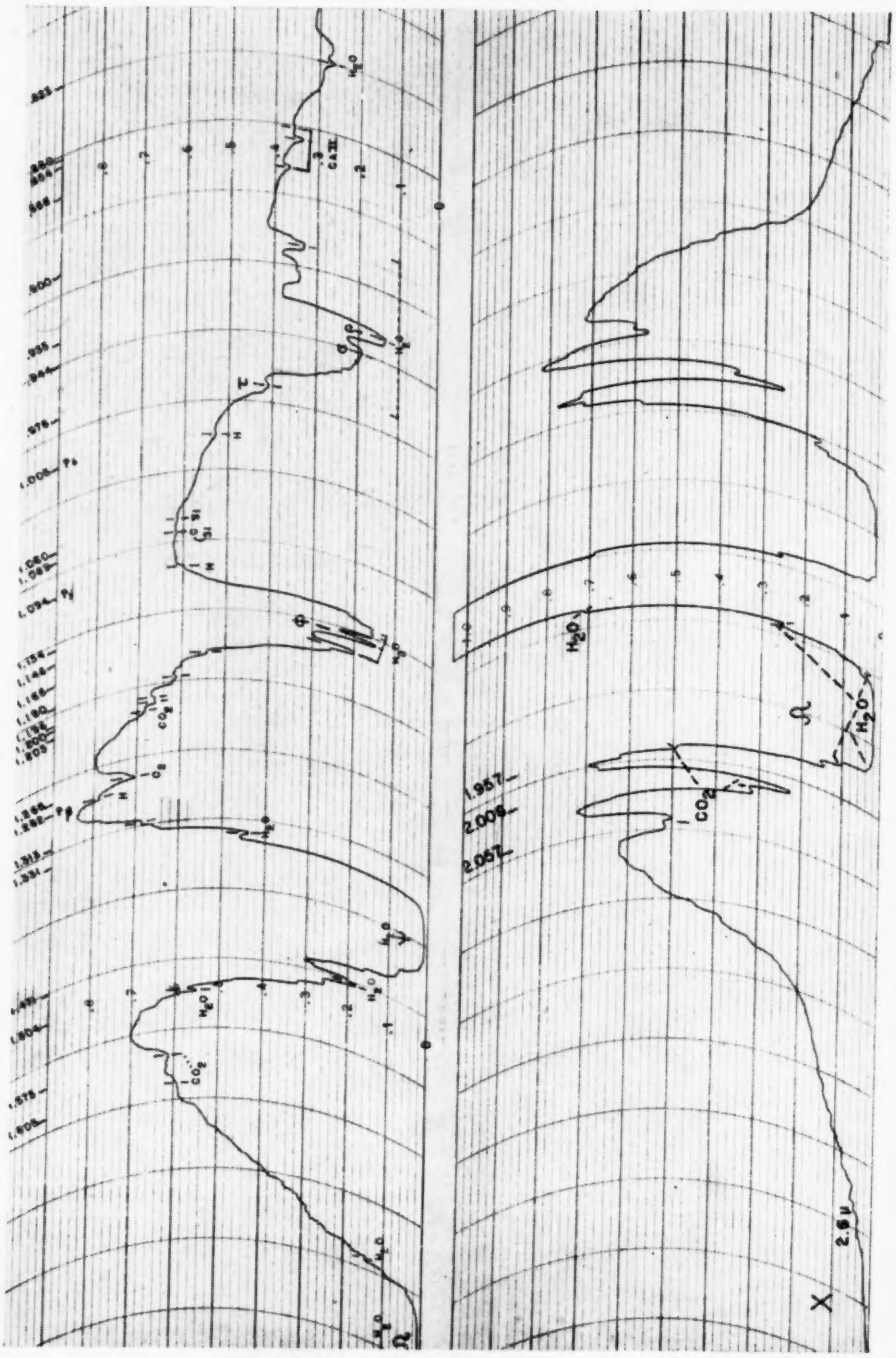

FIG. 1.—Solar spectrum taken at Yerkes Observatory, slit 0.05 mm

UNIV. OF MICH.

INFRARED SPECTRA OF PLANETS*

GERARD P. KUIPER
McDonald Observatory
Received June 20, 1947

ABSTRACT

Infrared spectra of Venus, Jupiter, and Saturn are shown, obtained with a PbS cell.

The extension of planetary spectra beyond the photographic range into the infrared is of interest on two counts: (*a*) the identification of bands and their quantitative interpretation, and (*b*) the heat balance in the planetary atmosphere is affected by these (usually heavy) absorptions.

So far, a number of records have been obtained for Venus, Jupiter, and Saturn. The records for Mercury[1] were affected by poor daytime seeing and have to be repeated. Mars has not yet been observed.

Except for Figure 1, the figures show tracings made by hand on transparent paper from the originals. Most of them show the range $\frac{3}{4}$–$2\frac{1}{2}$ μ (right to left), but two show a double run $2\frac{1}{2}$–1.7–$2\frac{1}{2}$ μ. In all cases the zero level and the noise level are indicated.

Figure 1 shows the solar spectrum for $\frac{3}{4}$–$2\frac{1}{2}$ μ, with the principal features identified. It was obtained at the Yerkes Observatory with an analyzing slit of 0.04 mm in front of the cell, thereby increasing the resolving power from the normal 50–80 to about 500. This value is similar to that used by Langley on the sun, nearly fifty years ago, and not quite so high as that used by Abbot and Freeman more recently.[2] It is reproduced here solely for comparison purposes with the planets.

Figures 8 and 9 show the spectrum of the sun reflected from a MgO block with the usual low resolution. The air masses were 2 and 9, respectively (McDonald Observatory). The dotted curve indicates the approximate position of the spectrum if the telluric bands had been absent. The slight dip at 1.4 μ is due to the absorption in the flint prisms.

Figures 2–4 show the spectrum of Venus. Nine strong CO_2 bands are shown: 1.205 and 1.220 μ, blended; 1.433 μ, shown as a dent in the H_2O band ψ; the group of four bands, 1.536, 1.574, 1.604, and 1.645 μ; and the three bands ω_0, ω_1, ω_2, at 1.957, 2.006, and 2.057 μ. The bands at 1.2 μ had been found previously in the Venus spectrum by Herzberg, by use of 1Z plates.

The declination of Venus was about $-20°$ when these records were obtained, and the daytime seeing there was usually poor. The first results were obtained with the slit parallel to the crescent; but it is seen that this position, while admitting the most light, is the poorest when the image is boiling. Later records, including Figures 2 and 3, were obtained with the slit at right angles to the crescent. In this way variations in the amount of admitted light were minimized. But all records obtained are regarded as provisional because of the unfavorable position of the planet. It is not clear whether or not the dip suggested by Figure 3 at 2.2 μ, is real. It could not be the CO band at 2.3 μ.

The dotted line in Figure 2 would be the approximate spectrum in the absence of the Venus CO_2 bands and the telluric bands. It shows that outside the CO_2 bands the reflection by Venus is nonselective (i.e., white) for the interval $\frac{3}{4}$–2 μ.

Figure 5 shows the Jupiter spectrum. It is heavily cut up by bands, probably due to CH_4 and NH_3. For comparison, a solar spectrum seen through the same terrestrial atmosphere is added. The comparison shows Jupiter to be "blue" in the $\frac{3}{4}$–2-μ region.

* *Contributions from the McDonald Observatory, University of Texas*, No. 140.

[1] *Ap. J.*, **106**, 243, 1947.

[2] *Smithsonian Misc. Coll.*, Vol. **82**, 1929.

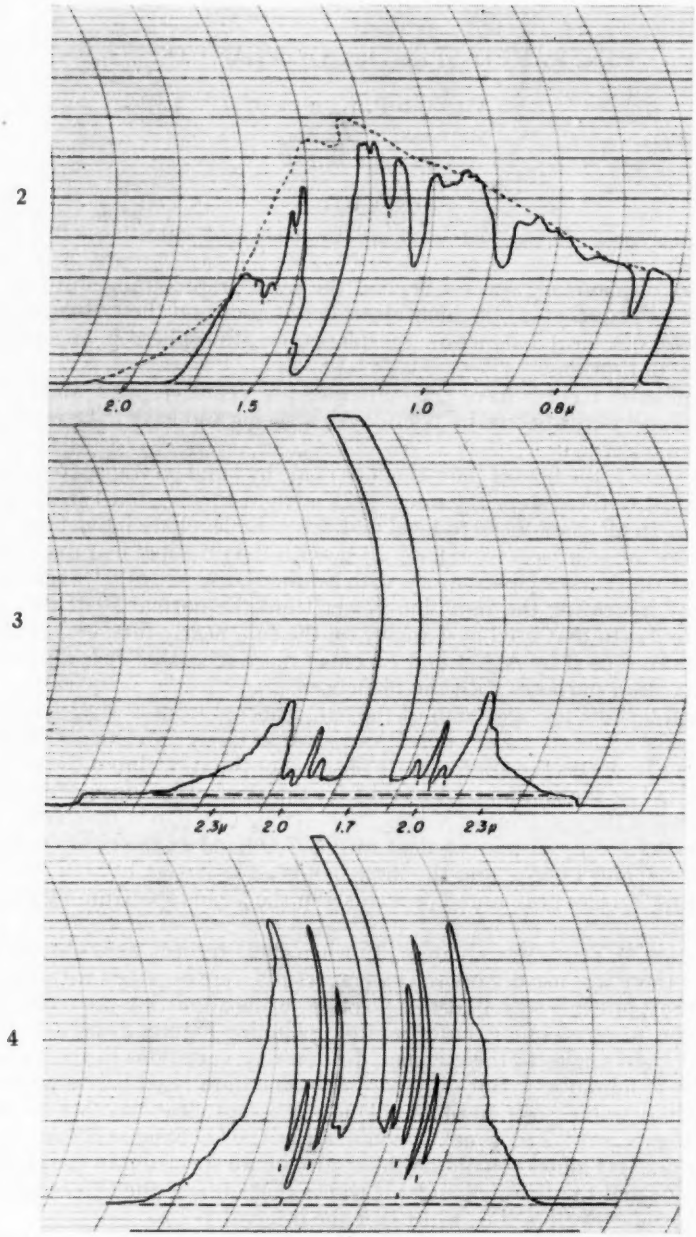

FIGS. 2–4.—Venus spectrum; slit 0.7 mm; $A = 1.55, 1.53, 1.71$

U OF MICH.

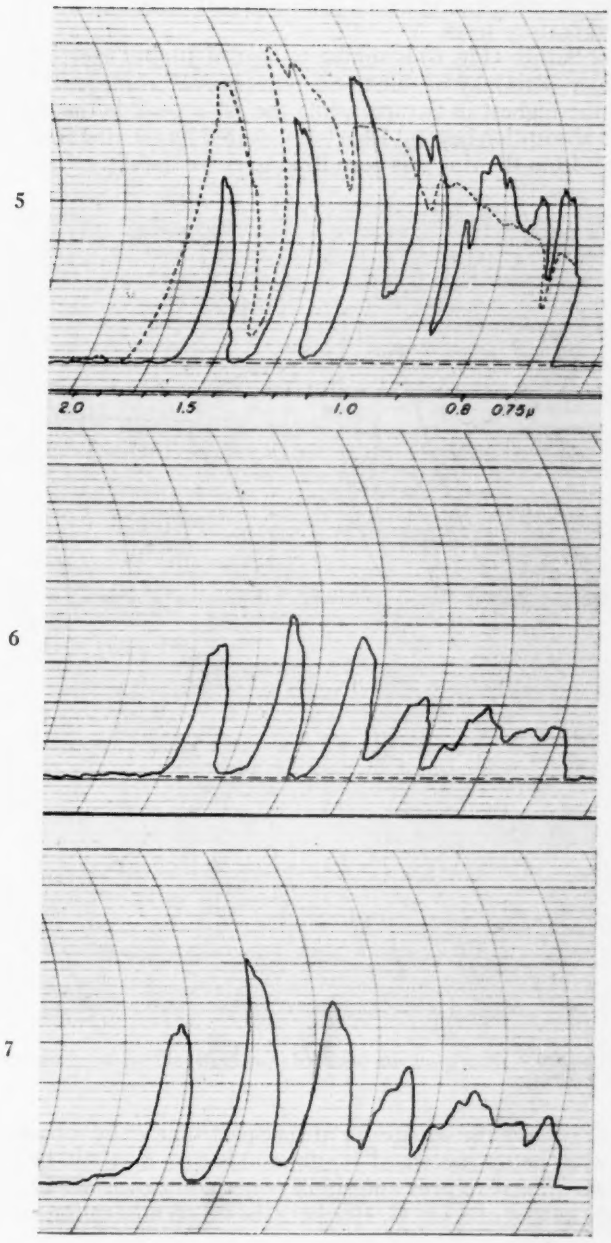

FIG. 5.—Jupiter spectrum; slit 1.0 mm; $A = 1.58$.

FIGS. 6, 7.—Saturn spectrum; slit 1.0, 1.5 mm; $A = 1.04, 1.15$

Whether this is due to overlapping bands or to a general selective absorption cannot be decided without laboratory tests.

The spectrum of Saturn (Fig. 6) is similar to that of Jupiter except that the 1.6-μ reflection peak is wider. This may be due to the reduced NH_3 content. It is also noted that the 1.3-μ peak is the highest in Saturn, while the 1.1-μ peak is the highest in Jupiter. That the complete absorption beyond 1.6 μ is not shared by the ring is shown by Figure 7, in which some light from the ring was permitted to enter the slit.

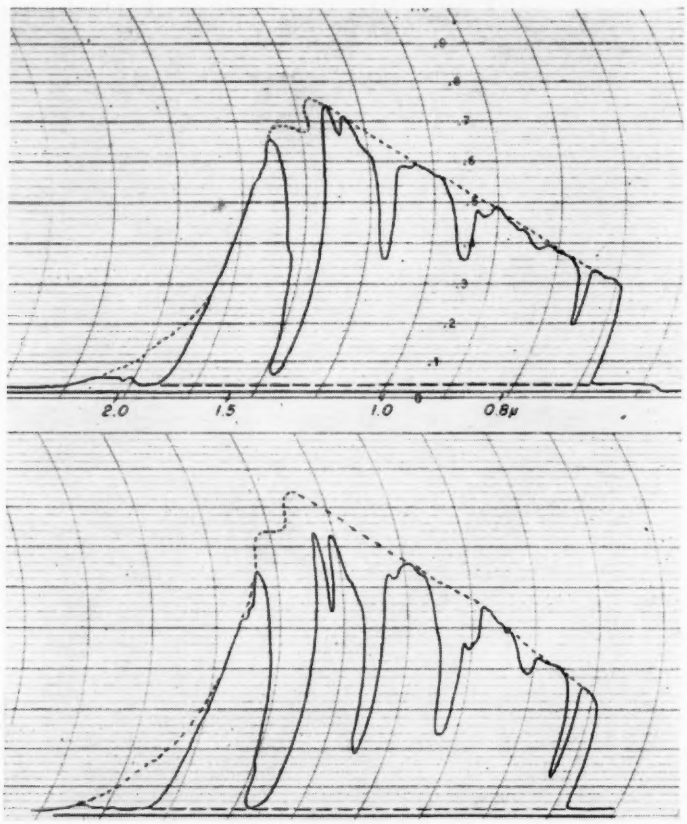

FIGS. 8, 9.—Solar spectrum reflected from *MgO;* slit 0.7 mm; air masses A = 2.0, 9.1.

If attempts to improve the sensitivity of the spectrometer by a cooling technique are successful, somewhat better spectra of Jupiter and Saturn may still be obtained. The interpretation of the present records and similar ones not shown will be treated later in a joint paper by the author and Dr. G. Herzberg, based on absorption measures with long paths.

THE SPECTRUM OF THE ECLIPSING BINARY UX MONOCEROTIS*

OTTO STRUVE
Yerkes and McDonald Observatories
Received June 23, 1947

ABSTRACT

The system of UX Monocerotis consists of a small A-type star and a large, more massive G-type star. The spectrum is characterized by emission lines of *H*, which become very strong only during the first half of the total eclipse and which are very weak during secondary eclipse. They are moderately strong at the elongations. There are also present peculiar absorption lines of *H* and *Ca* II. The *H* lines are usually strong, but double, at phases near 0.25 *P* and are weak and sometimes double at phases near 0.75 *P*. Usually the violet absorption component is the stronger at both elongations, but occasionally the intensities are reversed. This can happen at both elongations. The *Ca* II lines are also sometimes double, but usually the violet component alone is present at phases near 0.25 *P*, and the red component is very much the stronger at phases near 0.75 *P*. The luminosities of the two stars are approximately the same at about λ 4230. At λ 3933 the A star greatly predominates. Hence it is suggested that at phase 0.25 *P* we observe a stream of *Ca* II gas flowing out in front of the advancing hemisphere of the A star and that at phase 0.75 we observe a stream flowing into the receding hemisphere of the A star. Similarly, there is a stream flowing out of the advancing hemisphere of the G star, which presumably connects with the stream flowing into the A star; and there is also a stream flowing into the receding hemisphere of the G star which may represent the end of the stream which starts from the A star.

The changes in the intensities of the peculiar *H* and *Ca* II lines, as well as in their radial velocities, are rapid: major changes occur in less than 6 days, and small changes can be detected in about 1 hour. They occur apparently in an irregular manner. The phenomenon probably resembles a dense field of prominences whose integrated absorptions give rise to the peculiar lines.

The radial velocities of the G- and A-type components of the system do not vary from cycle to cycle. The entire material gives the following circular elements: $V_0 = -20$ km/sec; $K_G = 60$ km/sec; $K_A = 140$ km/sec; $a_G \sin i = 4.9 \times 10^6$ km; $a_A \sin i = 11.4 \times 10^6$ km; $m_G \sin^3 i = 3.40\ \odot$; $m_A \sin^3 i = 1.5\ \odot$; $m_G/m_A = 2.3$.

The variation in light of UX Monocerotis was discovered in 1926 by Miss Ida E. Woods at the Harvard Observatory.[1] The light-elements were determined by E. Hertzsprung[1] from Miss Woods's observations:

$$\text{Principal minimum} = \text{JD}2418602.84 + 5.90464\,E\,.$$

The spectrum, as determined at Harvard, is A3, the photographic magnitude at maximum is 8.42, the primary range is 1.74 mag., and the secondary range is 0.14 mag. The orbital elements were determined by Mrs. M. B. Shapley[1] and are given in the accompanying tabulation. The star designated by the subscript 2 is that whose spectral type

Solution	Uniform	Darkened
Computed secondary range	0.04 mag.	0.11 mag.
D	0.92 day	1.06 day
d	0.34 day	0.26 day
L_1	0.201	0.201
L_2	0.799	0.799
J_2/J_1	20.5	11.0
i	89°	90°
r_1	0.33	0.34
r_2	0.14	0.20
ρ_1	0.0035	0.003
ρ_2	0.089	0.031

* *Contributions from the McDonald Observatory, University of Texas*, No. 138.

[1] *Harvard Bull.*, No. 854, 1928. The variable star is BD−7°2291 = HD 65607 (A3), and its position for 1900 is: $\alpha = 7^h54^m24^s$; $\delta = -7°14'.0$.

is described as A3. Dugan[2] has called attention to the low density of the secondary. The spectrum, during the total eclipse and outside it, was observed by A. B. Wyse[3] at the Lick Observatory. That of the brighter component was found to be A5, that of the fainter dG1p. As far as I am able to determine, the reason for the designation of the spectrum of the secondary as "peculiar" is Wyse's observation that "the iron and hydrogen lines in the spectrum of the secondary are weak relative to λ 4227." Apparently, Wyse observed no emission lines.

In December, 1944, S. Gaposchkin undertook a spectrographic study of UX Mon at the McDonald Observatory.[4] When he and I examined the first few spectrograms, we at once realized that the character of the spectrum was peculiar. The *H* lines show emission components, which vary in intensity with the phase. The absorption lines of *H* and *Ca* II undergo strange variations with phase and also from cycle to cycle. The material collected by Gaposchkin consisted of 32 spectrograms; it was not sufficient to disentangle the remarkable changes which he had discovered. I have therefore made a new investigation of the spectrum of UX Mon, using for this purpose 152 spectrograms obtained with the Cassegrain spectrograph attached to the 82-inch McDonald reflector between January 22 and April 11, 1947. Between January 22 and February 21, inclusive, all nights were clear, and UX Mon was observed nightly in order to follow the course of the spectral changes. After February 21 another program had the precedence, and only occasional spectrograms of UX Mon were secured. For these later spectrograms I am indebted to Dr. W. A. Hiltner and Dr. Y. C. Chang. All spectrograms were obtained on Eastman 103*a*-O film with an *f*/2 Schmidt camera and two glass prisms, giving a linear dispersion of 76 A/mm at *Hγ*. The slit was 0.10 mm in width, which projected to 0.018 mm on the film. The length of the slit was 2.5 mm. The exposure time was 15–20 minutes during maximum light. The dispersion was slightly smaller than that used by Gaposchkin, but this was more than compensated for by the greater density of the exposures and by their shorter duration. It was particularly desired to secure numerous exposures during the total eclipse. This would not have been possible with the greater dispersion of the quartz prisms and the 500-mm camera.

There is still some uncertainty concerning the exact period of UX Mon. The light-elements as given in the 1941 edition of Schneller's *Katalog* of variable stars are

$$\text{Principal minimum} = \text{JD}2418602.84 + 5.904604\,\text{E}\,, \qquad (1)$$

and these have been used throughout in the present investigation. In 1943 A. Soloviev[5] derived from 64 plates the elements

$$\text{Principal minimum} = \text{JD}2418602.84 + 5.904701\,\text{E}\,.$$

His normal minimum occurred on JD 2429638.722 (E = 1869). He also gave $D = 0.767$ day (?) and $d = 0.178$ day (?). Gaposchkin, from his discussion of the Harvard patrol plates, at first concluded that the period required a small correction, making the new period 5.904504 days. He also suggested that the epoch of principal minimum be set at JD 2427855.527. However, these values were not consistent with my spectroscopic observations; hence, after some correspondence, Gaposchkin proposed the following elements:

$$\text{Principal minimum} = \text{JD}2427536.506 + 5.904604\,\text{E}\,,$$

and these were published in his recent article. The period is identical with that given in Schneller's *Katalog*. The epoch is probably also that given by Schneller, simply brought forward by means of his period; it does not agree with the epoch listed in Gaposchkin's Table 6, which was JD 2427536.552, with an estimated departure of 0.

[2] *Contr. Princeton U. Obs.*, No. 15, p. 16, 1945.

[3] *Lick Obs. Bull.*, No. 464, p. 37, 1934.

[4] *Ap. J.*, **105**, 258, 1947.

[5] *Astr. Circ. Acad. Sci. Soviet Union*, No. 19, July 30, 1943.

In view of the importance of the spectrographic observations, it is regrettable that the period and epoch are not accurately known. As far as I was able to judge from the spectra, formula (1) fits the observations best.

Gaposchkin's investigation of UX Mon is of exceptional interest because it has called attention to the extraordinary spectral variations in this star. In particular we call attention to the first five "unusual characteristics," which he listed on page 259 of his article. These characteristics have been confirmed in my present investigation. However, certain details of Gaposchkin's work may be subjected to criticism.

His photometric investigation, based upon estimates made on focal images, gives $A_1 = 1.03$ mag., $A_2 = 0.04$ mag. These values differ greatly from those of Miss Woods and Hertzsprung, but Gaposchkin has assured us that the latter's results were vitiated by "a less standardized magnitude scale" than that used by himself. He also asserts that the photometric orbit is eccentric and that "the secondary minimum . . . . seems to be much wider than the primary." He has even attempted to derive the eccentricity of the orbit from the light-curve, $e = 0.3$, with a question mark. The procedure is not described; usually only the value of $e \cos \omega$ can be determined from the spacings of the two minima. Whether e was found from a determination of $e \sin \omega$ by measuring the difference in the widths of the two minima or by assuming the value of ω, which he derived from the spectrographic observations, is not clear. In any case, it is fairly obvious from the scatter of the normal magnitudes that little confidence can be placed upon the secondary minimum. Gaposchkin, for example, places the latter at his phase 0.150 P (or at my phase 0.585 P, the latter being counted from primary mid-eclipse). But an independent inspection of his light-curve suggests a more conspicuous indentation at his phase 0.200 P (or at my phase 0.635 P). This would, if real, give a very large value for

$$e \cos \omega = \frac{\frac{\pi}{P}\left(t_2 - t_1 - \frac{P}{2}\right)}{\operatorname{cosec}^2 i + 1} = 0.135\,\frac{\pi}{2} = 0.2\,.$$

It is doubtful whether any significance can be attributed to this result. Even less trustworthy would be the determination of $e \sin \omega$ from the relation $e \sin \omega = (D_2 - D_1)/(D_2 + D_1)$. Gaposchkin's derivation of the spectroscopic values of e and ω are also illusory. His curves in his Figure 2 and Table 4 show double lines at almost all phases, and the curves as drawn by him do not represent binary motion. It is quite certain that from his material no determination of e and ω can be obtained. Hence the values $e = 0.08$ and $\omega = 316°$ must be discarded. As a matter of fact, the measures gave double lines for the metals at his phases 0.304 P and 0.336 P and single lines at his phase 0.334. Surely, this cannot be the time of zero relative velocity near secondary conjunction? The measurement of the A- and the G-type components is extremely difficult, as Gaposchkin has himself pointed out. Hence, it is best to disregard his results for e and ω and to accept, with caution, only his determination K_G and V_0 (velocity of the center of mass).

For convenience I have arranged the new spectrographic material in fourteen consecutive cycles. Cycle I starts on January 22 and ends on January 27; cycle II starts on January 28 and ends on February 2, etc. Cycles I, II, III, IV, and V have been observed completely, the rest only incompletely. Figures 1–9 contain representative reproductions of spectrograms for each night of observation.

Outside eclipse, the spectrum shows complex lines of *H* and *Ca* II, whose intensities vary over a large range. There are also emission features of *H* and probably of *Ca* II, of variable intensity, and predominantly on the red sides of the corresponding absorption lines. The spectrum shows a large number of faint lines of *Fe* I, *Fe* II, *Sr* II, *Ca* I, etc., all of which can occur in spectral classes from A to G. These lines are often diffuse. Sometimes they are clearly double, especially at phases near 0.75 P; and in that case one component is attributed to the G star, the other to the A star. During total eclipse the lines

of the G star are observed with great strength. They show no *Fe* II 4233, so that presumably all *Fe* II lines may be attributed to the A star alone. But even at principal minimum the lines of *H* and *Ca* II are peculiar.

From the photometric data we conclude that the eclipse is certainly total. The spectra show that at the principal minimum the G star is in front. The lines of the A star, especially *Fe* II 4233, are completely invisible during mid-eclipse. Hence we may suppose that this eclipse is total or nearly total. At phases near 0.5 *P* the lines of *Fe* II are strengthened. Hence the A star is then in front. This strengthening of the lines of the A star is interesting in view of the very small value of A_2, the range of secondary minimum. According to Gaposchkin, $1 - \lambda_2 = 0.027$, while $1 - \lambda_1 = 0.613$. It is difficult to understand how a change of only 3 per cent in the total light can produce so conspicuous a strengthening of the *Fe* II lines.

In this connection we notice that the degree of intensification of the *Fe* II lines near secondary minimum is not the same in all cycles. It was particularly pronounced on January 30 (cycle II) and on April 11 (cycle XIV). On these two dates the spectrum showed all normal lines of spectral type A5 except those of *H*, with greater intensity than in the other cycles. During cycle II there was a general tendency for the peculiar *H* lines to be weaker than in most other cycles, but the material for cycle XIV is insufficient to confirm this correlation. In a tentative manner we might suggest that the opacity produced by the *H* atoms in an outer ring or shell tends to weaken the metallic lines in the same way as has been observed in peculiar shell stars (γ Cas and others). We conclude that the strength of the *Fe* II lines is not constant but depends upon conditions which vary from cycle to cycle. We cannot, therefore, rely upon these intensities to give us an accurate estimate of the relative total brightnesses of the two stars L_A/L_G.

Because of the variable character of the *Fe* II lines, the question might arise as to whether these lines belong to the A star at all. When we examine our new spectrograms, or those obtained by Gaposchkin, throughout each cycle, we notice that the pair of lines *Ca* I 4227 and *Fe* II 4233 are quite close to each other at phases around 0.2 *P* and 0.3 *P* and are much farther separated at phases around 0.6 *P* and 0.7 *P*. This is fairly conclusive proof that the *Fe* II line actually belongs to the A-type star. It must be remembered, however, that there are no other lines of the A star in the region adequately covered by my plates that are not more or less seriously blended with lines of the G-type star or with lines originating in the gaseous streams.

From the radial velocities in Table 1 we infer that the range is much larger for the A star than for the G star. Hence the mass of the G star must be the larger (Gaposchkin had obtained equal masses).

The presence at λ 4233 of a line of the A-type component and at λ 4227 of a line of the G-type component suggests that (disregarding the variations of the A-type lines), as to order of magnitude, the total luminosities of the two component stars are about the same at λ 4230. At λ 4045 a strong line of *Fe* I is often observed double, with the G-type component always much the stronger. Since, normally, *Fe* I would be weaker in class A than in class G, we can only infer that even at λ 4045 the luminosities are still comparable. To the violet of λ 4045 the G-type component is certainly less luminous than the A-type component. This may be inferred from the conspicuous fact that, outside eclipse, the energy distribution of the continuous spectrum on the violet side of λ 4000 is that of a blue star, while during total eclipse the region of *Ca* II 3933 required exposure times of the order of five to ten times those normally used, while the region of $H\gamma$ required exposure times of the order of twice those normally used. It is evident that with the normal exposure times of about 15–20 minutes the continuous spectrum of a G star would be very little registered on the photographic emulsion in the region of λ 3933. We conclude that in the ordinary photographic region

$$L_G \sim L_A .$$

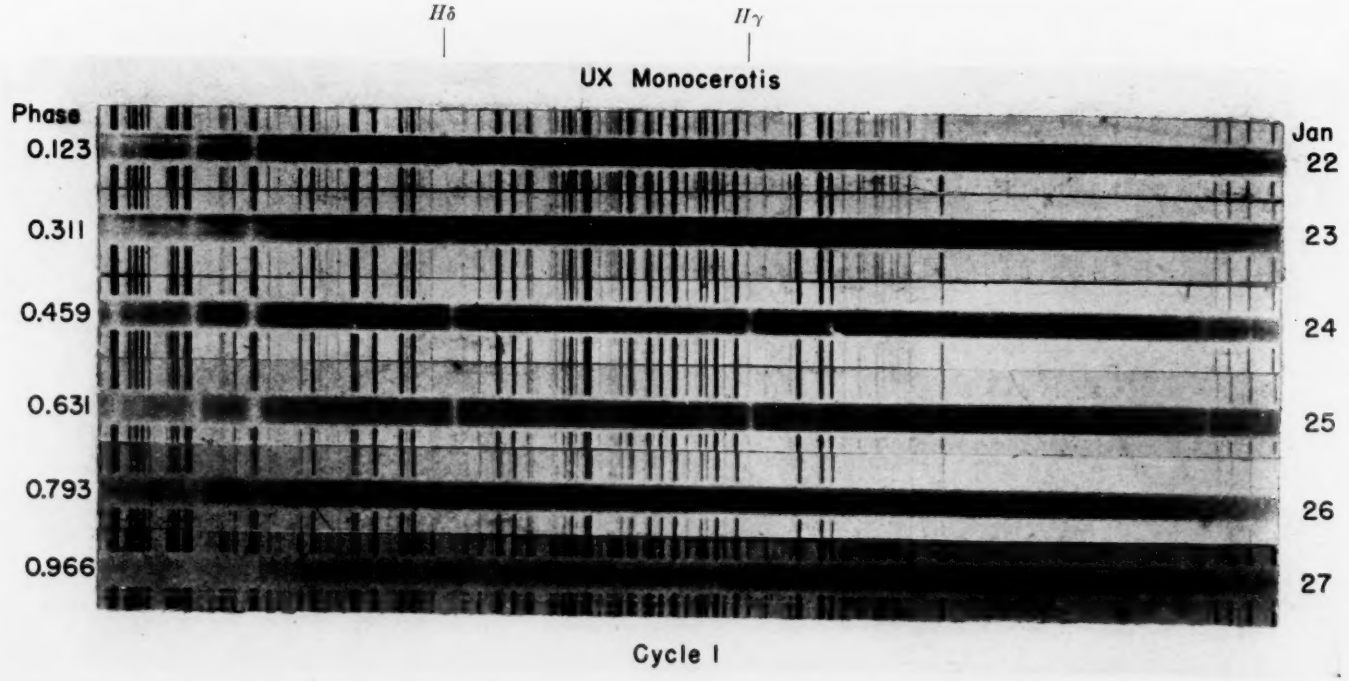

FIG. 1.—Notice the doubling of $H\delta$ and $H\gamma$ at phases 0.311 P and 0.793 P. At both phases the violet components are the stronger, but at phase 0.793 P the total intensities of the H lines are much smaller than at phase 0.311 P.

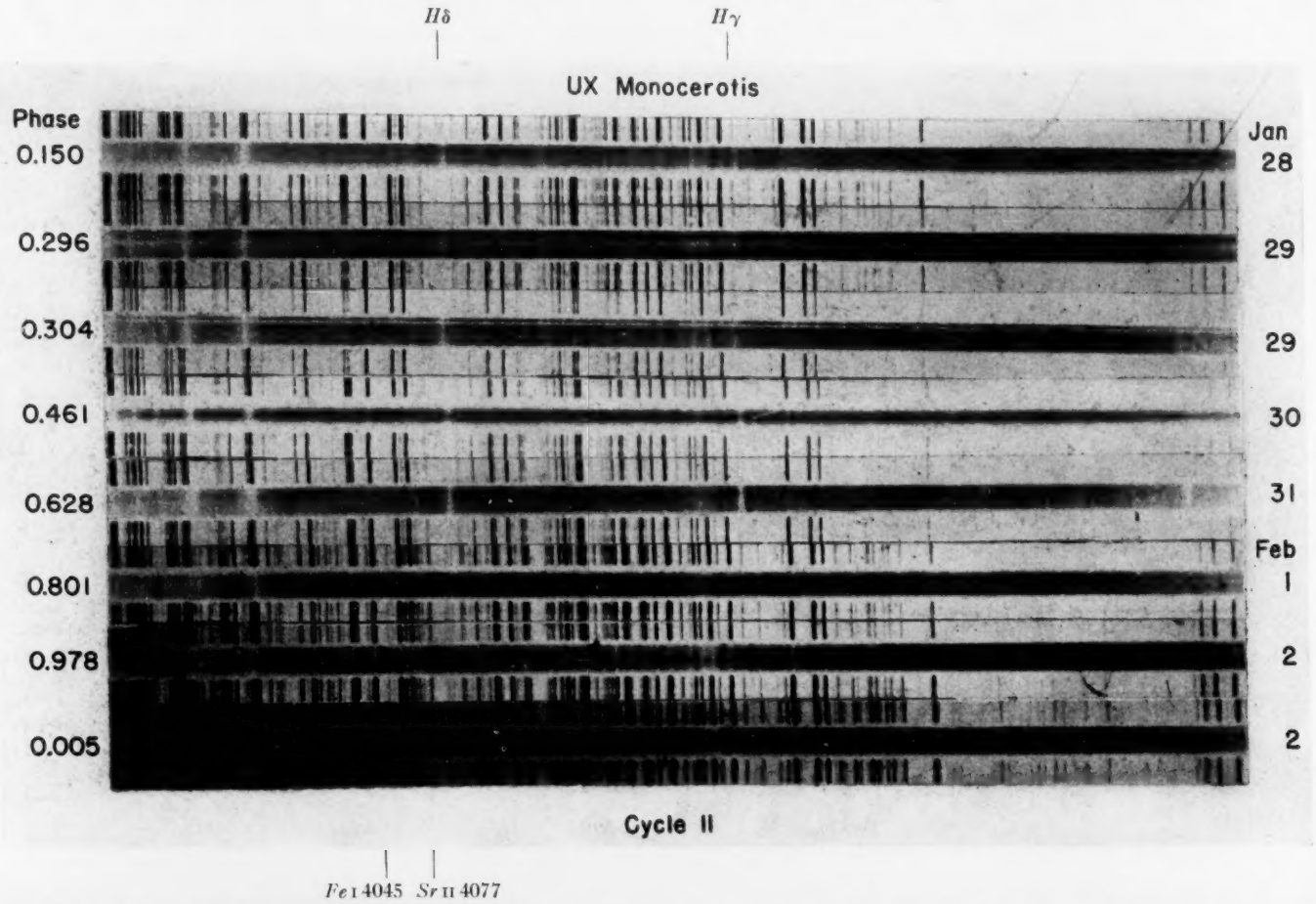

FIG. 2.—Notice the great intensity of the *Fe* II lines belonging to the A star at phase 0.461 *P*—near secondary eclipse. During the first half of totality the bright *H* lines are much stronger than during the second. Notice that, during totality, *Sr* II 4077 is slightly stronger than *Fe* I 4045. At phase 0.304 *P* the double *H* components are much weaker than in Cycle I.

totality the bright H lines are much stronger than during the second. Notice that, during totality, *Sr* II 4077 is slightly stronger than *Fe* I 4045. At phase 0.304 P the double H components are much weaker than in Cycle I.

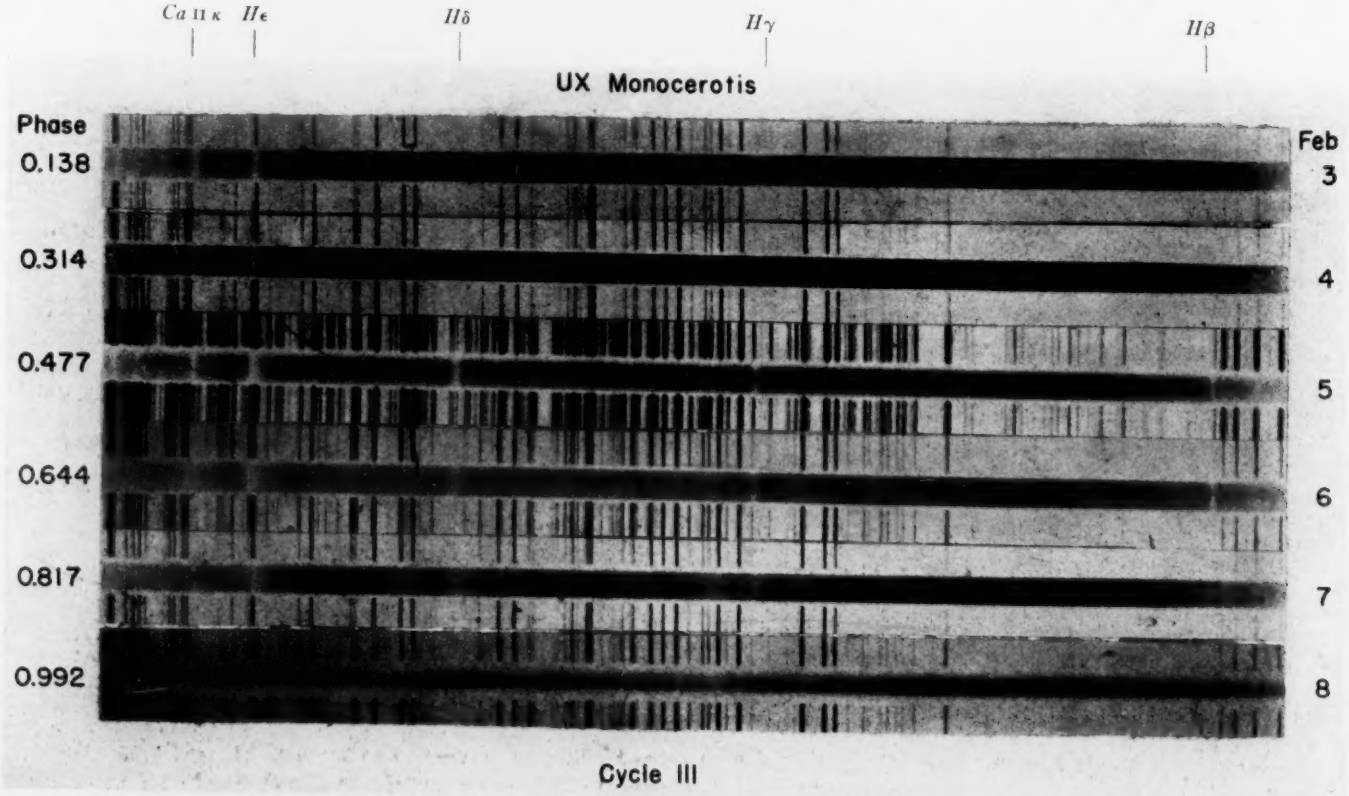

FIG. 3.—Notice the great intensity of the H absorption lines at secondary eclipse, phase 0.477 P. At phase 0.644 P, *Ca* II 3933 is double with r = v.

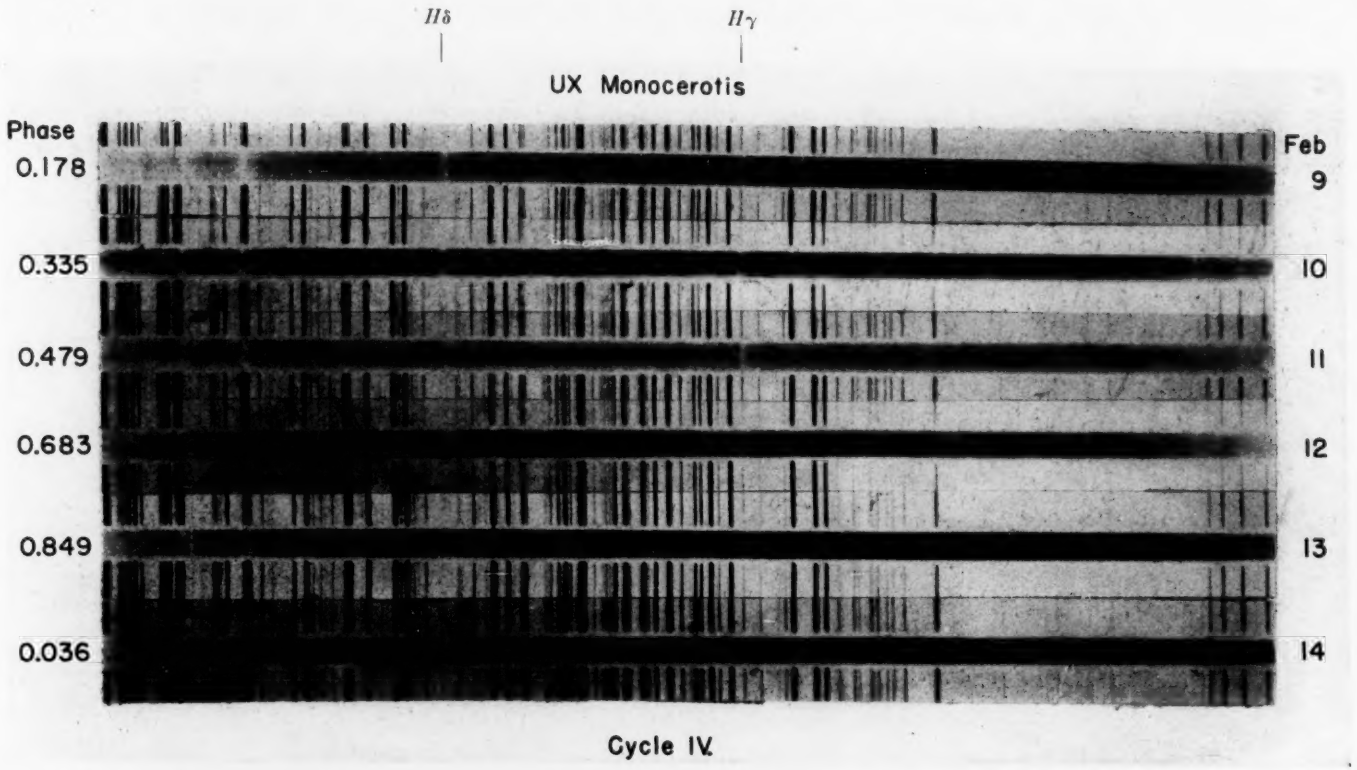

FIG. 4.—At phase 0.683 *P* the *H* and *Ca* II lines are double with r < v, but at phase 0.849 *P* the lines are single. At the end of totality, phase 0.036 *P*, the emission lines are weak.

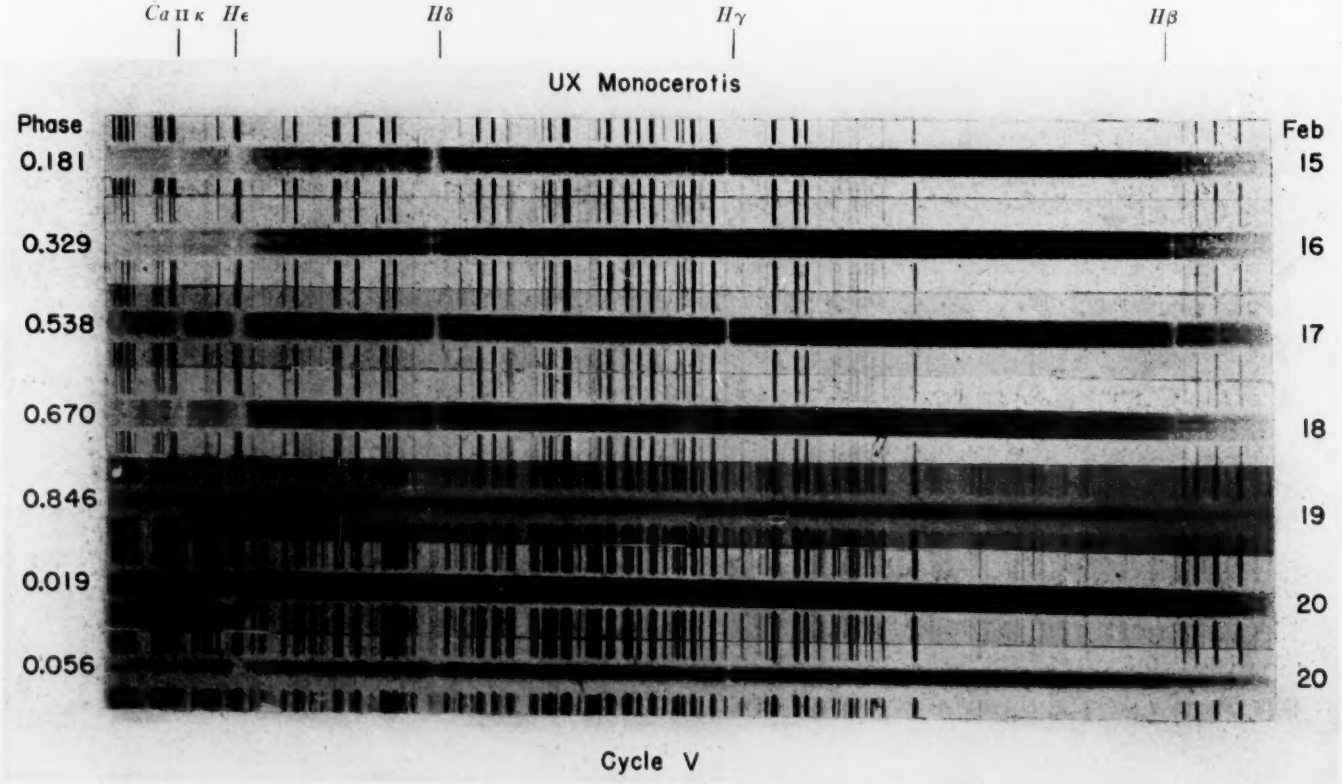

FIG. 5.—At phase 0.670 *P* the *H* lines are broad but not so widely double as in the preceding cycle at phase 0.683 *P*

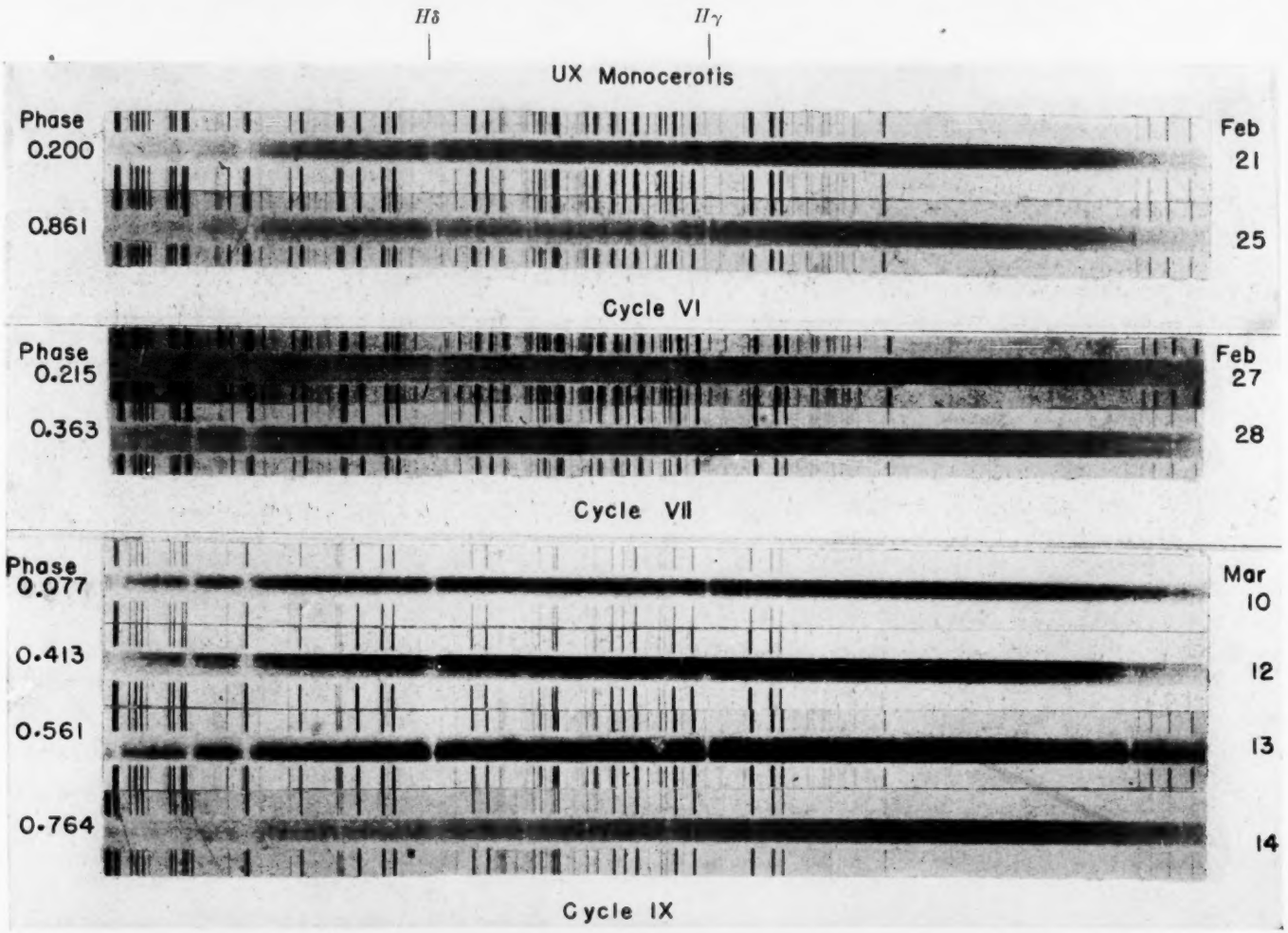

FIG. 6.—Notice that in Cycle VII at phase 0.363 *P* the *H* lines are double with r < v. This is unusual. In Cycle VI at phase 0.200 *P* the *H* lines are weak. In Cycle IX at phase 0.413 *P*—not far from conjugation—the *H* lines are double with r = v.

are weak. In Cycle IX at phase 0.413 P—not far from conjugation—the H lines are double with $r = v$.

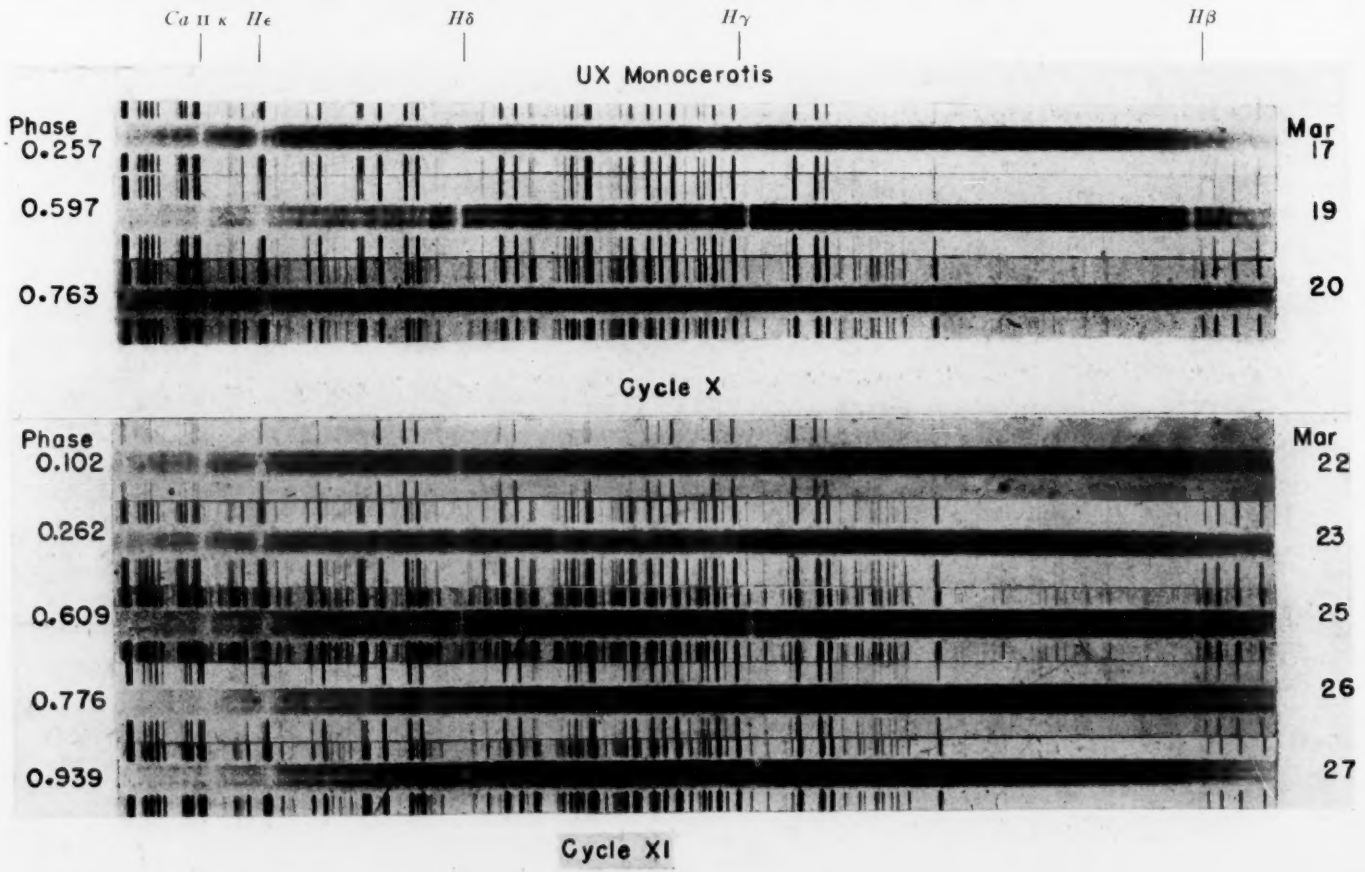

FIG. 7.—In Cycle XI the emission lines of H are strong, especially at phase 0.609 P. Compare $H\beta$ in this cycle with Cycles I, II, and III

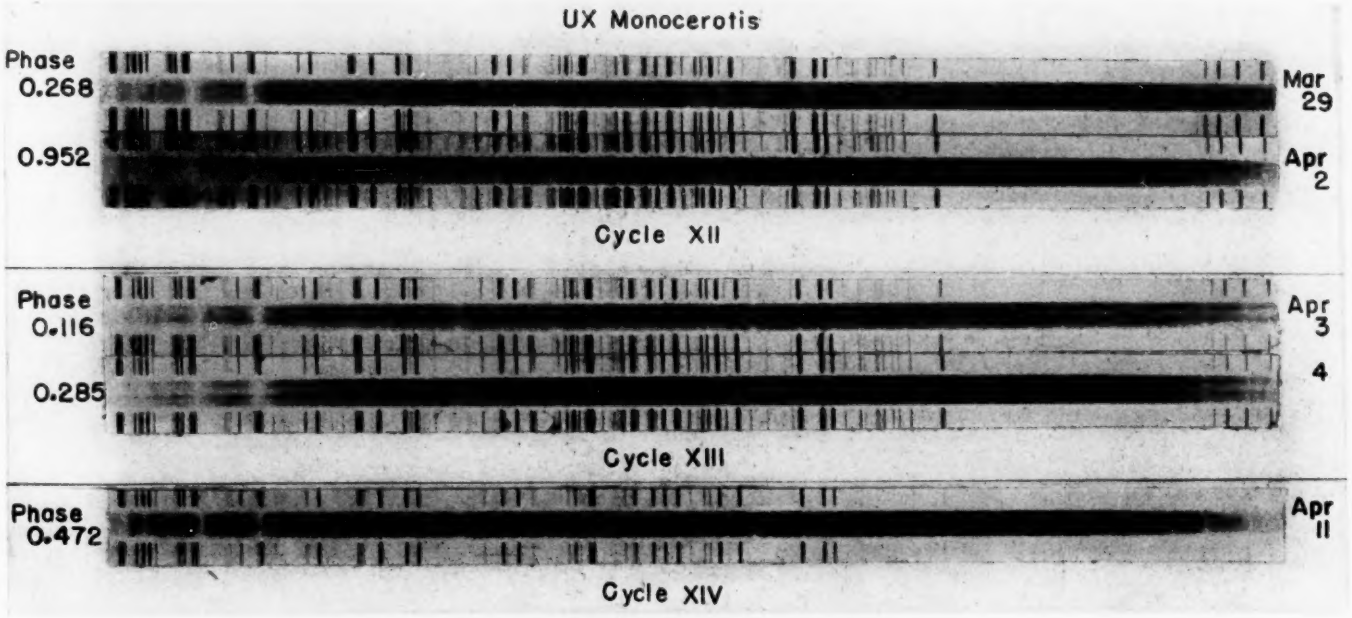

FIG. 8.—In Cycle XIV at phase 0.472 *P* the lines of *Fe* II of the A star are unusually strong, as in Cycle II

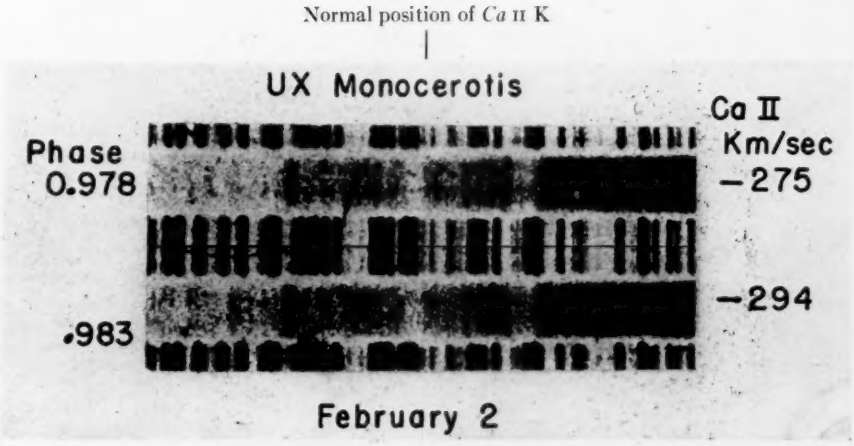

FIG. 9.—The broad absorption line of *Ca* II 3933 has a velocity of about −250 km/sec. The two spectrograms were taken during the first half of totality. Hence the rapidly approaching *Ca* II prominences must have been in front of the G star. This highly displaced *Ca* II line seems to be always present in the first half of totality.

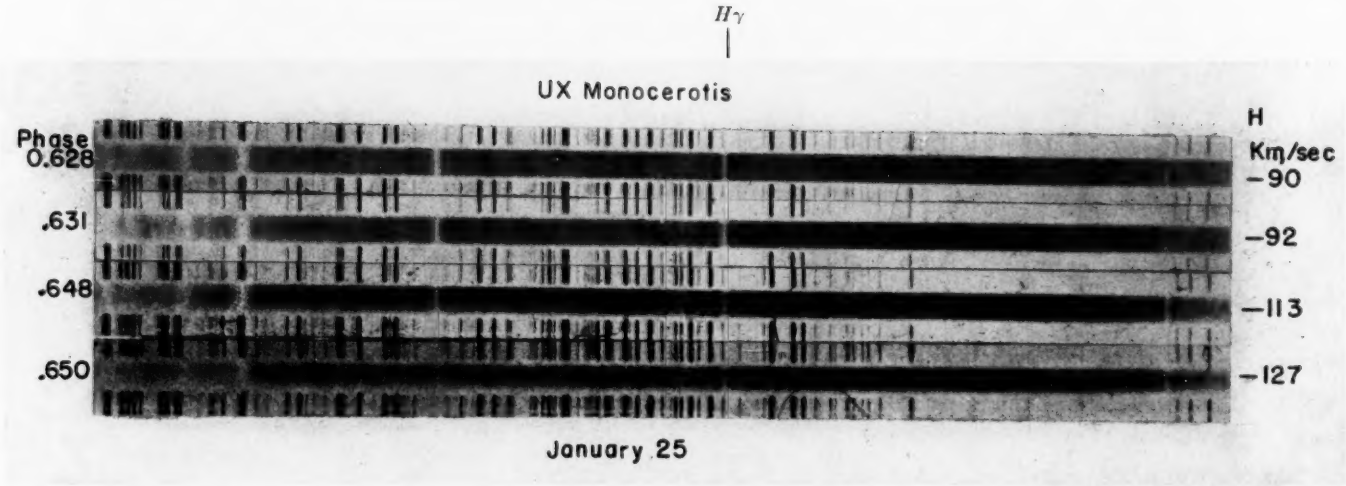

FIG. 10.—Changes in the appearance of $H\gamma$ during the night of January 25. Notice that the line shifted with respect to the comparison line, *Fe* I 4337.

TABLE 1

RADIAL VELOCITIES OF UX MONOCEROTIS

PLATE*	DATE (1947)	U.T.	PHASE IN PERIOD	RADIAL VELOCITIES (KM/SEC)					
				Ca II		*H*		G Star	A Star
				I	II	I	II		
8927	Jan. 22	6:36	0.123	− 32	.....	− 14	.....	+ 38	.....
8928	22	6:53	.125	− 73	.....	− 5	.....	+ 32	.....
8930	22	8:05	.134	− 69	.....	− 25	.....	+ 26	.....
8931	22	8:28	.136	− 62	.....	− 27	.....	+ 53	.....
8942	23	8:43	.307	−182	.....	−284	+168	+ 27	.....
8943	23	9:10	.311	−178	.....	−309	+109	+ 34	.....
8953	24	6:09	.459	− 93	.....	−205	+ 15	− 13	0
8954	24	6:36	.462	−145	.....	−162	.....	− 23	+ 5
8959	24	8:47	.477	− 97	.....	−130	.....	− 12	− 10
8960	24	9:14	.480	− 70	.....	−100	.....	− 6	+ 24
8970	25	6:07	.628	− 15	.....	− 90	.....	− 66	+ 53
8971	25	6:36	.631	+ 30	.....	− 92	.....	− 68	.....
8975	25	8:56	.648	+ 34	.....	−113	.....	− 80	.....
8976	25	9:20	.650	− 4	.....	−127	.....	− 63	.....
8985	26	5:08	.790	+115	−271	−172	+140	− 94	+ 92
8986	26	5:30	.793	+115	−287	−181	+170	− 32	+130
8994	26	9:27	.821	+111	−250	−198	+189	− 44	+122
8995	26	9:56	.824	+ 67	−177	−155	+193	− 20	+140
9003	27	5:39	.963	.....	.....	− 39	.....	− 11	+ 52
9004	27	6:03	.966	.....	.....	− 18	.....	− 17	.....
9007	27	8:14	.981	.....	.....	− 21	.....	− 4	− 21
9008	27	8:45	.985	.....	.....	− 48	.....	− 11	.....
9009	27	9:17	.989	.....	.....	− 44	.....	− 40	.....
9010	27	9:49	.993	.....	.....	− 51	.....	+ 27	.....
9017	28	7:14	.144	− 72	.....	− 36	.....	+ 28	.....
9018	28	7:40	.147	− 65	.....	− 38	.....	+ 45	.....
9019	28	8:06	.150	− 69	.....	− 49	.....	+ 16	.....
9020p	28	8:47	.155	.....	.....	− 55	.....	+ 3	.....
9027	29	4:43	.296	−117	.....	−173	+154	+ 35	−102
9028	29	5:08	.298	−147	.....	−219	+131	+ 2	.....
9029	29	5:34	.301	−125	.....	−222	+136	− 32	.....
9030	29	6:00	.304	−103	.....	−213	+134	− 46	.....
9031	29	6:32	.308	−166	.....	−211	+116	− 41	.....
9037	30	4:09	.461	− 39	.....	+ 1	.....	0	+ 30
9038	30	5:13	.468	− 13	.....	− 30	.....	− 2	+ 11
9039	30	6:17	.476	− 17	.....	− 15	.....	0	+ 50
9040	30	7:22	.484	− 32	.....	− 33	.....	− 6	+ 21
9045	31	3:44	.627	+ 65	−270	− 68	.....	− 72	.....
9046	31	4:08	.630	+ 46	−322	− 46	.....	− 40	+159
9056	31	9:21	.667	+ 57	.....	− 25	.....	− 46	+ 93
9057p	31	9:54	.671	.....	.....	− 10	.....	− 76	.....
9065	Feb. 1	4:00	.799	+ 86	.....	− 34	.....	− 20	.....
9066	1	4:21	.801	+ 60	.....	− 85	.....	− 53	.....
9067	1	4:43	.804	+ 82	.....	− 17	.....	− 81	+102
9076	1	9:23	.836	+ 94	.....	− 72	.....	− 48	.....
9088	2	5:30	.978	−275	.....	− 52	.....	0	.....
9089	2	6:08	.983	−294	.....	− 37	.....	+ 14	.....
9093	2	8:40	.001	−242	.....	− 36	.....	+ 14	.....
9094	2	9:14	.005	−153	.....	− 52	.....	− 5	.....
9101	3	4:08	.138	− 60	.....	− 34	.....	+ 19	.....
9102	3	4:31	.141	− 60	.....	− 30	.....	+ 8	.....
9108	3	8:24	.168	− 90	.....	− 78	.....	+ 52	.....
9109	3	9:17	.174	−105	.....	−109	.....	+ 28	.....
9119	4	4:40	0.311	−169	.....	−215	+132	+ 54	−148

* "p" designates a poor plate; "vp" designates a very poor plate.

TABLE 1—*Continued*

Plate*	Date (1947)	U.T.	Phase in Period	Radial Velocities (Km/Sec)					
				Ca II		*H*		G Star	A Star
				I	II	I	II		
9120	Feb. 4	5:08	0.314	−158	.....	−212	+142	+ 14	.....
9121	4	5:34	.318	−154	.....	−242	+124	+ 11	.....
9122	4	5:54	.320	−132	.....	−232	+151	+ 28	.....
9123	4	6:14	.322	−139	.....	−219	+143	− 4	.....
9126	5	3:28	.472	− 83	.....	− 83	.....	0	− 25
9127	5	4:09	.477	− 79	.....	−103	.....	− 17	− 1
9133	6	3:54	.644	+132	−248	−108	.....	− 68	+116
9134	6	4:26	.648	+128	−258	−124	.....	− 84	+109
9135	6	4:52	.651	+103	−310	−263	+ 33	− 78	+118
9148	7	4:19	.817	+ 69	−299	−100	+243	− 94	+ 47
9149p	7	5:02	.822	+ 42	.....	− 91	.....	− 85	.....
9152	7	8:23	.845	+ 91	.....	− 66	.....	− 32	+138
9153	7	8:49	.848	+ 61	.....	− 47	.....	− 42	.....
9154	7	9:17	.852	+106	.....	− 62	.....	− 36	+ 99
9161	8	4:22	.987	−245	+153	− 58	.....	0	.....
9162	8	5:05	.992	−215	.....	− 42	.....	+ 16	.....
9164	8	7:14	.007	−219	.....	− 59	.....	− 2	.....
9166	9	6:32	.171	−119	.....	−117	.....	+ 56	.....
9167vp	9	6:59	.174	−144	.....	.....	.....	.....	.....
9168	9	7:26	.178	−152	.....	−109	.....	+ 49	.....
9169	9	7:48	.180	−186	.....	−102	.....	+ 35	.....
9170	9	8:09	.183	−115	.....	−124	.....	+ 62	.....
9178	10	4:55	.329	−172	.....	−298	+ 90	+ 5	.....
9179	10	5:42	.335	−201	+ 68	−309	+125	+ 28	.....
9183	11	1:44	.476	−105	.....	−120	.....	− 8	− 3
9184	11	2:13	.479	− 75	.....	−129	.....	− 32	+ 11
9190	12	1:45	.646	+ 40	.....	− 42	.....	− 89	+ 68
9191	12	2:13	.649	+ 63	.....	− 32	.....	− 72	+130
9196	12	6:37	.680	+100	.....	+ 67	.....	− 80	+122
9197	12	7:00	.683	+103	−328	+ 57	−388	− 80	+ 97
9206	13	3:08	.825	+103	.....	− 46	.....	− 77	+149
9207	13	3:33	.828	+111	.....	− 37	.....	− 84	+111
9212	13	6:37	.849	+114	.....	+ 22	.....	− 63	+144
9213	13	7:00	.852	+ 85	.....	− 2	.....	− 63	+130
9224	14	5:05	.008	.....	.....	− 34	.....	+ 3	.....
9225	14	6:42	.019	.....	.....	+ 2	.....	+ 19	.....
9226	14	7:29	.025	−188	.....	+ 8	.....	+ 30	.....
9232	15	2:56	.162	−144	.....	− 77	.....	+ 38	.....
9233	15	3:22	.165	−152	.....	− 95	.....	+ 50	.....
9236	15	5:41	.181	−114	.....	−134	.....	+ 38	.....
9237	15	6:04	.184	−148	.....	−161	.....	+ 50	.....
9240	15	7:44	.196	−192	.....	−188	.....	+ 58	.....
9241	15	8:10	.199	−144	.....	−192	.....	+ 28	.....
9251	16	2:44	.330	−222	.....	−353	+100	+ 31	.....
9252	16	3:08	.333	−281	.....	−345	+104	− 6	.....
9253	16	3:34	.336	−259	.....	−351	+132	− 18	.....
9254	17	3:09	.502	− 37	.....	−107	.....	− 29	+ 27
9255	17	4:11	.509	− 14	.....	−103	.....	− 7	+ 8
9256	17	5:04	.516	− 33	.....	− 87	.....	+ 2	+ 22
9257	17	5:35	.519	+ 8	.....	− 88	.....	− 22	+ 32
9259	17	7:12	.531	+ 1	.....	− 80	.....	− 7	+ 32
9260	17	7:40	.534	− 6	.....	− 96	.....	− 55	+ 70
9261	17	8:13	.538	− 22	.....	− 96	.....	− 24	− 2
9267	18	3:00	.670	+ 79	−390	− 7	.....	− 62	+133
9268	18	3:28	.674	+123	−282	− 22	.....	− 82	+104
9272	18	6:12	0.693	+108	.....	−123	+151	− 94	+ 85

TABLE 1—*Continued*

Plate*	Date (1947)	U.T.	Phase in Period	Radial Velocities (Km/Sec)					
				Ca II		*H*		G Star	A Star
				I	II	I	II		
9273p	Feb. 18	6:34	0.696	+105	.....	− 69	.....	−126	.....
9275	18	7:44	.704	+ 98	.....	−123	+162	− 96	+109
9276	18	8:12	.707	+ 75	.....	−114	+172	− 91	.....
9277	18	8:40	.710	+108	.....	−118	+121	− 92	+118
9284	19	3:50	.846	+130	.....	− 98	.....	− 54	+157
9287	20	2:55	.009	.....	.....	− 78	.....	+ 6	.....
9288	20	3:37	.014	.....	.....	− 42	.....	+ 11	.....
9289	20	4:24	.019	−201	.....	− 46	.....	+ 16	.....
9290	20	5:08	.024	−198	.....	− 54	.....	+ 27	.....
9291	20	6:02	.030	−168	.....	− 59	.....	+ 7	.....
9292	20	7:03	.038	−135	.....	− 46	.....	+ 18	.....
9293	20	7:58	.044	−105	.....	− 81	.....	+ 17	.....
9294p	20	8:44	.050	−146	.....	− 75	.....	+ 7	.....
9295	20	9:37	.056	− 42	.....	− 25	.....	− 10	.....
9301	21	5:38	.197	−180	.....	−206	.....	+ 35	.....
9302	21	6:02	.200	.....	.....	−256	.....	− 8	.....
9303	21	6:28	.203	−217	.....	−210	.....	− 49	.....
9304	21	7:03	.207	−180	.....	−228	.....	+ 47	.....
9305	21	7:52	.213	.....	.....	−192	.....	+ 60	.....
9306	21	8:42	.219	.....	.....	−179	.....	+ 41	.....
9310	25	3:42	.861	+113	.....	− 33	.....	− 36	.....
9311	25	4:10	.864	+ 65	.....	− 11	.....	− 38	+101
9312	25	4:37	.867	+ 84	.....	− 48	.....	− 62	+ 96
9321	27	5:48	.215	.....	.....	−178	.....	+ 30	+ 14
9325	28	2:53	.363	−123	.....	+ 78	−282	+ 20	− 25
9365	Mar. 10	5:45	.077	− 4	.....	+ 10	.....	+ 20	.....
9388	12	5:19	.413	−142	.....	−234	+ 90	+ 21	− 15
9396	13	2:18	.561	− 68	.....	− 90	.....	− 37	+ 48
9421	14	7:04	.764	.....	.....	−133	.....	−117	.....
9437	17	4:55	.257	−173	.....	−215	+132	+ 14	+ 60
9449	19	5:09	.597	− 3	.....	− 70	.....	− 52	+ 46
9458	20	4:41	.763	+ 87	−322	−192	+174	− 88	.....
9479	22	4:47	.102	− 70	.....	+ 4	.....	+ 4	+ 21
9487	23	3:20	.262	−161	.....	−201	.....	−107	+ 85
9502	25	4:30	.609	+ 71	.....	− 48	.....	− 30	.....
9513	26	4:12	.776	+148	−298	−151	+177	− 94	+121
9524	27	3:20	.939	+ 67	.....	+ 8	.....	− 16	+121
9533	29	2:00	.268	−113	.....	−171	+152	− 78	.....
9567	Apr. 2	2:52	.952	.....	.....	− 10	.....	− 20	.....
9569	3	2:02	.116	− 80	.....	− 24	.....	− 11	.....
9575	4	2:02	.285	−170	.....	−209	+127	+ 3	.....
9646	11	2:18	0.472	− 85	.....	−118	.....	− 15	+ 8

Since the eclipse is total and since the photometric data are of small precision (the two ranges of the eclipses are given as 1.74 and 0.14 mag. by Miss Woods and as 1.03 and 0.04 mag. by Gaposchkin) we can derive only very rough elements. If the stars are undarkened, we have

$$A_1 = 2.5 \log (1 + k^2\gamma) ,$$

$$A_2 = 2.5 \log \frac{1 + k^2\gamma}{1 + k^2\gamma - k^2},$$

where, as usual, $k = r_2/r_1$ and $\gamma = J_2/J_1$ is the ratio of the surface brightness of the smaller star to that of the larger star. These equations lead to two approximate sets of values, depending upon whether the deeper eclipse is total or annular:

$$\text{Principal eclipse is total } k = 0.3 ; \quad \gamma = 15 ; \tag{a}$$

$$\text{Principal eclipse is annular } k = 0.8 ; \quad \gamma = 0.06 . \tag{b}$$

In both cases the cooler star would be in front during the principal eclipse. But in case (*a*) the ratio of luminosities would be

$$\frac{L_A}{L_G} = \gamma k^2 = 1.35 , \tag{a}$$

while in case (*b*) the ratio would be

$$\frac{L_A}{L_G} = \frac{1}{\gamma k^2} = 26 . \tag{b}$$

Clearly, only case (*a*) is consistent with the spectrographic result $L_A \sim L_G$. This is the solution adopted (without attempt at a justification) by Gaposchkin. We shall follow the latter in adopting the following values for the radii of the two stars:

$$r_A = 0.08 (a_1 + a_2) ,$$

$$r_G = 0.28 (a_1 + a_2) ,$$

where a_1 and a_2 are the radii of the two orbits.

According to the photometric data, the eclipse lasts from 0.91 *P* to 0.09 *P*, and totality lasts from 0.95 *P* to 0.05 *P*. The spectrograms show an unblended G-type spectrum between phases 0.963 *P* and 0.030 *P*. It is definitely blended with the A-type spectrum at phase 0.038 *P* and later. There is no strengthening of the G-type spectrum at 0.077 *P*. On the other side, there is a noticeable strengthening of the G-type lines at phases 0.939 *P* and 0.952 *P*. There is no noticeable strengthening of the G-type spectrum at phases 0.852 *P*, 0.864 *P*, and 0.867 *P*. The spectrograms thus suggest the values shown in the accompanying tabulation. This would place mid-eclipse at phase 0.995 *P*, which

Beginning of eclipse at phase	0.91 *P*
Beginning of totality at phase	0.96 *P*
End of totality at phase	0.03 *P*
End of eclipse at phase	0.08 *P*

is in sufficiently good agreement with the elements in formula (1).

At phase 0.96 *P* the emission lines of *H* are very strong. They are entirely on the red sides of the corresponding absorption lines and are about 4 or 5 A in width. The centers of the emission lines would give large positive velocities, but this may be partly spurious because of the effect of the violet-displaced absorption lines. After phase 0.963 *P* the

emission lines decrease in intensity and become quite faint after phase 0.000 *P*. Only $H\beta$ remains visible with considerable strength and is somewhat stronger than at maximum light. This unsymmetrical change in the *H* emission lines is very remarkable. It shows that a mass of emitting hydrogen gas is not occulted until about mid-eclipse but is effectively blotted out by the G star after mid-eclipse. This would place the emitting mass of gas approximately within the shaded area of Figure 11.

An even more remarkable spectroscopic feature during the total eclipse is the appearance of the lines of *Ca* II, especially of λ 3933, which is unblended with *H*. The measured velocities give large negative values, of the order of −250 km/sec, and these velocities

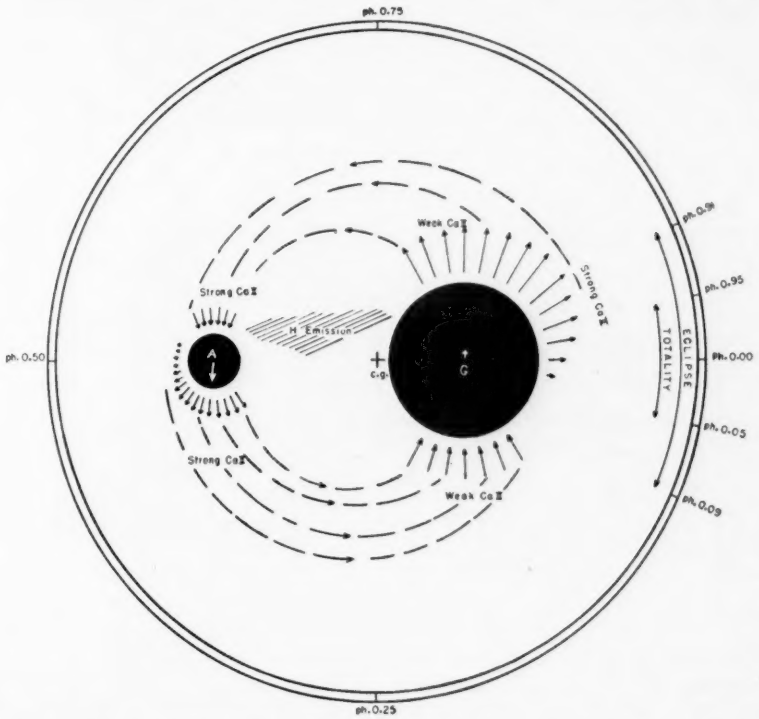

FIG. 11.—Schematic model illustrating the working hypothesis proposed in the text. The outflow and inflow of prominences are shown for *Ca* II.

seem to persist throughout totality. The absorption lines are broad and very conspicuous, but the contours are more shallow than ordinary *Ca* II lines in stars of type G. I have the impression that on the red sides of these broad absorption lines there is an indication of a faint and fairly broad emission line. It is this emission feature of *Ca* II which prevents us from seeing the normal, undisplaced *Ca* II absorption line of the G-type star. Since the violet-displaced absorption line is observed during total eclipse, when there are no features left belonging to the A-type star, we must conclude that the rapidly approaching *Ca* II atoms are located in front of the G star, as is indicated by the arrows in Figure 11. The contour of the absorption line presents an interesting problem. It is approximately symmetrical, with an over-all width of the order of about 10 A. If the expansion were radial with respect to the center of the G star, without appreciable turbulence, we should observe an unsymmetrical absorption line in the case of a layer

which is close to the G star's photosphere, or a broad emission line with a relatively narrow absorption line in the case of a very distant shell. The fact that we observe a symmetrical line suggests that the broadening is largely caused by turbulent motions. The shallow appearance of the line must be due to small optical depth of the expanding layer.

The expanding *Ca* II layer which is in front of the G star during principal eclipse does not give rise to hydrogen lines. We observe, during totality, only weak and narrow absorption lines of *H* on the violet borders of the emission lines already discussed. These lines give velocities of the order of -50 km/sec. There is no indication of other, broader absorption lines at -250 km/sec. We must conclude that the emitting gases which origi-

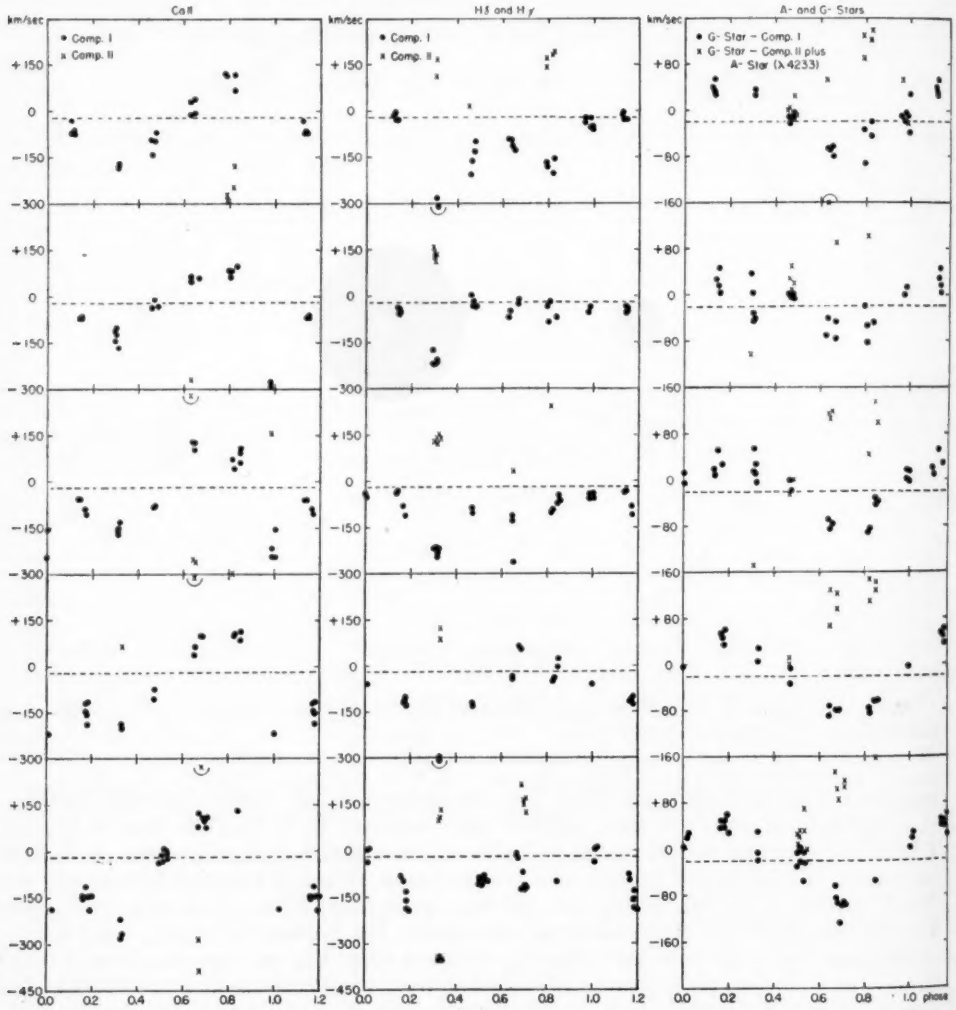

FIG. 12.—Radial velocities from *Ca* II, *H*, the lines of the G star, and the lines of the A star, plotted separately for each cycle.

nate in the G-type star are poor in *H* but rich in *Ca* II and that, moreover, the *H* atoms are driven out with a much smaller velocity than the *Ca* II atoms.[6] This is a phenomenon that reminds one of the early theoretical work by Milne and others on the expulsion of *Ca* atoms from the solar reversing layer. It is suggestive that the spectral types of the larger component of UX Mon and of the sun are approximately the same.

The radial velocities of the *Ca* II absorption lines between phases 0.96 *P* and 0.03 *P* show a tendency to increase algebraically, from about −250 km/sec to about −150 km/sec. This may be an effect of projection, so that we conclude that the *Ca* II atoms are expelled predominantly in the direction of phase 0.9 *P*. There is little or no expulsion in the direction 0.1 *P* or greater.

The radial velocities and the intensities of the *H* and *Ca* II lines, outside the two eclipses, are subject to large changes. Gaposchkin has already reported that the relative intensities of the double *H* lines are sometimes reversed in two consecutive cycles. The material in Figure 12 shows that such changes are quite common.

In a general way we notice the succession of intensities and velocities in a typical cycle, as shown in Table 2.

TABLE 2

Phase	*Ca* II			*H*			G Star	A Star
	Violet	Single	Red	Violet	Single	Red		
0.0	Strong		Absent		Weak		Predominates	Absent
.1		Strong			Strong		Small recession	Small approach
.2		Strong			Strong		Recession	Approach
.3	Strong		Absent	Strong		Weak or fairly strong	Recession	Approach
.4	Strong		Absent	Strong		Weak or fairly strong	Small recession	Small approach
.5		Strong as in class A5			Very strong		Absent or very weak	Strong
.6		Strong			Strong		Small approach	Small recession
.7	Weak or fairly strong		Strong	Weak		Very weak	Approach	Recession
.8	Weak		Strong	Weak		Very weak	Approach	Recession
0.9	Strong		Absent		Weak		Small approach	Small recession

Throughout all my observations the *H* lines were very weak in the second half of the cycle (near phase 0.75 *P*). In some cycles they were hardly visible. This was not the case in December, 1944, and January, 1945, when Gaposchkin's spectrograms were obtained. At that time strong double *H* lines were observed near phase 0.75 *P* and much weaker double lines near phase 0.25 *P*.

The variations from cycle to cycle are described in Table 3. An inspection of it shows that there is little correlation between the different entries. At phases around 0.3 *P* we notice that cycle II and also cycle VI had weak *H* lines. They were separated by about 3 weeks. But in cycle II, at phases near 0.8 *P*, the *H* lines were exceptionally weak, while in cycle VI they were strong. It is probable that the variations are irregular in character and that they occur at intervals which are often less than one complete cycle.

In order to test whether changes can be observed during single nights, I have obtained many series of consecutive spectrograms covering intervals of the order of 0.04 *P*, or about 6 hours. In several series unmistakable changes were detected which run contrary to the normal development within the cycle. These changes are never very conspicuous,

[6] We do not imply here that the abundance of *H* is small; only that the number of *H* atoms excited to the second energy level is small.

so that we can conclude that to accomplish a major change takes more than 6 hours, but often less than 6 days. Within intervals of even 1 or 2 hours appreciable changes in intensity and velocity take place, but they constitute only a small fraction of the entire range of these phenomena. A conspicuous case is illustrated in Figure 10. Other cases may be found in Table 1. Take, for example, the *H* lines on February 15, when they were single, strong, and sharp, as illustrated in the accompanying tabulation. Within

Phase	Mean Velocity	Phase	Mean Velocity
0.162 *P*	− 77 km/sec	0.184 *P*	−161 km/sec
0.165	− 95	0.196	−188
0.181	−134	0.199	−192

an interval of 0.037 *P*, or 5 hours, the radial velocity changed by more than 100 km/sec, a quantity which for such excellent lines as $H\gamma$ and $H\delta$ cannot be attributed to errors

TABLE 3*

CHANGES IN ABSORPTION-LINE INTENSITIES FROM CYCLE TO CYCLE

Cycle	0.1 *P*	0.3 *P*	0.5 *P*	0.8 *P*	1.0 *P*
I	*H* str., single *Ca* II str., single	*H* str., dble., v>r *Ca* II str., single, v	*H* very str., single *Ca* II str., single	*H* wk., dble., v>r *Ca* II str., dble., r>>v	*H* single, v *Ca* II single, v
II	*H* single *Ca* II single	*H* wk., dble., v>r *Ca* II str., v	*H* single *Ca* II single	*H* very wk., dble., v>r *Ca* II wk., r	*H* single, v *Ca* II single, v
III	*H* str., single *Ca* II str., single	*H* str., dble., v>r *Ca* II str., dble., v>>r	*H* very str., single *Ca* II str., single	*H* wk., single, v *Ca* II str., dble., r>>v	*H* single, v *Ca* II single, v
IV	*H* single *Ca* II single	*H* very str., dble., v>>r *Ca* II str., single, v	*H* str., single *Ca* II str., single	*H* str., dble., r>v *Ca* II str., dble., r>>v	*H* single, v *Ca* II single, v
V	*H* str., single *Ca* II str., single	*H* str., dble., v>r *Ca* II str., v	*H* str., single *Ca* II str., single	*H* wk., single, v *Ca* II single, r	*H* single, v *Ca* II single, v
VI	....	*H* wk., dble., v>r *Ca* II, single, v	....	*H* str., single, v *Ca* II str., single, r	....
VII	....	*H* dble., r>v *Ca* II single, r	....	....	....
IX	....	*H* str., dble., v=r *Ca* II single, r	*H* very str., single *Ca* II str., single	*H* very wk., v *Ca* II	....
X	....	*H* dble., v>r *Ca* II single, v	....	*H* wk., dble., v>r *Ca* II dble., r>>v	....
XI	*H* str., single *Ca* II str., single	*H* str., single, v *Ca* II str., single, v	*H* very str., single *Ca* II str., single	*H* wk., dble., v>r *Ca* II dble., r>>v	*H* str., single, v *Ca* II single, v
XII	....	*H* dble., v>r *Ca* II dble., v>>r	....	....	*H* single, v *Ca* II single, v
XIII	*H* str., single *Ca* II str., single	*H* str., dble., v=r *Ca* II str., single, v	....	....	....
XIV	....	....	*H* single *Ca* II str., single	....	....

* The letters "v" and "r" designate the violet and red absorption components; "wk." designates "weak"; "str." designates "strong"; "dble." designates "double."

of measurement or interpretation. While the *H* lines thus changed in velocity, the *Ca* II line remained approximately constant at −150 km/sec. This is, however, not especially surprising, because we have already seen that the velocities as derived from *H* and *Ca* II may be quite different.

It is abundantly clear that UX Mon presents a most complicated spectroscopic be-

havior. The lines of *Fe* I, *Ca* I, *Sr* II, *Ni* II, etc., undoubtedly originate in the reversing layer of a G-type star; those of *Fe* II come from an A-type star. But the lines of *Ca* II and *H* must come from streams of gas which during the time of observation happened to be between one or the other star and the observer. These streams, although subject to the gravitational attraction of the entire system, cannot be treated in the manner of the velocity-curves of spectroscopic binaries. It makes little sense to talk of the velocity of the "center of gravity for the *H* lines" and compare it to the velocity of the system of the two stars. In order to make progress in the unraveling of the peculiar phenomena in UX Mon, it is necessary that we should adopt, in a very tentative manner, a working hypothesis of the origin of the peculiar lines of *Ca* II and *H*. We shall present such a hypothesis in the following paragraphs and shall then show how it must be adjusted and modified to account for the known facts. I want to stress that I regard this hypothesis only as a convenient method for classifying and discussing the observations and not as a finished theory of stream-formation in binary stars.

The rapidity with which the absorption lines of *Ca* II and *H* change strongly suggests that we are concerned with prominence action, on a scale far surpassing that of the sun. On this hypothesis the observed component lines represent the integrated effect of absorption of a large mass of prominences. These prominences absorb mostly in *Ca* II and in *H*. They are subject to macroscopic variations which manifest themselves as the integrated effect of a large number of microscopic variations. If this interpretation is correct, we shall probably find that it is equally applicable to other cases of "stream motion" in close binaries and to the formation of "shells"—expanding or stationary—in rapidly rotating stars and in other peculiar objects. Our new interpretation provides an explanation of these phenomena and in no way contradicts them.

At the two elongations we observe double lines of *H* and *Ca* II. We therefore infer that when the two stars are observed side by side there are, somewhere in front of them, masses of prominences whose motions are predominantly those of approach and other masses whose motions are predominantly those of recession. In front of neither star are there any large masses whose motions are at right angles to the line of sight; if there were, such masses would produce strong undisplaced lines. There may, however, be in existence such a stream of gas that is not projected upon either star disk and which therefore would produce only an undisplaced emission line. Such a line probably exists: the space between the two absorption components is definitely stronger than the continuous spectrum at $H\beta$, and probably also at $H\gamma$ and $H\delta$. Incidentally, to remove any possible doubt, it is well to remember that the duplicity of the *H* absorption lines is not merely an effect of central reversal: the violet and red absorption components are often observed in places where there is normally only continuous spectrum and not the wing of a broad single absorption line. The absorption components are physically real.

We do not know whether the approaching and receding prominences are associated with only the A star, or with only the G star, or with both. An inspection of the double *H* lines at the two elongations, especially near phase 0.25 *P*, suggests that the central intensities of the components are cut down, as though the continuous spectrum of one star were covering the absorption component of the other. This would indicate that the streams are not present equally in front of both stars: there must be predominantly an outflow from one star and an inflow into the other; or there may be inflow and outflow in front of one star but not in front of the other. It is still impossible to decide which case is really present.

Perhaps we can reach a decision when we turn to *Ca* II. In the region of λ 3933, as we have already seen, $L_A \gg L_G$, so that the continuous spectrum is mostly that of the A star. A stream of gas in front of the G star, whether approaching or receding, would be very weak at λ 3933 because the continuous spectrum of a G star would be barely reg-

istered on the photographic emulsion. On the other hand, a stream of gas in front of the A star should produce a deep line, without the overlapping of continuous radiation from the G star. This latter prediction is in accordance with the facts: the *Ca* II components never give the impression of shallowness as do the *H* components.

It is interesting to note that for *Ca* II we normally observe the following: At phase 0.25 *P*, *Ca* II has only a strong violet component; at phase 0.75 *P*, *Ca* II has a very strong red component and a very weak violet component or no violet component at all. In the light of our discussion it is tempting to attribute the great predominance of the violet *Ca* II component at phase 0.25 *P* and of the red *Ca* II component at phase 0.75 *P* to a predominance of approaching prominences on the approaching hemisphere of the A star and a predominance of receding prominences on the receding hemisphere of the A star. It is also tempting to suggest that the *H* and *Ca* II prominences which rise from the approaching hemisphere of the A star curve around, giving rise to undisplaced emission lines, where the gases are effectively seen projected upon the empty space between the two component stars and finally fall into the receding side of the G star.

At phase 0.75 *P* we should observe weak components from those prominences which predominantly rise from the approaching hemisphere of the G star. If these prominences are similar to those which produce the large negative velocity of *Ca* II between phases 0.96 and 0.00 *P*, we should expect them to be rich in *Ca* II and poor in *H*. Again, it is reasonable to suppose that the stream of prominences curves around and finally falls into the receding side of the A star producing the strong red absorption components.

The proposed hypothesis, tentative as it is, agrees well with many obervational facts. It accounts, for example, for the tendency of the *H* emission lines to be stronger at the elongations than away from phases 0.25 *P* and 0.75 *P*. (The great apparent intensity of the *H* emission lines between phases 0.95 *P* and 0.00 *P* is caused by the longer exposures that are required during the total eclipse.) But it also meets with several difficulties.

In the first place, we notice that at least in one cycle, III, at phases near 0.644 *P* we have for *Ca* II, $v = r$. Although at phases near 0.8 *P*, we again have the usual $r \gg v$, it is clear that, at least in this one cycle, there existed in front of the receding hemisphere of the A star an approaching stream which was nearly as strong as the usual receding stream. We cannot, therefore, think of the streams as a regular flow of gas but only as an irregular mass of rising and falling prominences whose large-scale tendencies are reflected in the predominant motions which we have described.

Another unsatisfactory feature of our hypothesis is the fact that the unsymmetrical behavior of the *H* emission-line intensities during total eclipse requires for its explanation the postulation of a separate mass of gas, which we have indicated by the shaded area in Figure 11. These emission lines are shifted to the red so that the gas would move predominantly from the G star to the A star, that is, in the same direction as do the prominences in the same hemisphere. But it is not very satisfactory that this mass of gas cannot be identified with the flow of prominences: if it could, then the much greater intensity of the *H* absorption-line components at phases near 0.25 *P* than at 0.75 *P* would lead us to expect that the emission lines of *H* would be more intense after mid-eclipse than before it.

Despite these weaknesses, I have presented in Figure 11 a rough model of the proposed system, where the arrows outside the two stars represent the motions of the *Ca* II gases but are not drawn to scale.

We have not yet discussed the appearance of *H* and *Ca* II during the secondary eclipse. The lines are single, very strong, and suggestive of the bell-shaped contours associated with the concept of turbulence. The lines are deep because the continuous spectrum of the G star is weakened and because the prominences which flow out of the advancing hemisphere of the A star and flow into its receding hemisphere must absorb

at least a part of the light from the uneclipsed rim of the G star. The radial velocities of both *Ca* II and *H* are often negative at phases near 0.5 *P*—up to about −100 km/sec. But in several cycles the velocities were much closer to that of the system of the two stars. This variation shows that the general tendency at phase 0.5 *P* is one of outflowing prominences. As in the case of primary eclipse we linked the large negative velocity of *Ca* II during the first half of totality with the outflow of prominences from the advancing hemisphere of the G star, so we are inclined to see a connection between the moderate outflow of prominences at phase 0.5 *P* and the more violent outflow from the advancing hemisphere of the A star at phase 0.25 *P*.

The *H* emission lines are weaker at secondary eclipse than at the elongations and during the first half of total eclipse. This result is contrary to that announced by Gaposchkin. It is, of course, possible that the character of the spectrum has changed in this respect since 1944, as it has changed in other respects. But it fits into the picture we have presented, because during secondary eclipse at least a part of the shaded area in Figure 11 would be occulted by the disk of the A star, and those parts which would not be occulted would be seen in front of the uneclipsed rim of the G star and would contribute to the absorption line to the extent that pure scattering is responsible for the excitation of the *H* atoms.

The radial velocities listed in Table 1 depend upon *Ca* II 3933 for the column headed "*Ca* II"; upon *Hδ* and *Hγ* for the column headed "*H*"; upon the stronger components of the lines of *Fe* I, *Sr* II, *Ni* II, *Ti* II, and *Ca* I for the column headed "G Star"; and upon the average of *Fe* II 4233 and, whenever present, the fainter components of *Fe* I, *Sr* II and *Ca* I for the column headed "A Star." The velocities are plotted in Figure 12, separately for each cycle. The stronger components, in the case of double lines, are indicated by dots, the weaker components by crosses. There are large variations, from cycle to cycle, for *Ca* II and *H*. It is not possible to combine them into a single diagram.

The *Ca* II velocities are less complicated than are those of *H*. The curves show minima at phase 0.30 *P* and maxima near phase 0.80 *P*. Weak components are observed almost only between phases 0.60 *P* and 0.85 *P*. These components have large negative velocities and may be connected with the strong absorption lines observed at principal minimum. We can estimate the maximum and minimum velocities for the first five cycles, as in the accompanying tabulation. The mean velocities in all cycles are negative, the aver-

RADIAL VELOCITIES FROM STRONGER COMPONENTS OF *Ca* II

Cycle	Minimum		Maximum		Mean Velocity (Km/Sec)
	Phase *P*	Velocity (Km/Sec)	Phase *P*	Velocity (Km/Sec)	
I	0.30	−160	0.85	+120	−20
II	.30	−120	.85	+105	− 8
III	.30	−150	.75	+130	−10
IV	.30	−195	.75	+105	−45
V	0.30	−240	0.75	+120	−60
Mean	0.30	−173	0.79	+116	−29

age of the five cycles being −29 km/sec. This does not differ much from the velocity of the center of mass of the G and A stars, but the variations from cycle to cycle are so large that we can only conclude that there is no general tendency for the stronger com-

ponents of the *Ca* II lines to indicate a permanent tendency of the atoms to escape from the system. The velocities in the foregoing tabulation are, of course, referred to the sun. Now, at phase 0.3 *P*, the A star has a velocity of −160 km/sec with respect to the sun, or of −140 km/sec with respect to the center of mass. The velocity of the *Ca* II atoms with respect to the A star is therefore only −130 km/sec. Similarly, at phase 0.8 *P* the velocity of the *Ca* II atoms would be −4 km/sec with respect to the A star. If our picture in Figure 11 is correct, this means that the stream is practically stationary with respect to the A star. The stream of gas seems "to pay no attention" to the presence of the A star. This conclusion rests heavily upon the determination of the orbital velocity of the A star. If it were correct, we should probably not speak of prominences connected with the A star, but only of a stream of irregular masses of gas which flow along the same orbit as the A star but are not dynamically connected with it. It must, however, be remembered that Gaposchkin found only 68 km/sec for the orbital velocity of the A star. With his value there would be a real outflow of prominences, with a velocity of the order of 80 km/sec from the advancing hemisphere, and an inflow, with a velocity of the order of 50 km/sec into the receding hemisphere. At present, it is more probable that my result is correct, but only a new investigation can remove the doubt.

In the case of the fainter *Ca* II components, which we have, tentatively, associated with the G star, the evidence is even more uncertain. We again summarize the data in the accompanying tabulation. The maximum velocity depends upon a single observation.

RADIAL VELOCITIES FROM FAINTER COMPONENTS OF *Ca* II

Cycle	Maximum		Minimum	
	Phase *P*	Velocity (Km/Sec)	Phase *P*	Velocity (Km/Sec)
I	Not observed		0.8	−230
II	Not observed		.7?	300
III	Not observed		.8	300
IV	0.3?	+100	.7?	300
V	Not observed		0.7	−390

Nevertheless, there seems to be a very large preponderance of negative velocities, so that in this case we have probably a real departure from the velocity of the center of mass. At phases near 0.75 *P* the velocity of the G star is about −80 km/sec with respect to the sun. Hence at this phase the velocity of the *Ca* II prominences with regard to the G star is of the order of −220 km/sec. Similarly, at phase 0.25 *P* the velocity of the G star is +40 km/sec. That of the *Ca* II atoms is about +100 km/sec. They "fall" into the G star with a relative velocity of 60 km/sec.

It appears that we must look for the source of the *Ca* II prominences to the advancing hemisphere of the G star. The A star is not effective in producing them.

The interpretation of the velocities of the *H* lines is complicated by the fact that they reverse their intensities between elongations. It is, at first sight, tempting to adopt for the *H* lines a picture similar to that which we have used in the case of *Ca* II. The shallow appearance of the double components of $H\gamma$ and $H\delta$ shows that the inflowing and outflowing streams are not all equally distributed in front of both stars. But we do occasionally observe double lines of $H\zeta$ and $H\eta$, so that in these cases, at least, we are certain that inflow and outflow occur in front of the A star. Perhaps there is still a predominance of motions in the same sense as was proposed for *Ca* II, but this predominance

cannot be very pronounced. We can summarize the velocities as in the accompanying tabulation. The only definite conclusion that we can draw is that the *H* atoms have a

RADIAL VELOCITIES FROM *H* LINES

Cycle	Phase (Km/Sec)			
	0.30 *P*	0.80 *P*	0.30 *P*	0.80 *P*
I	−300	+180	+135	−180
II	−220	.....	+140	.....
III	−230	+140?	+150	−100?
IV	−300	.....	+110	.....
V	−345	+160	+120	− 90

large velocity of escape from the advancing hemisphere of the A star. They move, relative to it, with a velocity of the order of −150 km/sec and may well be thought of as explosive *H* prominences which originate in the A star. When they fall into the A star, they have small relative velocities. With respect to the G star, their velocities are appreciable, though much smaller than the velocity of escape from the A star. Perhaps we can think of them as streaming past the G star without being much disturbed by the latter. But if both outflow and inflow occur on each hemisphere of the A star, then there is little real evidence of the motion of *H* atoms in front of the G star, except for the evidence of the P Cygni type lines of *H* during total eclipse. We have already seen that the violet absorption components of these lines between phases 0.96 *P* and 0.03 *P* give velocities of the order of −50 km/sec. At the same phases the velocity of the G star must be that of the center of mass of the system, or −20 km/sec. The outflow of *H* from the G star near phase 0.0 *P* is thus about −30 km/sec.

We are thus led to propose that the *Ca* II prominences have their origin principally in the advancing hemisphere of the G star, while the *H* prominences originate primarily in the advancing hemisphere of the A star and produce strong lines of approaching gases and weaker lines of receding gases. If the *Ca* II prominences originate from the surface of the G star, then why do they produce faint lines of λ 3933 at phase 0.8 *P*? The answer is that the continuous spectrum of the G star is weak at λ 3933, relative to the continuous spectrum of the A star. It is perhaps also reasonable that after a complete turn around the orbit the infalling prominences produce still weaker lines in the combined spectrum at phase 0.3 *P*. But it is not so easy to explain why we often observe strong lines of *Ca* II with fairly large negative velocities at phases near 0.5 *P*. We present a summary of these velocities in the accompanying tabulation. Considering that the velocity of the system

RADIAL VELOCITIES OF *Ca* II DURING AND NEAR SECONDARY ECLIPSE

Cycle	Velocity (Km/Sec)	No. of Films	Cycle	Velocity (Km/Sec)	No. of Films
I	−101	4	IV	−90	2
II	25	4	V	−15	7
III	− 81	2	Mean	−62	.....

is −20 km/sec, it appears that there is an appreciable motion of *Ca* II away from the A star during the secondary eclipse. But perhaps this is to be considered a small complication that would not destroy the rest of the picture.

The contours of *H* absorption-line components are often unsymmetrical, with faint wings extending away from the geometrical center of the two components. These wings can only in part be caused by Stark effect, because they are variable; on some occasions they are absent; and when that happens the contours are bell-shaped, as in the case of turbulence broadening, except that the line centers are not so deep as in such stars as 17 Leporis or ϵ Aurigae. There is also a systematic difference between the velocities as measured for $H\gamma$ and $H\delta$, respectively, as shown in the accompanying tabulation.

DIFFERENCES IN VELOCITY: $H\gamma$–$H\delta$

Phases	Single Lines (Km/Sec)	Stronger Component	Weaker Component	Phases	Single Lines (Km/Sec)	Stronger Component	Weaker Component
0.95–0.05	−65.0	.....	.....	0.45–0.55	−39.6	− 2.0	−45.7
.05– .15	−27.4	.....	.....	.55– .65	−50.0	.....	.....
.15– .25	+30.0	.....	.....	.65– .75	−41.0	−12.3	− 3.2
.25– .35	+26.2	−14.8	+26.0	.75– .85	−75.6	−54.6	−15.0
0.35–0.45	.....	+10.8	+10.0	0.85–0.95	−53.7	.....	.....

Negative values predominate. They are especially large in the case of single lines; this suggests that the lines are unsymmetrical or consist of blended components, whose relative intensities are not the same for $H\gamma$ and $H\delta$.

There remains the question of the stars themselves. The plot of the velocities by cycles in Figure 12 shows that there are no appreciable changes in the velocities of the

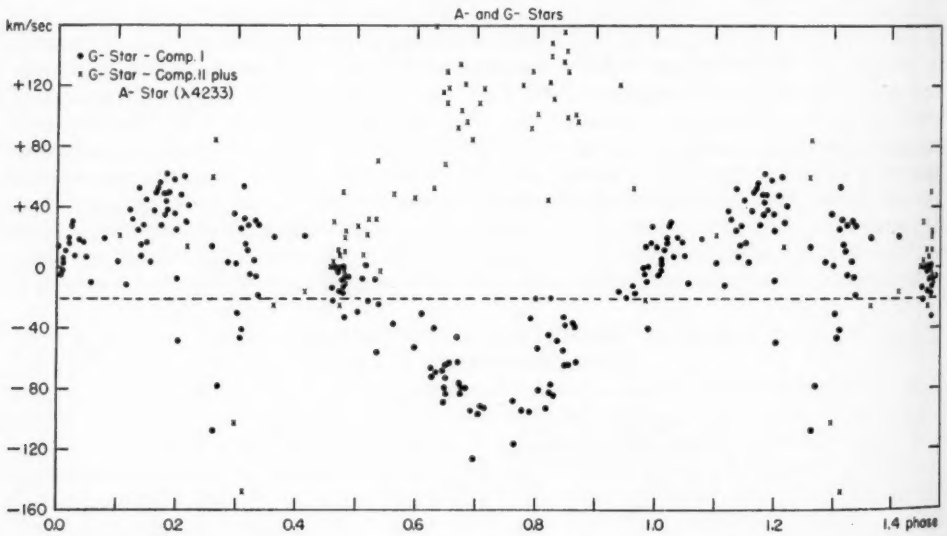

FIG. 13.—Radial velocities of G and A stars. The dots show the velocities of the G-type star. Crosses indicate the velocities of the A-type star.

G and A stars, from cycle to cycle. These velocities[7] have all been plotted together in Figure 13. The measures were very difficult because the lines are all faint and often somewhat diffuse. Nevertheless, we have a reasonably consistent velocity-curve for the G star. There is a suggestion that the maximum of the G star's velocity-curve is broader than the minimum, and perhaps this would account for the fact that double lines have been measured almost only between phases 0.6 P and 0.9 P. But this is certainly not the entire story. The line *Fe* II 4233 is not blended with a line of the G star. Yet *Fe* II 4233 was seen almost only from phase 0.45 P to phase 0.9 P, and almost never between phases 0.1 P and 0.4 P. Thus it is certain that the lines of the A star are more conspicuous in the second half of the cycle than in the first. This being the case, I am inclined to attribute the apparent asymmetry in the velocity-curve of the G star to a psychological effect; close double lines are often measured with greater separation than the real ones; and, because of the diffuse nature of the lines and the extreme faintness of the A star's component, the tendency has undoubtedly been to give preference to such lines as would best show the duplicities because of their peculiar grain structure. Under these circumstances it seems to me best to adopt circular elements for the two stars as follows:

$V_0 = -20$ km/sec

$K_G = 60$ km/sec

$K_A = 140$ km/sec

$T_G =$ Phase $0.75P =$ Time of minimum velocity

$T_A =$ Phase $0.25P =$ Time of minimum velocity

$a_G \sin i = 4.9 \times 10^6$ km

$a_A \sin i = 11.4 \times 10^6$ km

$m_G \sin^3 i = 3.4\odot$

$m_A \sin^3 i = 1.5\odot$

$$\frac{m_G}{m_A} = 2.3$$

Wyse has described the secondary's spectrum as dG1p. Gaposchkin gave G2p. It is doubtful whether the description of this star as dwarf can be maintained. Because of the peculiar character of the *Ca* II and *H* lines it is difficult to determine the type accurately. But it is probably not far from G0 or G2. During totality the line *Sr* II 4077 is very slightly stronger than *Fe* I 4045. Also, *Sr* II 4215 is a little stronger than *Fe* I 4250. These criteria, with the help of the *Atlas* by Morgan, Keenan, and Kellman, would indicate a luminosity class distinctly brighter than V and probably between III and IV. Perhaps the spectrum can best be described as that of a subgiant. In this respect the star would be similar to the cooler components of a large number of Algol-type variables with class A primaries. What makes the G star in the system of UX Mon unusual is its large mass. The mass of the cool companion in the usual Algol-type variable is less than $1\odot$, and it has a radius of 2–$3\odot$.

If my determination of $a_A \sin i$ and $a_G \sin i$ can be relied upon, we find, with Gaposchkin's photometric values of r_A and r_B in terms of $(a_A + a_G)$,

$$r_A = 1.3 \times 10^6 \text{ km} = 1.8\odot ,$$

$$r_G = 4.6 \times 10^6 \text{ km} = 6.6\odot .$$

These values are not unreasonable, although the cooler star appears to be considerably larger than is the case in ordinary Algol-type binaries.

[7] In Figs. 12 and 13 the weaker components of double lines whose stronger components belong to the G-star have been labeled as "G-star—Comp. II." These lines belong to the A star, as do also the single lines of *Fe* II 4233.

THE POSTMAXIMUM SPECTRUM OF χ CYGNI*

PAUL W. MERRILL
Mount Wilson Observatory
Received May 24, 1947

ABSTRACT

The spectrum of the long-period variable χ Cygni combines characteristics of classes M and S. Numerous bright lines are unusually intense. Spectrograms extending from the blue into the ultraviolet, dispersion 10 A/mm, were obtained over the interval from 41 to 162 days after maximum; the corresponding range of magnitude was from 6.3 to 11.4.

Dark lines.—The atomic-line spectrum resembles that of R Andromedae, class Se, but the *TiO* bands are as strong as in class M6. The velocities exhibit a very slight increase (algebraic) with advancing phase. Differences between various cycles are small. Residuals of individual lines behave as in other red variables.

Bright lines.—After maximum, bright lines of *Fe* I increased in number from 30 to almost 100. Most of them grew stronger throughout the period of observation, but a few high-excitation multiplets had their maximum intensities about 114 days after maximum. The behavior of multiplet (2) illustrates the tendency of bright lines to escape from the effects of the reversing layer as the phase advances. A peculiarity of physical interest is the inordinately high intensity of bright lines from upper levels z^5G_4 and z^5G_2. A third level possibly emphasized is w^5D_4, and others not so outstanding are y^5F_1 and y^5F_2. In *Zr* I level x^1G_4 is the only one that gives use to bright lines. In several other elements possible examples of excitation by line coincidence are noted.

Numerous bright lines of *Co* I and *Ni* I have been identified. Multiplets having certain *lower* levels are emphasized. This fact probably finds its explanation in the different relative intensities of absorption and emission lines at various excitation potentials.

Numerous bright lines of *Fe* II became outstanding with advancing phase; forbidden lines appeared about 100 days after maximum and strengthened rapidly during the next two months. Other bright lines discussed are those of *H*, *Mg* I, *Si* I, *Mn* I, *In* I, and the curious displaced components of *Al* I, *Ca* II, and other elements.

Velocities from lines of *H*, *Fe* II, and *Ti* II agree with one another and vary little with phase; velocities from *Fe* I lines increase slightly with excitation potential and with phase. Observations of R Andromedae and χ Cygni suggest that Se variables have smaller periodic variations in the positions of lines both bright and dark than do Me variables.

Wave lengths of numerous bright lines measured on Plate Ce 3505, phase +162 days, magnitude 11.4, are collected in Table 13. The table indicates how the intensity behaves as the phase advances. A number of strong lines remain unidentified.

The variability of χ Cygni, 194632, was discovered in 1686 by G. Kirch as a result of comparing the sky with Bayer's star atlas of 1603. The only variable stars discovered earlier are *o* Ceti (1596) and β Persei (1669). The period of χ Cygni is 406.5 days with a mean magnitude range of from 5.3 to 13.3. The extreme range has probably been 10 mag.; thus at the brighter maxima the star is about ten thousand times as bright as at the fainter minima.

The spectrum was classified Md at Harvard. Later observations with slit spectrographs have shown that it combines characteristics of classes M and S. Numerous bright lines are unusually intense. Previous observations of χ Cygni with slit spectrographs are listed in Table 1.

In the present investigation, spectrograms having dispersion 10.3 A/mm were obtained with the 100-inch telescope at four epochs after maximum light in 1944 and at one epoch in 1945 (Table 2). All were on the II*a*-O emulsion supplied by the Research Laboratory of the Eastman Kodak Company. In 1944 the plates were baked at 50° C for 3 days prior to exposure.

The dates of observation are marked on the light-curve in Figure 1. I am again indebted to Mr. Leon Campbell of the Harvard Observatory for the photometric data.

* *Contributions from the Mount Wilson Observatory, Carnegie Institution of Washington*, No. 735.

TABLE 1

PREVIOUS OBSERVATIONS WITH SLIT SPECTROGRAPHS

Observatory	Observer	Year	Reference
Potsdam	G. Eberhard	1901, 1902	*Ap. J.*, **18**, 198, 1903
Univ. Michigan	P. W. Merrill	1914	*Pub. Obs. Univ. Michigan*, **2**, 45, 1916
Victoria	F. S. Hogg	1932	Unpublished
Mount Wilson	P. W. Merrill	1920 1928	*Mt. W. Contr.*, *Ap. J.*
		1921 1932	No. 200 **53**, 185, 1921
		1923 1937	264 **58**, 215, 1923
		1926 1938	399 **71**, 285, 1930
		1927 1939	539 **83**, 272, 1936
			642 **93**, 40, 1941
			649 **94**, 171, 1941

TABLE 2

JOURNAL OF OBSERVATIONS

Plate Ce	Date	JD 243	Vis. Mag.	Phase (Days)	Exp. Min.	Rad Vel. from Abs. Lines	
						Km/Sec	No. Lines
3404	1944 Apr. 7	1188	7.9	+ 68	(44)	.....	.....
3406	Apr. 9	1190	8.0	+ 70	232	−3.0	31
3424	May 11	1222	9.3	+102	312	−3.6	47
3443	June 4	1246	10.2	+126	388	−6.5	28
3505	July 10–11	1282–83	11.4	+162–63	792	−5.7	21
3758	1945 Apr. 27	1573	6.3	+ 41	142		
3762	Apr. 28	1574	6.3	+ 42	142	−2.3	162
3766	Apr. 29	1575	6.4	+ 43	286		
3768	Apr. 30	1576	6.4	+ 44	12, (20)	.....	.....
3769	Apr. 30	1576	6.4	+ 44	(10), 30	.....	.....

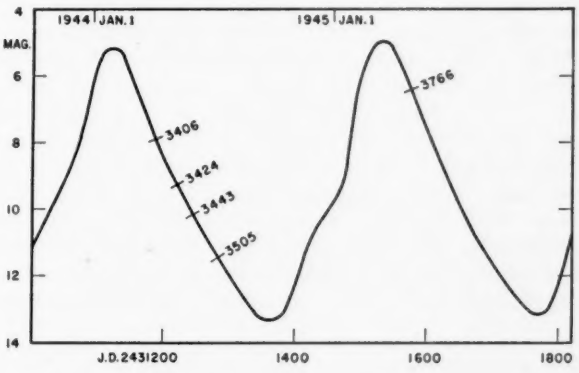

FIG. 1.—Light-curve of χ Cygni showing dates of spectrograms (see Table 2)

ABSORPTION LINES

The spectrum as a whole with its strong *TiO* bands has the general appearance of class M6, but (inconspicuous) *ZrO* bands[1] and the intensities of certain atomic lines suggest class S. The general atomic-line spectrum does not differ greatly from that of R Andromedae, class Se (although the excitation temperature appears to be somewhat lower), or from that of *o* Ceti, M6e. The numerous minor differences in line intensities call for future detailed study.

The mean radial velocities derived from absorption lines on spectrograms in the present series are recorded in Table 2. The velocities appear to decrease algebraically with advancing phase, but the changes are small. Likewise the differences from year to year (Table 3) are small.

TABLE 3

RADIAL VELOCITIES NEAR MAXIMUM LIGHT

Observatory*	Year	Abs. Lines (Km/Sec)	Emission Lines (Km/Sec)
Potsdam	1901	+2	−20
	1902	−2	−21
Univ. Michigan	1914	.....	−17
Mount Wilson	1920	−2	−18
	1923	−3	−18
	1928	0	−14
	1938	−4	−21
	1939	+4	−12
	1944	−3	−15
	1945	−2	−15

* For references see Table 1.

The residuals yielded by various lines behave much as in R Leonis[2] and other Me stars. The *K* lines λ 4044, λ 4047, are displaced shortward 3 km/sec with respect to the mean velocities adopted for absorption lines. Iron lines at excitation potential 1.0 volts are displaced longward 2 km/sec with respect to ultimate lines.

EMISSION LINES

Bright hydrogen lines are outstanding features of the maximum and early post-maximum spectrum. They appear on a long series of Harvard objective-prism photographs, the first of which was taken in 1890. A few additional bright lines were detected on some of the Harvard plates, but it remained for slit spectrograms to record scores of bright lines and to reveal the remarkable complexity of their behavior (see references in Table 1). The spectrograms discussed in this paper have higher dispersion than my earlier plates and make possible a more detailed study of the lines.

The bright lines, with their remarkable changes of intensity as the phase advances from maximum toward minimum, are similar to those in R Andromedae, class Se; and in both stars the chief lines and their cyclical changes follow the general pattern previously found to be typical of Me variables. The spectrograms of χ Cygni show an emission-line spectrum richer than that previously photographed in any long-period variable.

[1] The *ZrO* band λ 4619 is shown in P. W. Merrill, *Spectra of Long-Period Variable Stars* (Chicago: University of Chicago Press, 1940), Pl. II.

[2] P. W. Merrill, *Mt. W. Contr.*, No. 720; *Ap. J.*, **103**, 275, 1946.

Lines of Fe I.—About 30 bright lines of *Fe* I were identified during the first 2 months after maximum. The number increased to almost 100 on Plate Ce 3505, phase +162 days. Most of the lines grew stronger throughout the period of observation. An exception, however, was offered by multiplets (72), (73), (74), and (75), whose lines had their maximum intensities about 110 days after maximum.

The estimated intensities of lines of multiplet (2) at various phases are in Table 4. In the last column, phase +162 days, the relative intensities are nearly the same as in the laboratory. At earlier phases the intensities are modified, probably by *TiO* band absorption, as in R Leonis.[3] The behavior of this multiplet presents another example of the general tendency of bright lines to escape from the effects of the reversing layer as the phase advances.

Intensities in multiplet (3) are approximately the same as in the laboratory, except that λ 4216 is relatively weak, probably being interfered with by λ 4215 *Sr* II. A peculiarity of multiplet (4) is the absence in emission of the leading line λ 3860. Four of the stronger lines of (5) appear to be present at the later phases but, if correctly identified, yield negative displacements of about 15 km/sec with respect to other bright lines

TABLE 4

INTENSITIES OF EMISSION LINES OF *Fe* I MULTIPLET (2)

I.A.	Lab.	χ Cygni (Phase in Days)				
		+43	+69	+102	+126	+162
4375.93	9	1	1	2.5	3	3
4427.31	10	.....	.....	1	1	3
4461.65	8	.....	.....	1	2	2.5
4482.17	4	.....	.....	.....	0.7	2
4489.74	3	.....	.....	0.5	1	1.5
4389.24	2	.....	.....	.....	.....	0.5
4435.15	2	.....	.....	.....	0.5	tr

of *Fe* I. All lines of (20), with the possible exception of λ 3820, are present in moderate or low intensity; the intensities of the first five lines relative to the others are less than in the laboratory. In (21) several lines were noted as unusually sharp; lines with upper level y^5F_2, and possibly y^5F_1, seem relatively strong.

The extraordinarily high intensities of the bright *Fe* I lines with upper level z^3G_4 have been noted in the postmaximum spectra of many long-period variables.[2, 4, 5, 6] The behavior of multiplets (24) and (42) in which these lines occur is indicated in Table 5. Very similar behavior is now clearly shown by multiplets (23) and (41), in which lines from the upper level z^5G_2 are inordinately strong (Table 6). Another possible instance, not nearly so well marked, is supplied by multiplet (21), in which lines from upper levels y^5F_1 and y^5F_2 appear relatively stronger than in the laboratory.

In χ Cygni, as in many other red variables, an outstanding bright line at 3852.6, if correctly identified with an *Fe* I line of (73), is inordinately strong, compared with other lines of the multiplet. The upper level of this line w^5D_4 produces no other lines except λ 3171, (52), in the far ultraviolet and two weak lines λ 4373, (214), and λ 5787, (625); none of these has been observed in long-period variables, and the evidence for w^5D_4 as an emphasized upper level is thus less complete than for z^3G_4 and z^5G_2.

[3] P. W. Merrill, *Pub. A.S.P.*, **58**, 304, 1946. [4] Thackeray and Merrill, *Pub. A.S.P.*, **48**, 331, 1936.

[5] Merrill and Thackeray, *Pub. A.S.P.*, **49**, 120, 1937.

[6] A. D. Thackeray, *Mt. W. Contr.*, No. 580; *Ap. J.*, **86**, 499, 1937.

Measured displacements of 17 multiplets are arranged in Table 7 according to excitation potential and to phase in the light-cycle. The values tend to increase algebraically with both these parameters.[7] The change in displacement in passing from E.P. 3.1 (upper term) to 5.3 volts is about +8 km/sec and seems to be about the same at all phases. Similarly, the change in displacement in passing from phase +43 to +162 days, about +5 km/sec, is about the same for all excitation potentials. The effect is probably due in part to absorption components on the longward sides of many of the bright lines. The dark lines tend to become less intense relative to the bright lines with increasing

TABLE 5

EMISSION LINES OF *Fe* I MULTIPLETS (24) AND (42)

(24) a^5F-z^5G				(42) a^3F-z^3G			
I.A.	J	Intensity		I.A.	J	Intensity	
		Lab.	x Cyg*			Lab.	x Cyg*
3513.82	5–5	30	.....	4271.76	4–5	35	1
3521.26	4–4	25	8	4307.91	3–4	35	30
3526.17	3–3	15	.....	4325.76	2–3	35	1†
3466.50	5–4	3	0.3	4202.03	4–4	30	20
3483.01	4–3	3	.....	4250.79	3–3	25	0.5
3570.10	4–5	100R	.....	4147.67	4–3	10	.....
3565.38	3–4	60r	13				
3558.52	2–3	30	.....				

* Plate Ce 3505, phase +162 days. † Blend with an *Fe* I line of multiplet (2)?

TABLE 6

EMISSION LINES OF *Fe* I MULTIPLETS (23) AND (41)

(23) a^5F-z^5G				(41) a^3F-z^5G			
I.A.	J	Intensity		I.A.	J	Intensity	
		Lab.	x Cyg*			Lab.	x Cyg*
3581.20	5–6	250R	tr	4383.55	4–5	45r	2
3647.84	4–5	100R	.....	4404.75	3–4	30	1.5
3631.46	3–4	125R	.....	4415.12	2–3	20	1.5
3618.77	2–3	125R	tr	4294.13	4–4	15	0.5
3608.86	1–2	100R	5	4337.05	3–3	10	bl?
3589.11	5–5	8	.....	4367.91	2–2	2	1
3585.71	4–4	20	.....	4229.76	4–3	(1)	.....
3585.32	3–3	30	.....	4291.47	3–2	4	2.5
3586.98	2–2	30	4				
3528.94	5–4	.....	.....				
3540.71	4–3	3	.....				
3554.12	3–2	4	1				

* Plate Ce 3505, phase +162 days.

[7] A similar result, somewhat less marked, was shown by the *Fe* I lines in R Andromedae, as I pointed out in *Mt. W. Contr.*, No. 730; *Ap. J.*, **105**, 360, Table 8, 1947.

excitation potential and with increasing time after maximum light; naturally, as they become weaker, they have less effect in causing small displacements in the measured positions of the bright lines. The disturbing effect of the dark lines may not be the whole story; it certainly is not the main cause of the relatively large general displacement of bright lines with respect to the absorption spectrum.

Lines of Co I.—About 30 bright lines, mostly of moderate or low intensity, have been identified with *Co* I. Among the stronger are: multiplets (16) 4020.90; (28) 4131.32,

TABLE 7

RADIAL VELOCITIES FROM EMISSION LINES OF *Fe* I

(Km/Sec)

Multiplet	Upper Term		Phase (Days)					
	Desig.	E.P. (Volts)	+43	+69	+102	+126	+162	+100 (Mean)
2	z^7F	2.8	−25.6 1*	−22.5 1*	−18.0 4*	−17.0 5*	−18.8 7*	.....
3	z^7P	3.0	−23.3 2	−19.8 1	−18.8 4	−18.2 5	−19.0 5	.....
4	z^5D	3.2	.....	.....	.....	−21.5 2	−25.5 5	.....
Mean†	.....	3.1	−24.4 ..	−21.2 ..	−18.4 ..	−18.9 ..	−21.1 ..	−20.8
20	y^5D	4.1	−25.9 1	−20.6 2	−15.0 5	−18.7 10	−15.9 11	.....
21	y^5F	4.2	−20.8 2	−20.2 2	−18.6 4	−19.9 8	−18.8 10	.....
22	z^3P	4.2	.....	.....	−16.0 1	−15.2 3	−12.3 4	.....
23	z^5G	4.3	−26.1 3	−21.5 2	−16.2 3	−15.3 3	−13.9 4	.....
24	z^3G	4.4	−20.0 2	−19.1 2	−16.9 2	−17.6 3	−13.3 3	.....
Mean†	.....	4.2	−21.7 ..	−20.4 ..	−16.5 ..	−17.3 ..	−14.8 ..	−18.1
41	z^5G	4.4	.....	.....	−19.5 3	−15.0 3	−11.8 4	.....
42	z^3G	4.4	−20.8 2	−17.6 2	−15.6 3	−15.3 4	−15.5 5	.....
43	y^3F	4.6	−18.6 2	−16.6 2	−15.7 3	−16.7 4	−13.8 3	.....
45	y^3D	4.7	−13.8 1	−14.1 1	−15.6 4	−14.5 5	−13.4 5	.....
Mean†	.....	4.5	−17.7 ..	−16.1 ..	−16.6 ..	−15.4 ..	−13.6 ..	−15.9
68	x^5D	4.9	−14.8 1	.....	−15.3 1	−13.7 1	.....	.....
72	x^5P	5.3	−19.3 2	−11.4 3	− 7.8 3	− 7.1 3	− 8.6 3	.....
73	w^5D	5.4	−16.8 3	−14.4 3	−11.5 4	−11.9 5	−10.7 4	.....
74	w^5F	5.5	−13.3 4	−11.8 4	−10.1 4	−11.1 4	(−15.1) 2	.....
75	v^5D	5.5	−18.2 2	−14.0 2	−13.6 1	− 9.0 1	−10.1 1	.....
Mean†	.....	5.3	−16.5 ..	−12.9 ..	−11.7 ..	−10.6 ..	−11.1 ..	−12.6
Over-all mean	.....	4.3	−20.1 ..	−17.9 ..	−15.8 ..	−15.6 ..	−15.2 ..	−16.9

* Number of lines.

† The *lower* terms of the multiplets entering into the four sets of means have the respective excitation potentials 0.0, 0.9, 1.5, and 2.2 volts.

4118.77; (31) 3995.31; (32) 3935.96; 3997.90; (34) 3845.47; (58) 4086.30; all were measured also in the spectrum of R Andromedae. Most of the *Co* I lines appear to have their greatest intensity about 130 days after maximum light. Many of them are slightly diffuse.

Most of the lines have the lower term a^2F, E.P. 0.9 volts; three or four have the lower term b^4P, E.P. 1.9 volts. No ultimate lines have been detected; in this respect the be-

havior differs strongly from that of lines of *Fe* I. In *Co* a general tendency toward emission is apparently overcome in ultimate lines by the absorption of the numerous atoms in the ground level; although in *Fe* this appears to be true for some of the very strong lines, at the later phases the emission of certain lines becomes so intense that it cannot be hidden by absorption as weak as that in multiplets (2) and (3), for example.

Lines of Ni I.—About 15 bright lines, mostly of low intensity, have been identified with *Ni* I. Among the stronger ones are: multiplets (30) 3783.53, 3736.81; (32) 3858.30; (52) 4331.64; all were measured also in the spectrum of R Andromedae. The *Ni* I lines reach their greatest intensities later in the cycle than do the *Co* I lines; in fact, they appear to be growing stronger throughout the observed interval after maximum up to phase +162 days.

Most of the bright *Ni* I lines have the lower term a^1D, E.P. 0.4 volts. One rather strong line, λ 4331.65 (52), has the lower term b^1D, E.P. 1.7 volts. The measured wave length of this line is persistently greater than the laboratory value by 0.1 A. This discrepancy is probably an example of the tendency of high-excitation lines to have positive displacements, although, of course, it is possible that this line is blended or even wrongly identified.

One or two strong ultimate lines are probably present in low intensity. In this respect the behavior is intermediate between that of *Co* I and that of *Fe* I. In *Co* I ultimate lines have not been observed; in *Fe* I, at the later phases, they become outstanding. Ultimate lines of *Ni* I and possibly even those of *Co* I might be strong at phases later than those observed.

Lines of Si I.—The line λ 3905 appears to consist of two components only partially separated, the one of shorter wave length being the stronger. Table 9 gives two values for this line, the upper one corresponding to the stronger component, the lower to the effective center of the whole line. For some unknown reason, the line λ 4103 has a consistent positive displacement of about 10 km/sec with respect to the velocity yielded by most other elements.

Lines of Mn I.—As in R Andromedae, the strong components of lines of the triplet near λ 4030 have a persistent negative displacement of nearly 18 km/sec with respect to the bright lines of most other elements. At the later phases a weaker component appears about 0.4 A (30 km/sec) longward. It is hoped in a future *Contribution* to make a detailed report on the behavior of these *Mn* I lines in several variables.

Lines of Zr I.—The possibility that several emission lines of *Fe* I in Me spectra are excited by the strong ultraviolet line of *Mg* II, λ 2795.52, was noted by A. D. Thackeray[6] and P. W. Merrill[5] about ten years ago. A recent investigation by I. S. Bowen[8] shows that four lines in the postmaximum spectrum of χ Cygni (Table 13) are *Zr* I lines from the upper level, x^1G_4, probably excited by the same line of *Mg* II (see Table 12).

Line of In I.—As in several other variables, the line λ 4511 has a considerable positive residual with respect to bright lines of other elements. The accompanying tabulation, which gives the apparent difference in velocity, λ 4511 minus *H*, for four stars, suggests that the presence of strong *TiO* band absorption may cause the wave length of bright λ 4511 to be measured about 0.08 A too large.

Star	*TiO*	λ 4511 − *H*
R Hya	Yes	+5.5 km/sec
R Leo	Yes	+5.8
χ Cyg	Yes	+4.8
R And	No	−1.1

[8] *Pub. A.S.P.*, **59**, 196, 1947.

Lines of Fe II.—Numerous bright lines of *Fe* II are measurable on all the spectrograms. Most of them grow stronger with advancing phase until about +120 days, after which they tend to weaken. As in R Andromedae, multiplet (1) in the extreme ultraviolet is remarkably intense. The relative intensities of the lines are about the same as in R Andromedae,[9] except that λ 3255 is stronger, although it is still somewhat less intense than λ 3281, whereas in the laboratory it is slightly stronger. The radial velocities derived from several multiplets (Table 8) seem not to vary with phase or with excitation potential.

Forbidden lines begin to appear about 100 days after maximum and strengthen rapidly during the next 2 months. Their velocities agree with those from the permitted lines.

Lines of Ti II.—A number of lines of *Ti* II persist in low intensity during most of the observed portion of the light-cycle, the phase of greatest intensity being perhaps +120 days, with a noticeable weakening by +160 days.

TABLE 8

RADIAL VELOCITIES FROM EMISSION LINES OF *Fe* II

Multiplet	Upper Term		Phase (Days)					
	Desig.	E.P. (Volts)	+43	+69	+102	+126	+162	+100 (Mean)
1	z^6D	4.8	−15.2 5*	.....	−20.3 3*	.....	−15.1 7*	−16.2
3	z^6D	4.8	−11.4 1	−10.9 1*	−11.1 1	−12.6 1*	−12.3 1	−11.7
6	z^4D	5.5	.....	.....	.....	.....	−17.2 1	−17.2
27	z^4D	5.5	−15.3 3	−15.2 2	−13.3 4	−14.4 4	−14.6 5	−14.4
28	z^4F	5.6	(− 7.5) 1	(− 7.8) 1	− 9.4 1	−13.7 3	− 7.8 3	− 9.9
37	z^4F	5.5	.....	.....	.....	−11.8 2	−10.7 1	−11.4
38	z^4D	5.5	−13.1 1	.....	−13.8 2	−15.1 3	.....	−14.3
42	z^6P	5.3	−15.2 1	−16.2 1	−15.1 1	−16.9 1	.....	−15.8
Weighted mean	.....	.....	−14.7	−14.4	−15.3	−14.2	−14.6	−14.6

* Number of lines.

General.—The velocities yielded by the bright lines of several elements are compared in Table 9. As in R Andromedae, the displacements of *H*, *Fe* II, *Ti* II, and *Mg* I in multiplet (3) agree with each other and vary little with phase. Moreover, *Mg* I λ 4571 and the lines of *Fe* I, which at first appear as bright fringes on the shortward sides of dark lines and thus have negative residuals, tend as the cycle advances to assume the standard velocity.

Displacements of bright lines of various elements (e.g., *H* and *Fe* II) exhibit smaller differences in R Andromedae and χ Cygni than they do in Me variables; and variations with phase also are smaller. At the same time the light-ranges of R Andromedae and χ Cygni are relatively large. It thus appears doubtful that the complex behavior of the bright lines will find a simple explanation in terms of volume pulsation.

Displaced lines.—The general over-all displacement of the bright lines shortward with respect to the absorption spectrum has been observed and discussed for many years. Not so well known are the additional shortward displacements exhibited by bright lines which develop usually at the later phases in certain very strong lines of *Ca* II, *Al* I, *Cr* I, *Fe* I, and one or two other elements. These lines are slightly wide and often appear

[9] P. W. Merrill, *Mt. W. Contr.*, No. 730; *Ap. J.*, **105**, 360, Table 9, 1947.

slightly unsymmetrical, being more sharply bounded on the longward side. Their displacements, greatest for the lines which are strongest in absorption, tend to decrease with phase.

The displaced lines of *Ca* II, previously observed in the spectra of several long-period variables, become especially intense in χ Cygni. The anomalous reversal of the normal intensities of H and K is marked (Table 10). As in other variables, the intensities increase and the negative displacements decrease with advancing phase.

The strong *Al* I lines, λ 3944 and λ 3961 between H and K, also exhibit displaced emission (Table 10), although the intensities are much less and are more nearly the same in both lines than in the *Ca* II pair.

TABLE 9

RADIAL VELOCITIES FROM EMISSION LINES

(Km/Sec)

Element	Line or Multiplet	Phase (Days)					
		+43	+69	+102	+126	+162	+100 Mean
H	Many	−15.0	−15.6	−13.5	−14.5	−13.6	−14.4
Fe I	Table 5	−20.1	−17.9	−15.8	−15.6	−15.2	−16.9
Mg I	λ 4571	−21.8	−16.2	−15.7	−16.1	.....	.....
Mg I	(3)	−17.0	−17.6	−16.7	−17.8	−16.2	−17.1
Si I	λ 3905	−20.1	−21.1	−22.2	−22.1	.....	−21.4
		−13.4	−13.4	−12.2	−12.1	−10.9	−12.4
Si I	λ 4103	− 6.5	− 6.1	− 7.0	− 5.7	− 5.0	− 6.0
Mn I	(2)	−34.	−39.	−33.	−32.	−29.	−33.
In I	λ 4511	−11.7	−10.0	− 8.8	− 9.1	.....	− 9.9
Fe II	Table 6	−14.7	−14.4	−15.3	−14.2	−14.6	−14.6
[*Fe* II]	Several*	.....	.....	−14.8	−14.4	−13.5	−14.0
Ti II	(13)	−15.2	−13.8	−12.9	−14.3	−14.7	−14.2
Abs. lines	.....	− 2.3	− 3.0	− 3.6	− 6.5	− 5.7	− 4.2

* At the three epochs the numbers of lines measured were 3, 9, and 14, respectively.

TABLE 10

DISPLACEMENTS OF BROAD EMISSION LINES

(Corrected for Absorption-Line Velocities, Table 2)

Phase (Days)	Ca II				Al I			
	λ 3933		λ 3968		λ 3944		λ 3961	
	Int.	Displ. (Km/Sec)	Int.	Displ (Km/Sec)	Int.	Displ. (Km/Sec)	Int.	Displ. (Km/Sec)
+ 43	.....	.....	1	−100	tr	−64	tr	−72
+ 69	.....	.....	1	− 96	tr	.....	tr	.....
+102	3	−102	6	− 82	1	−58	1	−59
+126	4	− 94	7	− 67	1	−42	1	−45
+162	5	− 67	9	− 53	1	−29	1	−29

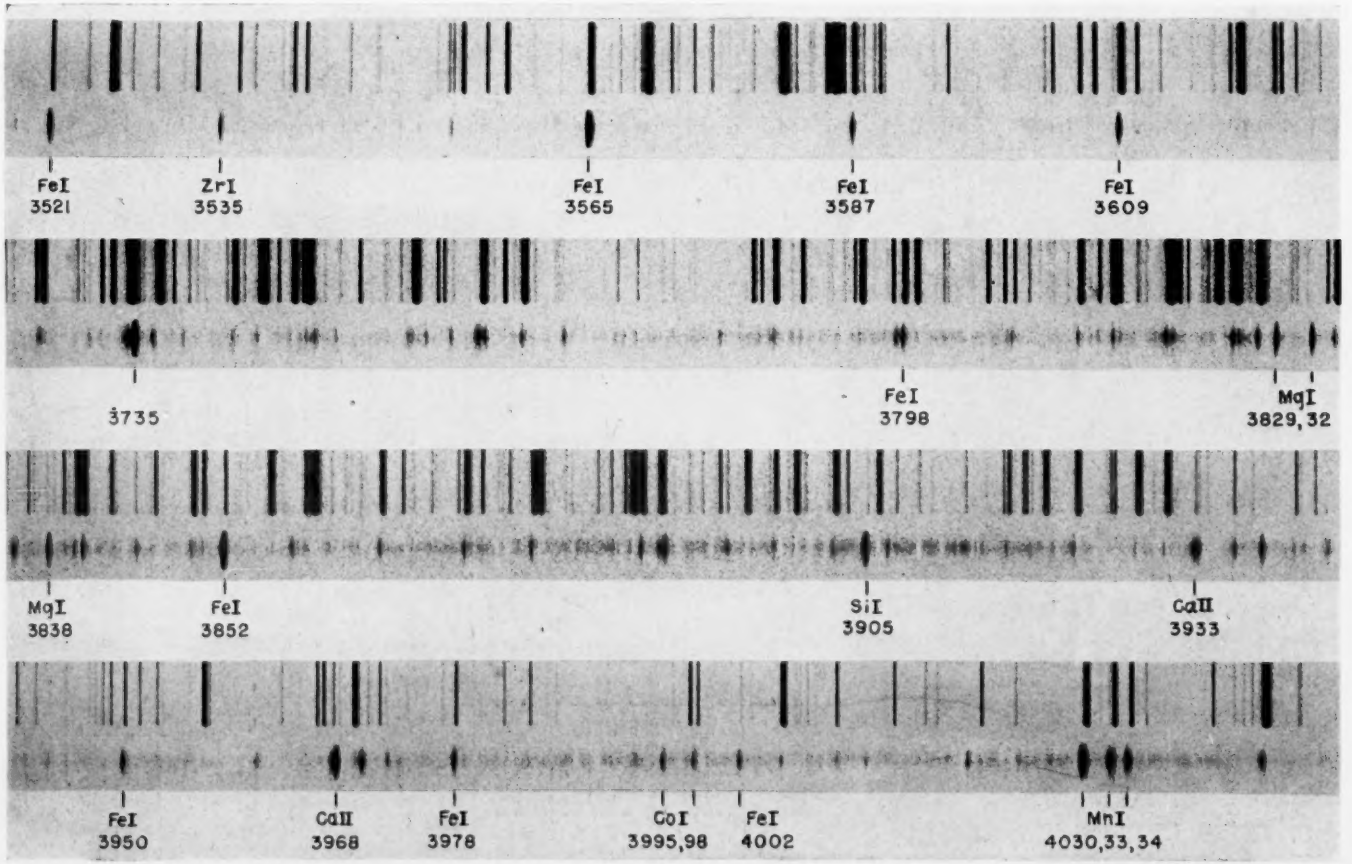

FIG. 2.—Ultraviolet spectrum of χ Cygni, 162 days after maximum light. Plate Ce 3505, 1944, July 10–11

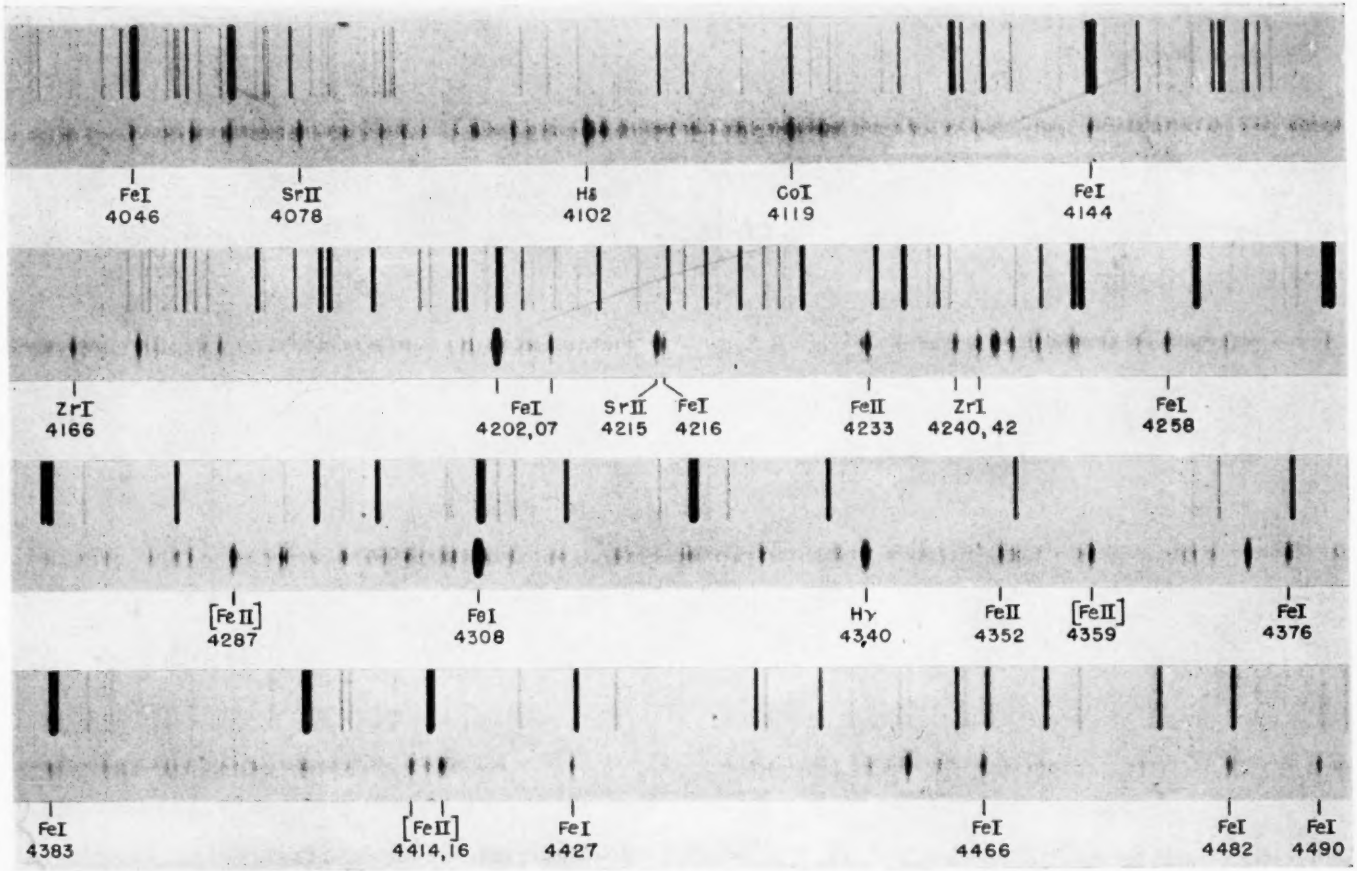

FIG. 3.—Spectrum of χ Cygni λλ 4050–4500, 162 days after maximum light. Plate Ce 3505, 1944, July 10–11

The *Sr* II lines, λ 4077 and λ 4215, also exhibit shortward displacements which decrease with advancing phase. The line λ 4215 is the stronger of the two (although weaker in the laboratory) and has somewhat smaller shortward displacements. The behavior thus has a resemblance to that of the analogous *Ca* II lines, λ 3933 and λ 3968.

An ingenious method of determining the probable structure of the strong unobserved lines λ 2795 and λ 2802 of *Mg* II, suggested by Ira S. Bowen, is outlined in Table 11,

TABLE 11

FLUORESCENT EXCITATION BY ULTRAVIOLET LINES OF *Mg* II

EXCITING LINE	OTHER CLOSE LINES		
	Element	Δλ	Observed Fluorescence
Mg II 2795.52	*Co* I	+0.71 A	No
	Co I	+0.30	No
	Fe I	+0.02	No
	Zr I	−0.39	Yes
	Fe I	−0.52	Yes
	Fe I	−0.83	Yes
Mg II 2802.70	*Fe* I	+0.47	No
	Ti I	−0.23	Yes?

TABLE 12

ATOMIC LEVELS YIELDING ABNORMALLY INTENSE EMISSION LINES

Element	Observed Lines	Upper Level	Line from Low Term	Exciting Line
Fe I	Table 5	z^3G_4	2795.01	*Mg* II 2795.53
Fe I	Table 6	z^5G_2		
Fe I	3852.57	w^5D_4	2794.70	*Mg* II 2795.53
Zr I*	3535.16, 4166.51, 4240.44, 4242.61	x^1G_4	2795.14	*Mg* II 2795.53
In I	4511.31	$6^2S_{1/2}$	4101.76	*Hδ* 4101.74
Sc I	3907.48	$y^2P_{2\frac{1}{2}}$	3933.38	*Ca* II 3933.66
Ti I	4372.38, 4400.60	v^1P_1	2802.47	*Mg* II 2802.70
Ga I	4172.05	$5^2S_{1/2}$	4032.98	*Mn* I 4033.07

* I. S. Bowen, *Pub. A.S.P.*, **59**, 196, 1947.

which lists lines of other elements lying near the *Mg* II lines. It appears that only those lines of somewhat shorter wave lengths than the *Mg* II lines produce fluorescent effects. This result suggests that the emission portions of the *Mg* II lines are displaced shortward as in the H and K lines of *Ca* II.

Atomic levels that yield abnormally intense emission lines, together with the probable exciting lines, are collected in Table 12. The identification of the observed lines ascribed to *Sc* I, *Ti* I, and *Ga* I is not considered wholly certain.

The bright lines measured on Plate Ce 3505, phase +162 days, magnitude 11.4, are listed in Table 13. The measured wave lengths have been corrected for a velocity (reduced to the sun) of −14.4 km/sec. Figures 2 and 3 show how strong many of these lines

TABLE 13

BRIGHT LINES MEASURED AT PHASE +162 DAYS (PLATE Ce 3505)

I.A.	Int.	Change with Phase*	Ident.		I.A.	Int.	Change with Phase*	Ident.	
3227.70	tr	.....	.73 *Fe* II	(6)	3761.32	1	+110	.32 *Ti* II	(13)
55.90	3	.....	.88 *Fe* II	(1)	63.44	1	.....	.....	
77.34	8	.....	.35 *Fe* II	(1)	63.78	1	.....	.79 *Fe* I	(21)
81.29	4	.....	.29 *Fe* II	(1)	64.14	1.5	.....	.21 *Fe* I	(74)?
95.80	2	.....	.81 *Fe* II	(1)	67.18	1	.....	.19 *Fe* I	(21)
3302.81	1	.....	.86 *Fe* II	(1)	70.4	1.5	Dec.	.63 *H* 11	
03.46	1	.....	.47 *Fe* II	(1)	74.86	tr	+120	.82 *Fe* I	(73)
13.99	tr	.....	.00 *Fe* II	(1)	75.57	tr	+130	.57 *Ni* I	(33)
71.9	tr	.....	.99 *Ni* I	(7)	76.51	tr	+110	.45 *Fe* I	(74)
3439.0	tr	.....	.98 *Mn* II	(1)	79.62	0.5	Dec.	.49 *Fe* I	(74)
44.33	tr	.....	.31 *Ti* II	(6)	83.47	1	.....	.53 *Ni* I	(30)
60.1	tr	.....	.04 *Mn* II	(1)	86.6	tr	Dec.	.68 *Fe* I	(22)
61.5	tr	.....	.50 *Ti* II	(6)	87.53	tr	Dec.	.....	
66.53	0.5	Inc.	.51 *Fe* I	(24)	87.87	0.5	Inc.?	.88 *Fe* I	(21)
77.2	tr	.....	.18 *Ti* II	(6)	89.36	tr n	.....	.....	
3518.4	0.5	Inc.?	.34 *Co* I	(36)?	90.14	tr	.....	.10 *Fe* I	(22)
21.25	8	Inc.!	.26 *Fe* I	(24)	90.96	tr	.....	.....	
30.9	tr	Dec.	.....		94.92	tr	.....	.00 *Fe* I	(21)
35.22	4	Inc.	.16 *Zr* I	(59)	97.98	1 n	Dec.	.90 *H* 10	
45.3	tr	Dec.	.19 *V* II	(5)	98.53	2	Inc.	.51 *Fe* I	(21)
49.95	0.5	Dec.	.87 *Fe* I	(48)	99.65	0.5 n	.....	.55 *Fe* I	(21)
51.54	tr	.....	.53 *Ni* I	(5)?	3807.08	tr	.....	.14 *Ni* I	(33)
54.14	1	.....	.12 *Fe* I	(23)	07.50	0.5	Dec.	.53 *Fe* I	(73)
65.41	14	Inc.!	.38 *Fe* I	(24)	12.98	1	.....	.96 *Fe* I	(22)
81.2	tr	.....	.19 *Fe* I	(23)	13.99	tr	Dec.	.....	
86.98	4	Inc.	.98 *Fe* I	(23)	14.61	0.5	.....	.58 *Ti* II	(12)
3608.85	5	Inc.	.86 *Fe* I	(23)	15.86	1	Inc.	.84 *Fe* I	(45)
18.6	tr	.....	.76 *Fe* I	(23)?	16.44	tr	+110	.34 *Fe* I	(73)?
19.3	0.5	.....	.39 *Ni* I	(35)	20.33	1	Inc.	.43 *Fe* I	(20)
24.7	tr	.....	.73 *Ni* I	(2)	20.79	0.5	+130	.....	
79.6	tr	.....	.92 *Fe* I	(5)	25.76	1.5	Inc.	.88 *Fe* I	(20)
85.21	tr	.....	.19 *Ti* II	(14)	26.25	0.5	+130	.....	
3705.4	tr	.....	.57 *Fe* I	(5)	27.83	1.5	Inc.	.82 *Fe* I	(45)
09.1	tr n	Dec.	.25 *Fe* I	(21)	29.33	4	.....	.35 *Mg* I	(3)
11.3	tr	.....	.30 *Fe* I	(75)?	32.27	4	.....	.30 *Mg* I	(3)
11.99	tr	Dec.	.97 *H* 15		34.16	1	Inc	.22 *Fe* I	(20)
19.52	3 n	Inc.	.94 *Fe* I	(5)	35.42	1.5 n	Dec	.39 *Hη*	
21.33	tr	Dec.	.28 *Fe* I	(75)	38.27	5	.....	.29 *Mg* I	(3)
21.93	tr	Dec.	.94 *H* 14		40.39	0.5	Inc.	.43 *Fe* I	(20)
27.43	2 n	.....	.62 *Fe* I	(21)	41.08	2	Inc.	.05 *Fe* I	(45)
31.62	1 n	.....	.03 *Cr* I	(2)?	45.52	1	.....	.47 *Co* I	(34)
34.44	0.5 n	.....	.37 *H* 13		49.95	0.5	.....	.97 *Fe* I	(20)
34.76	2	.....	.87 *Fe* I	(21)	50.78	tr	.....	.82 *Fe* I	(22)
35.31	10	Inc.!	.....		52.66	10	.....	.57 *Fe* I	(73)
36.84	2 n	Inc.	.13 *Fe* I	(5)	58.28	1	Inc.?	.30 *Ni* I	(32)
39.21	1	Inc.	.22 *Ni* I	(2)?	61.23	tr n	+130	.16 *Co* I	(33)
41.6	tr	.....	.63 *Ti* II	(72)	65.52	1	.....	.52 *Fe* I	(20)
43.33	0.5	.....	.36 *Fe* I	(21)	72.49	1	.....	.50 *Fe* I	(20)
45.34	0.5 n	.....	.56 *Fe* I	(5)	78.02	1.5	.....	.02 *Fe* I	(20)
48.07	0.5	.....	.26 *Fe* I	(5)	78.41	tr	.....	.57 *Fe* I	(4)?
48.89	0.5	Dec.	.04 *Ni* I	(1)?	84.70	tr n	+120	.60 *Co* I	(32)
49.38	1	.....	.49 *Fe* I	(21)	86.11	tr	Inc.?	.28 *Fe* I	(4)
50.03	1 n	Dec.	.15 *H* 12		87.08	1.5	Inc.	.05 *Fe* I	(20)
51.79	0.5	.....	.....		88.54	1	.....	.52 *Fe* I	(45)
57.98	1	.....	.24 *Fe* I	(21)	89.02	2 n	Dec.	.05 *Hζ*	
3759.29	1	+110	.29 *Ti* II	(13)	3894.14	0.5	Dec.	.07 *Co* I	(34)

* Inc., increasing intensity; Inc.!, marked increase from phase +126 days to +162 days; Dec., decreasing intensity. For lines which appear to have a maximum intensity between phases +43 days and +162 days, the approximate phase of maximum is indicated.

TABLE 13—*Continued*

I.A.	Int.	Change with Phase*	Ident.	I.A.	Int.	Change with Phase*	Ident.
3898.01	0.5	.....	.01 *Fe* I (20)	4132.0	tr	Dec.	.06 *Fe* I (43)
3903.00	0.5	.....	.95 *Fe* I (45)	34.29	0.5	Inc.	.34 *Fe* I (3)
05.58	6	.....	.53 *Si* I (3)	43.88	2	Inc.	.87 *Fe* I (43)
07.41	0.5	.....	.48 *Sc* I (8)?	56.8	tr n	Dec.	.....
12.97	tr	.....	.97 *Ni* I (15)	64.68	tr	Dec.	.64 *Ni* I (28)
14.53	tr	+130	.48 *Fe* II (3)?	66.58	3	+150	.51 *Zr* I
17.21	0.5	.....	.18 *Fe* I (20)	67.53	tr	+120	.....
22.75	1	Inc.?	.91 *Fe* I (4)	72.05	5	Inc.!	.05 *Ga* I (1)?
27.81	0.5	.....	.92 *Fe* I (4)	72.76	0.5	Inc.?	.75 *Fe* I (19)
30.17	0.5	.....	.30 *Fe* I (4)	73.48	1	+120	.45 *Fe* II (27)
32.90	4 n	Inc.	.66 *Ca* II (1)	77.65	0.5	.....	.....
36.02	1 n	+130	.96 *Co* I (32)	78.89	2	+130	.86 *Fe* II (28)
38.32	3	+110	.29 *Fe* II (3)	99.95	1	Inc.	.97 *Fe* I (3)
40.94	0.5	.....	.88 *Fe* I (20)	4202.07	20	Inc.	.03 *Fe* I (42)
41.7	0.5 n	.....	.73 *Co* I (17)	04.2	0.5	+110	.....
43.74	1 n	.....	.01 *Al* I (1)	06.63	3	Inc.	.70 *Fe* I (3)
45.27	0.5	+130	.21 *Fe* II (3)?	15.51	5	Inc.	.52 *Sr* II (1)
50.03	3	.....	.95 *Fe* I (72)	16.05	2	Inc.	.18 *Fe* I (3)
61.25	1 n	.....	.52 *Al* I (1)	32.67	1	Inc.	.72 *Fe* I (3)
67.89	8 n	Inc.	.47 *Ca* II (1)	33.15	4	.....	.17 *Fe* II (27)
70.06	2 n	Dec.	.07 *He*	40.48	2	+140	.44 *Zr* I
72.21	1 n	Inc.	.17 *Ni* I (29)	42.49	2	Inc.!	.61 *Zr* I, —
77.81	3	.....	.74 *Fe* I (72)	43.68	3	Inc.!	.....
78.7	tr	.....	.65 *Co* I (17)	44.00	3	Inc.	.98 *Fe* II (21F)
93.0	0.5 n	.....	.....	45.26	3	Inc.!	.....
95.35	2	.....	.31 *Co* I (31)	46.83	tr	.....	.83 *Sc* II (7)
97.97	2	+120	.90 *Co* I (32)	47.45	2	Inc.!	.....
4001.75	2	+110	.67 *Fe* I (72)	50.31	1	Inc.!	.....
05.28	1	Inc.	.25 *Fe* I (43)	50.73	0.5	.....	.79 *Fe* I (42)
09.94	0.5	+110	.71 *Fe* I (72)?	53.9	tr n	.....	.35 *Cr* I (1)
12.38	0.5	+120	.37 *Ti* II (11)	55.88	0.5	Inc.?	.....
20.92	1	.....	.90 *Co* I (16)	58.28	3	Inc.	.32 *Fe* I (3)
25.09	tr	+120	.14 *Ti* II (11)	63.20	1	Inc.	.....
30.52	6	+130	.76 *Mn* I (2)	71.76	1	Inc.	.76 *Fe* I (42)
30.91	3	Inc.!		74.6	0.5	Inc.?	.80 *Cr* I (1)
				76.85	1	Inc.!	.83 *Fe* II (21F)
32.88	3	Inc.	.07 *Mn* I (2)	80.47	1.5	Inc.!	.....
33.26	2	Inc.!		82.65	2 n	Inc.	.41 *Fe* I (71) bl?
				83.83	2	Inc.!	.....
34.29	3	+160	.49 *Mn* I (2)	87.41	5	Inc.!	.40 *Fe* II (7F)
34.59	2	Inc.!		90.27	tr	.....	.22 *Ti* II (41)
45.68	2 n	.....	.80 *Fe* I (43)	91.44	3	Inc.	.47 *Fe* I (3)
63.59	1.5	.....	.60 *Fe* I (43)	91.85	2	Inc.!	.....
66.42	0.5	.....	.36 *Co* I (36)	94.2	0.5 n	.....	.13 *Fe* I (41)
68.60	2	.....	.62 *S* II (1F)?	96.69	2 n	Inc.	.57 *Fe* II (28)?
71.26	0.5	Inc.	.....	4300.10	0.5	.....	.05 *Ti* II (41)
71.75	2	.....	.74 *Fe* I (43)	02.01	1 n	+130	.93 *Ti* II (41)
77.68	2	Inc.	.71 *Sr* II (1)	03.16	0.5	+130	.17 *Fe* II (27)
81.46	0.5	Inc.!	.....	05.89	1.5	Inc.	.90 *Fe* II (21F)
84.49	1	Inc.!	.....	07.92	30	Inc.	.91 *Fe* I (42)
86.34	1	+120	.30 *Co* I (58)	09.7	tr	+130	.62 *Y* II (5)
88.01	1	Inc.!	.....	14.23	tr n	.....	.....
90.7	0.5 n	Inc.?	.....	15.07	0.5 n	Inc.?	.98 *Ti* II (41)
92.30	2 n	Inc.?	.39 *Co* I (29)	19.61	1 n	Inc.!	.62 *Fe* II (21F)
95.54	2	Inc.	.....	20.6	tr n	Inc.?	.....
4101.7	6 n	Dec.	.74 *Hδ*	25.09	0.5	Dec.	.....
03.06	2 n	Dec.	.93 *Si* I (2)	25.68	0.5	+150	.76 *Fe* I (42)
08.84	0.5	Inc.	.....	31.77	2	Inc.	.....
18.81	3	+140	.77 *Co* I (28)	38.14	0.5 n	Inc.	.....
19.53	tr	Dec.	.....	40.44	8 n	Dec.	.47 *Hγ*
4121.36	1	+140	.32 *Co* I (28)	4347.0	tr n	.....	See note

TABLE 13—*Continued*

I.A.	Int.	Change with Phase*	Ident.	I.A.	Int.	Change with Phase*	Ident.
4351.78	2	.....	.76 *Fe* II (27)	4442.4	tr	+120?	.34 *Fe* I (68)
52.78	0.8	Inc.	.78 *Fe* II (21F)	43.9	0.5	+120	.80 *Ti* II (19)?
53.25	0.5	Inc.	.....	52.13	1 n	Inc.	.11 *Fe* II (7F)
54.97	tr	Inc.	.....	55.34	4	Inc.!	.....
56.60	tr	Inc.?	.....	57.94	1 n	Inc.!	.95 *Fe* II (6F)
58.43	0.8	Inc.	.37 *Fe* II (21F)	61.60	3	Inc.	.65 *Fe* I (2)
59.35	3	Inc.!	.34 *Fe* II (7F)	66.58	tr	Inc.?	.57 *Fe* I (2)
67.13	0.5	Inc.!	.....	74.89	tr	Inc.	.91 *Fe* II (7F)
67.99	1	+120	.90 *Fe* I (41)	82.09	2	Inc.!	.17 *Fe* I (2)
69.53	1	Inc.!	.....	89.65	2	Inc.	.74 *Fe* I (2)
72.50	6	+140	.38 *Ti* I (277)?	94.56	tr	Inc.?	.57 *Fe* I (68)
75.88	3	+140	.93 *Fe* I (2)	4501.26	0.5	+120?	.27 *Ti* II (31)
79.81	1	Inc.	.....				
83.52	2 n	+120	.54 *Fe* I (41)				
84.40	0.5 n	Inc.	.....				
85.36	tr	.....	.38 *Fe* II (27)				
88.15	1 n	Inc.!	.....				
89.23	tr	Inc.?	.24 *Fe* I (2)				
93.35	0.8	Inc.!	.....				
94.07	tr	+120	.12 *Fe* I (41)				
95.04	0.5	+120	.03 *Ti* II (19)				
98.02	tr	.....	.02 *Y* II (5)				
99.02	0.5	Inc.?	.....				
4400.64	1	Inc.	.....				
04.81	1 n	+120	.75 *Fe* I (41)				
08.5	tr	.....	.42 *Fe* I (68)?				
13.81	2.5 n	Inc.!	.78 *Fe* II (7F)				
15.16	1.5 n	+120	.12 *Fe* I (41)				
16.32	3.5	Inc.!	.27 *Fe* II (6F)				
27.25	3	Inc.	.31 *Fe* I (2)				
4435.0	tr	+120?	.15 *Fe* I (2)?				

Phase +126 Days (Ce 3443)

I.A.	Int.	Change with Phase*	Ident.
4511.39	2	Dec.	.31 *In* I (1)
18.72	1	.....	.....
20.20	1	.....	.22 *Fe* II (37)
22.64	0.5	.....	.63 *Fe* II (38)
28.63	2 n	.....	.61 *Fe* I (68)
31.20	0.5	.....	.15 *Fe* I (39)
34.05	1 n	.....	See note
49.48	2	.....	.47 *Fe* II (38)
55.97	1 n	.....	.89 *Fe* II (37)
71.08	15	Inc.	.10 *Mg* I (1)
83.79	2	.....	.83 *Fe* II (38)
4861.18	10 n	.....	.33 *Hβ*
4923.89	2	.....	.92 *Fe* II (42)

NOTES TO TABLE 13

λ 3565.41 The line appears to consist of two components, one at λ 3565.34, intensity 10; another at λ 3565.60, intensity 3. The longward component developed rapidly after phase +100 days.

λ 3757.98 The line appears to consist of two components, one at λ 3757.84, intensity 1; the other at λ 3758.19, intensity 0.5.

λ 3852.66 At earlier phases a faint companion lies 0.4 A shortward.

λ 3905.58 At earlier phases components were measured at λ 3905.43 and λ 3905.71. The intensity on the longward component gradually increased from 0.4 to about 1.4 times the intensity of the other.

λ 3945.27 Possibly blended with λ 3945.33 *Co* I (29).

λ 4045.68 At earlier phases this line may have a component (possibly a companion line of another element) about 0.3 A shortward.

λ 4092.30 Possibly double, with components of nearly equal intensity at λ 4092.12 and λ 4092.44.

λ 4215.51 Unsymmetrical; main component at λ 4215.43, with a fringe or faint component at λ 4215.62.

λ 4247.45 The remarkable preminimum bright line previously observed with low dispersion (P. W. Merrill, *Mt. W. Contr.*, No. 539; *Ap. J.*, **83**, 272, 1936) at λ 4245 is here resolved into several lines from λ 4242.49 to λ 4247.45. The line λ 4242.49 is probably a blend of λ 4242.61 *Zr* I with an unidentified line, whose wave length might be λ 4242.4.

λ 4315.07 Possibly blend with λ 4315.09 *Fe* I (71).

λ 4325.68 Possibly blend with λ 4325.74 *Fe* I (2).

λ 4347.0 Possibly blend of λ 4346.85 *Fe* II (21F) with λ 4347.24 *Fe* I (2).

λ 4352.78 Possibly blend with λ 4352.74 *Fe* I (71).

λ 4375.88 At the earlier phases the wave length was shorter by about 0.1 A. The increasing relative intensity of emission with respect to absorption on the longward side may account for the slight increase in wave length.

λ 4511.39 This line and the following ones were measured at phase +126 days, Plate Ce 3443. Wave lengths greater than λ 4510 are not on Plate Ce 3505.

λ 4534.05 Possibly a blend of λ 4533.97 *Ti* II (50) and λ 4534.17 *Fe* II (37).

are, in comparison with the underexposed background of continuous spectrum. Unidentified bright lines from Table 13 and a few measured only at earlier phases are collected in Table 14; the wave lengths, derived from all available measures, may differ slightly from those in Table 13.

In Tables 13 and 14 an attempt has been made to give an idea of the behavior of each line as the cycle advances. The indicated phase of maximum observed intensity is, of course, only approximate but should be helpful in checking possible identifications. The lines may be grouped according to the time of maximum intensity as follows:

I. Lines whose intensities decrease steadily after maximum light. The phase of greatest intensity in the present series of spectrograms is +40 days. Two of the strongest unidentified lines are λ 4138.53 and λ 4521.72.

TABLE 14

SURVEY OF UNIDENTIFIED BRIGHT LINES

I.A.	Max. Obs. Int.		I.A.	Max. Obs. Int.		I.A.	Max. Obs. Int.	
	Int.	Phase* (Days)		Int.	Phase* (Days)		Int.	Phase* (Days)
3421.2	tr	+(80)	3952.86	1	+ 40	4283.83	2	+ 160!
3531.0	0.5	+(60)	92.96	0.5	+ 150	91.85	2	+ 160!
3724.4	0.5	+ 90	4081.46	0.5	+ 160!	92.45	1	+ 70
26.9	0.5	+ 70	84.49	1	+ 160!	4325.11	1	+ 70
35.34	10	+ 160!	88.01	1	+ 160!	31.75	2	+ 160
42.31	0.5	+ 40	95.52	2	+ 140	38.14	0.5 n	+ 160
51.81	0.5	+ 140	98.95	1	+ 50	53.25	0.5	+ 160
63.3–63.4	2	+ 110	4119.46	1	+ 40	67.13	0.5	+ 160!
85.99	0.5	+ 40	34.88	0.5	+ 110	69.53	1	+ 160!
87.54	1	+ 40	38.53	2	+ 40	72.52 *Ti* I?	6	+ 140
94.52	1	+ 40	56.86	1	+ 70	79.81	1	+ 160
3814.01	2	+ 100	72.05 *Ga* I?	5	+ 160!	84.40	0.5 n	+ 160
20.8	1	+ 130	4243.68	3	+ 160!	88.15	1 n	+ 160!
22.87	0.5	+ 40	45.25	3	+ 160!	93.35	0.8	+ 160!
26.3	1	+ 130	47.45	2	+ 160!	4400.6	1	+ 160
44.92	1	+ 40	50.31	1	+ 160!	55.34	4	+ 160!
3907.44 *Sc* I?	1	+ 120	55.90	0.5	+ 160	4518.72	1	+(160)
13.6–13.7	1	+ 100	63.19	1	+ 160	21.72	3	+ 40
52.2	1	+ 40	80.47	1.5	+ 160!			

* An exclamation mark (160!) indicates that the line was much stronger than at earlier phases.

II. Lines which have their greatest intensities at intermediate phases. Lines of *Co* I, *Fe* II, *Ti* II, *V* II, and high excitation lines of *Fe* I fall in this group; other lines of *Fe* I appear to be intermediate between groups II and III.

III. Lines which grow stronger rapidly after phase +130 days. These are marked "Inc.!" in Table 13 or "+160!" in Table 14. Most of the identified lines are due to [*Fe* II]. Whether most of the unidentified lines of type III also are forbidden remains to be determined.

The numerous unidentified lines constitute an engaging problem. The same lines probably occur in many or all typical variables of classes Me and Se, although they appear to be especially strong in χ Cygni. Further data concerning these lines (and possibly additional lines) can eventually be obtained from suitable spectrograms taken closer to minimum light.

I am indebted to Ira S. Bowen for helpful discussions of the identification and behavior of the bright lines.

THE ABSORPTION LINES WITHIN THE HYDROGEN EMISSION OF MIRA CETI*

ALFRED H. JOY
Mount Wilson Observatory
Received June 14, 1947

ABSTRACT

On spectrograms taken with the high dispersion of the coudé spectrograph, most of the absorption minima within the emission lines of Mira Ceti may be identified with metallic lines of the reversing layer of the star. Sixty-five lines were thus assigned to thirteen elements, and four other lines in $H\gamma$ were attributed to *TiO*. The measurements seem to furnish sufficient proof that the hydrogen producing the emission lines is at a lower level than the source of the numerous metallic absorption lines of the star's atmosphere.

In 1899, W. W. Campbell[1] reported that the bright hydrogen lines $H\gamma$ and $H\delta$ in the three-prism spectra of *o* Ceti were not single lines but were made up of three components. W. H. Wright[2] found but two components of $H\gamma$ at the following maximum, but in 1909 the three components were again seen. Three components of both lines were recorded[3] in 1925 on Mount Wilson spectrograms taken with the three-prism spectrograph. On coudé spectrograms of high dispersion, taken before or shortly after maximum light, similar abnormalities have been seen in each of the hydrogen lines observed in Mira Ceti and other long-period Me variables. The broad emission lines seem to be broken up into several components by absorption lines having different widths and intensities. The appearance of some of the lines is well shown by reproductions of coudé spectrograms[4] and by the microphotometer curves of Figures 1 and 2. An obvious and perhaps sufficient explanation of the peculiar structure of the hydrogen lines is that they originate at a comparatively low level in the star's atmosphere and are so greatly widened that the overlying atoms of other elements of the reversing layer absorb narrow portions of the outgoing radiation in the characteristic lines of those elements. The apparent components of the bright lines are then the remaining wave lengths of emission not affected by such absorption lines as happen to occur at positions intermediate between the extremities of the hydrogen radiation. This explanation was, in principle, advanced many years ago by Miss A. Clerke[5] to account for the weakness and disappearance of $H\epsilon$ in the spectrum of *o* Ceti at certain phases and was later applied by C. D. Shane[6] to the weakened ultraviolet hydrogen lines $H\zeta$, $H\kappa$, $H\lambda$, $H\mu$, and $H\xi$. P. W. Merrill[7] strongly supports this theory as a general explanation of the mutilation of the emission lines in long-period variables. He was able to identify some of the absorption minima within $H\zeta$, $H\eta$, $H\theta$, and $H\iota$ with lines which might be expected in the reversing layer; he also suggested that

* *Contributions from the Mount Wilson Observatory, Carnegie Institution of Washington*, No. 737.

[1] *Ap. J.*, **9**, 31, 1899.

[2] *Lick Obs. Bull.*, **6**, 60, 1910.

[3] A. H. Joy, *Mt. W. Contr.*, No. 311; *Ap. J.*, **63**, 303, 1926.

[4] P. W. Merrill, *Spectra of Long-Period Variable Stars* (Chicago: University of Chicago Press, 1940), opp. p. 57 (*H* 11, U Ori; $H\delta$ and $H\gamma$, *o* Cet); *Mt. W. Contr.*, No. 713; *Ap. J.*, **102**, opp. p. 349, 1945 ($H\gamma$ and $H\delta$, U Ori); *Pub. A.S.P.*, **57**, opp. p. 179, 1945 (*H* 10 and *H* 11, *o* Cet); W. S. Adams, *Mt. W. Contr.*, No. 638, *Ap. J.*, **93**, opp. p. 14, 1941 (*H* 16, *o* Cet).

[5] *Problems in Astrophysics* (London, 1903), p. 226.

[6] *Lick Obs. Bull.*, **10**, 132, 1922.

[7] *Spectra of Long-Period Variable Stars*, p. 72; *Pub. A.S.P.*, **57**, 178, 1945.

the low intensity of $H\alpha$, $H\beta$, and $H\gamma$ might be due to the absorption of the *TiO* bands. W. S. Adams[8] identified certain lines of iron, chromium, and vanadium with the absorption lines in $H\delta$, $H\zeta$, H 10, and H 16.

An extensive series of spectrograms of Mira Ceti obtained by Dr. P. W. Merrill and the writer during the years from 1934 to 1947 now makes it possible to study this interesting problem in greater detail than has hitherto been possible. Eighty-eight spectrograms were used in measuring the wave lengths of the absorption lines within the hydrogen emission lines. Of these, 75 were taken with the coudé spectrograph of the 100-inch telescope and 13 with the three-prism ultraviolet spectrograph at the 60-inch. The approximate mean dispersions are: 40 plates, 3 A/mm; 33 plates, 10 A/mm; 10 plates, 15 A/mm; and 5 plates, 20 A/mm. Nineteen of the spectrograms extend to H 18, λ 3696, in the ultraviolet, but only a few scattered measures were possible in the complicated region of shorter wave length, where the distinction between bright lines and spaces separating absorption lines is difficult.

The means of the measured wave lengths of the absorption lines within and near the emission lines of hydrogen are shown in Table 1. For each spectrogram the measured values were corrected for the radial velocity of the star as determined from the other absorption lines of the same plate or of other plates taken at about the same date. Only such lines as occur within about 1 A of the center of the hydrogen lines are included in the table. Since the total width of the strong hydrogen emission is usually not much greater than 1 A, some of the absorption lines may fall on the edge of, or partly outside, the principal emission.

The intensities in the third column of Table 1 are rough relative estimates made from spectrograms where the lines are easily seen. The estimates are greatly influenced by the density of the near-by emission. For such lines as are evidently blends the other contributing line is in the last column. Variations in the intensity of the absorption lines during the cycle of the light-variation are largely masked by the changes in the position and strength of the emission lines. The microphotometer curves of Figures 1 and 2 illustrate the appearance of the absorption lines within or near some of the hydrogen lines at phases before and after maximum. The curves for $H\gamma$ are at four phases of the same cycle.

The identifications in the fifth and sixth columns are based chiefly on agreement in wave length, the average difference being 0.036 A, or about 3 km/sec in terms of velocity. This difference includes the error in determining the velocity of the star and the error in the laboratory wave length, as well as the errors of measurement of the particular line in the star. The intensities in the seventh column are from the *M.I.T. Wavelength Tables*. Although only about half the 65 identifications pertain to strong or well-known lines, the excellent agreement of the wave lengths points to the probability that most of the identifications are justified. The distribution of the identifications among the elements is quite reasonable for a star of low temperature. The number of lines identified for the several elements are: *Ca*, 1; *Ti* I, 8; *Ti* II, 1; *V*, 14; *Cr*, 4; *Mn*, 1; *Fe*, 24; *Co*, 3; *Ni*, 5; *Y*, 1; *Zr*, 1; *Mo*, 1; *In*, 1. The identification of the *In* line λ 4101.764, as suggested by P. W. Merrill for U Orionis[9] and R Leonis,[10] is interesting and provides a mechanism by which electrons of indium atoms may be raised to the level at which they can emit the line λ 4511.310. A search for similar fluorescent effects in other elements was not fruitful.

The 24 *Fe* lines identified within the bright hydrogen lines show the same correlation between displacement and excitation potential as that found by W. S. Adams[11] for *Fe* lines in *o* Ceti and by P. W. Merrill[12] in U Orionis, R Serpentis, and R Hydrae. The mean

[8] *Mt. W. Contr.*, No. 638; *Ap. J.*, **93**, 18, 1941.

[9] *Mt. W. Contr.*, No. 713; *Ap. J.*, **102**, 352, 1945.

[10] *Mt. W. Contr.*, No. 720; *Ap. J.*, **103**, 285, 1946.

[11] *Mt. W. Contr.*, No. 638; *Ap. J.*, **93**, 19, 1941.

[12] *Mt. W. Contr.*, No. 713; *Ap. J.*, **102**, 348, 1946; *Mt. W. Contr.*, No. 717; *Ap. J.*, **103**, 6, 1946.

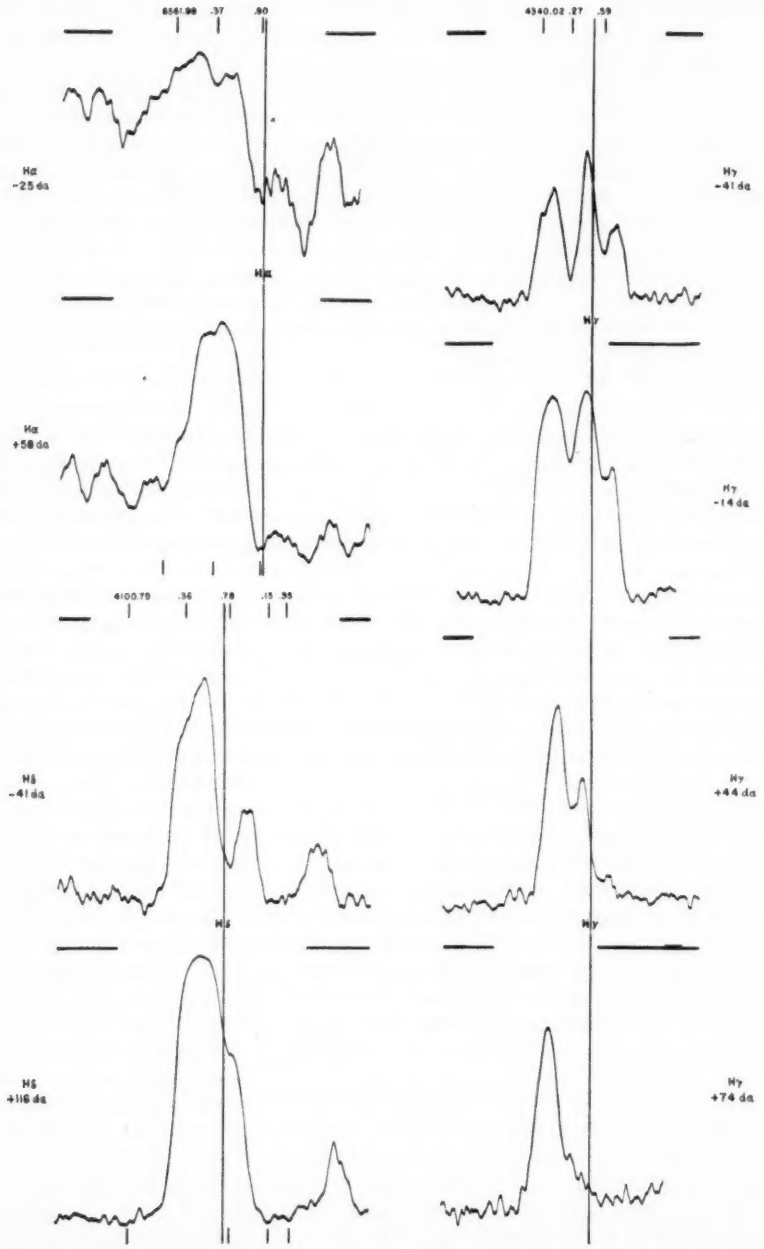

FIG. 1.—Microphotometer curves of *o* Ceti, showing the emission lines $H\alpha$ and $H\delta$ at phases before and after maximum, and $H\gamma$ at four different phases of the same cycle. The vertical line indicates the undisplaced (laboratory) position of the hydrogen line, and the numbers above are the wave lengths of the absorption lines.

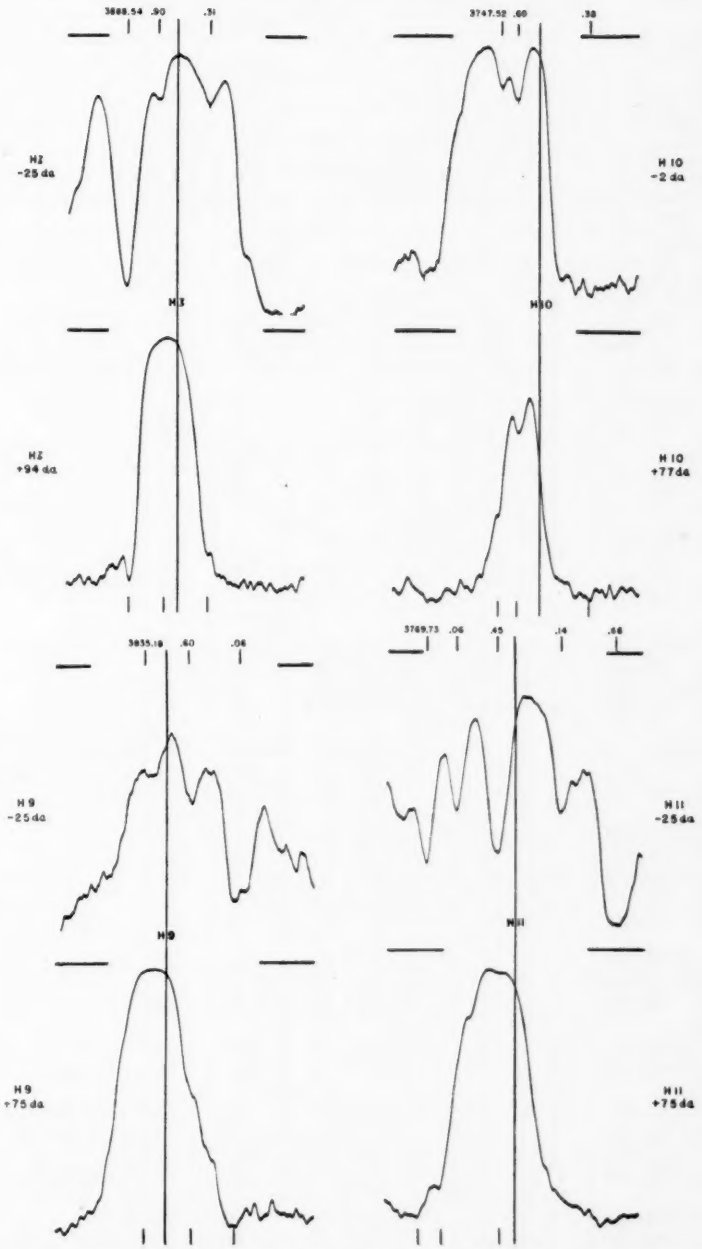

FIG. 2.—Microphotometer curves of *o* Ceti showing the emission lines $H\zeta$, $H9$, $H10$, and $H11$ at phases before and after maximum. The vertical line indicates the undisplaced (laboratory) position of the hydrogen line, and the numbers above are the wave lengths of the absorption lines.

TABLE 1

WAVE LENGTHS AND IDENTIFICATION OF ABSORPTION LINES WITHIN OR NEAR THE HYDROGEN EMISSION OF *o* CETI

HYDROGEN LINE	MEAN MEASURED λ	INT.	NO. PLATES	IDENTIFICATION				REMARKS
				λ	Element	M.I.T. Int.	Multiplet No.	
Hα	6561.982	2	4	.....	.....	.....	.....	
	62.369	2	3	.....	.....	.....	.....	
	62.801	5	5	.....	.....	.....	.....	
Hγ	4340.022	1	3	4340.011	*TiO*	.....	.....	
	40.271	2	40	40.304	*TiO*	.....	.....	
	40.593	4	40	40.593	*TiO*	.....	.....	
	41.015	4	2	40.986	*TiO*	.....	.....	4341.013 *V* 60 (5)
Hδ	4100.792	5	5	4100.745	*Fe*	80	18	
	01.358	2	6	01.272	*Fe*	40	698	
	01.784	10	42	01.764	*In*	2000	1	Identified by P. W. Merrill
	02.153	2	3	02.159	*V*	30	41	
	02.347	3	4	02.376	*Y*	150	7	
Hζ	3887.969	2	9	3888.020	*Ti*	15	175	
	88.545	10	42	88.517	*Fe*	400	45	Identified by W. S. Adams
	88.901	1	19	88.825	*Fe*	40	488	Identified by W. S. Adams
	89.313	2	14	.....	.....	.....	.....	
H 9	3834.673	1	4	3834.735	*Cr*	25	70	
	35.183	1	5	35.185	*V*	30	.....	
	35.598	2	29	35.560	*V*	50	44	
	36.055	5	28	36.054	*V*	10	44	
H 10	3797.520	2	9	3797.517	*Fe*	300	607	Identified by W. S. Adams
	97.690	3	46	97.716	*Cr*	100	139	Identified by W. S. Adams
	98.381	4	12	98.259	*Mo*	1000	1	3798.513 *Fe* 400 (21)
H 11	3769.730	3	17	3769.736	*Ti*	10	.....	
	70.061	1	18	69.995	*Fe*	80	387	
	70.450	10	40	70.405	*Fe*	4	177	
	71.143	2	24	.....	.....	.....	.....	
	71.657	5	30	71.652	*Ti*	70	17	
H 12	3749.526	5	16	3749.487	*Fe*	1000	21	Identified by C. D. Shane
	50.306	1	2	50.349	*Cr*	20	27	
	50.786	1	9	50.763	*Mn*	60	24	
H 13	3733.336	12	22	3733.319	*Fe*	400	5	
	34.849	10	23	34.867	*Fe*	1000	21	Identified by C. D. Shane
H 14	3721.386	1	6	3721.358	*V*	10	11	3721.396 *Fe* 3 (131)
	21.638	1	10	21.632	*Ti* II	60	13	3721.606 *Fe* 6 (437)
	22.016	1	6	21.998	*V*	70	91	
	22.564	15	20	22.564	*Fe*	500	5	Identified by C. D. Shane
H 15	3711.340	4	23	3711.411	*Fe*	50	494	
	12.110	1	14	12.177	*Co*	40	84	
H 16	3703.003	2	23	3702.942	*Ti*	20	132	
	03.603	3	28	03.584	*V*	200	29	Identified by C. D. Shane
	04.107	1	10	04.060	*Co*	300	35	
H 17	3696.685	1	18	.....	.....	.....	.....	Unidentified molecular band

TABLE 1—*Continued*

Hydrogen Line	Mean Measured λ	Int.	No. Plates	Identification				Remarks
				λ	Element	M.I.T. Int.	Multiplet No.	
H 17	97.172	1	15	.....	.....	.....	.....	Unidentified molecular band
	97.657	2	15	.....	.....	.....	.....	Unidentified molecular band
H 18	3690.762	1	5	3690.730	*Fe*	80	807	
	91.136	1	11	.....	.....	.....	.....	Unidentified molecular band
	91.509	1	18	.....	.....	.....	.....	Unidentified molecular band
	91.888	1	14	.....	.....	.....	.....	Unidentified molecular band
	92.263	3	11	3692.225	*V*	200	29	
H 19	3686.040	2	1	3685.998	*Fe*	150	385	
	87.379	12	3	87.458	*Fe*	400	21	
H 20	3682.293	2	3	3682.226	*Fe*	400	772	
	83.052	5	5	83.047	*Co*	200	99	
H 21	3678.974	2	3	3678.98	*Fe*	5	124	
	79.861	20	3	79.915	*Fe*	500	5	
H 22	3675.716	3	2	3675.700	*V*	100	29	
	76.352	1	2	76.314	*Fe*	200	228	
	76.631	1	1	76.684	*V*	300	115	
	77.050	2	1	77.085	*V*	25	.....	
H 23	3674.098	12	3	3674.15	*Ni*	200	32	
H 24	3670.814	1	1	3670.810	*Fe*	12	133	
	71.230	2	1	71.205	*V*	100	70	
	71.653	5	4	71.672	*Ti*	150	19	
H 25	3668.994	3	1	3668.965	*Ti*	100	18	
	69.204	3	1	69.241	*Ni*	150	2	
	69.580	1	2	69.523	*Fe*	200	291	
	70.371	6	1	70.427	*Ni*	150	4	
H 26	3667.105	5	1	3667.252	*Fe*	80	570	3666.944 *Fe* (46)
	67.747	1	1	67.741	*V*	80	114	
	68.024	2	1	67.999	*Fe*	60	438	
	68.444	1	1	.....	.....	.....	.....	
H 27	3665.990	1	1	3665.980	*Cr*	20	48	
	66.176	3	1	66.19	*Cr*	12	46	
H 28	3664.049	10	1	3664.095	*Ni*	300	4	
	64.618	3	1	64.537	*Fe*	35	391	
	65.223	2	2	65.142	*V*	100	115	
H 30	3661.931	4	1	3661.951	*Ni*	50	16	
H 31	3661.271	5	3	3661.20	*Zr*	18	12	
H 32	3660.558	8	3	3660.631	*Ti*	90	18	
H 35	3658.043	8	3	3658.097	*Ti*	150	19	

displacement for E.P. 0.53 volts is —0.6 km/sec, based on laboratory wave lengths, while for E.P. 2.85 volts it is +2.8 km/sec. This result indicates that the *Fe* lines within the hydrogen emission have the same characteristics as those outside.

The probable occurrence of the identified lines has also been checked by noting the presence in the star's spectrum of other lines of similar intensity belonging to the same multiplets.

Of the 81 lines measured, only 3 remain unidentified, aside from the lines of *Hα*, *H* 17, and *H* 18, which are probably molecular. The lines in *Hγ*, which were first observed in 1898 by W. W. Campbell and have since been measured on a large number of spectrograms, have, until the present time, defied identification. The failure to trace the origin of these best-known features of the *Hγ* emission in Mira Ceti has doubtless delayed the acceptance of the hypothesis of absorption by gases of the reversing layer—a hypothesis which now seems entirely probable. The individual absorption lines of the *TiO* bands, however, seem to furnish the needed source of absorption for these lines of *Hγ*. Two laboratory spectrograms of *TiO*, dispersion 2.7 A/mm, kindly supplied by Dr. R. B. King, were measured in the region of *Hγ*. Four *TiO* band lines have mean wave lengths as follows: λλ 4340.011, 4340.304, 4340.593, 4340.986. These lines agree well in wave length with the 4 lines of *Hγ*, measured in the star. The last line is probably largely due to the vanadium line, λ 4341.013. Similar identifications with *TiO* would doubtless result from measures of laboratory plates in the region of *Hα* and *Hβ*. A well-marked overlying molecular band whose origin has not yet been traced is responsible for six unidentified lines in *H* 17 and *H* 18. The stellar lines λ 3696.885 *Ti* 20 (177) and λ 3697.426 *Fe* 100 (389) should be present but seem to be lost in the band structure.

Wave lengths determined at different phases of the star's light-variation show no significant correlation with phase, indicating that the changes in the emission strata have little effect on the stability of the absorbing layers. On the assumption that there is no variation of wave length with phase, the average deviation of a single plate from the mean measured wave length of a line is 0.030 A or 2.1 km/sec for the lines at *Hγ* and *Hδ*. The high accuracy obtained for the mean wave lengths gives considerable confidence in the identifications suggested and proves beyond question that absorption by atoms of the reversing layer sufficiently explains the abnormalities of the bright hydrogen lines in Mira Ceti and other long-period Me variables.

UNIV. OF MICH.

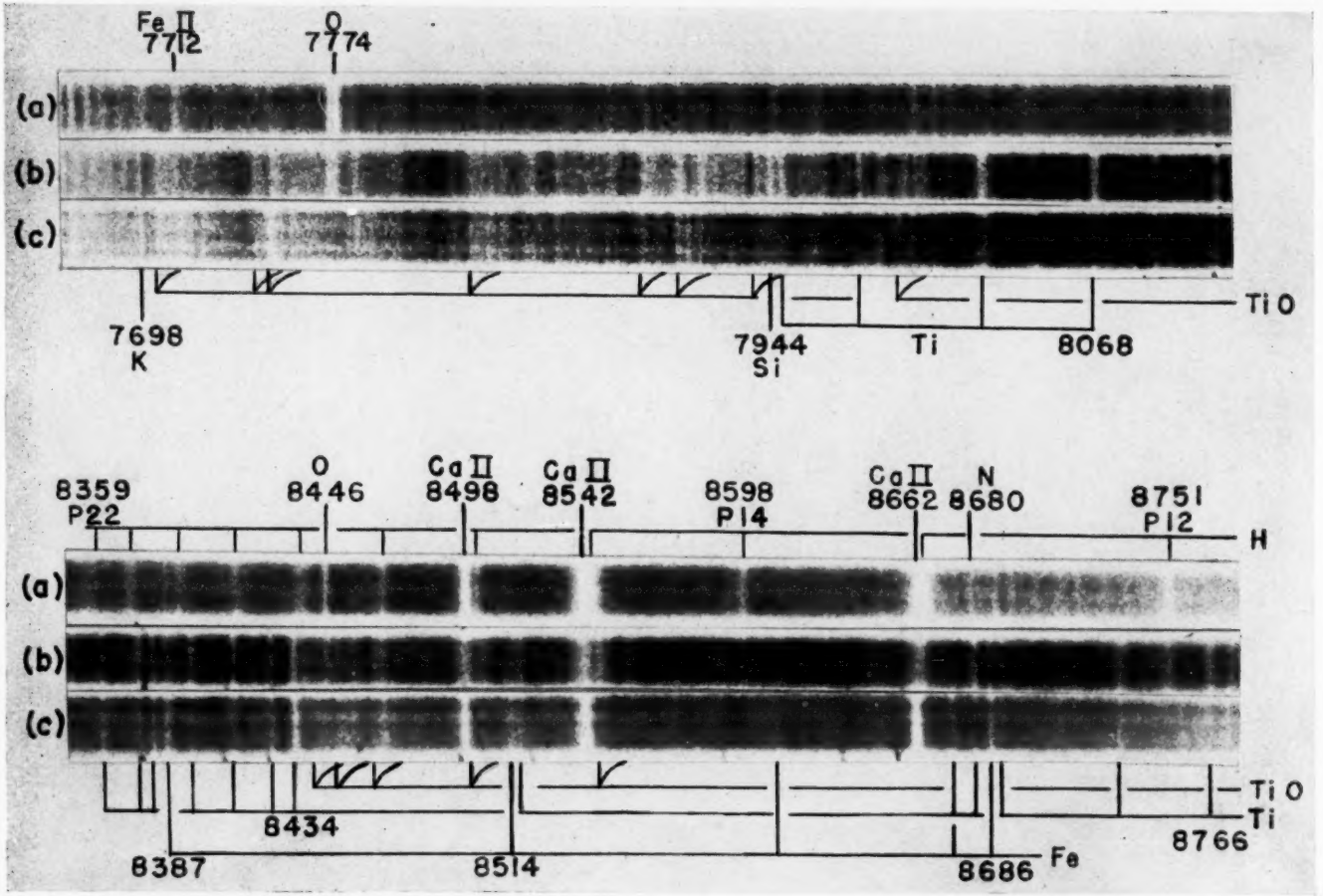

FIG. 1.—Infrared spectra of ρ Cas (image *b*); δ CMa, F8 I*a* (image *a*); and δ^2 Lyr, M4 III (image *c*)

THE INFRARED SPECTRUM OF ρ CASSIOPEIAE IN 1946

PHILIP C. KEENAN
Perkins Observatory
Received June 17, 1947

ABSTRACT

At its minimum of light in 1946 the supergiant ρ Cas possessed an absorption spectrum which, in the infrared as well as in the photographic region, comprised a remarkable mixture of high-excitation lines with lines and bands normally found in low-temperature stars of type M. In particular, the infrared bands of *TiO* were as well developed as in an M4 star.

This peculiar spectrum cannot be described as a superposition of spectra of normal stars. The infrared lines of *Si* I and some of the multiplets of *Ti* I are unusually strong, while the lines of *Fe* I, which are usually enhanced in late-type stars of high luminosity, are weak. Negative radial velocities of the order of -50 to -80 km/sec are shown by lines of all elements measured, but there appear to be systematic differences between lines of different elements, particularly *Ti* (-79 km/sec) and *Fe* (-56 km/sec).

The supergiant ρ Cassiopeiae, which has usually fluctuated in brightness through the visual range $4^m.7$–$5^m.1$, underwent a deep minimum in 1946. Throughout the year the star remained close to $6^m.0$–$6^m.2$, and it was not until the spring of 1947 that it rose again to approximately its former brightness.[1] It was noticed by D. M. Popper[2,3] that the spectrum, which for several years previously had been of class F8 I*a*, had correspondingly undergone radical changes. During the decline to minimum, strong bands of *TiO* and many of the atomic lines characteristic of an M-type star had developed, while the features characteristic of the F-type spectrum were weakening.

In order to study the behavior of the infrared region of the spectrum during the minimum phase, several plates were taken with the grating spectrograph on the 69-inch Perkins reflector. The exposures were made on Eastman I-N plates, and the average dispersion over the range 7300–8700 A is 48 A/mm. Two strong spectrograms, taken with exposure times of about 4 hours each, were obtained on September 5 and October 3, respectively. On these spectrograms the intensities and wave lengths of the lines and bands appear identical, and additional weaker plates, obtained on June 15, June 23, and July 8, agree in showing that no marked changes in the infrared spectrum took place during the summer and fall of 1946. We may therefore speak of a "minimum spectrum" as existing during this period.

The more interesting portions of the infrared region (the portions least distorted by telluric bands) are reproduced in Figure 1. The comparison stars are δ CMa, F8 I*a*, which in the blue region of its spectrum is known to be very similar to ρ Cas as the latter appeared before it underwent its marked change, and δ^2 Lyr, a normal M4 giant, in which the *TiO* bands can be seen to match rather closely those in ρ Cas.

It can be seen clearly in the reproduction that throughout the infrared, just as in the other spectral regions, the spectrum of ρ Cas in 1946 comprised an unusual mixture of absorption features of high and low excitation. This complexity made the sorting-out of the blended lines and bands difficult, and it was only by comparison with matched prints of spectra of early- and late-type standard stars that it was possible to identify the contributing elements with fair confidence. Also of great help in the task of identification was the catalogue of lines in the spectrum of β Peg which Mrs. Dorothy Davis Locanthi has prepared from measurements of Mount Wilson coudé spectrograms.[4]

FIG. 1.—Infrared spectra of ρ Cas (image *b*); δ CMa, F8 I*a* (image *a*); and δ^2 Lyr, M4 III (image *c*)

[1] D. M. Popper, *Harvard Announcement Card*, No. 816, May, 1947.

[2] *Ibid.*, No. 752, June, 1946. [3] *A.J.*, **52**, 129, 1947.

[4] *Ap. J.*, **106**, 28, 1947. I am greatly indebted to Mrs. Locanthi for making several sections of this valuable table available in advance of its publication.

In Table 1 are listed the lines which were clearly present on both of the best spectrograms of ρ Cas, No. 1652 (Sept. 5) and No. 1740 (Oct. 3). No systematic displacement of the lines between these two dates could be detected, and the tabulated wave lengths and line intensities are the means of the measurements from the two plates. The wave lengths are reduced to the sun but are not corrected for the radial velocity of ρ Cas, since there is evidence that the Doppler shift in this star varies considerably with the element responsible for the line. For most of the strong lines in the infrared region the displacements range from 1.5 to 2.0 A to the violet of the laboratory positions, which are given in the columns for identification. In these columns the figures in parentheses are the multiplet numbers as given in the revised edition of *A Multiplet Table of Astrophysical Interest*.[5]

Telluric lines have been included in the table only when they contribute to blends in which a stellar component is evidently present. The listing of *TiO* bands is also incomplete, for many of them overlap and are visible only as a weakening of broad strips of the continuous spectrum. All features listed in Table 1 are absorption lines or bands. If any emission lines are present, they are too weak to be readily recognized.

The radial velocities derived from the relatively few lines which appear nearly free of blending are collected in Table 2. The systematic differences between several of the elements are suggestive, but from this small amount of data only the difference between *Ti* (-79 km/sec) and *Fe* (-56 km/sec) appears clearly established. It is striking that practically all the elements show negative radial velocities considerably greater than the value of -42.6 ± 0.3 km/sec assigned to ρ Cas in Moore's catalogue of radial velocities.

Among the discrepancies in the positions of individual lines the most striking is that of *Ca* II 8662, which has an apparent velocity shift only half that of the other two lines of the infrared triplet, λ 8498 and λ 8542. Since both plates show this effect, it is probably real.

In considering the intensities of lines of different elements, it is natural to split them into two groups according to whether they normally appear in the spectrum of an F-type supergiant or in an M-type spectrum. It can be seen in Figure 1 that the only stellar features conspicuously present in both comparison stars are the lines of the *Ca* II triplet. We accordingly make this division of the material.

LINES CHARACTERISTIC OF AN F-TYPE SUPERGIANT

All the features which are strong in the spectrum of δ CMa are present in that of ρ Cas at minimum, but most of them are considerably weakened. These include the Paschen series of hydrogen, the blends of *O* I at λ 7774 and λ 8446, several lines of *N* I near λ 8700, and *Fe* II 7712. The single marked exception among the elements is *Si*. Normally the lines of *Si* I reach their maximum near type G0, and in δ CMa the chief infrared lines—$\lambda\lambda$ 7405, 7409, 7416, 7423, 7918, 7932, and 7944 (all arising from levels having excitation potentials between 5 and 6 volts)—are either weak or moderately strong. In ρ Cas at minimum these lines, in spite of blending with other metallic lines, are strengthened to such a degree that they are more conspicuous than in the spectrum of any other star which has been photographed here in the infrared region. The least blended of these lines, λ 7944, has been marked on the upper set of exposures in Figure 1, where it appears just to the left of the equally strong *Ti* 7949.

LINES AND BANDS CHARACTERISTIC OF M-TYPE SPECTRA

The strength of the *TiO* bands in ρ Cas corresponds to a spectral type close to M4. The lines of most of the neutral metals that normally would appear in an M-type spectrum are present also. The only marked peculiarities are shown by the *Ti* lines, which are somewhat stronger than in most M-type stars, and by the *Fe* lines, which are much weaker. If the spectra of ρ Cas and of δ^2 Lyr in Figure 1 are compared, the conspicuous

[5] C. E. Moore, *Princeton Univ. Obs. Contr.*, No. 20, 1945.

TABLE 1

LINES IN THE MINIMUM SPECTRUM OF ρ CAS, REGION 7300–8825 A

Measured Wave Length	Intensity	Chief Contributors	Weak Contributors	Remarks
7342.90	5	*Ti* (97) 44.72	Atm H_2O 43.95	
7355.47	5	*Ti* (97) 57.74 *Cr* (93) 55.94	*V* (117) 56.51	Blend
7362.10	4n	*Ti* (97) 64.11	*Al* (11) 61.59 *Al* (11) 62.31 *V* (117) 63.16	
7389.2	2 (Bl on R)	*Fe* (1077) 89.42 — (β Peg) 90.41 *Si* (75) 92.18	.....	Blend
7392.5	2 (Bl on V)	*Ni* (109) 93.63	.....	
7398.35	2	*Cr* (93) 00.23	.....	
7404.9	2n (Bl on R)	*Si* (23) 05.85	.....	
7408.7	3n (Bl on V)	*Si* (23) 09.11 *Ni* (139) 09.39	.....	Blend
7414.67	3	*Si* (22) 16.00	.....	
7422.04	4	*Si* (23) 23.54 *Ni* (139) 22.30 *Ti* (97) 23.17	.....	Blend
7430.89	2	— (β Peg) 32.69	.....	
7438.4	3n	*Zr* (23) 39.89 *Ti* (225) 40.60	.....	Blend
7444.27	1	*Fe* (1077) 45.78	.....	
7448.8	1	*Fe* II (73) 49.34 (?)*Y* II (25) 50.32	.....	Blend present in δ CMa
7461.0	3	*Cr* (93) 62.37	.....	Plate 1740 gives discrepant wave length
7467.97	2+n	— (β Peg) 69.95 *N* (3) 68.29	.....	Blend
7473.20	2n	(?)*Ti* (142) 74.94	.....	
7478.3	1n	(?)*Fe* (683) p 78.87 (?)*Fe* (266) p 81.74	.....	Both lines present in sun and β Peg
7482.30	3	— (β Peg) 83.30 *La* II (1) 83.48	.....	Probably blend
7488.04	2 (Bl on R)	*Ti* (225) 89.61	.....	
7493.84	3	*Fe* (1077) 95.09 *Ti* (225) 96.12	*Fe* (33) p 94.72	Blend
7509.55	1	*Fe* (1077) 11.04	.....	
7544.92	1	*Fe* (unc.) 46.18	.....	
7553.64	2+w	*Ni* (117) 55.60 *Zr* (23) 54.73	.....	Blend
7573.42	2	*Ni* (156) 74.08	*Cb*—74.57	
7587.6±	.....	*TiO* γ 89.62	.....	Band head
7666±	4	*K* (1) 64.91 Atm O_2 64.87 Atm O_2 65.94	.....	Blend; mainly telluric
7696.32	4	*K* (1) 98.98 Atm O_2 95.84 Atm O_2 96.87	.....	Blend; mainly stellar
7703.8	3n	*TiO* γ 05.21	.....	Band head
7741.5	.....	*TiO* γ 43.24	.....	Band head
7748.4	.....	*TiO* γ 49.76	.....	Band head
7772.13	8	*O* (1) 73.68	.....	Lab. wave length is mean for the triplet.
7781.2	.....	*TiO* γ 83.44	.....	Band head

TABLE 1—*Continued*

Measured Wave Length	Intensity	Chief Contributors	Weak Contributors	Remarks
7797.8.....	4w	*TiO* γ	*Rb* (1) 00.23	Probably blend
7819.5.....	3n	*TiO* γ 20.11	.....	Band head
7826.4.....	.....	*TiO* γ 28.04	.....	Band head
7850.12.....	3n	*Ti* (34) 52.74 *TiO* γ	.....	Blend with band head
7860.7.....	2n	*TiO* γ 61.00	.....	Band head
7881.5.....	3wn	*TiO* γ ⊙, β Peg 81.7	.....	Probably blend with band head
7893.3.....	.....	*TiO* γ	.....	Band head
7907.62.....	5n	*TiO* γ 07.33 Atm H_2O 08.75	*Cr* (316) 08.30 Atm H_2O 08.44	Blend
7912.88.....	1s	*TiO* γ (?)*Fe* (12) 12.86	.....	Identification uncertain
7916.3.....	4n	*TiO* γ Atm H_2O 15.64 *Si* (57) 18.38	*Ni* (109) 17.48 *Cr* (316) 17.85 Atm H_2O 16.80	Blend
7931.97.....	2 Bl on V	*Si* (57) 32.20 *TiO* γ	*Cu* (6) 33.13	Blend
7937.56.....	3	*TiO* γ *Fe* (1136) 37.17	.....	Blend
7942.56.....	4	*Si* (57) 43.94	*Ti* (308) 43.93	
7947.01.....	4	*Ti* (125) 49.17	*Rb* (1) 47.60 *TiO* γ 48.60	
7976.75.....	3s	*Ti* (151) 78.88 *Ti* (308) 78.88	.....	
7986.2.....	3n	*TiO* γ 88.05 *Co* (89) 87.36	.....	Blend
7991.38.....	1	β Peg 92.31 β Peg 93.61	*TiO* γ *Mo* 92.55	Blend
7994.29.....	2	*Ti* (308) 96.53	*TiO* γ 95.98	
7998.62.....	2	*Fe* (1136) 98.97 Atm H_2O 00.3	*Vt* 99.33	Blend
8002.27.....	2n	Atm H_2O 02–03 β Peg 02.52	.....	Blend
8019.8.....	2n	*TiO* γ	Atm H_2O 20–21	
8023.91.....	6w	*Ti* (151) 24.84 β Peg 25.61 *V* (30) 27.36	.....	Blend
8043.6.....	3n	*Fe* (1136) 8046.07 *Fe* (12) 8047.60 Atm H_2O 43–45	.....	Blend
8052.88.....	1	*TiO* γ	.....	
8060.8.....	3n	*Zr* (40) 63.10	Atm H_2O 60.2	
8067.31.....	6w	*Ti* (151) 68.24 *Zr* (40) 70.12	(?)*Sm* II (68) 68.46	
8080.46.....	1n	*TiO* γ (?)	.....	
8083.8.....	0n	*Fe* (1136) 85.20 Atm H_2O δ CMa	.....	
8091.08.....	3+	*Cu* (6) 92.63 *V* (30) 93.51	.....	Blend
8114.52.....	4s	*V* (30) 16.82 Atm H_2O 13.6, 13.9	.....	Blend
8130.65.....	4s	*Zr* (40) 33.00 *Ti* — 31.41 Atm H_2O 30.46 Atm H_2O 31.21	.....	Blend
8181.44.....	4	*Na* (4) 83.26	Atm H_2O 81.85	
8192.96.....	5s	*Na* (4) 94.82	Atm H_2O 93.11	

TABLE 1—*Continued*

Measured Wave Length	Intensity	Chief Contributors	Weak Contributors	Remarks
8210.89.....	3	*Mn* (unc.) 12.43 *Zr* (40) 12.59	Atm H_2O	Blend
8304.56.....	6	*Zr* (40) 05.94 *Ti* (33) 07.41 Atm H_2O 05.09	(?)*Sm* II (69) 05.79	Blend
8332.65.....	6	*Ti* (33) 34.37	(?)*C* (10) 35.19 Atm H_2O 33.58	Mostly *Ti*, but there appears to be a line of slightly longer wave length strengthened in δ CMa
8362.01.....	4	*Ti* (33) 64.28	Atm H_2O 62.00 Atm H_2O 62.30	
8371.56.....	1n	*H* (P21) 74.48 β Peg — 73.99	Atm H_2O 70–71	Blend
8380.59.....	4	*Ti* (33) 82.54 *Ti* (33) 82.82	.....	Blended wave length of 82.65 used for radial velocity
8386.5.....	3nn	*Ti* (182) 89.5 *Fe* (60) 87.78	.....	Blend
8394.75.....	4	*Ti* (33) 96.93	.....	
8410.53.....	4	*Ti* (33) 12.36	*H* (P 19) 13.32	
8418.22.....	1n	*Ti* (182) 18.05 β Peg, ⊙ 19.88 β Peg, ⊙ 20.49	.....	Blend
8424.51.....	3+	*Ti* (33) 26.50	*Ti* (182) 24.41	
8432.54.....	5	*Ti* (33) 34.98 *Ti* (33) 35.68 *TiO* γ	.....	Blend
8436.29.....	1	*H* (P18) 37.96 *Ti* (224) 38.93	.....	Blend
8445.01.....	2n	*O* (4) 46.49	*Fe* (12) p	Lab. wave length is mean for the doublet
8449.6.....	1nn	*Cr* (56) 50.26 *Ti* (224) 50.89	.....	Blend
8455.61.....	1nn	*Ti* (141) 57.10 *TiO* γ 57.1	*Cr* (56) 55.24	Blend
8464.65.....	4wn	*Ti* (182) 67.17 *H* (P17) 67.26	*Zr* (40) 64.65	Blend
8470.54.....	2nn	*Fe* (1270) 71.75 *TiO* γ 71.6	.....	Blend
8495.52.....	8n	*Ca* II (2) 98.02	.....	
8503.48.....	3nn	*H* (P16) 02.49 *TiO* γ 04.9	.....	Blend
8512.89.....	1n	*Fe* (60) 14.08 *Fe* (401) 15.08 *TiO* γ 13.5	.....	Blend
8515.72.....	3n	*Ti* (182) 18.05 *Ti* (150) 18.37	.....	Blend
8539.60.....	10n	*Ca* II (2) 42.09	*TiO* γ 41.7	
8544.98.....	3n	*Ti* (150) 48.07 *H* (P15) 45.38	.....	
8555.10.....	2nn Bl on R	*Si* (45) 56.64 β Peg 58.83	*Cr* (56) 55.54	
8567.9.....	2n	*Ti* (209) 69.72	.....	
8589.55.....	1n	(?)*V* — 91.06 (?)*La* — 90.94 *TiO* γ 91.1	.....	Blend

TABLE 1—*Continued*

Measured Wave Length	Intensity	Chief Contributors	Weak Contributors	Remarks
8596.42.....	2n	*H* (P14) 98.39	.....	
8610.6.....	1n	*Fe* (339) 11.81 *Ti* (141) 12.91	.....	Blend
8627.1.....	2	?	.....	
8646.7.....	3nn	*Si* (unc.) 48.89 ⊙ — 48.47	(?)*Na* (19) 49.6	Wide blend
8660.76.....	9	*Ca* II (2) 62.14	*H* (P13) 65.02	
8666.3.....	1n	(?) *Si* (55)p 67.40 (?)*Fe* (166)p 67.37	.....	
8672.8.....	1n	*Ti* (68) 75.38 *Fe* (339) 74.75	.....	Blend
8680.45.....	4	*Ti* (68) 82.99	.....	
8685.74.....	2	*Fe* (60) 88.63 *N* (1) 86.13	.....	Probably blend
8690.20.....	2	*Ti* (68) 92.34	.....	
8693.1.....	0	⊙, β Peg 94.05	.....	
8701.6.....	1n	*N* (1) 03.24	*Ni* (83) 02.49	
8709.43.....	0n	*N* (1) 11.69	*Ba* II (5) 10.82 *Fe* (1267) 10.29	
8716.50.....	2n	*N* (1) 18.82 β Peg, ⊙ 17.78	.....	Blend
8733.0.....	3+	*Ti* (68) 37.70	.....	
8749.9.....	3n	*H* (P12) 50.48 *Si* (43) 52.17	.....	
8756.3.....	0	*Fe* (333) 57.19	.....	
8764.40.....	4n	*Ti* (68) 66.64	.....	
8771.28.....	2 Bl on R	*TiO* γ 74.5 *Al* (9) 72.88 *Al* (9) 73.91	.....	Blend
8804.7.....	4n	*Mg* (7) 06.8	.....	Blended *Mg* triplet
8821.90.....	4nn	*Fe* (60) 24.23 *Ti* (139) 21.14 *TiO* γ 19.3	.....	Blend

TABLE 2

RADIAL VELOCITIES FROM RELATIVELY UNBLENDED LINES

LINE	V_r (KM/SEC)	MEAN V_r (KM/SEC)
	Ti	
7344.7	−74.4	
7364.1	81.8	
7949.2	83.6	
7978.9	82.2	
7996.5	85.8	
8377.9	82.0	
8382–83	73.8	
8396.9	82.8	−79.0 ±1.8 m.e.
8412.4	65.2	
8426.5	70.8	
8675.4	88.5	
8683.0	89.1	
8692.3	73.8	
8734.7	74.8	
8766.6	−76.2	
	Fe	
7445.8	−60.8	
7511.0	59.3	−55.8
7546.2	49.9	
7568.9	−53.0	
	Mg	
8806.8	−69.0	−69.0
	Si	
7416.0	−53.8	−52.9
7943.9	−52.0	
	Na	
8183.3	−66.6	−67.5
8194.8	−68.4	

LINE	V_r (KM/SEC)	MEAN V_r (KM/SEC)
	Cr	
7400.2	−76.3	−62.6(?)
7462.4	−49.0(?)	
	Ni	
7393.6	−47.0	
7522.8	48.5	−40.0(?)
7574.1	−24.6(?)	
	Cu	
8092.6	−57.6	−57.6
	H	
8598.4	−68.7	−68.7
	O	
7773.7	−59.7	−56.1
8446.5	−52.5	
	N	
8703.2	−56.4	
8711.7	77.6	−71.1
8718.8	−79.4	
	Ca II	
8498.0	−88.5	
8542.1	87.5	(?)
8662.1	−44.0(?)	

weakening of *Fe* 8387, 8514, and 8686 in contrast to neighboring *Ti* lines can be easily seen. Since these same iron lines, of excitation potential near 2.2 volts, are the ones which are usually most enhanced in passing from giants to supergiants of type M,[6] their weakening in the supergiant ρ Cas as compared to a normal M-type giant is in the wrong direction to be explained as a luminosity effect and should be described as a peculiarity in ρ Cas.

On the other hand, the lines of the alkali metals of low ionization potential, *Na* and *K*, which are strong in ρ Cas, are consistent with their behavior in other highly luminous stars of type M, such as μ Cep.

It can be noticed in Figure 1 that the lines of the triplet of ionized calcium are much weaker in ρ Cas than in either of the comparison stars. Microphotometer tracings show that they have about their usual width but are very shallow. This may be due to filling of the line centers by incipient emission. There is also another possible explanation. Since these *Ca* II lines become very weak in spectra of type later than M4, it might be that in ρ Cas they are actually produced in an atmosphere of considerably lower temperature than that corresponding to type M4. In that event we should have to assume that level effects or generally increased opacity prevent the *TiO* band heads from being as conspicuous as in type M5 or M6. This latter explanation of the *Ca* II weakening seems improbable, however, for in most late M-type stars these lines are narrow and rather deep, in marked contrast to their shallowness in ρ Cas.

The Perkins spectrograms also furnish some qualitative information about the color of ρ Cas. The exposure times required to obtain the infrared spectrum at minimum correspond to the infrared index of a giant near type K0. This is not greatly different from the color of this star when at its usual brightness and indicates that during the drop of minimum the color did not change much, in spite of the great alteration of the line spectrum. Similar conclusions were drawn by Popper from a comparison of the blue and visual regions.[3]

Although any interpretive discussion of ρ Cas must be based upon detailed investigation of the whole accessible spectral range, the data for the infrared portion do offer a few suggestive points which may be worth noting. In the first place, it does not seem possible to ascribe the complexity of the minimum spectrum to the superposition of spectra of two stars of contrasting type. If that were the case, the star of earlier type would dominate the violet region, and the redder star would produce the infrared spectrum. Actually, the blending of features of high and low excitation seems to be much the same over the whole range from 4000 to 8700 A, and it appears necessary to conclude that a single source is responsible for the entire continuous spectrum. Furthermore, the relative intensities of lines of different elements, particularly *Si*, *Ti*, and *Fe*, cannot be reconciled with any simple mixture of normal spectra. The star has a definitely peculiar spectrum, and the evidence for systematic differences in the velocities of different elements immediately suggests that we have to deal with stratification effects.

[6] Keenan and Hynek, *Ap.J.*, **101**, 57, 1945.

THE NEW ECLIPSING VARIABLE BD — 6°2376

CHANG YUIN
Harvard College Observatory
Received May 26, 1947

ABSTRACT

The writer has estimated the light-changes of this star on 1415 Harvard patrol plates and has found that it is a normal eclipsing system with a fairly constant period of 3.8735833 days. The photographic light-curve exhibits a small reflection effect and a secondary minimum, slightly asymmetrical to the primary minima. The photographic elements are: Min = 2427562.220 + 3.8735833 E; Max = 9^m39; $Min_1 = 10^m59$; $Min_2 = 9^m43$; the relative elements are: $k = 0.35$; $r_1 = 0.30$; $r_2 = 0.11$; $L_2 = 0.669$; $i = 78°40'$; and $\gamma = 18.6$. The spectral class of the brighter component is B5 and the computed one of the fainter component is F3. The absolute dimensions of the components are: Masses, 3.7 ⊙ and 5.9 ⊙; radii 7.1 ⊙ and 2.5 ⊙. Absolute photographic magnitudes are: 0^m45 and -0^m27. Distance is 1000 parsecs.

Dr. Y. C. Chang of Yerkes Observatory announced in a letter of February 26, 1947, that the star BD−6°2376 in Monoceros is variable. With Dr. Chang's permission I have observed the star on the large number of Harvard patrol plates taken over a period longer than forty-seven years, and I thank him for this opportunity to publish the results.

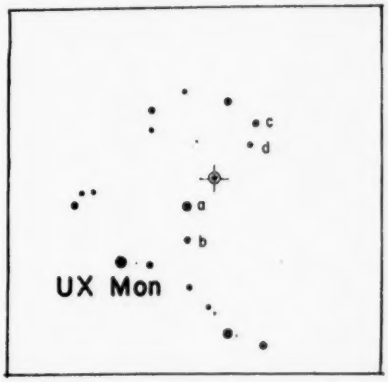

FIG. 1.—Field of BD−6°2376

TABLE 1

Comparison Stars	Steps	IPg	Comparison Stars	Steps	IPg
a	8	9^m19	c	− 3	10^m08
b	3	9.62	d	−15	10.84

The positions of the near-by stars are plotted in Figure 1. The stars a, b, c, and d were selected as comparison stars, and the estimates were made in steps. The steps and the international photographic magnitude (IPg) of those stars are shown in Table 1.

The IPg magnitudes were determined from *Harvard Observatory Mimeograms* for Selected Area No. 124 (−15°) (C. P. and S. Gaposchkin, Series II, No. 1 [1935]). Each photographic magnitude was computed by the formula IPg = $9^m8 - 0^m074 \times$ steps.

The brightness of the star was estimated on 1415 Harvard patrol plates taken between October 16, 1898 (JD 2414579.899) and March 18, 1946 (JD 2431898.537) covering a period of over forty-seven years. Most of these plates were taken with the $1\frac{1}{2}$-inch Cooke lens (AC and AM), some with the 3-inch Ross-Fecker lens (RB and RH).

In Table 2 there are 56 of the 1415 estimates fainter than −6 (steps) or $10^{m}.24$ (IPg). The approximate period derived from this table is

$$P = 3^{d}.8735833 \qquad \text{or} \qquad P^{-1} = 0^{d}.2581589 .$$

The mean photographic light-curve was drawn as in Figure 2, through 35 normal points given in Table 3, columns (1) and (2). All magnitudes outside primary minimum have a probable error of $\pm 0^{m}.033$ at maximum.

TABLE 2

Steps	JD	Steps	JD	Steps	JD
− 6	2414949.885	− 7	3103.658	−11	8193.667
9	5383.666	8.5	2423107.569	8	8197.417
8	6820.806	10	3905.520	12	2428491.889
9.5	7521.876	9	4141.807	15	8592.586
8	7622.637	11	4145.683	13	8925.711
8.5	7955.686	7	4172.750	15.5	9196.893
7	8158.849	6	4908.728	10	9591.895
7	8292.777	6.5	4916.638	11.5	9665.642
8	8397.307	6	5327.259	11	30138.214
7	8420.541	9.5	5946.862	14	0343.435
6	8621.917	8.5	5981.710	13	0401.528
6	8660.814	13	6090.232	11	0668.886
8	8691.716	11.5	6651.857	11	1110.325
8	8761.331	12	7387.906	14	1141.400
10	9795.708	9	7418.814	7	1172.320
10	20465.845	13	7562.221	12	1416.497
8.5	0934.561	8	7895.261	14	1768.905
10	1364.492	9	8158.807	−11.5	1834.722
− 7	2975.900	− 6	8166.435		

In Figure 2 the secondary minimum is slightly asymmetrical to primary minima. The type of eclipse is shown to be total, and a slight reflection effect is indicated. The result of this effect is shown in Figure 3, in which the ordinates are photographic magnitudes and the abscissae are phases.

The correction for the reflection effect is $\Delta m = 0.02 \cos\varphi$, with which I have recomputed all normal points in Table 3, columns (3) and (4), where φ is the phase reduced to the middle of the primary minimum ($\varphi_0 = 0^{p}.432$) as the zero point.

The corresponding light-curve is given in Figure 4, in which the crosses indicate the computed curve within primary minimum; they are in harmony with the observed one.

From this rectified light-curve, the following elements are derived:

Max = $9^{m}.39$ Min$_1$ = $10^{m}.59$ $\Delta m_1 = 1^{m}.20$
Min$_2$ = 9.43 $\Delta m_2 = 0.04$
Duration of eclipse, $D = 0^{p}.13 = 0^{d}.5036$
Duration of total eclipse, $d = 0^{p}.016$

The method of Scharbe (*Poulkova Bull.*, **94**, 31, 1932), slightly modified by S. Gaposchkin, was used for computing the relative dimensions of the system. The spectral class of

the brighter component is classified by Mrs. Mayall on Harvard plates as B5, and that of the fainter derived from the difference of their surface brightness is F3.

The absolute dimensions were computed in accordance with S. Gaposchkin's formula (*Harvard Reprint*, No. 201, 1940). Tables 4 and 5 give the results. The relative dimensions for this system are shown in Figure 5.

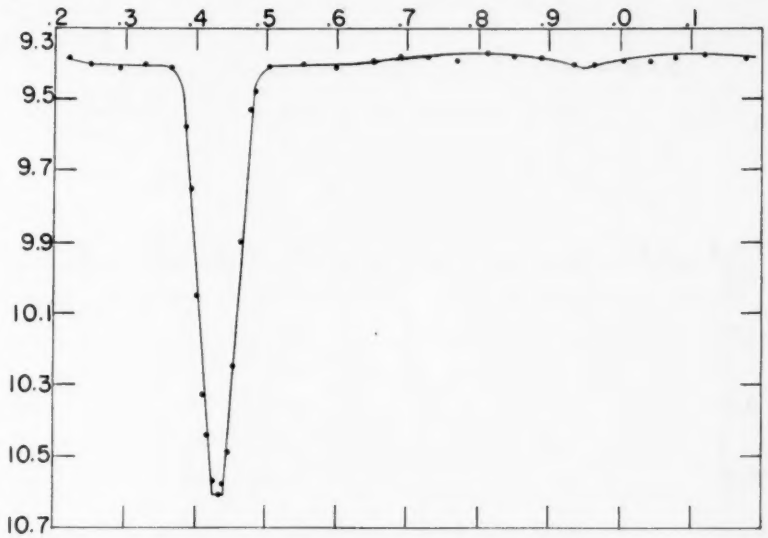

FIG. 2.—Light-curve of BD−6°2376

TABLE 3

(1) Phase	(2) Mag (IPg)	(3) φ (In Period)	(4) Mag+ Δm (IPg)	(5) No. of Obs.	(1) Phase	(2) Mag (IPg)	(3) φ (In Period)	(4) Mag+ Δm (IPg)	(5) No. of Obs.
−0.039	9m40	−0.471	9m42	58	+0.438	10m58	+0.006	10m56	7
+ .004	9.39	.428	9.41	39	.446	10.49	.014	10.47	9
+ .040	9.39	.392	9.41	64	.454	10.25	.022	10.23	5
+ .076	9.38	.356	9.39	63	.463	10.90	.031	9.88	16
+ .118	9.37	.314	9.38	52	.476	10.53	.044	9.51	13
+ .175	9.38	.257	9.38	56	.483	10.48	.051	9.46	14
+ .219	9.38	.213	9.37	63	.504	10.41	.072	9.39	42
+ .250	9.40	.182	9.37	53	.551	10.40	.119	9.38	71
+ .290	9.41	.142	9.40	44	.597	9.41	.165	9.40	62
+ .327	9.40	.105	9.38	62	.650	9.39	.218	9.39	73
+ .364	9.41	.068	9.39	39	.687	9.38	.255	9.38	70
+ .385	9.58	.047	9.56	10	.729	9.38	.299	9.39	54
+ .394	9.75	.038	9.73	11	.768	9.39	.336	9.40	62
+ .401	10.05	.031	10.03	14	.811	9.37	.379	9.38	44
+ .410	10.33	.022	10.31	13	.849	9.38	.417	9.40	54
+ .417	10.44	.015	10.42	11	.887	9.38	.455	9.40	75
+ .426	10.57	.006	10.55	11	+0.932	9.40	+0.500	9.42	72
+ .432	10.61	−0.000	10.59	9					

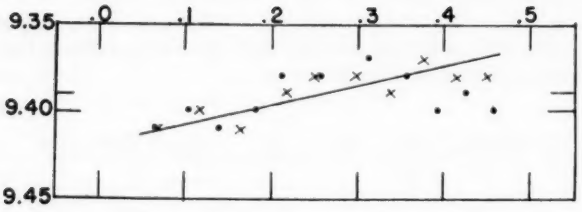

FIG. 3.—Reflection effect for BD−6°2376

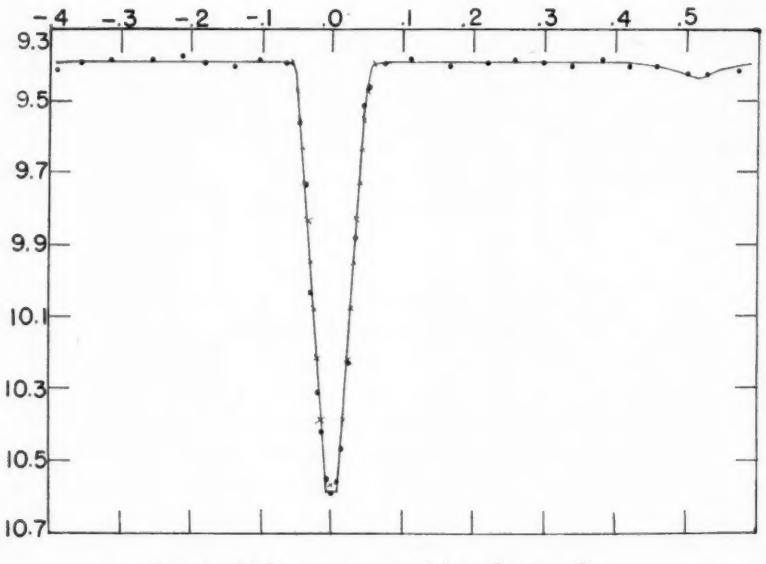

FIG. 4.—Light-curve corrected for reflection effect

TABLE 4

THE SYSTEM OF BD−6°2376

Photometric Elements	Relative Elements
Max = $9^{m}39$	Ratio of radii, $k = 0.35$
Min_1 = 10.59	Ratio of surface brightness, $\gamma = 18.6$
Min_2 = 9.43	Inclination of orbit, $i = 78°40'$
$D = 0^{p}13$	Radius of brighter component, $r_2 = 0.11$
$d = 0^{p}016$	Radius of fainter component, $r_1 = 0.30$

It is interesting to note that our eclipsing variable, according to Dr. Gaposchkin, resembles the newly discovered eclipsing variable by Baade in the extragalactic nebula IC 1613 (No. 31), of which the period is 3.77 days and the spectral class is B5. But this system seems brighter, around -2^m5 (absolute magnitude [IPg]), and the secondary minimum is deeper.

TABLE 5

ABSOLUTE DIMENSIONS

	B Star	F Star	Notes
Radius R	2.50⊙	7.11⊙	(1)
Mass μ	5.89⊙	3.71⊙	(1)
Absolute magnitude (IPg)	-0^m27	0^m45	(2)
Apparent magnitude (IPg)	9.84	11.59	

(1) Computed by S. Gaposchkin's formula.
(2) Computed by Russell, Dugan, and Stewart's formula.

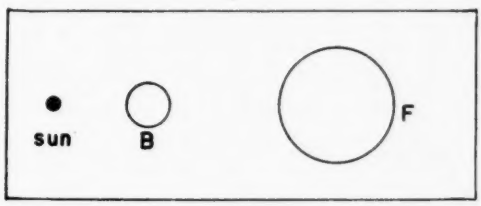

FIG. 5.—Relative dimensions of system

A further discussion and the spectroscopic orbital elements will, I hope, soon be derived from Dr. Y. C. Chang's observations at Yerkes and McDonald observatories. The writer is greatly indebted to Dr. S. Gaposchkin for his very friendly aid in this work and also to Mrs. Mayall for her spectral classification of the star.

NOTES

VELOCITY-CURVE OF BD−6°2376, A NEW ECLIPSING VARIABLE

On plates taken on December 17, 1946, for photometric measurement of UX Monocerotis, the brightness of the star BD−6°2376 was found to have a sudden drop of over 1 mag. Dr. S. Gaposchkin kindly confirmed that its variability had not been announced before and suggested that it might be an eclipsing variable. Its light-curve and elements have been derived by Dr. Chang Yuin, of Harvard, and published elsewhere in the *Astrophysical Journal*.

TABLE 1

Date (U.T.)	JD 24322	Phase	Rad. Vel. (Km/Sec)	Date (U.T.)	JD 24322	Phase	Rad.Vel. (Km/Sec)
1947 Mar. 13....	57.666	0.165	− 49	25....	69.717	0.278	− 20
14....	58.761	.448	− 29	26....	70.699	.530	+ 34
16....	60.725	.955	+ 75	27....	71.700	.788	+ 76
17....	61.737	.216	− 68	31....	75.732	.829	+116
19....	63.747	.735	+ 8	1947 Apr. 3....	78.616	.574	− 11
20....	64.750	.994	0	4....	79.611	.831	+ 24
22....	66.743	.509	+ 13	11....	86.638	0.645	+ 19
23....	67.715	0.760	+ 24				

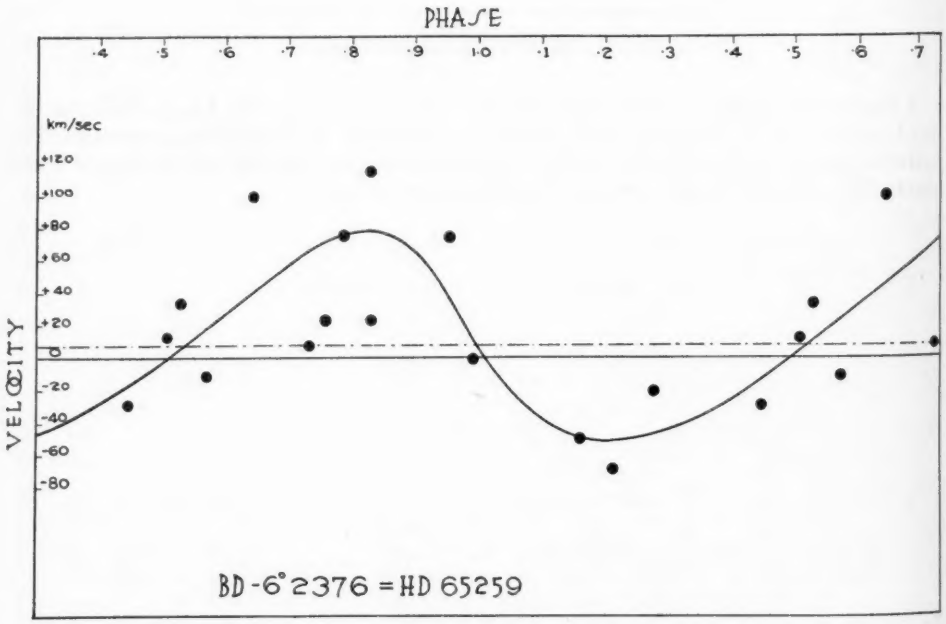

FIG. 1

Fifteen spectrograms of the eclipsing variable were obtained with the McDonald G $f/2$ spectrograph. Three helium lines, λλ 4026, 4387, and 4471 were measured for radial velocity, except in the case of a spectrogram taken at light-minimum, where only the spectrum of the fainter component is visible. The spectral types of the brighter and the fainter components were estimated by Dr. W. W. Morgan as B5 and F2, respectively. In general, only the spectrum of the brighter component could be measured. Table 1 gives the radial velocities.

The phases here are computed with the period of 3.87358 days as given in the paper by Dr. Chang Yuin. When plotted, the velocities show considerable scattering. This is not surprising, considering the fact that the spectral lines are diffuse and broad. A standard velocity-curve with $\omega = 60°$, $e = 0.20$, seems to give a fair representation of the plotted points (Fig. 1). We have therefore the following spectroscopic elements:

$$\gamma = +7 \text{ km/sec} \qquad \omega = 60°$$
$$P = 3.8735 \text{ days} \qquad a \sin i = 3{,}370{,}000 \text{ km}$$
$$e = 0.20$$
$$K = 65 \text{ km/sec} \qquad \frac{m_1^3 \sin^3 i}{(m + m_1)^2} = 0.104$$

Introducing the photometric element $i = 78°40'$, we may reduce the last two quantities to

$$a = 3{,}440{,}000 \text{ km}, \qquad \frac{m_1^3}{(m + m_1)^2} = 0.111 .$$

I am deeply indebted to Dr. W. A. Hiltner, who took the spectrograms for me.

Y. C. CHANG*

YERKES OBSERVATORY
June 20, 1947

A NOTE ON THE PERIOD-SPECTRUM RELATION AMONG CEPHEIDS

The spectral types of eleven of the cepheids listed in Table 1 were determined throughout the light-variation by comparing the variables with a sequence of standard supergiants belonging to luminosity classes I*a*, I*b*, and II.[1] Most of the plates were taken with the small one-prism spectrograph used in the preparation of the *Atlas of Stellar Spectra*. This spectrograph, attached to the 40-inch refractor, gives a dispersion of 125 A/mm at $H\gamma$. The remainder were taken with a similar spectrograph, giving about the same dispersion, attached to the Yerkes 12-inch refractor. It is found that the general features of the cepheid spectra match those of standard supergiants well. The hydrogen lines, as pointed out by Struve,[2] are abnormally strong at maximum, and the cyanogen band near λ 4215 is found to be abnormally weak at minimum.

The spectral types are listed in Table 1 and are plotted in Figure 1 against the logarithm of the periods; the italicized magnitudes are photographic. The seven cepheids marked with asterisks in the table and plotted on the diagram as squares are those studied by Struve,[2] the open circles and squares refer to the types at maximum light, and the filled figures are the types at minimum light.

* On leave from the Institute of Astronomy, Academia Sinica, Nanking, China.

[1] See Morgan, Keenan, and Kellman, *An Atlas of Stellar Spectra* (Chicago, 1943).

[2] *Observatory*, **65**, 257, 1944.

TABLE 1

SPECTRAL TYPES OF EIGHTEEN CEPHEIDS

Star	Period (Days)	log P	Max. Mag.	Δm	Spectral Type (M.K.K. System)	Δ Sp.
SU Cas	1.95	0.29	6.05	0.38	F5 I–II—F7 I–II	0.1
DT Cyg	2.50	0.40	5.66	0.39	F5.5 I–II—F7 I–II	0.15
SZ Tau	3.15	0.50	*6.78*	*0.60*	F6 I*b*—F9 I*b*	0.3
V386 Cyg	5.24	0.72	*10.0*	*1.0*	F5 I*b*—G1 I*b**	0.6
δ Cep	5.37	0.73	*3.71*	*0.72*	F5 I*b*—G2 I*b*	0.7
MW Cyg	5.96	0.78	*10.0*	*1.0*	F8 I*b*—G1 I*b**	0.3
η Aql	7.18	0.86	3.69	0.71	F6 I*b*—G4 I*b*	0.8
VY Cyg	7.86	0.90	*10.1*	*1.2*	F6 I*b*—G1 I*b**	0.5
S Sge	8.38	0.92	*5.79*	1.02	F6 I*b*—G5 I*b*	0.9
BZ Cyg	10.14	1.01	*11.2*	*0.8*	F8 I*b*—G5 I*b**	0.7
ζ Gem	10.15	1.01	3.73	0.37	F7 I*b*—G3 I*b*	0.6
Z Lac	10.89	1.03	*8.64*	*1.36*	F6 I*b*—G6 I*b*	1.0
TX Cyg	14.71	1.17	*10.4*	*1.9*	F5 I*b*—G6 I*b**	1.1
SZ Cyg	15.11	1.18	*9.7*	*1.3*	F8 I*b*—G8 I*b**	1.0
X Cyg	16.39	1.21	*6.53*	*1.56*	F7 I*b*—G8 I*b*	1.1
CD Cyg	17.07	1.23	*9.0*	*1.5*	F8 I*b*—K0 I*b**	1.2
T Mon	27.01	1.43	5.80	0.95	F7 I*a*–I*b*—K1 I*a*–I*b*	1.4
SV Vul	45.13	1.65	*8.43*	*0.90*	F7 I*a*—(K0)	(1.3)

* These spectral types are given by O. Struve in *Observatory*, **65**, 257, 1944.

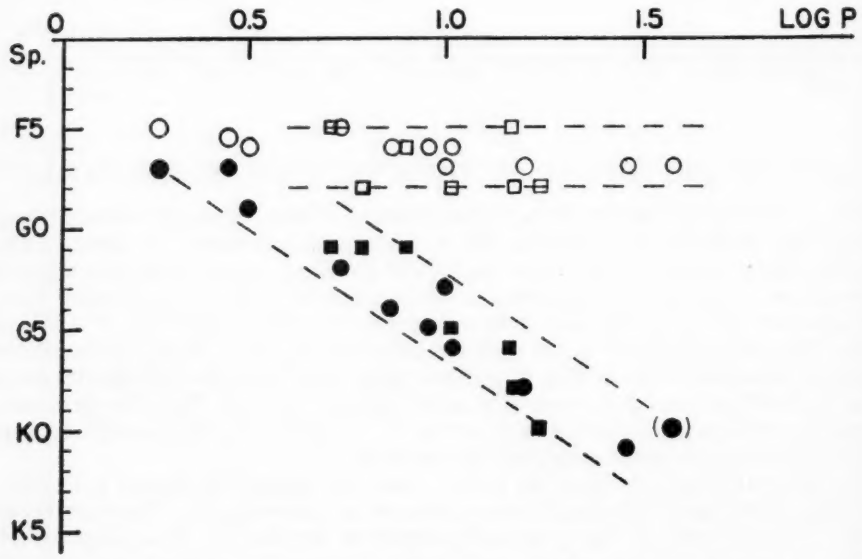

FIG. 1.—Spectral types at maximum (*open circles* and *squares*) and minimum phases for cepheids. Circles are observations by Code; squares are those by Struve.

An examination of the plot shows that the types at maximum light are nearly the same for all the cepheids studied and that the progressive lateness of the median spectral type with increasing period (the standard period-spectrum relation) is due to the systematic change in type at minimum light. The near-equality of the spectral type at maximum light for cepheids of all periods suggests that the unreddened colors obtained at maximum should be about the same. For δ Cephei it is found that the spectrum matches α Persei, F5 I*b*, at maximum light, and β Draconis, G2 I*b*, at minimum. The variation in color type determined by Stebbins[3] is from cF4 to cG2. However, Stebbins calls α Persei cF4. The indication is that the cepheids have the colors of normal supergiants of equivalent type. The value of the new period-spectrum relation for problems of galactic structure and absorption is then clear. It is necessary only to make color observations of cepheids at maximum light, assign the normal color of an F6 or F7 supergiant, and then determine the color excess. Since the range of maximum spectral types is from F5 to F8 and the colors are probably those of normal supergiants, the assumed color cannot be in error by more than around 0.1 mag.

ARTHUR D. CODE

YERKES OBSERVATORY
June 26, 1947

A NOTE ON β CEPHEI

The lines in the spectrum of β Canis Majoris are known to show changes in appearance and intensity which have a period slightly different from that of the velocity variation.[1] Although β Cephei appears to belong to the same class of stars,[2] no such changes in the appearance of the lines have been announced for it. However, since β Cephei has not

TABLE 1

Plate No. Cd	Date 1941 July	Julian Day* 2430+	Phase†	Velocity (Km/Sec)	Plate No. Cd	Date 1941 July	Julian Day* 2430+	Phase†	Velocity (Km/Sec)
140.....	16	191.887	47.356	−14.5	155.....	19	194.784	62.565	−17.7
141.....	16	191.933	47.599	−19.1	156.....	19	194.831	62.817	+ 3.4
144.....	17	192.746	51.866	+ 5.6	157.....	19	194.883	63.085	+15.5
145.....	17	192.789	52.092	+ 5.8	158.....	19	194.932	63.342	−11.6
146.....	17	192.869	52.512	−13.7	160.....	20	195.738	67.576	−20.6
148.....	18	193.732	57.042	+14.7	161.....	20	195.791	67.851	+12.4
149.....	18	193.779	57.289	−10.8	162.....	20	195.851	68.166	+ 2.6
150.....	18	193.824	57.525	−19.4	163.....	20	195.902	68.434	−19.2
151.....	18	193.869	57.761	− 2.7	164.....	20	195.955	68.712	− 4.7
152.....	18	193.915	58.003	+14.8	166.....	21	196.819	73.248	− 4.8
153.....	18	193.962	58.250	− 2.5	168.....	21	196.933	73.846	+11.0

* For the middle of the exposure.

† Counted from the maximum at JD 2430182.866 (July 7, 1941), using the period 0.1904886 day (Smith, *Ap. J.*, **98**, 82, 1943).

been studied previously with a dispersion greater than 10 A/mm, it is valuable to examine the profiles on plates of the highest dispersion available. For this purpose, plates were taken with the coudé spectrograph of the McDonald Observatory by O. Struve in July, 1941. These plates, having a dispersion of 3.5 A/mm at $H\gamma$, were turned over to me for discussion.

[3] *Ap. J.*, **101**, 47, 1945.

[1] See, e.g., Underhill, *Ap. J.*, **104**, 388, 1946.

[2] Struve and Swings, *Ap. J.*, **94**, 99, 1941.

A careful visual study of the plates was made to discover a change in the appearance of the lines with phase. However, no systematic variation was found, and any change which may be present is small enough to be masked completely by photographic effects. Figure 1 shows six *O* II lines and $H\gamma$ at four phases of the velocity variation. The lines are always narrower than in β Canis Majoris.

Table 1 gives the radial velocities obtained, and Figure 2 shows these results graphically. For the mean curve, the γ-velocity is -2.8 km/sec and K is 17 km/sec. These

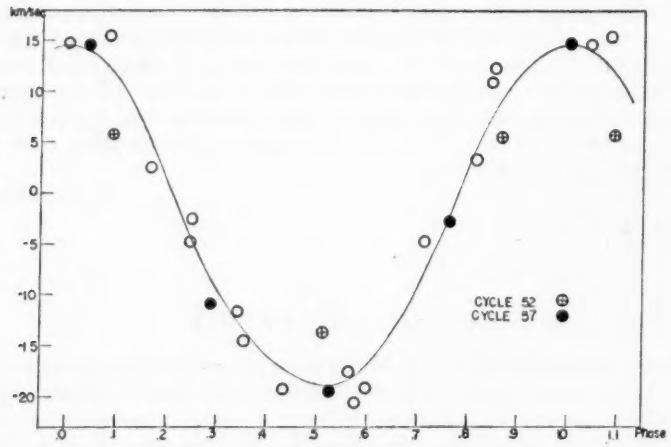

FIG. 2.—Velocity-curve of β Cephei

results agree with those obtained by Burke Smith[3] from plates taken at the Yerkes Observatory covering the same time interval. Although, owing to the short period, not more than five plates were obtained during any one cycle, in every case the velocities for each cycle indicate that a smooth curve would be obtained if more points were available (cf. cycle 57). The observed scatter seems to be due to differences in the velocity-curve from cycle to cycle, a result also found by Smith.[3] Note particularly that, for cycle 52, the amplitude is decidedly smaller than the mean amplitude. A comparison of the velocity-curve obtained from $H\gamma$ and $H\delta$ and of that from three *He* I lines with the curve obtained from thirteen lines of *O* II shows no indication of any systematic differences.

NANCY G. ROMAN

YERKES OBSERVATORY
April 30, 1947

NOTES

EDITOR'S NOTE

Referring to note 4 in K. O. Kiepenheuer's paper (*Ap. J.*, **105**, 408, 1947), Mr. A. H. Shapley has drawn our attention to a paper by J. H. Bartels (*Terr. Mag.*, **51**, 181, 1946), where δR, δW, and δP are defined as deviations "from normals valid for medium solar activity, about $R = 50$; these deviations are all uniformly standardized as to have the same standard deviation $\sigma = 25$."

[3] *Ap. J.*, **98**, 82, 1943.

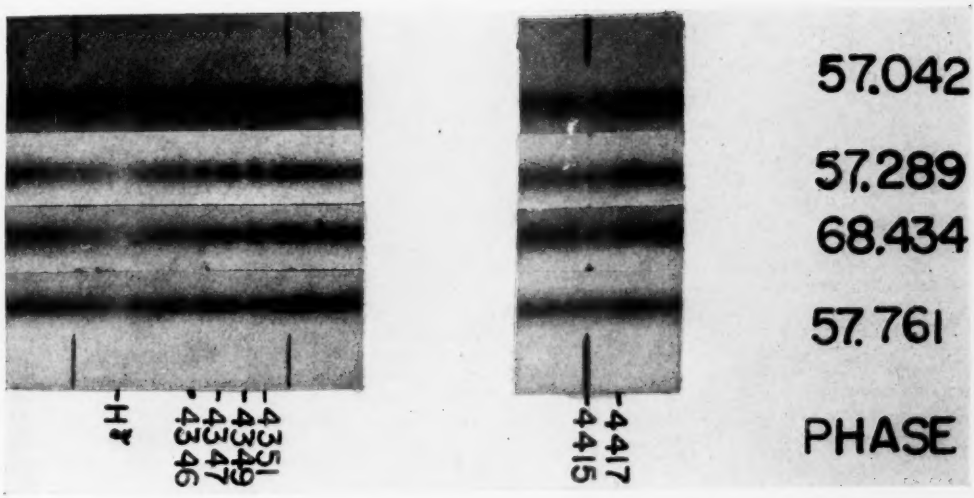

FIG. 1.—Appearance of lines in β Cephei at different phases

UNIV. OF MICH.